The role of inflammation in hereditary spastic paraplegia type 11

Die Rolle von Entzündungsreaktionen bei hereditärer spastischer Paraplegie Typ 11

Dissertation for a doctoral degree

at the Graduate School of Life Sciences,

Julius-Maximilians-Universität Würzburg,

Section Neuroscience

submitted by

Michaela Hörner

from

Woluwe-Saint-Lambert, Belgium

Würzburg, September 2022

Submitted on:

Members of the Promotionskomitee:

Chairperson: Prof. Dr. Carmen Villmann

Primary Supervisor: Prof. Dr. Rudolf Martini

Supervisor (Second): Prof. Dr. Lutz

Supervisor (Third): Prof. Dr. Chi Wang Ip

Date of Public Defense:

Date of Receipt of Certificates:

Affidavit

I hereby confirm that my thesis entitled "The role of inflammation in hereditary spastic paraplegia type 11" is the result of my own work. I did not receive any help or support from commercial consultants. All sources and/or materials applied are listed and specified in the thesis.

Furthermore, I confirm that this thesis has not yet been submitted as part of another examination process neither in identical nor in similar form.

Place, date   Signature

Eidesstattliche Erklärung

Hiermit erkläre ich an Eides statt, die Dissertation „Die Rolle von Entzündungsreaktionen bei hereditärer spastischer Paraplegie Typ 11" eigenständig, d.h. insbesondere selbständig und ohne Hilfe eines kommerziellen Promotionsberaters, angefertigt und keine anderen als die von mir angegebenen Quellen und Hilfsmittel verwendet zu haben.

Ich erkläre außerdem, dass die Dissertation weder in gleicher noch in ähnlicher Form bereits in einem anderen Prüfungsverfahren vorgelegen hat.

Ort, Datum   Unterschrift

Inhalt

Parts of the results presented in this thesis have been published:

The published manuscript and this thesis contain similar text passages in adapted form in some sections.

Flow cytometry was performed under the supervision of PD. Dr. Janos Groh.

Sara dos Santos partially contributed to the immunohistochemical stainings in the corpus callosum, as part of her bachelor thesis, under my supervision.

1 Abstract

Hereditary spastic paraplegias (HSPs) are genetically-determined, neurodegenerative disorders characterized by progressive weakness and spasticity of the lower limbs. Spastic paraplegia type 11 (SPG11) is a complicated form of HSP, which is caused by mutations in the *SPG11* gene encoding spatacsin, a protein possibly involved in lysosomal reformation. Based on our previous studies demonstrating that secondary neuroinflammation can be a robust amplifier of various genetically-mediated diseases of both the central and peripheral nervous system, we here test the possibility that neuroinflammation may modify the disease outcome also in a mouse model for SPG11. *Spg11*-knockout (*Spg11$^{-/-}$*) mice develop early walking pattern and behavioral abnormalities, at least partially reflecting motor, and behavioral changes typical for patients. Furthermore, we detected a progressive increase in axonal damage and axonal spheroid formation in the white and grey matter compartments of the central nervous system of *Spg11$^{-/-}$* mice. This was accompanied by a concomitant substantial increase of secondary inflammation by cytotoxic CD8$^+$ and CD4$^+$ T-lymphocytes. We here provide evidence that disease-related changes can be ameliorated/delayed by the genetic deletion of the adaptive immune system. Accordingly, we provide evidence that repurposing clinically approved immunomodulators (fingolimod/FTY720 or teriflunomide), that are in use for treatment of multiple sclerosis (MS), also improve disease symptoms in mice, when administered in an early (before neural damage) or late (after/during neural damage) treatment regime.

This work provides strong evidence that immunomodulation can be a therapeutic option for the still untreatable SPG11, including its typical neuropsychological features. This poses the question if inflammation is not only a disease amplifier in SPG11 but can act as a unifying factor also for other genetically mediated disorders of the CNS. If true, this may pave the way to therapeutic options in a wide range of still untreatable, primarily genetic, neurological disorders by repurposing approved immunomodulators.

2 Zusammenfassung

Hereditäre spastische Paraplegien (HSPs) sind genetisch-determinierte, neurodegenerative Erkrankungen, die durch eine progressive Schwäche und Spastizität der unteren Extremitäten charakterisiert sind. Die spastische Paraplegie Typ 11 (SPG11) ist eine komplizierte Form der HSP, die durch eine Mutation des *SPG11* Gens hervorgerufen wird. Dieses Gen kodiert Spatacsin, ein Protein, das wahrscheinlich in der lysosomalen Reformation eine Rolle spielt. Frühere Studien unserer Arbeitsgruppe konnten zeigen, dass sekundäre Entzündungsreaktionen verschiedene genetisch-determinierte Krankheiten des zentralen und peripheren Nervensystems verstärken können. Daher haben wir hier untersucht, ob neuroinflammatorische Reaktionen auch in einem Mausmodell für SPG11 den Krankheitsverlauf beeinflussen. *Spg11*-knockout (*Spg11$^{-/-}$*) Mäuse entwickeln frühzeitige Gangveränderungen und Verhaltensauffälligkeiten, welche die Veränderungen der Patienten, zumindest teilweise, abbilden. Außerdem konnten wir eine progressive Zunahme von axonalem Schaden und die Bildung von axonalen Schwellungen in der weißen und grauen Substanz des zentralen Nervensystems von *Spg11$^{-/-}$* Mäusen feststellen. Dies wurde von einer deutlichen Zunahme einer sekundären Entzündungsreaktion in der weißen und grauen Substanz durch zytotoxische CD8$^+$ und CD4$^+$ T-Lymphozyten begleitet. Wir zeigen hier, dass diese krankheitsbedingten Veränderungen durch eine genetische Deletion von Teilen des adaptiven Immunsystems verbessert bzw. ihr Auftreten hinausgezögert werden können. Entsprechend zeigen wir, dass eine Behandlung mit klinisch etablierten Immunomodulatoren (Fingolimod/FTY720 oder Teriflunomid), die zu der Behandlung der Multiplen Sklerose (MS) eingesetzt werden, den Krankheitsverlauf positiv beeinflusst, wenn sie in einem frühzeitigen (Gabe vor neuronalem Schaden) oder späten (Gabe nach/während neuronalem Schaden) Behandlungsversuch appliziert werden.

Diese Arbeit deutet stark darauf hin, dass Immunomodulation eine Therapiemöglichkeit für die noch nicht behandelbare Krankheit SPG11 sein könnte, inklusive der typischen neuropsychologischen Auffälligkeiten. Das wirft die Frage auf, ob sekundäre Entzündungsreaktionen nicht nur einen krankheitsverstärkenden Effekt in SPG11 haben, sondern als ein vereinender Faktor für andere genetisch determinierte Krankheiten des ZNS fungieren können. Dies könnte den Weg dahin ebnen das Fortschreiten anderer unheilbarer, primär genetisch bedingter, neurologischer Erkrankungen durch eine individuelle Behandlung mit auf dem Markt verfügbaren immunomodulatorischen Medikamenten zu verlangsamen.

3   Introduction

Genetically mediated disorders of the central nervous system (CNS) are usually orphan diseases with poor treatment options (Groh & Martini, 2017). Lack of knowledge of the basic pathomechanism is often cause of limited therapeutic options. The situation is even more complicated since many of the genetically mediated diseases are characterized by not only physical manifestations, like motor symptoms, but display additional psychological abnormalities. Interestingly, previous studies from our group identified secondary neuroinflammation as a robust amplifier of disease progression (Groh & Martini, 2017). These findings conceptionally influenced the present work with the aim to decipher the pathomechanism underlying clinical changes in a complicated form of hereditary spastic paraplegia (HSP), HSP type 11 (SPG11).

3.1   The role of inflammation in hereditary neurodegenerative disorders of the central and peripheral nervous system

Pathomechanistic research and clinical observations during the last decades delivered substantial evidence that some disorders of the peripheral nervous system (PNS) and CNS, like Guillain-Barré-syndrome (GBS), chronic inflammatory demyelinating polyneuropathy (CIDP) or multiple sclerosis (MS) are classical immune-mediated disorders (Ueda & Kusunoki, 2011). However, in the last decade it was shown that chronic, low-grade, secondary inflammation can act as a robust amplifier of disease progression in various other genetically mediated disorders of both the peripheral and central nervous system (e.g. Charcot-Marie Tooth neuropathy (CMT), amyotrophic lateral sclerosis (ALS), leukodystrophies, storage disorders, multiple system atrophy) that are not classically considered as being immune-mediated (Schmid *et al.*, 2000; Kobsar *et al.*, 2002; Kobsar *et al.*, 2003; Ip *et al.*, 2006; Kroner *et al.*, 2009; Hooten *et al.*, 2015; Groh *et al.*, 2016a; Groh & Martini, 2017). Despite the heterogenous nature of molecular changes and the distinct mutations that underlie them, all these diseases show secondary inflammation as a common disease modifier. For example, mouse models of two forms of severe lysosomal storage diseases, neuronal ceroid lipofuscinosis (CLN) type 1 and type 3, display disease-amplifying neuroinflammation (Groh *et al.*, 2016b; Groh *et al.*, 2017; 2021a) and treatment with the clinically approved immunomodulators fingolimod (Melzer & Meuth, 2014) or teriflunomide (Melzer & Meuth, 2014; Klotz *et al.*, 2019) substantially improve the disease outcome. Interestingly, also other mouse models of so far untreatable neurological diseases show secondary neuroinflammation and therapeutically respond to fingolimod or teriflunomide: Mice carrying mutations in the myelin-related proteolipid protein-

1 (*PLP1)* gene, initially identified in patients with progressive multiple sclerosis (PMS) (Warshawsky *et al.*, 2005) or relapsing-remitting MS (RRMS) (Gorman *et al.*, 2007), show disease-amplifying neuroinflammation and neuropathological features relevant for PMS and a subform of hereditary spastic paraplegia (HSP/SPG2) (Groh *et al.*, 2016a). Moreover, they also respond to treatment approaches with the aforementioned immunomodulators (Groh *et al.*, unpublished data; Groh *et al.*, 2018).

3.2 Hereditary spastic paraplegias (HSPs) and relevant structures of the nervous system

Hereditary spastic paraplegias are genetically-determined, neurodegenerative disorders, characterized by progressive weakness and spasticity of the lower limbs (Harding, 1983; Stevanin *et al.*, 2007). Unlike SPG2 which is primarily mediated by mutations in the myelin gene *PLP1*, the majority of HSPs are caused by mutations in genes involved in cell metabolism, leading to compromised shaping of the ER, abnormal lysosomal function, disturbed lipid metabolism, and other cellular dysfunctions. However, the exact pathomechanism resulting in neuropathology and clinical disease is often incompletely understood (Boutry *et al.*, 2019a; Gumeni *et al.*, 2021; Toupenet Marchesi *et al.*, 2021). HSPs constitute the second most common group of motor neuron diseases and affects between 3-10 per 100.000 births (Klebe *et al.*, 2015), with varying ages of onset (early childhood to 70 years) (Finsterer *et al.*, 2012). Most patients have a normal life span; therefore, only a limited number of post-mortem, neuropathological investigations of HSP patients have been published (Blackstone, 2012). Up to this day no cure for HSPs is available. Treatment options for HSP diseases are confined to mostly spasmolytic drugs, botulinum toxin and physiotherapy (Boutry *et al.*, 2019a; Gumeni *et al.*, 2021). HSPs are among the most clinically and genetically heterogeneous diseases of the human CNS with over 70 distinct genetic loci and about 60 mutated genes (Stevanin *et al.*, 2008b; Klebe *et al.*, 2015; Tesson *et al.*, 2015). However, they prefigure only a small number of common themes at a cellular level, within a limited number of predicted processes, e.g., myelination, endoplasmic reticulum network morphology, lipid synthesis and metabolism, or endosomal dynamics, among others (Soderblom & Blackstone, 2006; Depienne *et al.*, 2007; Salinas *et al.*, 2008; Blackstone *et al.*, 2011). The respective mutations can be inherited in autosomal dominant or autosomal recessive mode, in X-linked manner or by maternal transmission, with autosomal dominant HSPs constituting the most common form (Finsterer *et al.*, 2012; Klebe *et al.*, 2015). Classifications of HSPs into different types are based on the mutated gene, kind of inheritance as well as phenotype and divide between pure and complex forms of HSP (Harding, 1983). Patients with pure HSPs show the leading clinical

characteristics, consisting of mainly isolated pyramidal signs, including spasticity and motor deficits. These symptoms of HSPs are mainly caused by progressive axonal degeneration of the ascending (spinocerebellar) and descending (corticospinal) tracts of the spinal cord, beginning at the distal ends, and degeneration of upper motor neurons (UPNs), which are located in the motor cortex (Blackstone *et al.*, 2011; Parodi *et al.*, 2017). The motor cortex is localized within one of the four major lobes of the cerebral cortex, the frontal lobe. It is known to be affected in individuals with various forms of HSP (Pelosi *et al.*, 1991; Geevasinga *et al.*, 2015; Lin *et al.*, 2020). From the cerebral cortex, the spinocerebellar and the corticospinal tracts conduct to the spinal cord and allow the control of motor functions. The corticospinal tract origins in UPNs, also called Betz cells, of layer V of the primary motor cortex, which are essential for voluntary movement (Blackstone *et al.*, 2011; Parodi *et al.*, 2017). Most axons decussate in the caudal medulla, and form the lateral corticospinal tract, connecting with interneurons, which in turn connect to lower motor neurons (LMNs). The anterior corticospinal tract consist of the uncrossed axons, directly forming synapses to LMNs which control the contraction of skeletal muscles (Blackstone, 2018). The cerebellum and the basal ganglia, two subcortical regions, constantly modulate the motor cortex (Kandel *et al.*, 2000). Additionally, the somatosensory cortex, which is found in the parietal lobe, another of the four major lobes of the cerebral cortex, provides sensory inputs from the periphery to the motor cortex (Zagha *et al.*, 2013).

In addition to the pure forms, some forms of HSPs show superimposed clinical and neurological features of high variance, like optic atrophy, mental decline and cerebellar ataxia (Salinas *et al.*, 2008; Klebe *et al.*, 2015; Boutry *et al.*, 2019a). These forms are referred to as complex HSPs. Advances in molecular diagnosis have revealed genetic and clinical overlaps between HSPs and other neurodegenerative diseases, which include, but are not limited to, ALS (Orlacchio *et al.*, 2010), CMT (Timmerman *et al.*, 2013; Montecchiani *et al.*, 2016), and MS (Rubegni *et al.*, 2017). Many of these diseases show progressive low-grade secondary inflammation (Kobsar *et al.*, 2003; Hooten *et al.*, 2015; Groh *et al.*, 2016a) making it plausible that inflammation could also be a secondary disease amplifier in HSPs. In this work, we focus on a model of such a complex HSP, SPG11, caused by mutations in the lysosome-related spatacsin gene.

3.3 Hereditary spastic paraplegia type 11

Hereditary spastic paraplegia type 11 (SPG11) is an autosomal recessive form of HSP, and is caused by a mutation in the KIAA1840/SPG11 gene on chromosome 15 (Blackstone, 2018). SPG11 has its onset during the first decade of life. The protein product of *SPG11*, spatacsin, is highly expressed in neurons forming the corticospinal tract in humans, but expression can also

be detected in neurons of the hippocampus, cerebellum, and corpus callosum (Murmu *et al.*, 2011). Most mutations identified in SPG11 patients are frameshift or nonsense mutations, predicted to lead to a loss of function of the protein (Stevanin *et al.*, 2008b; Orlacchio *et al.*, 2010; Montecchiani *et al.*, 2016). Spatacsin associates with the adaptor protein complex 5 (AP-5) and Spastizin/zFYVE26, both causative of HSP, SPG48 or SPG15 respectively, when mutated (Hanein *et al.*, 2008; Slabicki *et al.*, 2010). Patients with SPG11 and SPG15 show similar symptoms, which is in line with the idea that similar cellular mechanisms are involved in these two disease forms (Hanein *et al.*, 2008). A variety of pathogenic mechanisms have been suggested to be causative of SPG11 and SPG15, e.g., endolysosomal dysfunction, impaired autophagy, lysosomal reformation or membrane trafficking (Slabicki *et al.*, 2010; Hirst *et al.*, 2011; Hirst *et al.*, 2013; Khundadze *et al.*, 2013; Chang *et al.*, 2014; Renvoise *et al.*, 2014). It has also been shown, that AP-5 coprecipitates not only with spastizin and spatacsin but also with the lysosomal-associated membrane protein 1 (LAMP1) (Slabicki *et al.*, 2010; Hirst *et al.*, 2011; Hirst *et al.*, 2013). However, mutations in SPG11 show a pleiomorphic nature and can also account for other disease conditions, e.g., autosomal-recessive CMT (Montecchiani *et al.*, 2016), as well as slowly progressive juvenile-onset autosomal recessive ALS (Daoud *et al.*, 2012). It was observed that a mutation in SPG11 can cause two different diseases within one family (Orlacchio *et al.*, 2010; Daoud *et al.*, 2012), making an exact determination of the underlying pathomechanism difficult. Recent studies introduced the idea that SPG11 is divided in a neurodevelopmental and neurodegenerative component (Pozner *et al.*, 2020). Dysfunction of the autophagy-lysosomal machinery has been proposed to mediate the pathogenic effects of SPG11 in neurodevelopment and neurodegeneration, causing developmental defects and over time resulting in neurodegeneration (Pozner *et al.*, 2020).

As typical for complicated forms patients show not only spastic gait disorders, but also additional symptoms including cognitive impairment, mental retardation, peripheral neuropathy, cerebellar ataxia, retinal degeneration, as well as neuropsychological abnormalities including anxiety, depression and learning difficulties, among others (Stevanin *et al.*, 2008a; Anheim *et al.*, 2009; Puech *et al.*, 2011; Faber *et al.*, 2018a). Thin corpus callosum (TCC) is one of the lead features of this HSP subform (Stevanin *et al.*, 2007). The corpus callosum, a large bundle of axons, connects the two cerebral hemispheres (De Leon Reyes *et al.*, 2020). It facilitates not only bilateral sensory integration but also higher-order functions of the cerebral cortex, like coordination of sensory-motor responses, associative and executive tasks, and management of social and emotional stimuli (Brown *et al.*, 1999; Paul *et al.*, 2003). Additionally, patients often present with frontal lobe syndrome (Faber *et al.*, 2018a). The frontal

lobe is a structure that is implicated in a variety of processes, e.g. motivation, planning, social behavior, and speech production (Pirau & Lui, 2021) and has an important inhibitory role in emotion and fight / flight response through interconnections with paralimbic structures (Pirau & Lui, 2021). More recently, an ongoing study by Klebe *et al.* (unpublished data; University hospital Essen; University hospital Wuerzburg) provides evidence that neuropsychological abnormalities occur early in the disease, pointing towards them being the first disease symptoms, even before worsened motor performance. Therefore, neuropsychological abnormalities should be considered as an additional area of interest for research.

3.4   Mouse models for SPG11

To better understand the pathophysiological mechanisms underlying SPG11, two mouse models have been generated (Varga *et al.*, 2015; Branchu *et al.*, 2017). Both mouse models show a disruption in the *Spg11* gene and consequently display symptoms mimicking SPG11 (Varga *et al.*, 2015; Branchu *et al.*, 2017). Vargas *et al.* generated the SPG11 mouse model by inserting a gene trap cassette into intron 1 of *Spg11*, leading to encoding of a premature cytoplasmic fusion protein and a subsequent loss of full-length spatacsin (Varga *et al.*, 2015). In contrast, the SPG11 mouse model of Branchu *et al.* was generated by inserting two stop codons in Exon 32 of the *Spg11* gene, the most common mutation found in humans, predicted to lead to a loss of spatacsin (Branchu *et al.*, 2017). We focus on the SPG11 mouse model that was generated and previously described by Branchu *et al.*, here named *Spg11$^{-/-}$* mouse. *Spg11$^{-/-}$* mice do not only show progressive impairment of gait and motor function beginning early in life but also progressive neurodegeneration of the motor cortex and cerebellum, accompanied by dystrophic axons in the corticospinal tract, thus recapitulating the human disease (Branchu *et al.*, 2017). Furthermore, this mouse model shows a loss of large caliber neurons in the gray matter of the lumbar spinal cord and a high proportion of fragmented neuromuscular junctions, suggesting relevant histopathological changes are not limited to the CNS but are also present in the PNS (Branchu *et al.*, 2017). On a cellular level, loss of spatacsin leads to an accumulation of lipid material in lysosomes, an observation that was similarly made in brains of humans with SPG11 (Denora *et al.*, 2016). This accumulation occurs early in the development of the disease and is likely due to the loss of lipid clearance in lysosomes, which is normally promoted by spatacsin. More recent work using embryonic fibroblasts from *Spg11$^{-/-}$* mice could show that the clearance of cholesterol from lysosomes is disturbed, since loss of spatacsin leads to an inhibition of the formation of tubules on lysosomes (Boutry *et al.*, 2019b). This in turn decreases cholesterol levels in the plasma membrane and increases resting

cytosolic calcium levels by enhancing the influx of calcium by store-operated calcium entry (Boutry *et al.*, 2019b). These findings suggest that loss of spatacsin leads to an altered lipid metabolism in lysosomes, linking lysosomal dysfunction to lipid metabolism (Branchu *et al.*, 2017), two mechanisms for which proteins are recurrently encoded by the wide variety of genes associated with HSP. Of note, other investigations in a different mouse model of SPG11 found accumulation of intracellular autofluorescent material preceding neuronal loss, suggesting impaired autolysosomal clearance (Varga *et al.*, 2015). This is reminiscent of lysosomal storage disorders, like NCL (Seehafer & Pearce, 2006; Groh *et al.*, 2013). None of the previous studies have investigated if secondary neuroinflammation influences histopathological and clinical (gait and behavioral) changes in these mouse models for SPG11. This is of interest in the here presented study.

3.5 Immunomodulatory treatment of hereditary neurodegenerative disorders of the central nervous system and relevance for SPG11

More evidence points towards secondary inflammation as a common disease modifier in orphan diseases (Groh & Martini, 2017). In a mouse model overexpressing the *Plp1* gene *(Plp*^{tg} mice*)*, a model of the HSP subform SPG2, activation of microglia and elevated numbers of T-lymphocytes in the CNS are pathologically relevant (Ip *et al.*, 2006; Ip *et al.*, 2007). Crossbreeding experiments in this mouse model with mice devoid of mature T- and B-lymphocytes (*Rag1*$^{-/-}$ mice), and therefore lacking an adaptive immune response, ameliorated the histopathological phenotype, demonstrating a strong impact of the adaptive immune system in the pathogenesis of this disease (Ip *et al.*, 2006). By performing reconstitution experiments in *Plp*^{tg}*Rag1*$^{-/-}$ mice, CD8$^+$ effector T-lymphocytes were identified as an important pathomechanistic player (Ip *et al.*, 2006). Notably, this crossbreeding approach led to more preserved corpora callosa (Ip *et al.*, 2006), a structure also implicated in SPG11 (Klebe *et al.*, 2015), suggesting that inflammation might also be implicated in other complicated HSPs with TCC, like SPG11. However, despite these intriguing links between inflammation and histopathological alterations in neurodegenerative diseases, corresponding clinical approaches appear to be rare (Marteyn & Baron-Van Evercooren, 2016).

Investigations of our group have focused on using the clinically approved immunomodulators fingolimod (FTY720) and teriflunomide as a treatment approach for genetically-determined, neurodegenerative disorders. Fingolimod is a modulator of the sphingosine-1-phosphate (S1P) receptor and impairs emigration of lymphocytes from secondary lymphatic organs, and therefore the infiltration into the brain (Brinkmann *et al.*, 2010; Chun & Brinkmann, 2011;

Melzer & Meuth, 2014). Teriflunomide inhibits the dihydroorotate dehydrogenase (DOHDH) and therefore the de novo synthesis of pyrimidine nucleotides, leading to reduced proliferation and function of activated T- and B-lymphocytes while the resting population remains unaffected (Bar-Or *et al.*, 2014; Melzer & Meuth, 2014). Previous work could provide robust evidence that targeting neuroinflammation in mouse models of NCL (Groh *et al.*, 2017; 2021a), and of PMS and SPG2 (Groh *et al.*, 2018) ameliorates the histopathological and clinical outcome of the diseases. The commonalities in neuroinflammation and pathomechanistic processes in distinct neuronal diseases might explain the occasionally observed transitions between disorders (Groh & Martini, 2017); e.g., HSPs, such as SPG2 or SPG11 display similarities with MS. Thus, it is plausible to assume that inflammation can be viewed as a unifying factor in distinct CNS diseases, posing the question of whether and how inflammation impacts disease progression in SPG11.

Even though it has been shown that neuroinflammation impacts neural damage-related symptoms, little research has investigated the effect of secondary neuroinflammation in HSPs on histopathological and clinical alterations. Finding evidence for an involvement of secondary inflammation as a disease amplifier could extend the treatment options to targeting these disease-amplifying immune cells for this, so far, only poorly treatable disorder.

3.6 Aim of the study

The aim of this study was to analyze the pathogenic impact of immune cells in a mouse model for hereditary spastic paraplegia type 11 (*Spg11$^{-/-}$* mice) by addressing the following sub aims:

1) Analyze different structures of the CNS implicated in SPG11 in an age-dependent manner for characterization of pathological alterations and inflammation in *Spg11$^{-/-}$* mice.

2) Determine whether *Spg11$^{-/-}$* mice show clinical (gait and behavioral) abnormalities that reflect the human SPG11 disease.

3) Investigate the functional impact of immune reactions by crossbreeding *Spg11$^{-/-}$* mice with mice devoid of mature T- and B-lymphocytes (*Rag1*-deficient mice) and analyze the effect on histopathological and clinical alterations in the resulting double mutants.

4) Investigate the potential therapeutic properties of targeting the immune system with clinically approved immunomodulators fingolimod (FTY720) or teriflunomide in an early and (more clinically relevant) late treatment approach and analyze the effect on histopathological and clinical alterations in treated *Spg11$^{-/-}$* mice

5) Investigate whether *Rag1*-deficiency influences histopathological and clinical properties of wild-type mice.

6) Investigate whether long-term treatment with fingolimod (FTY720) or teriflunomide influences histopathological and clinical properties of wild-type mice.

4   Material and methods

4.1   Equipment, buffers and solutions, antibodies and primer sequences

Technical equipment (Appendix 8.1), software (Appendix 8.2), reagents (Appendix 8.3), buffers and solutions (Appendix 8.4), primer sequences for genotyping (Appendix 8.5) and antibodies for immunohistochemical stainings and flow cytometry (Appendix 8.6) are listed in detail in the appendices.

4.2   Animals

All mice were on a *C57BL/6J* genetic background. Animals were kept in individually ventilated cages under barrier conditions at the Center of Experimental Molecular Medicine, University of Würzburg with a 14h/10h day/night rhythm (<300 lux during day). Colonies were maintained at 20–24 °C and 40–60% humidity, with free access to food and water. All animal experiments were approved by the local authority of the Government of Lower Franconia, Germany (AZ 2-214 & AZ 2-1347).

Spg11$^{-/-}$ mice were used as an SPG11 disease model, and age-matched wild-type (wt, *Spg11$^{+/+}$*) littermates were used as control animals (Branchu *et al.*, 2017). *B6J* refers to *C57BL/6J* mice bought from Charles River Laboratories. Mice of either sex were analyzed for histopathological readout parameters, as we did not detect sex-related differences in *Spg11$^{+/+}$*, *Spg11$^{-/-}$* or *B6J* mice. Genotypes were determined by conventional PCR using isolated DNA from ear punch biopsies as previously described (Branchu *et al.*, 2017). In experiments aimed to genetically inactivate the adaptive immune reactions, *Spg11$^{-/-}$* mice were crossbred with *Rag1*-deficient (*Rag1$^{-/-}$*) mice (Mombaerts *et al.*, 1992), devoid of mature T- and B-lymphocytes, lacking an adaptive immune response according to previously published protocols (Ip *et al.*, 2006; Groh *et al.*, 2013). *Rag1$^{-/-}$* mice did not display any abnormalities in longevity, behavior, and body weight under the standardized conditions applied (specific pathogen-free).

4.3   Immunomodulatory treatment

Fingolimod (FTY720; Sigma-Aldrich; SML0700) was dissolved in autoclaved water at 3 µg per milliliter and provided *ad libitum*, corresponding to a dose of 0.5 mg/kg body weight in a mouse with an average body weight of 30 g and an approximate water consumption of 5 ml per day. Teriflunomide (Biorbyt, orb146201) was dissolved in autoclaved drinking water containing 0.6% Tween 80 at 60 µg per milliliter and provided *ad libitum*, corresponding to a dose of 10 mg/kg body weight per day. These concentrations are based on previous animal

experiments of our group (Groh *et al.*, 2017) and other laboratories (Metzler *et al.*, 2008; Merrill *et al.*, 2009), implicating dose conversion scaling (Nair & Jacob, 2016). *Spg11$^{-/-}$* mice receiving water containing only 0.6% Tween 80 did not show any abnormalities in inflammation, longevity, behavior, or body weight (data not shown). Autoclaved drinking water without the compounds was provided to non-treated controls. The water with or without compounds was changed weekly. Mice were treated for 450 days (early treatment), starting at 3 months of age, or 90 days (late treatment), starting at 15 months of age and monitored daily regarding defined burden criteria and phenotypic abnormalities. No obvious side effects were detectable during treatment.

4.4   Spectral domain optical coherence tomography

Optical coherence tomography (OCT) was performed using a commercially available device (Spectralis OCT; Heidelberg Engineering, Heidelberg, Germany) with additional lenses, reaching a digital resolution of 3.9 µm and a measurable thickness change of 1 µm (Wolf-Schnurrbusch *et al.*, 2009), as previously described (Groh *et al.*, 2014; Groh *et al.*, 2021b; Hörner *et al.*, 2022). Thickness of the innermost retinal composite layer, comprising of the nerve fiber layer (NFL), ganglion cell layer (GCL) and inner plexiform layer (IPL) was assessed at different ages for longitudinal analysis in high-resolution peripapillary circle scans (at least 10 measurements per scan) by an investigator unaware of the genotype and potential treatment. Mice were anesthetized with an intraperitoneal injection of Ketavet (Pfizer) and Xylavet (CP-Pharma) (100 mg Ketavet and 6.7 mg Xylavet per kilogram body weight). Thickness of the retina was determined in the same mice at different ages for longitudinal analysis.

4.5   Behavioral evaluation

At least 3 – 11 animals per genotype and age were tested. All behavioral procedures were performed between 7 am and 2 pm. By randomly selecting mice for testing, regardless of their genotype and possible treatment, bias was minimized. For catwalk analysis, mice were tested at the ages of 6, 12, 15, and/or 18 months of age. For behavioral evaluation, mice were tested at 6, 12 and 18 months of age.

4.5.1   Catwalk analysis

For gait analysis, the CatWalkXT (10.6) by Noldus was used. Briefly, mice voluntarily crossed an approximately 45 cm long walkway with a glass floor, in a darkened room, while being filmed by a CCD camera using infrared light from above the walkway, enabling collection of paw prints (Hörner *et al.*, 2022). Run criteria were defined (minimum run duration: 1 second;

maximum run duration: 25 seconds; minimum number of compliant runs to acquire: 3; maximum allowed speed variation: 40%). Automated values of the CatWalk analysis of selected parameters (find details for selection in the results) of at least three runs per mouse were extracted and manual measurements (print length, print width) were performed by an investigator unaware of the genotype and the potential treatment of mice.

4.5.2 Behavioral analysis

A behavioral test battery was designed to longitudinally investigate mice (Figure 1). The test battery consisted of the cliff avoidance reaction (CAR) analysis for investigation of impulsivity-like behavior, the dark/light box (DLB) analysis for investigation of anxiety-like behavior, the open field (OF) analysis for investigation of exploratory and hyperactivity-like behavior, the novel object recognition (NOR) analysis for investigation of short-term, non-spatial learning and recognition, and the social interaction and novelty (SI) analysis for investigation of social interest and novelty behavior. The tests were performed in the previously described order, depending on the level of stress-induction: starting with less stress-inducing towards more stress-inducing tests. All tests were recorded using a camera and evaluated using the EthoVisionXT (Noldus Information Technology) video tracking software v.116. All tests were performed in a room with only the investigator present. Mice were placed in the testing room to habituate 30 minutes prior to each test. Between each trial, arenas, objects and/or cages, were cleaned using 10% ethanol and the arena was aired out for approximately 3 minutes to minimize behavioral disturbance by olfaction. No more than two tests per week were performed to minimize stress bias. The investigator was unaware of genotypes and possible treatment of the mice during testing.
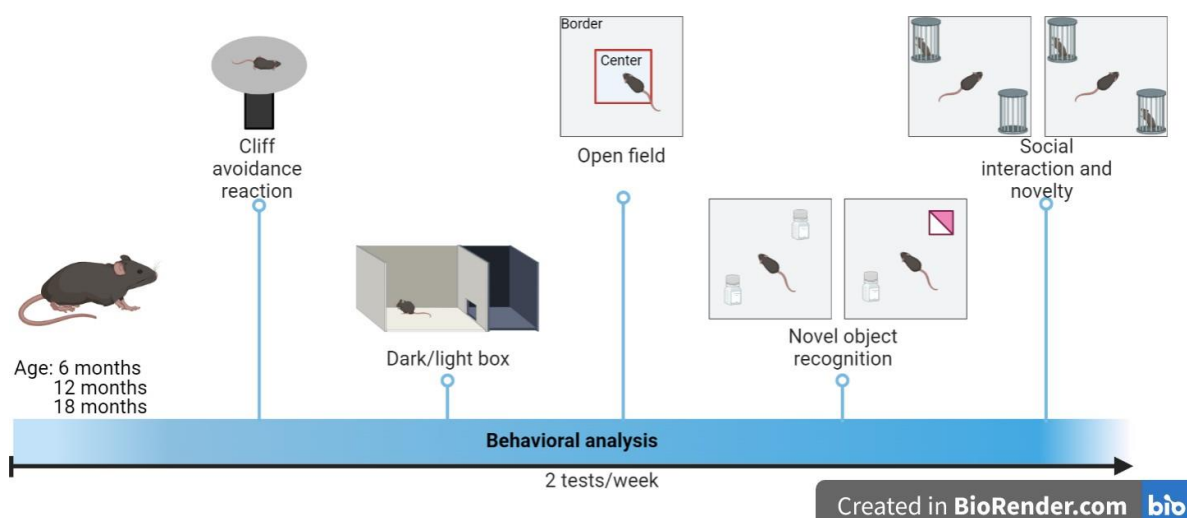
Figure 1: Behavioral test battery for mice.
Mice were subjected to a behavioral test battery in the following order: cliff avoidance reaction (CAR) analysis, dark/light box (DLB) analysis, open field (OF) analysis, novel object recognition (NOR)

analysis and social interaction and novelty (SI) analysis at the age of 6, 12 and 18 months. The order is structured from less stress-inducing to more stress-inducing tests. Each week a maximum of two tests was performed. Scheme by Hörner *et al.*, unpublished (generated with BioRender).

4.5.2.1 Cliff avoidance reaction (CAR) analysis

To assess impulsivity-like behavior, the CAR analysis was used. CAR was evaluated by using a round, non-transparent, plastic platform (diameter: 25 cm; thickness: 2 cm), supported by a plastic rod (height: 15.5 cm). The platform was divided into a center zone (diameter: 20 cm) and a border zone (width: 2.5 cm). To initiate the test, one mouse was gently placed in the center of the platform and the behavior was recorded. The investigator recorded the latency to jump off the platform, the number of jumps, and the time the mouse spent leaning over the edge of the platform. The definition of "leaning over the edge of the platform" is depicted in Figure 2. A behavior was considered "leaning over the edge of the platform" when the eyes of the mouse crossed the horizontal axis of the platform rim (Figure 2c, d).
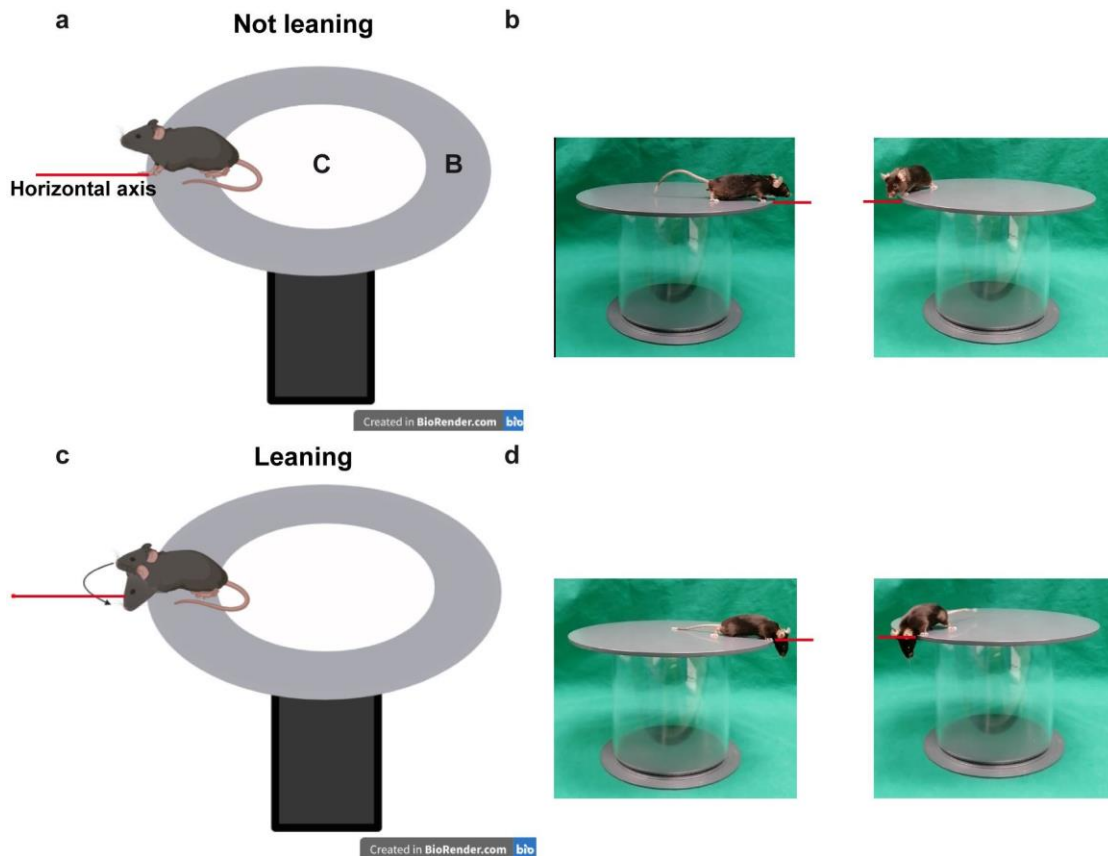
Figure 2: Definition of leaning over the edge of the CAR platform.
(a) Not leaning: A horizontal axis (red line) defines if a mouse is leaning (C= center zone, white; B= border zone, grey). If the eyes of the mouse do not cross the horizontal axis of the platform rim the mouse is not considered leaning. **(b)** Representative images of mice not leaning over the edge of the CAR platform. Note that the eyes do not cross the horizontal axis of the platform rim. **(c)** Leaning: If the eyes of the mouse cross the horizontal axis of the platform rim the movement is considered leaning. **(d)** Representative images of mice leaning over the edge of the CAR platform. Note that the eyes cross the horizontal axis of the platform rim. Scheme by Hörner *et al.*, unpublished (generated with BioRender).

The CAR was considered abnormal when the mouse voluntarily jumped off the platform. After 10 minutes the mouse was taken off the platform, disregarding if it had jumped off or not. The CAR was calculated as % intact CAR for each group: [number of mice that did not jump off the platform/ total number of mice] x 100. After each jump, the mice were immediately returned to the center of the platform. The walking distance was recorded by the EthoVisionXT software.

4.5.2.2 Dark/light box (DLB) analysis

To evaluate anxiety-like behavior in mice, DLB analysis was used. The DLB consists of a dark compartment (10cm x 20cm), and a light compartment (40cm x 40 cm; < 300 lx), connected by a small doorway. To begin the experiment, one mouse was placed in a random corner of the dark compartment of the box, facing the wall and away from the doorway. Corners were randomly alternated between mice to minimize bias. The mouse was allowed to explore freely and recorded in the light, but not dark compartment. After 10 minutes, the mouse was taken out of the arena, disregarding if it had entered the light compartment or not. The investigator measured the latency of the mouse to enter the light compartment with the whole body and the time spent in the light compartment. The walking distance in the light compartment was recorded by the EthoVisionXT software.

4.5.2.3 Open field (OF) analysis

To evaluate the general exploratory and hyperactivity-like behavior of mice, the OF analysis was used. A white, non-transparent, wooden box (29.5 cm x 29.5 cm) was divided into a center (diameter: 10 cm) and a border zone (diameter: 19.5 cm). To begin the experiment, one mouse was gently placed in a corner of the arena, facing the wall. The corners were randomly selected and alternated between different mice. One trial lasted a total of 10 minutes. Total walking distance and time spent in center/border zone was assessed by the EthoVisionXT software. The time the mouse stood on its hindlimbs, either assisted with one or both front paws by a wall or unassisted, was considered rearing and recorded by the investigator.

4.5.2.4 Novel object recognition (NOR) analysis

For assessment of the short-term, non-spatial learning and recognition, the NOR analysis was used as previously described (Groh *et al.*, 2016a; Groh *et al.*, 2021b). The test was performed in an OF box (29.5 cm x 29.5 cm), which was divided into quadrants of the same size. For the training trial, two identical objects were placed in opposite quadrants of the arena. The quadrants were randomly alternated between the tests to minimize bias. To start the experiment, one mouse was gently placed in a corner of a quadrant not containing an object, facing the wall. The corners were randomly selected and alternated between mice. After the training trial, the

mouse was taken out of the arena and placed back in its home cage for 60 minutes. For the test trial, one of the objects was replaced by an unfamiliar object that was of similar dimensions and colors but yielded enough discrimination properties and did not show spontaneous preference in prior testing (data not shown). The mouse was placed back into a corner of the arena in a quadrant not containing an object, facing the wall. During both trials, the mouse was allowed to explore freely for 10 minutes while being recorded. The total walking distance was recorded by the EthoVisionXT software. In both trials, the time spent actively interacting with each object (sniffing, touching) was recorded by the investigator. The object preference was calculated for training and test trial: [time spent with object 1/time spent with object 2] x 100. In the test trial object 1 refers to the unfamiliar object.

4.5.2.5 Social interaction and novelty (SI) analysis

For assessment of social interaction and novelty behavior, the SI analysis was used. Two small, identical cages were placed in an OF box (29.5 cm x 29.5 cm) in opposite corners of the arena. The corners containing the cages were chosen randomly and alternated between different tests to minimize bias. In the social interest trial (trial 1), one of the cages contained a gender-matched mouse that was unfamiliar to the test mouse. The cage containing the mouse was chosen randomly and alternated between tests to minimize bias. The test mouse was gently placed in one of the corners of the arena, not containing a cage, facing the wall. The corners were alternated randomly between mice. The social novelty trial (trial 2) was carried out directly following the social interest trial (trial 1). A second, unknown, gender-matched mouse was placed in the empty cage of the arena. To start the social novelty trial (trial 2), the test mouse was gently placed in a corner, not containing a cage, facing the wall. The test mouse was allowed to explore freely for 10 minutes. The time spent with the mice or the empty cage (direct interaction; sniffing or touching) was recorded by the investigator. The object preference was calculated for both trials. Social interest preference (trial 1): [time spent with animal 1/time spent with empty cage] x 100. Social novelty preference (trial 2): [time spent with animal 2/time spent with animal1] x 100. Animal 1 being the first unfamiliar animal, and animal 2 being the second unfamiliar animal. When the unfamiliar mice were taken out of the cages, the cages were cleaned using 10% ethanol and given time to air out for approximately 3 minutes. The mice used as unfamiliar mice were placed in the cages for 5 minutes each day starting three days prior to testing day for habituation.

4.6 Analysis of visual acuity

The visual acuity of mice was analyzed using a commercially available OptoDrum device (Striatech), using automated optokinetic reflex tracking as previously described (Groh *et al.*, 2021b). In summary, mice were placed on an elevated platform (diameter: 5 cm) that was surrounded by monitors and presented with a rotating stripe pattern with maximum contrast and a constant rotation speed (12 deg s^{-1}). The OptoDrum software v.1.2.6. automatically detected and analyzed the head movements following the rotating stripes in an unbiased manner. To find the threshold of the animals' visual acuity, the stimulus pattern (cycles) was repeatedly adjusted.

4.7 Dissection and processing of nervous tissue

Mice were euthanized using CO_2 (according to guidelines by the State Office of Health and Social Affairs Berlin). Mice were transcardially perfused with phosphate-buffered saline (PBS) containing heparin followed by 2% paraformaldehyde in PBS. Subsequently, tissue was harvested, post-fixed, dehydrated in 30% sucrose, and processed as previously described (Groh *et al.*, 2016a). Optic nerve, brain and spinal cord were embedded in TissueTek$^®$ O.C.T.™ compound. Before embedding the brain, the olfactory bulb was removed, and the cerebrum and cerebellum were separated at defined positions.

4.8 Histochemistry and immunofluorescence

Immunohistochemistry was performed on 10 µm thick longitudinal optic nerve cryo-sections, 40 µm thick coronal brain cryo-sections (Bregma 0.90 to 0.60 mm), 40 µm thick coronal cerebellum cryo-sections (Bregma -6.00 to -6.30 mm) or 10 µm thick coronal lumbar spinal cord cryo-sections (L1 to L5). Sections were post-fixed in ice-cold acetone or 4% PFA/PBS for 10 minutes and blocked using 5% bovine serum albumin (BSA) in PBS. Sections were incubated over night at 4°C with one or a combination of up to two of the following primary antibodies: rat anti-CD4 (1:1000, Bio-Rad AbD Serotec, MCA1767), rat anti-CD8 (1:500, Bio-Rad AbD, Serotec MCA609G), rat anti-CD11b (1:100, Bio-Rad AbD Serotec MCA74G), rat anti-CD169 (binding to sialoadhesin, Sn, 1:300, Bio-Rad ABD Serotec MCA947G), rabbit anti-TMEM119 (1:500, abcam ab209064) and mouse anti-SMI32 (1:1000, BioLegend 801701). Primary antibody binding was visualized using respective fluorescently labeled secondary antibodies (1:300, Dianova) or the streptavidin-biotin-peroxidase complex (Vector Laboratories) using diaminobenzidine-HCl and H_2O_2. Nuclei were stained using DAPI (4´,6-diamidino-2-phenylindole) (Sigma-Aldrich). Light and fluorescence images were acquired

using an Axiophot 2 microscope (Zeiss) equipped with a CCD camera (Visitron Systems) or an Axio Imager M2 microscope (Zeiss) with ApoTome.2 structured illumination equipment, attached Axiocam cameras and corresponding software (ZEN v.2.3 blue edition). Images were minimally processed (rotation, cropping, and addition of symbols) using Photoshop CS6 (Adobe). For quantification of immunoreactive cells, the cells were counted in at least three non-adjacent longitudinal cryo-sections of the optic nerve, in at least three coronal cerebrum or cerebellum cryo-sections, or in at least five coronal spinal cord cryo-sections for each animal and related to the area of the section using the cell counter plugin in ImageJ (National Institutes of Health, Bethesda USA). For quantification of Brn3a/RBPMS$^+$ retinal ganglion cells, free floating retina preparations were fixed and frozen in PBS containing 2% Triton X-100, thawed, washed, and blocked for 1 hour in a blocking solution containing 5% BSA, 5% Donkey Serum and 2% Triton-X in PBS. The sections were incubated overnight at 4°C on a slow shaker with the following primary antibodies: guinea pig anti-RBPMS (1:300, Merck ABN1376) and goat anti-Brn3a (1:100, Santa Cruz, sc-31984). The next day, sections were rinsed (PBS/2% TritonX-100) and washed three times on a slow shaker. Primary antibody binding was visualized using respective fluorescently labeled secondary antibodies (1:500, Dianova). Retinae were flat-mounted, and the number of RBPMS$^+$ retinal ganglion cells was assessed, in at least three images of the middle retinal region per flat mount, by an investigator unaware of the genotype and potential treatment of the mice. While antibodies against RBPMS stain the cell body of RGC, antibodies against Brn3a stain the cell nuclei of the large majority of RGC. This enables a more refined analysis and easier distinction of individual RGC in close vicinity. Almost all RBPMS$^+$ RGCs were also positive for Brn3a, as previously shown (Groh *et al.*, 2021b).

4.9   Flow cytometry

Flow cytometry was performed under the supervision of PD. Dr. Janos Groh. Blood was removed by transcardial perfusion with PBS containing heparin. Whole brains including leptomeninges and choroid plexus were dissected, collected in ice-cold PBS, and cut into small pieces. Tissue was digested in 1 ml of Accutase (Merck Millipore) per brain at 37 °C for 30 min and triturated through 70-μm cell strainers, which were rinsed with 10% FCS in PBS. Cells were purified by a linear 40% Percoll (GE Healthcare) centrifugation step at 650 g without brakes for 25 min and the myelin top layer and supernatant were discarded. Mononuclear cells were resuspended in fluorescence-activated cell sorting buffer (1% BSA and 0.1% sodium azide in PBS) and isolated cells were counted for each brain. Viable cells were identified by

LIVE/DEAD stain (Thermo Fisher Scientific L34965), Fc receptors were blocked for 15 min with rat anti-CD16/32 (1:200, catalog no. 553141; BD Biosciences) and cells were washed and labeled with the following antibodies for 30 min at 4 °C: rat anti-CD45 APC (1:100, BioLegend 103111), rat anti-CD8a PerCP/Cyanine5.5 (1:100, BioLegend 100733), rat anti-CXCR6 PE/Cyanine7 (1:100, BioLegend 151118), rat anti-CXCR4 PE (1:100, BioLegend 146505), armenian hamster anti-CD103 BV605 (1:100, BioLegend 121433), rat anti-Ly-6A/E FITC (1:100, BioLegend 108105). Cells were washed twice; single viable cells were gated, and CD45^{high}CD8$^+$ cells were analyzed using an FACSLyric (BD Biosciences) and Flowjo (version 10). Calculation of the total number of CD8$^+$ T cells per brain was performed by extrapolating their frequencies to the counted total number of isolated cells.

4.10 Experimental design and statistical analysis

Quantifications and clinical analyses were performed by investigators unaware of the genotype and potential treatments of mice, by assigning uniquely coded labels to animals. Mice were randomly placed into experimental and control groups according to genotyping results and by using a random generator (https://www.randomizer.org/, accessed 2021/08/29). For biometrical sample size estimation, the G*Power program (version 3.1.3) was used (Faul *et al.*, 2007). Calculation of the appropriate sample size groups was performed in *a priori* power analysis by comparing the mean of three to four groups with a defined adequate power of 0.8 (1-beta-error) and an *α*-error of 0.05. To determine the prespecified effect size *d*, previously published data were considered comparable reference values (Groh *et al.*, 2017; 2021a). Statistical analysis was performed using Prism 8 (GraphPad). The Shapiro-Wilk test was used to assess data sets for normal distribution and the *F* test was used to check for variance homology. If more than two groups or multiple timepoints (OCT, CatWalk, behavioral assessment) were compared, differences were evaluated by one-way ANOVA, followed by Tukey's post-hoc test. For body weight analysis two-way ANOVA with multiple comparisons was used. Student's t-test was used to compare two groups. Significance levels are indicated by asterisks (*), hashtags (#), or circles (°) and considered significant according to the following scheme: */#/°p<0.05; **/##/°°p<0.01; ***/###/°°°p<0.001. Measurements and quantifications are shown as individual values (circles, squares, triangles = mean value of one mouse) and mean ± standard deviation (SD). Graphs were generated with Prism 8.

5   Results

5.1   *Spg11^{-/-}* mice display substantial neuroinflammation in the CNS

We here evaluate whether a mouse model of SPG11 shows disease-amplifying neuroinflammation and investigate whether genetic depletion of the adaptive immune response or treatment with established immunomodulatory drugs, targeting the adaptive immune cells, leads to an improved disease outcome.

At first, we investigated whether there are indeed elevated numbers of adaptive immune cells detectable in the CNS of *Spg11^{-/-}* mice and quantified CD8$^+$ and CD4$^+$ T-lymphocytes in the visual system (optic nerve, ON), a valuable surrogate tissue for genetically mediated diseases of the CNS (Kroner *et al.*, 2009; Ip *et al.*, 2012; Groh *et al.*, 2016a; Ip *et al.*, 2016; Groh *et al.*, 2017; 2021a) (Figure 3a, b). The corpus callosum (CC) was chosen since it is often affected in complicated HSPs, like SPG11 (Stevanin *et al.*, 2008a; Klebe *et al.*, 2015) (Figure 3c, d). Additionally, we investigated the cerebral cortex (CO), including the motor cortex, and the folium of the cerebellum (CB), structures relevant for impaired motor performance in HSPs (Blackstone *et al.*, 2011; Lin *et al.*, 2020) (Figure 3e– h). Moreover, spinal cord cross-sections (SC) were investigated due to the reported atrophy and axonal degeneration of the corticospinal tract and the relevance for HSPs (Branchu *et al.*, 2017) (Figure 4).

In CO and CB of mutant mice, the number of CD8$^+$ T-lymphocytes was already increased at 12 months, followed by CC at 15 and ON at 18 months (Figure 3a – h). Of note, CB displayed the most robust increase in the number of CD8$^+$ T-lymphocytes compared to all other investigated compartments (Figure 3g). The number of CD4$^+$ T-lymphocytes was increased in the CO and CB at 12 months, followed by the ON at 18 months (Figure 3b, f, h). The number of CD4$^+$ T-lymphocytes was not increased in the CC of *Spg11^{-/-}* mice at any investigated timepoint (Figure 3d). Overall, we realized that CD8$^+$ T-lymphocytes outnumbered CD4$^+$ T-lymphocytes (Figure 3a – h).
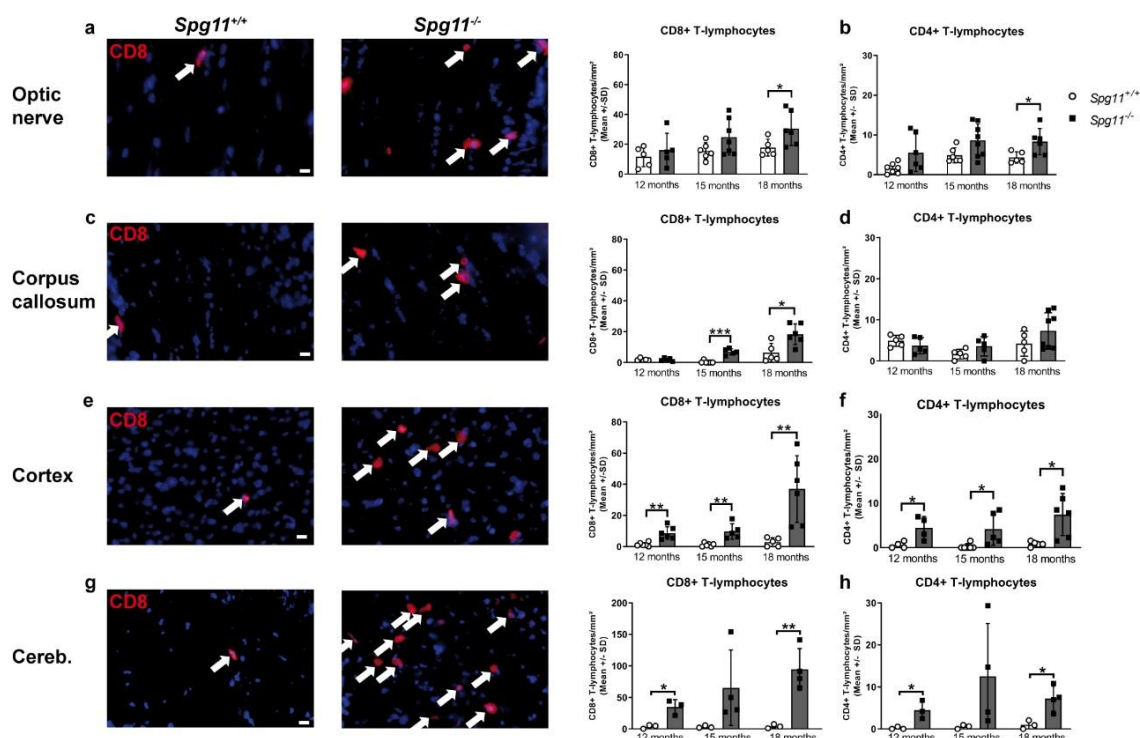
Figure 3: Progressive accumulation of T-lymphocytes in distinct CNS compartments of *Spg11*^{-/-} mice.

(**a, c, e, g**) Representative images of CD8^{+} T-lymphocytes (red, arrows) in distinct CNS compartments of 18-month-old *Spg11*^{+/+} and *Spg11*^{-/-} mice (left) and corresponding quantification at different ages (right). Nuclei are labeled with DAPI (blue). Scale bar: 10 µm. (**a**) In longitudinal sections of ON, the number of CD8^{+} T-lymphocytes is significantly increased at 18 months. (**c**) In coronal sections of CC, the number of CD8^{+} T-lymphocytes is significantly increased at 15 and 18 months. (**e**) In coronal sections of CO, the number of CD8^{+} T-lymphocytes is significantly increased at 12, 15, and 18 months (**g**). In coronal sections of CB, the number of CD8^{+} T-lymphocytes is significantly increased at 12 and 18 months. Note the different scale of the Y-axis in g) compared to a), c), e) due to the high number of CD8^{+} T-lymphocytes in CB of *Spg11*^{-/-} mice. (**b, d, f, h**) Quantification of CD4^{+} T-lymphocytes in distinct CNS compartments of *Spg11*^{+/+} and *Spg11*^{-/-} mice at distinct ages. (**b**) In ON, the number of CD4^{+} T-lymphocytes is significantly increased at 18 months. (**d**) In CC, the number of CD4^{+} T-lymphocytes is not increased. (**f**) In CO, the number of CD4^{+} T-lymphocytes is significantly increased at 12, 15, and 18 months. (**h**) In CB, the number of CD4^{+} T-lymphocytes is significantly increased at 12 and 18 months. Note the lower number of CD4^{+} compared to CD8^{+} T-lymphocytes. Error bars represent the standard deviations (circles, squares = mean value of one mouse). Significance of *Spg11*^{-/-} compared to *Spg11*^{+/+} mice is determined by Two-tailed Student's t-test (*$p < 0.05$, **$p < 0.01$, ***$p < 0.001$).

In SC of *Spg11*^{-/-} mice, the number of CD8^{+} and CD4^{+} T-lymphocytes was lower than in the other investigated compartments at 18 months (Figure 4a, b). However, we detected an elevated number of CD8^{+} T-lymphocytes in the SC white and grey matter of 18-month-old *Spg11*^{-/-} mice compared to *Spg11*^{+/+} mice, while the number of CD4^{+} T-lymphocytes remained unaffected (Figure 4a, b).
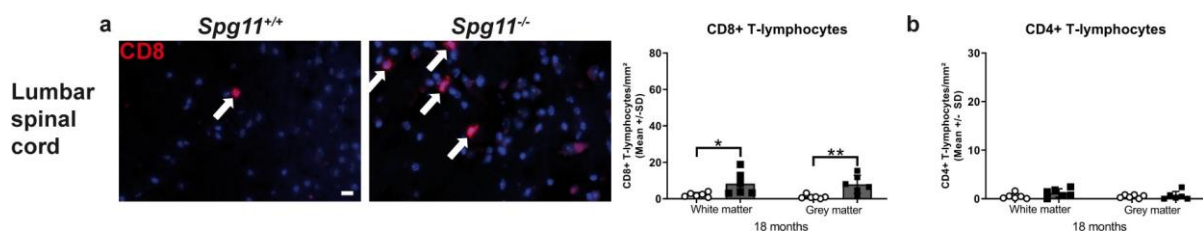
27

Figure 4: The number of CD8⁺ T-lymphocytes is mildly increased in SC white and grey matter of *Spg11⁻/⁻* mice.
(a) Representative images of CD8⁺ T-lymphocytes (red, arrows) in coronal sections of lumbar spinal cord (SC) of 18-month-old *Spg11⁺/⁺*, and *Spg11⁻/⁻* mice (left) and quantification (right). Nuclei are labeled with DAPI (blue). Scale bar: 10 µm. In SC of *Spg11⁻/⁻* mice, the number of CD8⁺ T-lymphocytes is increased in white and grey matter. (b) Quantification of CD4⁺ T-lymphocytes in SC of 18-month-old *Spg11⁺/⁺*, and *Spg11⁻/⁻*. In SC of *Spg11⁻/⁻* mice, the number of CD4⁺ T-lymphocytes is not increased. Error bars represent the standard deviations (circles, squares = mean value of one mouse). Significance of *Spg11⁻/⁻* compared to *Spg11⁺/⁺* mice is determined by Two-tailed Student's t-test (*$p < 0.05$, **$p < 0.01$).

Our group could previously identify cytotoxic CD8⁺ T-lymphocytes as pathogenic executors in various disease models and during aging (Ip *et al.*, 2006; Groh *et al.*, 2013; Groh *et al.*, 2016a; Groh *et al.*, 2021b). This prompted us to further characterize isolated CD8⁺ T-lymphocytes from whole brains of 15-month-old *Spg11⁺/⁺* and *Spg11⁻/⁻* mice for expression of distinct subtype and activation markers by flow cytometry (Figure 5). We could confirm a significant increase in the total number of CD8⁺ T-lymphocytes per brain of *Spg11⁻/⁻* mice compared to wt littermates (Figure 5a, b). Among these cells, the large majority expressed CXCR6 (Figure 5c – g), which is a marker of tissue recruitment and residency for activated CD8⁺ T-lymphocytes (Urban *et al.*, 2020). CXCR4 was expressed by a smaller population of T-lymphocytes (Figure 5c – g), usually associated with CNS trafficking of T helper cells (Galli *et al.*, 2019). Most of the CD8⁺CXCR6⁺CXCR4⁻ T-lymphocytes also expressed the activation marker Ly6A/E and some of them were positive for CD103, a marker of tissue-resident memory T-lymphocytes (Figure 5e – g) (Urban *et al.*, 2020). While the total number of most populations increased proportionally to the number of CD8⁺ T-lymphocytes, there was a disproportional increase of CD8⁺CXCR6⁺CXCR4⁻CD103⁺ T-lymphocytes in brains of *Spg11⁻/⁻* mice (Figure 5e, f). This cytotoxic population has been identified to be activated in the white matter during normal aging (Groh *et al.*, 2021b) and accumulates in MS patients (Machado-Santos *et al.*, 2018).

a

b CD8+ T-lymphocytes

c Gated for CD8+ T cells

$Spg11^{+/+}$ $Spg11^{-/-}$

d Gated for CD8+ T-lymphocytes

e Gated for CD8+CXCR6+CXCR4- T cells

$Spg11^{+/+}$ $Spg11^{-/-}$

f Gated for CD8+CXCR6+CXCR4- T-lymphocytes

g CD8+ T-lymphocytes
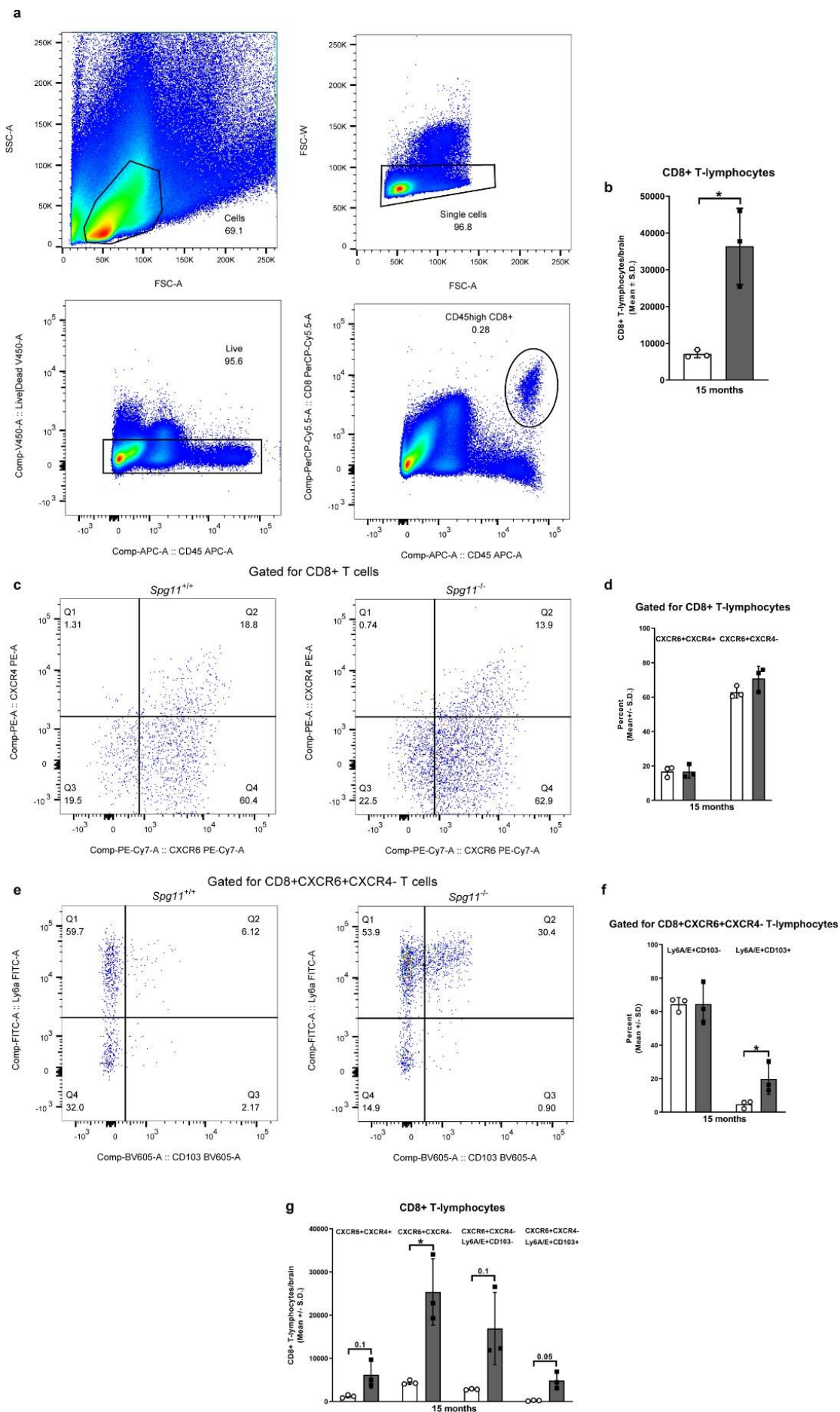
29

Figure 5: *Spg11^{-/-}* mice show a significantly increased number of CD8⁺ tissue resident memory T-lymphocytes in the CNS.

(a) Gating strategy for flow cytometric analysis of CD8⁺ T-lymphocytes in whole brains of 15-month-old *Spg11^{+/+}* and *Spg11^{-/-}* mice and (b) quantification. In whole brains of *Spg11^{-/-}* mice, the total number of CD8⁺ T-lymphocytes is significantly increased. (c) Gating strategy for flow cytometric analysis of CD8⁺ T-lymphocytes in whole brains of 15-month-old *Spg11^{+/+}* and *Spg11^{-/-}* mice for CXCR6 and CXCR4 and (d) quantification. The percentage of CD8⁺CXCR6⁺CXCR4⁻ T-lymphocytes is higher than CD8⁺CXCR6⁺CXCR4⁺ T-lymphocytes but comparable between *Spg11^{+/+}* and *Spg11^{-/-}* mice. (e) Gating strategy for further flow cytometric analysis of CD8⁺CXCR6⁺CXCR4⁻ T-lymphocytes in whole brains of 15-month-old *Spg11^{+/+}* and *Spg11^{-/-}* mice for Ly6A/E and CD103 and (f) quantification. The percentage of CD8⁺CXCR6⁺CXCR4⁻Ly6A/E⁺CD103⁺ is significantly increased in *Spg11^{-/-}* mice. (g) Flow cytometric analysis of CD8⁺ T-lymphocytes of whole brains from 15-month-old *Spg11^{+/+}* and *Spg11^{-/-}* mice. Total number of CD8⁺CXCR6⁺CXCR4⁻ T-lymphocytes per brain are significantly increased in *Spg11^{-/-}* mice. Most of these cells express the activation marker Ly6A/E, while some are additionally positive for CD103, a marker of tissue-resident memory T-lymphocytes. Error bars represent the standard deviations. Significance *Spg11^{-/-}* compared to *Spg11^{+/+}* mice is determined by Two-tailed Student's t-test (*p < 0.05, **p < 0.01, ***p < 0.001). Figure generated by PD. Dr. Janos Groh, with slight modifications by Michaela Hörner.

The previously presented data clearly indicate that *Spg11^{-/-}* mice show robust upregulation of secondary inflammation, with a disproportionally high increase of CD103⁺ T-lymphocytes. These findings support the previously described heterogeneity of CD8⁺ CNS-associated T-lymphocytes (Groh *et al.*, 2021b) and reveal some commonalities between T cell reactions in aging, neuroinflammatory disease, and this model of SPG11.

It has been previously described that not only T-lymphocytes can act as a pathogenic amplifier of disease, but microglia and their activation state have also been implicated to influence the disease progression in other mouse models (Ip *et al.*, 2007; Groh *et al.*, 2016b). Even though the focus of the present study was on targetable, neuroinflammatory cells of the adaptive immune system, we investigated microglia in different CNS compartments of *Spg11^{+/+}* and *Spg11^{-/-}* mice using CD11b as pan-marker and sialoadhesin (CD169, Sn) as an activation marker (Groh *et al.*, 2016b; Bogie *et al.*, 2018). The vast majority of CD11b⁺ cells expressed the resident microglial marker TMEM119 (Bennett *et al.*, 2016) (Figure 6a), indicating that blood-derived monocytes are most likely rare within the parenchyma (Prinz *et al.*, 2017). We could find an increase in the number of CD11b⁺ cells in ON of *Spg11^{-/-}* mice at 12 and 18 months (Figure 6b). Importantly, the number of activated (Sn⁺) microglial cells was significantly increased at 15 and 18 months (Figure 6c). In CC and CO of *Spg11^{-/-}* mice, microglia numbers were increased from 12 months onwards (Figure 6d, f). While the CC displayed an increased number of activated microglia from 15 months onwards, the CO showed an increased number only at 18 months (Figure 6e, g). Of note, the increase in the CO was generally lower than in all other investigated compartments (Figure 6g). In CB of *Spg11^{-/-}* mice,

the number of CD11b$^+$ cells was increased at 18 months (Figure 6h), but activation of microglial cells was already detectable at 12 months (Figure 6i). Investigation of SC of 18-month-old *Spg11$^{-/-}$* mice revealed an increased number of CD11b$^+$ cells in the grey and white matter (Figure 6j). Interestingly, increased microglial activation was only detectable in the SC white matter of *Spg11$^{-/-}$* mice (Figure 6k).
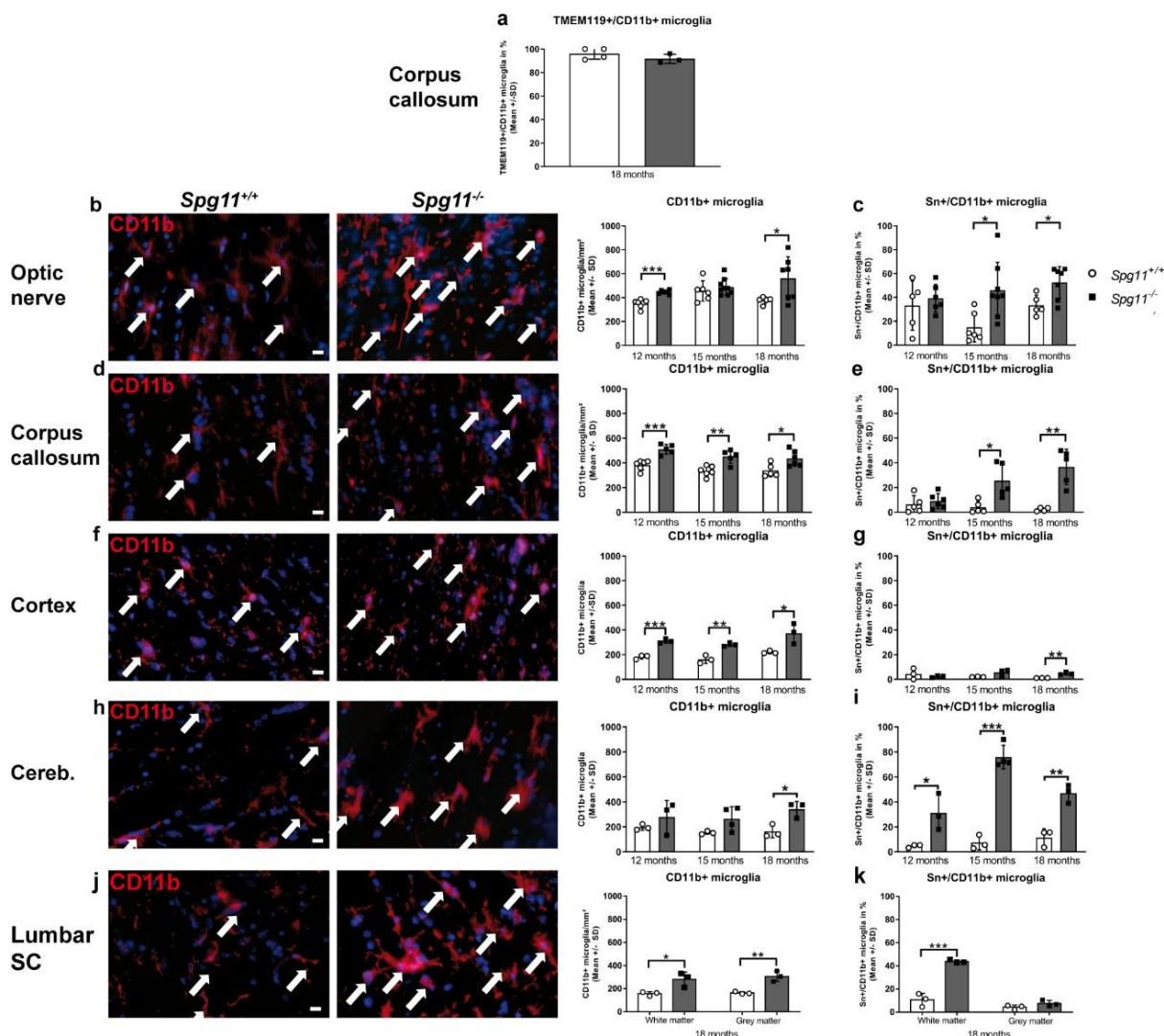

Figure 6: Increase in number and activation of microglia in the CNS of *Spg11$^{-/-}$* mice.
(a) As exemplified in the CC, the vast majority of CD11b$^+$ cells are positive for the microglial marker TMEM119$^+$. **(b, d, f, h, j)** Representative images of CD11b$^+$ cells (arrows), a pan myeloid marker, in distinct CNS compartments of 18-month-old *Spg11$^{+/+}$* and *Spg11$^{-/-}$* mice (left) and corresponding quantification at distinct ages (right). Nuclei are labeled with DAPI (blue). Scale bar: 10 µm. **(b)** In ON of *Spg11$^{-/-}$* mice, the number of CD11b$^+$ cells is significantly increased at 12 and 18 months. **(d)** In CC and **(f)** CO of *Spg11$^{-/-}$* mice, the number of CD11b$^+$ cells is significantly increased at 12, 15, and 18 months. **(h)** In CB of *Spg11$^{-/-}$* mice, the number of CD11b$^+$ cells is significantly increased at 18 months. **(j)** In SC, the number of CD11b$^+$ cells is significantly increased in white and grey matter at 18 months. **(c, e, g, i, k)** Percentage of CD11b$^+$ cells showing the microglial activation marker Sn in distinct CNS compartments of *Spg11$^{+/+}$* and *Spg11$^{-/-}$* mice at distinct ages. **(c)** The number of Sn$^+$ cells is significantly increased from 15 months onwards in ON and **(e)** CC, at 18 months in **(g)** CO, from 12 months onwards in **(i)** CB, and at 18 months in **(k)** SC. Error bars represent the standard deviations (circles, squares = mean value of one mouse). Significance of *Spg11$^{-/-}$* compared to *Spg11$^{+/+}$* mice is determined by Two-tailed Student's t-test (*p < 0.05, **p < 0.01, ***p < 0.001).

In summary, we found that CNS-related CD11b^{+} cells are mainly TMEM119^{+} resident microglial cells displaying mildly increased numbers in *Spg11^{-/-}* mice in comparison to wt mice, while their activation was robust in most compartments.

5.2 *Spg11^{-/-}* mice display significant axonal perturbation and neural damage in white and grey matter compartments of the CNS

We next scored pathological alterations in these distinct CNS compartments applying electron microscopy (EM) and immunocytochemistry (IC) at the ages of 12, 15 and 18 months. In cross sections of ON of *Spg11^{-/-}* mice, EM analysis revealed axonal perturbation in the form of typical, organelle-rich swellings, here and in the following designated as spheroids (Figure 7a, b). As an additional axonopathic feature, we quantified axonal profiles with altered axoplasm and/or contorted cytoskeleton (Figure 7a, b). In *Spg11^{-/-}* mice we found an increase of axonopathic features from 15 months onwards (Figure 7a, b). In contrast, we detected a higher percentage of axons with redundant myelin in the ON of *Spg11^{-/-}* mice at 15 but not 18 months (Figure 7c), possibly reflecting that these axons are prone to degenerate. Indeed, *Spg11^{-/-}* mice showed a reduced number of axons at 15 months, that was even more pronounced at 18 months (Figure 7d). Accordingly, these histopathological alterations resulted in a reduced ON area (Figure 7e). Investigations using SMI32-immunoreactivity, identifying non-phosphorylated neurofilaments, confirmed a progressive increase in the number of spheroids in ON (Figure 7f). Additionally, double-immunofluorescence staining for CD8 and SMI32 revealed that spheroids were frequently in close proximity to CD8^{+} T-lymphocytes (Figure 7g). A higher number of SMI32^{+} axonal spheroids was also detectable in the CC, CO, and CB of 18-month-old *Spg11^{-/-}* mice (Figure 7h – j) and *Spg11^{-/-}* mice showed a significant reduction of brain weight at 18 months compared to their wt littermates (Figure 7k).
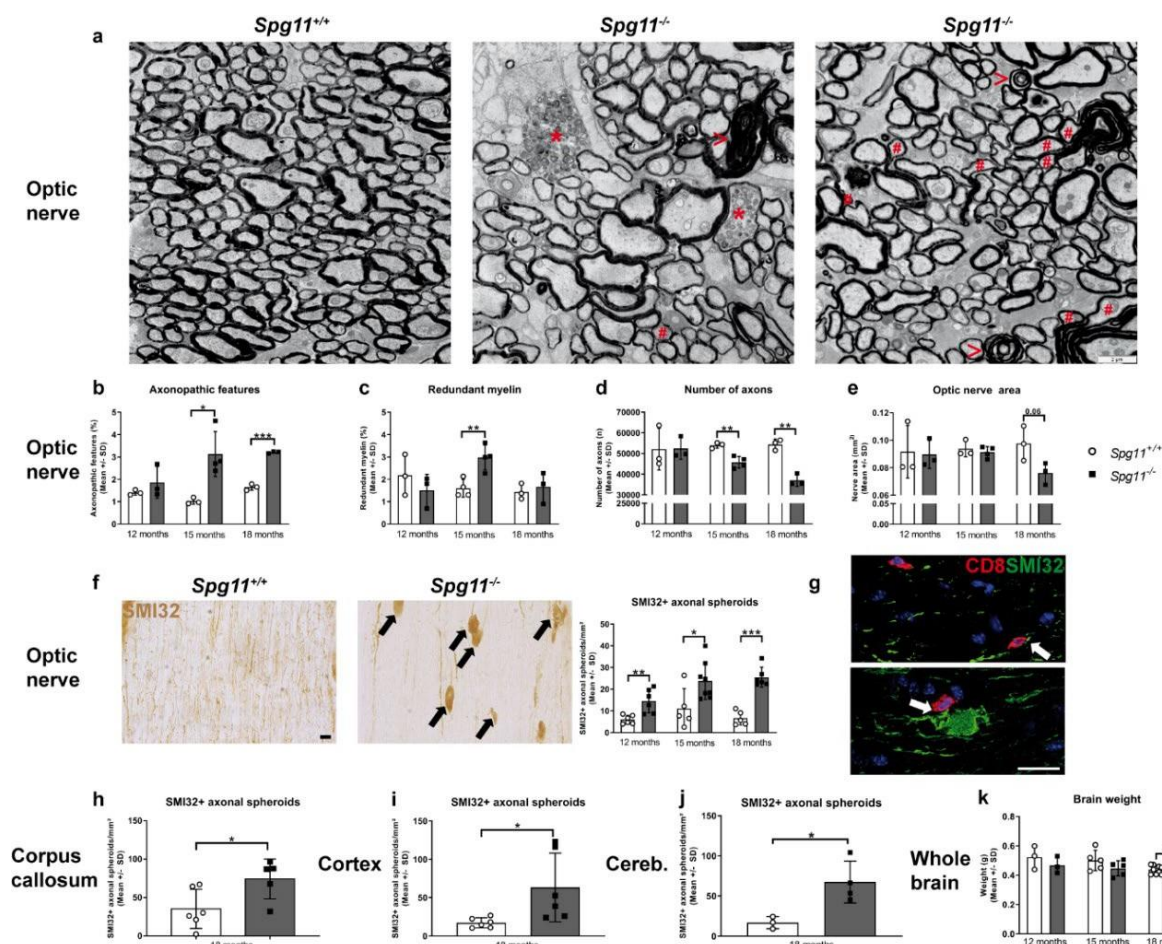
Figure 7: Progressive increase of neural damage in distinct CNS compartments of *Spg11⁻/⁻* mice.

(a) Representative electron micrographs of ON cross sections of 18-month-old *Spg11⁺/⁺* and *Spg11⁻/⁻* mice. (b-e) EM-based quantification of pathological alterations at distinct ages. Asterisks indicate axonopathic features, hashtags axons with redundant myelin, open arrowheads myelin fragments. Scale bar: 2 µm. (b) Axonopathic features are more frequent in *Spg11⁻/⁻* mice at 15 and 18 months. (c) The percentage of axons with redundant myelin is increased at 15 months. (d) At 15 and 18 months, the number of axons is reduced, likely contributing to (e) a reduced ON area. (f) Representative images of SMI32⁺ axonal spheroids (arrows) in ON of 18-month-old *Spg11⁺/⁺* and *Spg11⁻/⁻* mice (left) and corresponding quantification (right). Scale bar: 10 µm. The number of SMI32⁺ axonal spheroids is significantly increased in *Spg11⁻/⁻* mice. (g) Representative images of CD8/SMI32 double-immunofluorescence in ON of 18-month-old *Spg11⁻/⁻* mice. Nuclei are labeled with DAPI (blue). Scale bar: 20 µm. CD8/SMI32 staining reveals close contact (arrows) between CD8⁺ T-lymphocytes and SMI32⁺ perturbed axon (top) or axonal spheroid (bottom). (h) Quantification of SMI32⁺ axonal spheroids in CC, (i) CO, and (j) CB of 18-month-old *Spg11⁺/⁺* and *Spg11⁻/⁻* mice. The number of SMI32⁺ axonal spheroids is significantly increased in *Spg11⁻/⁻* mice at 18 months. (k) *Spg11⁻/⁻* mice show a significant reduction of brain weight compared to wt mice at 18 months. Error represents standard deviations (circles, squares = mean value of one mouse). Significance of *Spg11⁻/⁻* compared to *Spg11⁺/⁺* mice is determined by Two-tailed Student's t-test (*$p < 0.05$, **$p < 0.01$, ***$p < 0.001$).

Regarding the visual system, we also investigated the retina for pathological alterations. In retinal flat mount preparations, we found a significant reduction of retinal ganglion cell bodies (RGCs) when using the pan marker RBPMS (Figure 8a). Previous reports indicated, that patients with complicated forms of HSP show thinning of the retinal nerve fiber layer (RNFL),

as detected with spectral domain optical coherence tomography (SD-OCT) (Vavla *et al.*, 2019). Work of our group provided evidence, that thinning of the innermost composite layer of the mouse retina, which is composed of the nerve fiber layer (NFL), the ganglion cell layer (GCL) and the inner plexiform layer (IPL), can serve as a robust indicator of disease progression and treatment efficacy in various mouse models of hereditary neurodegenerative diseases (Groh *et al.*, 2014; Groh *et al.*, 2016a; Groh *et al.*, 2017; Groh *et al.*, 2018; Groh *et al.*, 2021a). Therefore, we investigated retinal thickness of $Spg11^{+/+}$ and $Spg11^{-/-}$ mice longitudinally by using a commercially available SD-OCT device with slight modifications (Groh *et al.*, 2014). We could detect that $Spg11^{-/-}$ mice show a significant thinning of the innermost retinal layer from 12 months onwards compared to wt mice (Figure 8b). Of note, the visual acuity of $Spg11^{-/-}$ mice remained intact at 18 months of age (Figure 8c).
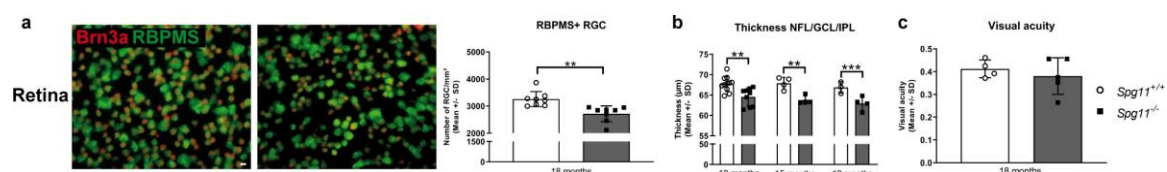

Figure 8: $Spg11^{-/-}$ mice display pathogenic alterations in the retina.
(a) Representative images of Brn3a/RBPMS$^+$ RGCs in whole-mount retinae of 18-month-old $Spg11^{+/+}$ and $Spg11^{-/-}$ mice (left) and corresponding quantification (right). Scale bar: 50 µm. Densities of RBPMS$^+$ RGCs are significantly reduced in $Spg11^{-/-}$ mice. Most RBPMS$^+$ cells are Brn3a$^+$. **(b)** Longitudinal analysis of the thickness of the innermost retinal composite layer (NFL/GCL/IPL) of $Spg11^{+/+}$ and $Spg11^{-/-}$ mice by OCT reveals significant retinal thinning in $Spg11^{-/-}$ mice from 12 months onwards. **(c)** $Spg11^{-/-}$ mice do not have altered visual acuity compared to $Spg11^{+/+}$ mice at 18 months. Error bars represent standard deviations (circles, squares = mean value of one mouse). Significance of $Spg11^{-/-}$ compared to $Spg11^{+/+}$ mice is determined by Two-tailed Student's t-test or one-way ANOVA and Tukey's post hoc test (**$p < 0.01$, ***$p < 0.001$).

These data suggest that $Spg11^{-/-}$ mice show progressive increase in axonal and neural perturbation in the CNS.

5.3 $Spg11^{-/-}$ mice display reduced gait coordination, attenuated strength and reduced body weight

As gait abnormalities are one of the leading features in SPG11, we next focused on a detailed description of the walking pattern of $Spg11^{+/+}$ and $Spg11^{-/-}$ mice at 6 and 18 months of age. For this the CatWalk analysis was used, a gait analysis that is also used in humans. Two different categories of gait parameters, likely relevant to SPG11, were chosen. The first category, consisting of paw angle movement vector variation (Figure 9c), paw angle body axis variation (Figure 9d), step cycle variation (Figure 9e), print position (Figure 9f) and regularity index (Figure 9g), comprised parameters related to the variability of stepping patterns and interlimb coordination. These parameters will, in the following, be summarized as gait coordination. The

second category consisted of parameters most likely related to strength, like maximal contact area, print area and print width of the hind paws (Figure 9h – j).

We could detect distinct walking pattern abnormalities in *Spg11*⁻/⁻ mice, as early as 6 months of age (Figure 9a – j). *Spg11*⁻/⁻ mice displayed abnormalities in gait coordination compared to wt littermates: We detected an increased paw angle and step cycle variation at 18 months (Figure 9c – e), while the print position was already increased at 6 months (Figure 9b, f). Furthermore, we detected a reduction in the regularity index in 18-month-old *Spg11*⁻/⁻ mice (Figure 9g). *Spg11*⁻/⁻ mice also showed indicators of reduced strength at 18 months, like the reduction of the maximal contact area, print area, and print width of the hind paws (Figure 9a, i – j).
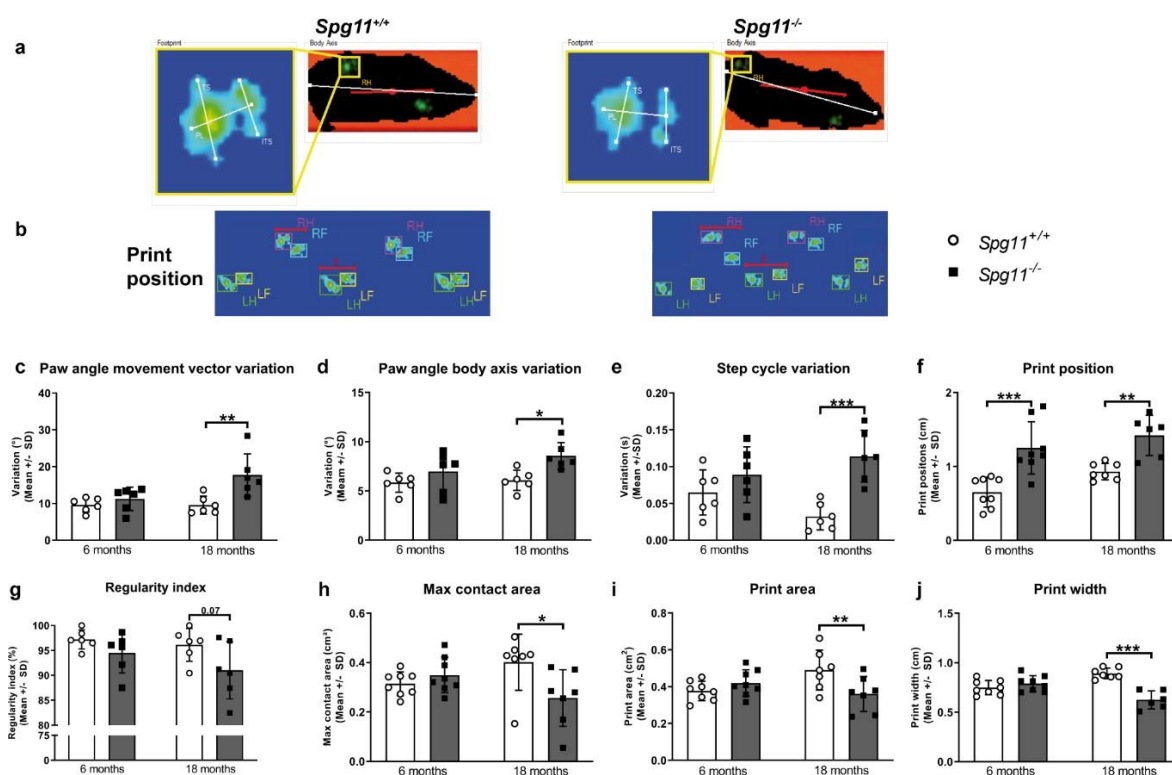

Figure 9: *Spg11*⁻/⁻ mice display abnormalities in gait coordination and reduced strength.
(a) Representative images of body contour, footprints and **(b)** print positions of 18-month-old *Spg11*⁺/⁺ and *Spg11*⁻/⁻ mice while crossing the CatWalk device (ITS: intermediate toe spread; TS: toe spread; PL: print length; RF: right front paw; LF: left front paw; RH: right hind paw; LH: left hind paw). Red line (top) indicates the body axis, red line segment (bottom) indicates print position. **(c)** In *Spg11*⁻/⁻ mice, paw angle movement vector variation and **(d)** paw angle body axis variation, both parameters reflecting variability of stepping pattern, are increased at 18 months. **(e)** In *Spg11*⁻/⁻ mice, step cycle variation, another parameter reflecting variability of stepping pattern, is increased at 18 months. **(f)** In *Spg11*⁻/⁻ mice, the print position, a parameter for interlimb coordination, is increased at 6 and 18 months while **(g)** the regularity index, another parameter for interlimb coordination, is reduced at 18 months. **(h)** In *Spg11*⁻/⁻ mice, the maximal contact area, **(i)** the print area and **(j)** the print width of the hind paws, all parameters likely reflecting strength, are reduced at 18 months. Error bars represent the standard deviations (circles, squares = mean value of three consecutive runs of one mouse). Significance of *Spg11*⁻/⁻ compared to *Spg11*⁺/⁺ mice is determined by one-way ANOVA and Tukey's post hoc test (*p < 0.05, **p < 0.01, ***p < 0.001).

In addition, *Spg11⁻/⁻* mice showed a significantly lower stride length at 6 and 18 months compared to wt littermates (Figure 10a). Correspondingly, the number of steps needed to cross the walkway was increased at the same ages (Figure 10b).
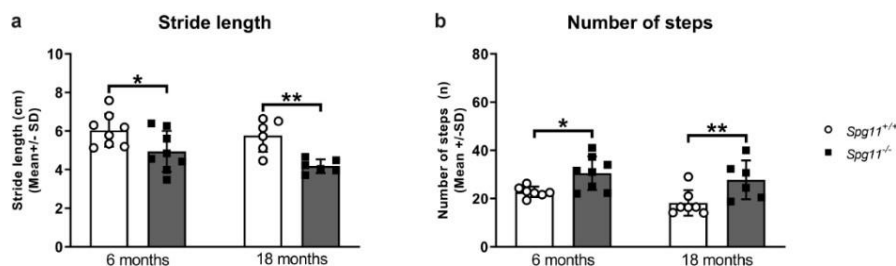

Figure 10: *Spg11⁻/⁻* mice display distinct gait abnormalities.
(a) In *Spg11⁻/⁻* mice, the stride length is decreased at 6 and 18 months, corresponding to (b) an increased number of steps. Error bars represent the standard deviations (circles, squares = mean value of three consecutive runs of one mouse). Significance of *Spg11⁻/⁻* compared to *Spg11⁺/⁺* mice is determined by one-way ANOVA and Tukey's post hoc test (*$p < 0.05$, **$p < 0.01$).

Furthermore, we detected a reduced body weight in male and female *Spg11⁻/⁻* mice compared to their wt littermates (Figure 11a, b). While male *Spg11⁻/⁻* mice showed a reduced body weight starting at 12 months, female *Spg11⁻/⁻* mice showed reduced a body weight already from 8 months onwards (Figure 11a, b).
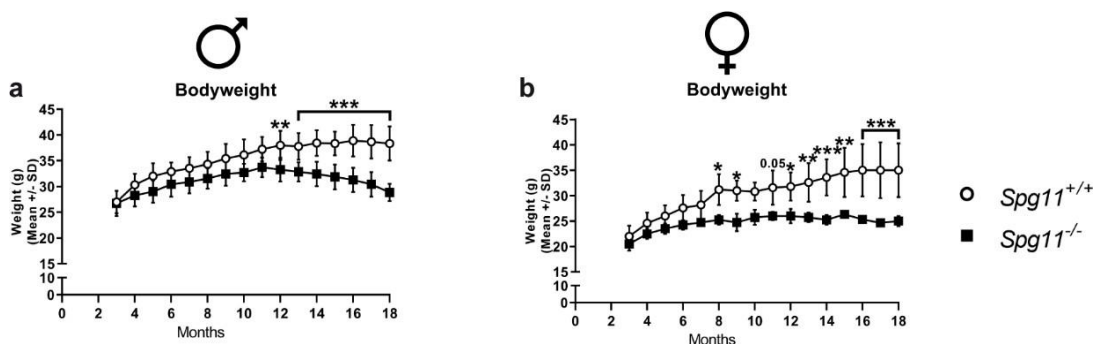
Figure 11: Male and female *Spg11⁻/⁻* mice show reduced body weight.
(a) Body weight of male *Spg11⁺/⁺* and *Spg11⁻/⁻* mice starting from 3 months. Male *Spg11⁻/⁻* mice show a reduced body weight compared to wt mice starting from 12 months onwards. (b) Body weight of female *Spg11⁺/⁺* and *Spg11⁻/⁻* mice starting from 3 months. Female *Spg11⁻/⁻* mice show a reduced body weight compared to wt mice from 8 months onwards. Error bars represent standard deviations (circles, squares = mean value at one age). Significance of *Spg11⁻/⁻* compared to *Spg11⁺/⁺* mice is determined by two-way ANOVA with multiple comparisons (*$p < 0.05$, **$p < 0.005$, ***$p < 0.001$).

Together, these data provide evidence, that *Spg11⁻/⁻* mice show robust histopathological alterations in distinct CNS compartments, body weight loss and an early alteration of their walking pattern, which is in accordance with gait alterations of SPG11 patients. Interestingly, we could show, that *Spg11⁻/⁻* mice display walking pattern abnormalities connected to intra- and interlimb coordination as early as 6 months of age while parameters related to attenuated strength were only visible at 18 months.

5.4 *Spg11^{-/-}* mice display distinct behavioral abnormalities, including abnormal social behavior

It has been previously shown, that HSP patients present with distinct neuropsychological abnormalities, including anxiety, impulsivity, learning and memory difficulties, as well as social abnormalities (Osmolak *et al.*, 2012; Faber *et al.*, 2018a). Therefore, we examined whether we could detect similar behavioral alterations in *Spg11^{-/-}* mice. For this, we designed a behavioral test battery, trying to closely mimic symptoms seen in patients (see material and methods; Figure 1). We tested for social interaction and novelty behavior, non-spatial, short-term memory and recognition, general exploratory, and hyperactivity-like behavior, anxiety-like behavior, and impulsivity-like behavior.

As social abnormalities are a prominent neuropsychological feature of SPG11 patients (Klebe *et al.*, unpublished data), we aimed to investigate whether *Spg11^{-/-}* mice showed abnormal social behavior. For this the social interaction and novelty (SI) analysis, consisting of a social interest (trial 1) and novelty trial (trial 2), was used (Figure 12a). Male *Spg11^{-/-}* mice showed a significant reduction of social interest and novelty preference compared to wt mice at 18 months (Figure 12b, c). Furthermore, male *Spg11^{-/-}* mice spent less time with the unfamiliar animals during the social novelty trial (trial 2) compared to their wt littermates at 18 months (Figure 12d), indicating abnormal social behavior.
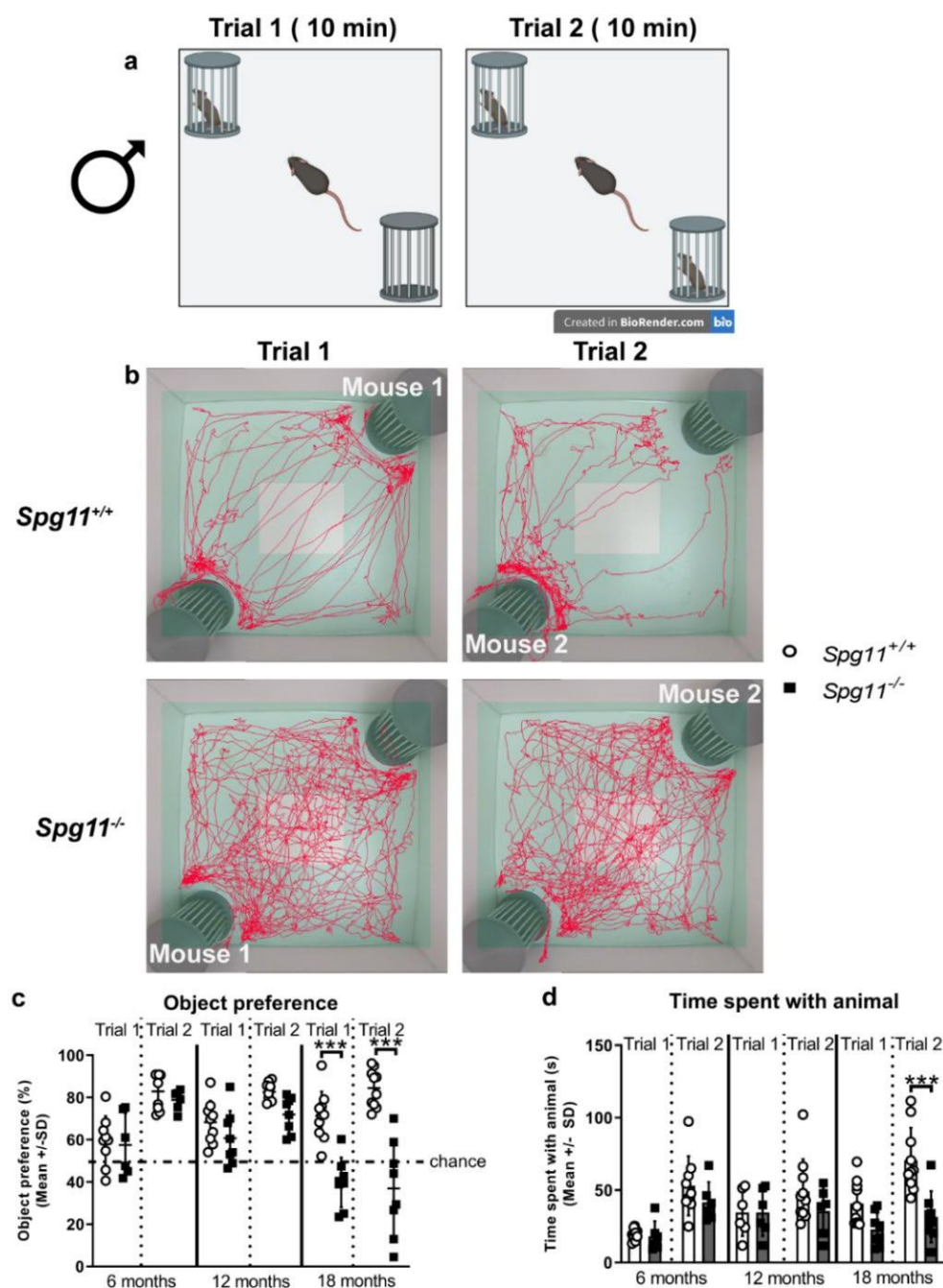
Figure 12: Male *Spg11⁻/⁻* mice show abnormal social behavior.
(a) Graphic depiction of SI analysis. A test mouse is placed in an OF box containing two small cages. In the social interest trial (trial 1), one cage contains an unfamiliar mouse, while the other cage remains empty. In the social novelty trial (trial 2) a second unfamiliar mouse is placed in the empty cage. **(b)** Representative images of social interest (trial 1, left) and novelty (trial 2, right) analysis of 18-month-old male *Spg11⁺/⁺* (top row) and *Spg11⁻/⁻* mice (bottom row). Light square indicates the center zone of the arena, green area indicates the border zone. Red line represents the walking track. Mouse 1 indicates the cage in which the first unfamiliar mouse is placed, mouse 2 in which the second unfamiliar mouse is placed. **(c)** Male *Spg11⁻/⁻* mice show lower social interest and novelty preference and **(d)** spend less time with the unfamiliar animals during the social novelty trial (trial 2) compared to wt littermates at 18 months. Chance indicates equal time spent with the empty cage/animals (50%). Error bars represent standard deviations (circles, squares = value of one mouse). Significance of *Spg11⁻/⁻* compared to *Spg11⁺/⁺* mice is determined by one-way ANOVA and Tukey's post hoc test (***$p < 0.001$). Scheme by Hörner *et al.*, unpublished (generated with BioRender).

Similar to the findings in the male mutant mice, female *Spg11*^{-/-} mice displayed reduced social interest (trial 1) and novelty (trial 2) preference compared to their wt littermates at 18 months (Figure 13a, b). Additionally, they spent less time with the unfamiliar animals (Figure 13c), indicating abnormal social behavior. Interestingly, even though the social novelty preference was still comparable to wt mice in 12-month-old *Spg11*^{-/-} mice (trial 2), they already spent less time with the unfamiliar animals (Figure 13b, c).
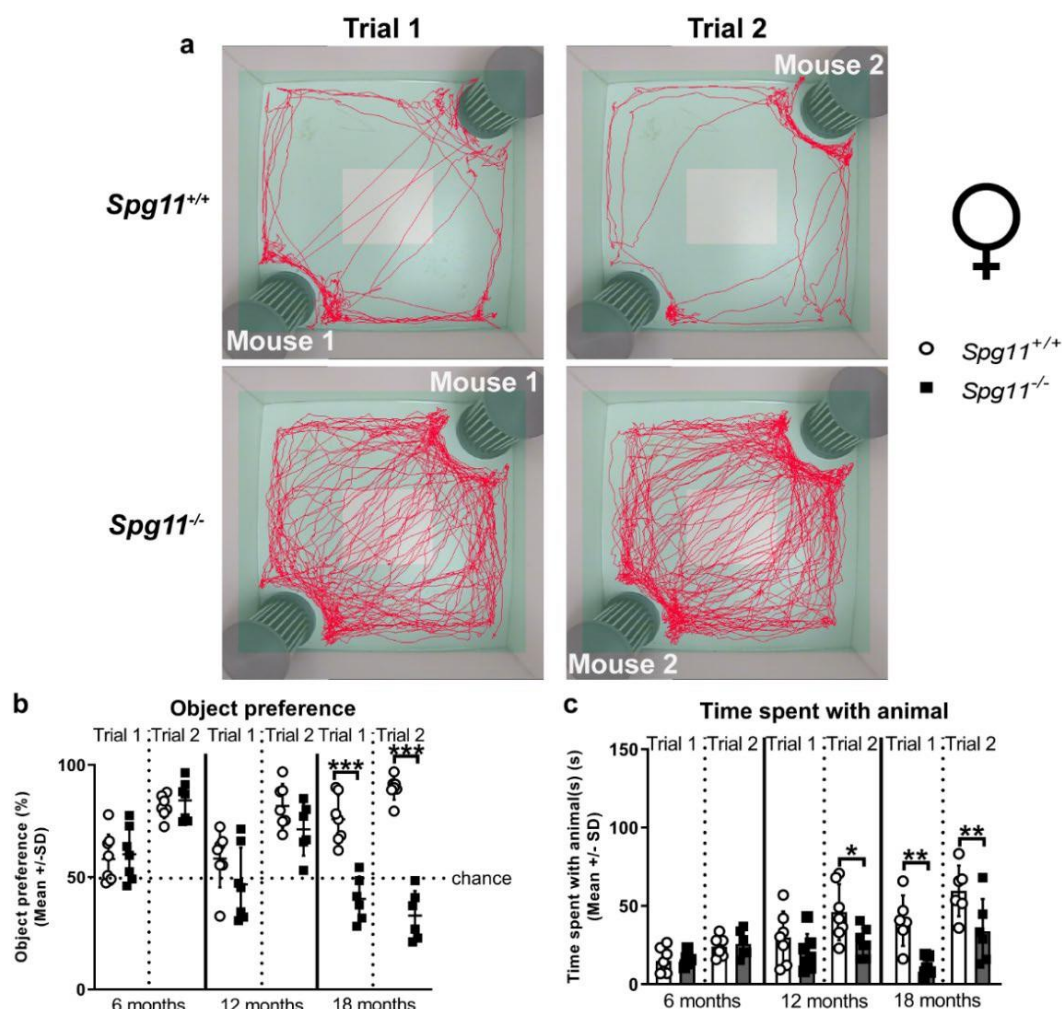
Figure 13: Female *Spg11*^{-/-} mice show abnormal social behavior.
(a) Representative images of social interest (trial 1, left) and novelty (trial 2, right) analysis of 18-month-old female *Spg11*^{+/+} (top row) and *Spg11*^{-/-} mice (bottom row). Light square indicates the center zone of the arena, green area indicates the border zone. Red line represents the walking track. Mouse 1 indicates the cage in which the first unfamiliar mouse is placed, mouse 2 in which the second unfamiliar mouse is placed. **(b)** Female *Spg11*^{-/-} mice show lower social interest and novelty preference compared to their wt littermates at 18 months. Chance indicates equal time spent with the empty cage/animals (50%). **(c)** Female *Spg11*^{-/-} mice spend less time with the unfamiliar animals compared to their wt littermates in the social interest trial (trial 1) at 18 months, and in the social novelty trial (trial 2) at 12 and 18 months. Error bars represent standard deviations (circles, squares = value of one mouse). Significance of *Spg11*^{-/-} compared to *Spg11*^{+/+} mice is determined by one-way ANOVA and Tukey's post hoc test ($*p < 0.05$, $**p < 0.005$, $***p < 0.001$).

As it has been previously shown that cognitive dysfunction is a prominent feature in HSPs (Faber *et al.*, 2016), we aimed to investigate whether cognitive dysfunction was also present in our mouse model for SPG11 using the novel object recognition (NOR) analysis. It consists of two trials, a training trial offering two identical objects and a test trial offering a familiar and an unfamiliar object, each lasting 10 minutes with a 60-minute break (Figure 14a). Male and female *Spg11*$^{-/-}$ mice elicited the expected lack of object preference in the training trial (approximately 50%), while they showed a clear preference for the novel object during the test trial (Figure 14b, c), suggesting that non-spatial, short-term memory and recognition were intact.
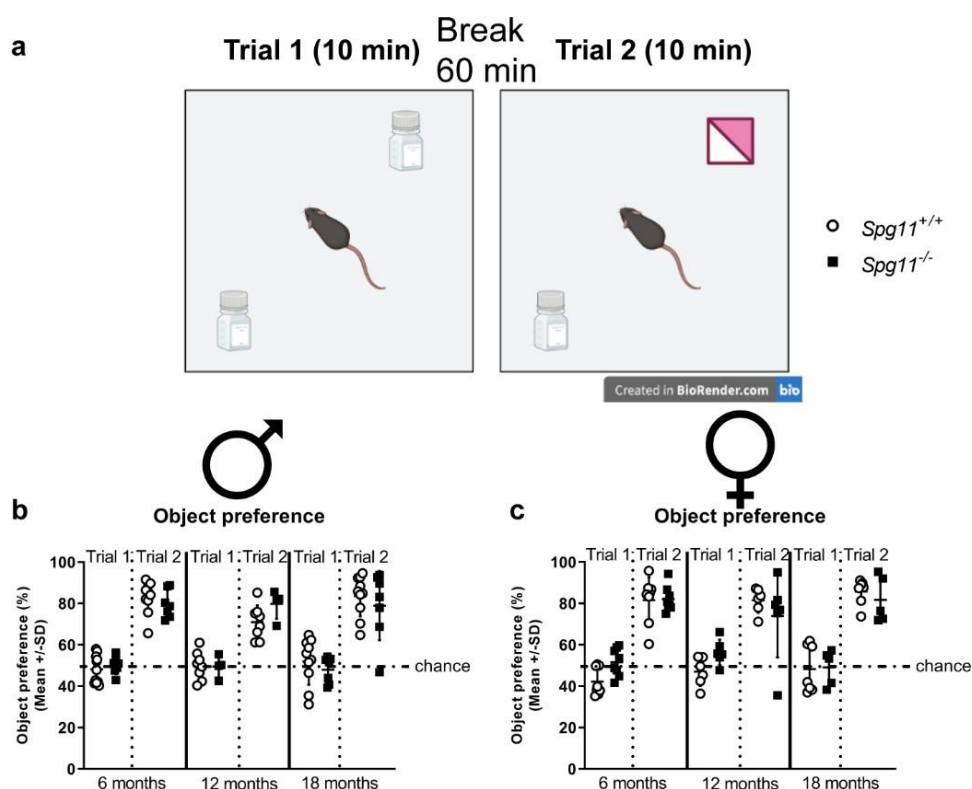
Figure 14: *Spg11*$^{-/-}$ mice do not show altered object preference in the NOR analysis.
(a) Graphic depiction of NOR analysis. A mouse is placed in an OF box, containing two identical objects. The mouse is free to investigate. After a 60-minute break, one object is replaced by an unfamiliar object of similar proportions and the mouse is placed back into the box. **(b)** Male or **(c)** female *Spg11*$^{-/-}$ mice do not show altered object preference in the NOR analysis compared to their wt littermates. Chance indicates equal time spent with both objects (50%). Error bars represent standard deviations (circles, squares = mean value of one mouse). Significance of *Spg11*$^{-/-}$ compared to *Spg11*$^{+/+}$ mice is determined by one-way ANOVA and Tukey's post hoc test. Scheme by Hörner *et al.*, unpublished (generated with BioRender).

To investigate exploratory and hyperactivity-like behavior, the open field (OF) analysis was used. It was performed in a wooden, non-transparent box, that was divided into a center and a border zone (Figure 15a). Male *Spg11*$^{-/-}$ mice walked a longer distance and showed a higher movement duration at 6 and 18 months compared to wt mice (Figure 15b – d), indicating

hyperactivity-like behavior. While the time male $Spg11^{-/-}$ mice spent in the center zone of the arena remained unaffected (Figure 15e), they spent more time rearing, with or without support of the front paws, at 6 but not 12 or 18 months (Figure 15f), possibly reflecting the previously described disturbances in gait coordination and loss of strength with progressing age. In contrast, female $Spg11^{-/-}$ showed an increased walking distance and movement duration only at 18 months of age (Figure 15g – i), while the center time and the time spent rearing remained unaffected compared to wt mice at all investigated ages (Figure 15j, k).
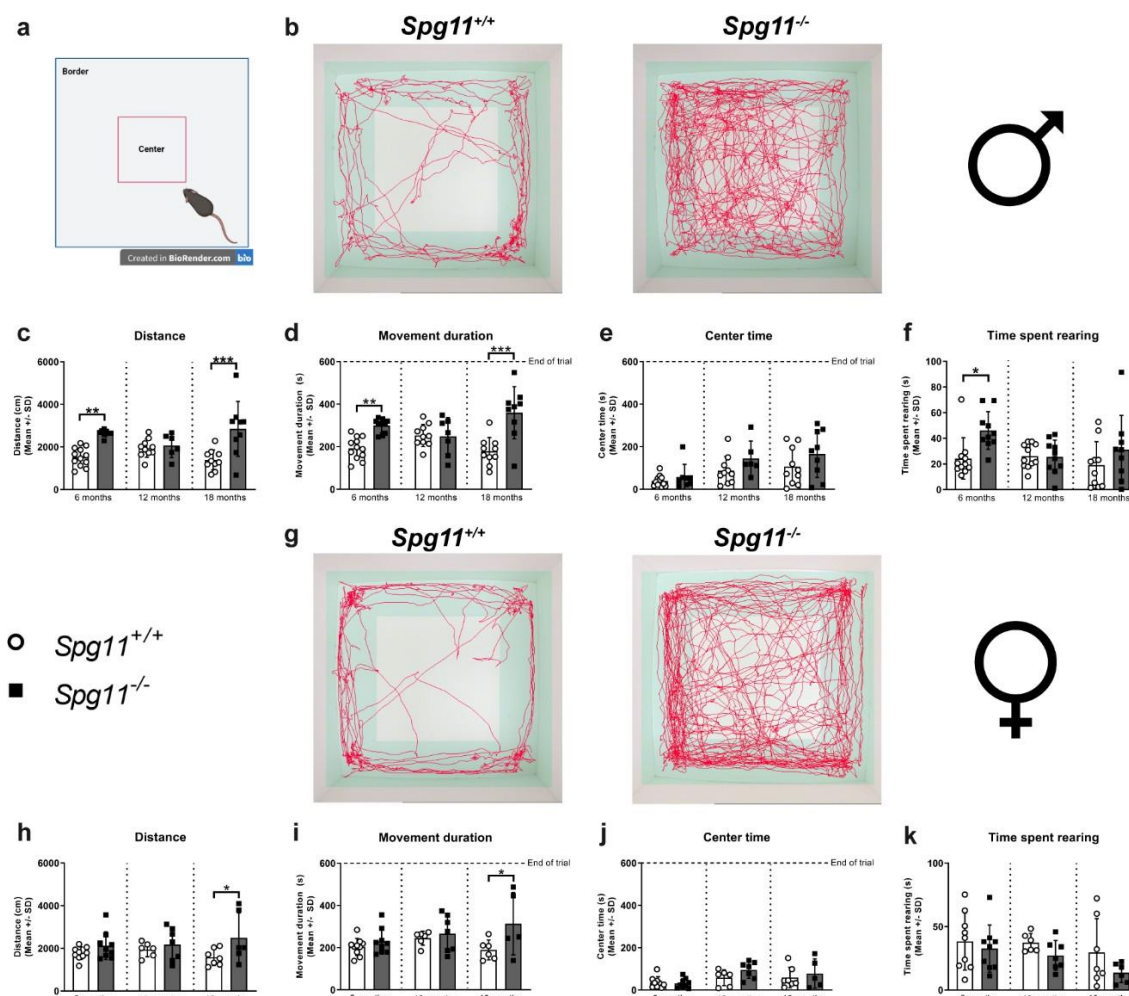
Figure 15: $Spg11^{-/-}$ mice show a hyperactivity-like phenotype.
(**a**) Graphic depiction of the OF box. The box is divided into a center (red square) and border zone. (**b**) Representative images of OF analysis of 18-month-old male $Spg11^{+/+}$ and $Spg11^{-/-}$ mice. Light square indicates the center zone of the arena, green area indicates the border zone. Red line represents the walking track. (**c**) Male $Spg11^{-/-}$ mice walk a greater distance and (**d**) show a higher movement duration at 6 and 18 months compared to wt mice, while (**e**) the center time remains unaffected. (**f**) Male $Spg11^{-/-}$ mice spend more time rearing compared to wt mice at 6 months. (**g**) Representative images of OF analysis of 18-month-old female $Spg11^{+/+}$ and $Spg11^{-/-}$ mice. Light square indicates the center zone of the arena, green area indicates the border zone. Red line represents the walking track. (**h**) Female $Spg11^{-/-}$ mice walk a greater distance and (**i**) show a higher movement duration at 18 months compared to their wt littermates. (**j**) The center time and (**k**) time spent rearing remains unchanged. Error bars represent standard deviations (circles, squares = value of one mouse). Significance of $Spg11^{-/-}$ compared to $Spg11^{+/+}$ mice is determined by one-way ANOVA and Tukey's post hoc test (*$p < 0.05$, **$p < 0.01$, ***$p < 0.001$). Scheme by Hörner *et al.*, unpublished (generated with BioRender).

Next, we examined anxiety-like behavior in male and female $Spg11^{+/+}$ and $Spg11^{-/-}$ mice using the dark/light box (DLB) analysis. The DLB consists of two compartments, a light compartment (< 300lx) and a dark compartment, which are connected by a doorway through which the mouse can walk voluntarily and freely (Figure 16a). While we did not see differences in the behavior of male $Spg11^{-/-}$ mice compared to their wt littermates (Figure 16b – f), we did detect distinct differences between female $Spg11^{-/-}$ and $Spg11^{+/+}$ mice at 18 months (Figure 16g – k). While female $Spg11^{-/-}$ mice did not show an altered latency to enter the light compartment, they walked a greater distance and spent more time in the light compartment than their wt littermates (Figure 16g – j), indicating reduced anxiety-like behavior. The time female $Spg11^{-/-}$ mice spent in the center part of the light compartment remained unaffected (Figure 16k).
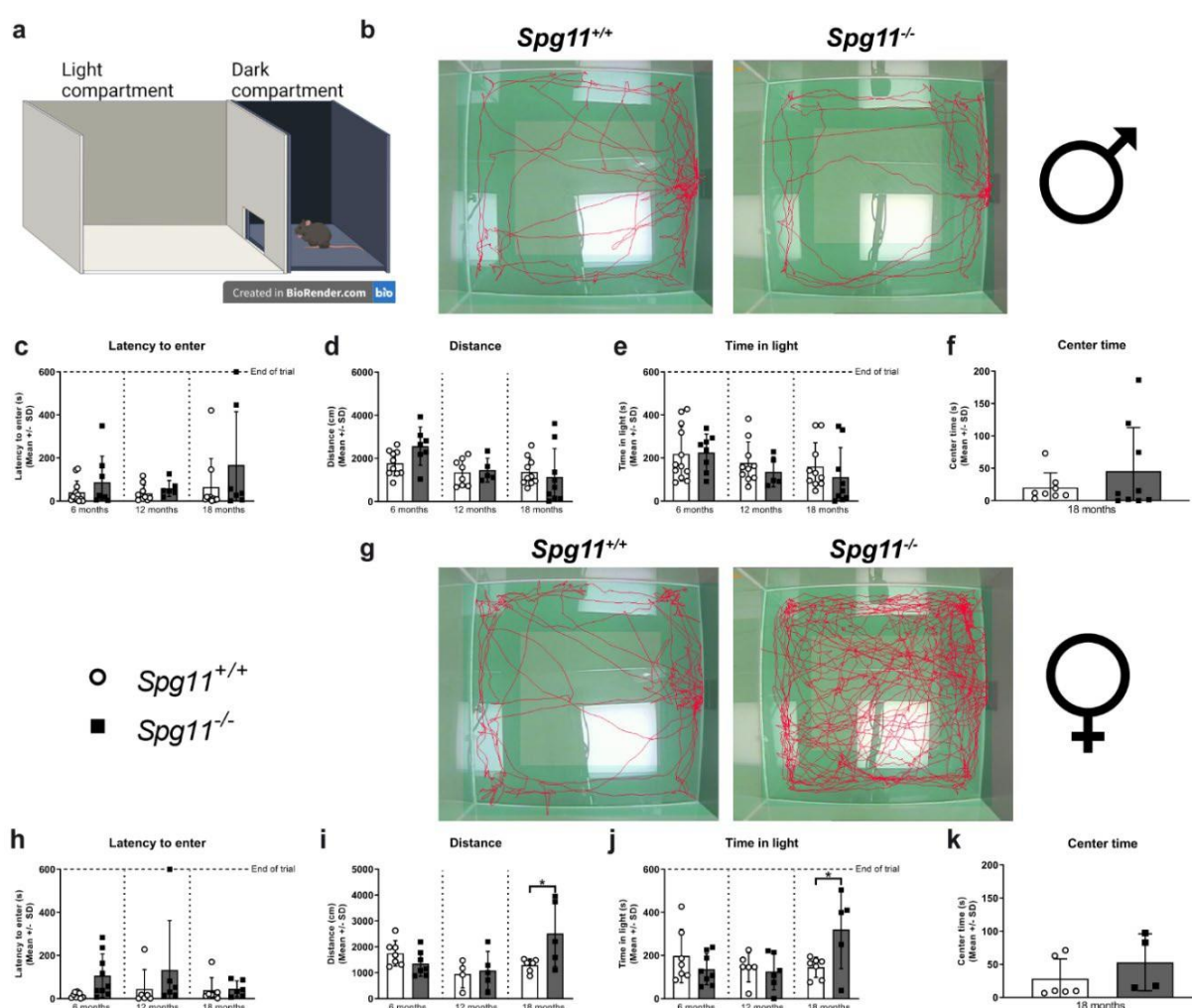
Figure 16: Female $Spg11^{-/-}$ mice show reduced anxiety-like behavior.
(a) Setup of the DLB analysis. The DLB consists of a light compartment (<300lx) and a dark compartment, connected by a doorway through which the mouse can walk freely. **(b)** Representative images of DLB analysis of 18-month-old male $Spg11^{+/+}$ and $Spg11^{-/-}$ mice. Light square indicates the center zone of the arena. Red line represents the walking track. **(c)** Male $Spg11^{-/-}$ mice do not show an altered latency to enter the light compartment, **(d)** walking distance, **(e)** time in light compartment or **(f)** center time compared to wt mice at any age investigated. **(g)** Representative images of DLB analysis of 18-month-old female $Spg11^{+/+}$ and $Spg11^{-/-}$ mice. Light square indicates the center zone of the arena.

Red line represents the walking track. **(h)** Female *Spg11*$^{-/-}$ mice do not show an altered latency to enter the light compartment compared to wt mice. **(i)** Female *Spg11*$^{-/-}$ mice walk a greater distance and **(j)** spend more time in the light compartment than wt mice at 18 months. **(k)** The center time is not altered in female *Spg11*$^{-/-}$ compared to wt mice. Error bars represent standard deviations (circles, squares = mean value of one mouse). Significance of *Spg11*$^{-/-}$ compared to *Spg11*$^{+/+}$ mice is determined by one-way ANOVA and Tukey's post hoc test (*$p < 0.05$). Scheme from BioRender.

Using the cliff avoidance reaction (CAR) analysis, we investigated impulsivity-like behavior. The CAR platform is round and non-transparent on a plastic rod (height 15.5 cm) and divided into a center and border zone (Figure 17a). Resembling our findings of the OF analysis, we found that 18-month-old male *Spg11*$^{-/-}$ mice walked a greater distance than their wt littermates (Figure 17b, c). The time spent leaning over the edge of the platform was increased in 18-month-old male *Spg11*$^{-/-}$ compared to wt mice (Figure 17d). At the same age, male *Spg11*$^{-/-}$ mice showed a reduced latency to jump off the platform, and consequently displayed an abnormal CAR compared to wt littermates, indicating increased impulsivity-like behavior (Figure 17e, f). Interestingly, female *Spg11*$^{-/-}$ mice did not walk a greater distance and showed only a tendency to spend more time leaning over the edge of the platform than their wt littermates at 18 months (Figure 17g – i). However, they displayed a decreased latency to jump off the platform and an abnormal CAR, indicating increased impulsivity-like behavior (Figure 17j, k). Note that wt mice of either gender rarely jumped off the platform at any investigated age (Figure 17f, k).
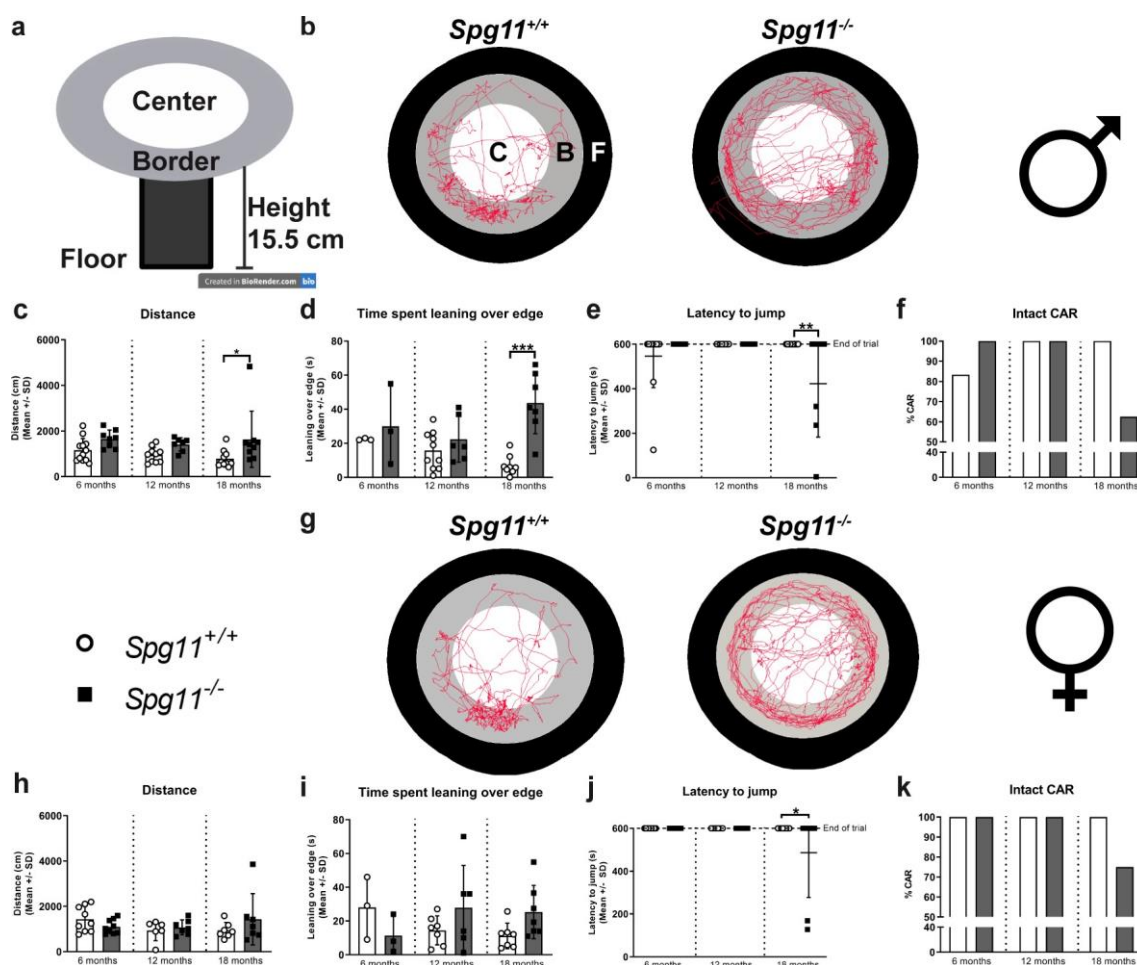
Figure 17: *Spg11⁻ᐟ⁻* **mice show increased impulsivity-like behavior.**
(**a**) Graphic depiction of the CAR platform. The platform is approximately 15.5 cm high, non-transparent, and divided into a center and a border zone. (**b**) Representative images of CAR analysis of 18-month-old male *Spg11⁺ᐟ⁺* and *Spg11⁻ᐟ⁻* mice. Red line represents the walking track (C= center zone, white; B= border zone, grey; F = floor zone, black). (**c**) Male *Spg11⁻ᐟ⁻* mice walk a greater distance than their wt littermates and (**d**) spend more time leaning over the edge of the platform at 18 months. (**e**) Male *Spg11⁻ᐟ⁻* mice show a lower latency to jump off the platform and (**f**) an abnormal CAR compared to their wt littermates at 18 months. (**g**) Representative images of CAR analysis of 18-month-old female *Spg11⁺ᐟ⁺* and *Spg11⁻ᐟ⁻* mice. Red line represents the walking track. (**h**) Female *Spg11⁻ᐟ⁻* mice do not show alterations in walking distance compared to wt mice. (**i**) Female *Spg11⁻ᐟ⁻* show a tendency towards more time spent leaning over the edge of the platform compared to wt mice at 18 months. (**j**) Female *Spg11⁻ᐟ⁻* mice show a lower latency to jump off the platform and (**k**) an abnormal CAR compared to their wt littermates at 18 months. Error bars represent standard deviations (circles, squares = value of one mouse). Significance of *Spg11⁻ᐟ⁻* compared to *Spg11⁺ᐟ⁺* mice is determined by one-way ANOVA and Tukey's post hoc test (*$p < 0.05$, **$p < 0.01$, ***$p < 0.001$). Scheme by Hörner *et al.*, unpublished (generated with BioRender).

In summary, the here presented data indicate that male and female *Spg11⁻ᐟ⁻* mice show behavioral abnormalities, consisting of reduced social interest and novelty behavior, as well as increased hyperactivity-like and impulsivity-like behavior. Additionally, female *Spg11⁻ᐟ⁻* mice show reduced anxiety-like behavior. Non-spatial, short-term memory and recognition remained unaffected in *Spg11⁻ᐟ⁻* mice. Of note, the detected social abnormalities were not due to a general reduction of exploratory behavior or recognition, or increased anxiety-like behavior. Together

with the previously published observations (Branchu *et al.*, 2017), this suggests that this mouse model recapitulates a large proportion of the clinical spectrum of SPG11.

5.5 Genetic inactivation of the adaptive immune system ameliorates pathological alterations in white and grey matter compartments of the CNS

Based on the observation that $Spg11^{-/-}$ mice show substantial neuroinflammation we investigated whether the adaptive immune system is causally involved in the development of the disease. Therefore, we evaluated the putative impact of lymphocytes in $Spg11^{-/-}$ mice, by crossbreeding them with $Rag1$-deficient ($Rag1^{-/-}$) mice, lacking mature T- and B-lymphocytes (Mombaerts *et al.*, 1992). These double-knockout mice are, hence, completely devoid of an adaptive immune response and T-lymphocytes were completely absent in the CNS (data not shown).

Examining the impact of immune cells on axonopathic features, we found that 18-month-old $Spg11^{-/-}Rag1^{-/-}$ mice presented with significantly less axonopathic features in cross-sections of ON, as demonstrated by EM analysis (Figure 18a, b). Redundant myelin remained unchanged in all investigated groups at this timepoint (Figure 18c). $Rag1$-deficiency restored the number of axons in the ON, and likely contributed to a preserved optic nerve area (Figure 18d, e). By IC, we detected a significant reduction in the number of SMI32$^+$ axonal spheroids in longitudinal ON sections of $Spg11^{-/-}Rag1^{-/-}$ mice compared to $Spg11^{-/-}$ mice (Figure 18f). These findings were not confined to the visual system, as we could also detect a reduction in spheroid numbers in CC (Figure 18g), CO (Figure 18h), and CB (Figure 18i). Interestingly, even though we detected a substantial reduction of pathogenic alterations, $Rag1$-deficiency did not dampen brain weight decline, typically occurring in $Spg11^{-/-}$ mice (Figure 18j).
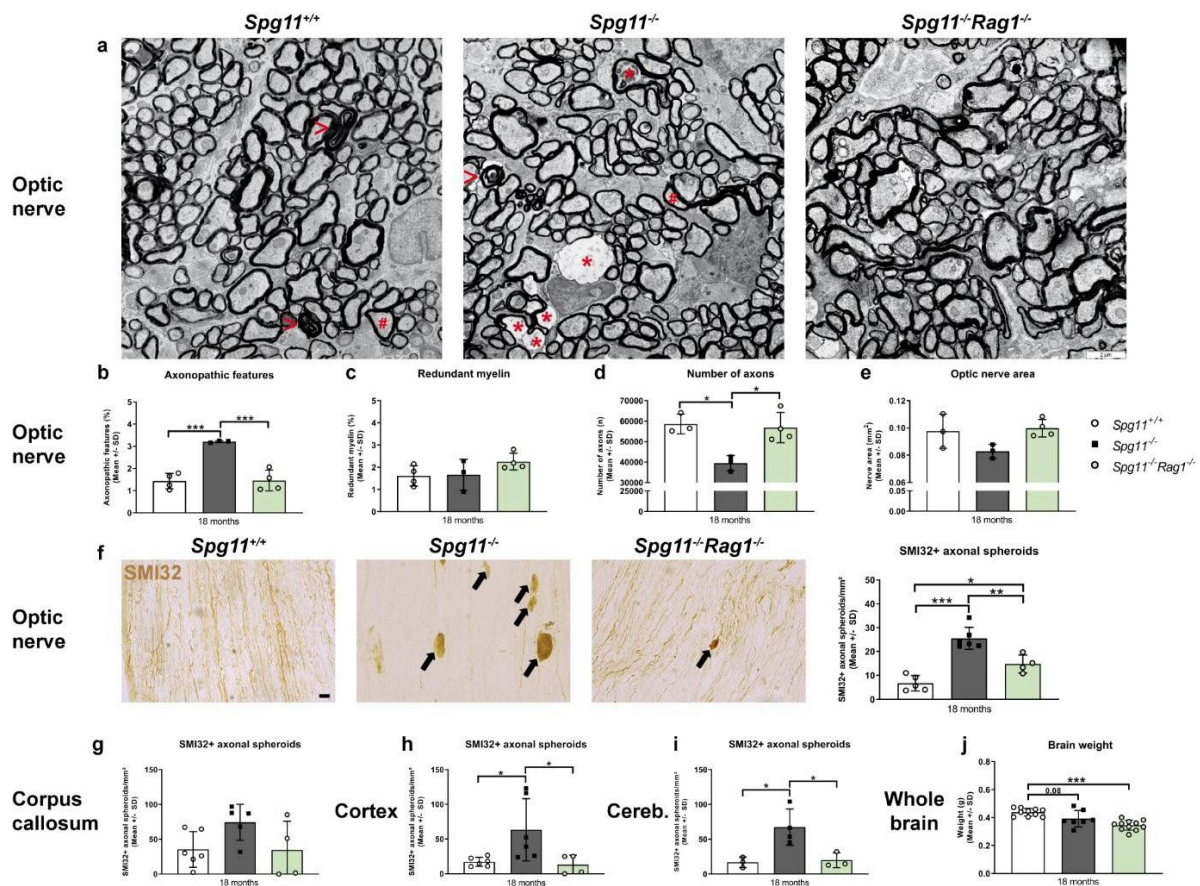
Figure 18: *Rag1*-deficiency reduces neural damage in the CNS of *Spg11*$^{-/-}$ mice.
(**a**) Representative electron micrographs of ON cross sections of 18-month-old *Spg11*$^{+/+}$, *Spg11*$^{-/-}$ and *Spg11*$^{-/-}$*Rag1*$^{-/-}$ mice, and (**b − e**) EM-based quantification of pathological alterations. Asterisks indicate axonopathic features, hashtags axons with redundant myelin, open arrowheads myelin fragments. Scale bar: 2 µm. (**b**) *Rag1*-deficiency reduces axonopathic features, typically occurring in *Spg11*$^{-/-}$ mice. (**c**) At this age, redundant myelin is not changed in either genotype. (**d**) *Rag1*-deficiency increases number of axons. (**e**) ON area remains preserved. (**f**) Representative images of SMI32$^+$ axonal spheroids (arrows) in longitudinal ON sections of 18-month-old *Spg11*$^{+/+}$, *Spg11*$^{-/-}$ and *Spg11*$^{-/-}$*Rag1*$^{-/-}$ mice (left) and corresponding quantification (right). Scale bar: 10 µm. *Rag1*-deficiency reduces the formation of SMI32$^+$ axonal spheroids, typically occurring in *Spg11*$^{-/-}$ mice. (**g**) Quantification of SMI32$^+$ axonal spheroids in coronal sections of CC, (**h**) CO and (**i**) CB of 18-month-old *Spg11*$^{+/+}$, *Spg11*$^{-/-}$ and *Spg11*$^{-/-}$*Rag1*$^{-/-}$ mice. *Rag1*-deficiency prevents the increased number of SMI32$^+$ axonal spheroids, typically present in *Spg11*$^{-/-}$ mice. (**j**) *Rag1*-deficiency does not dampen brain weight decline, typically occurring in *Spg11*$^{-/-}$ mice. Error bars represent standard deviations (circles, squares = mean value of one mouse). Significance of *Spg11*$^{-/-}$*Rag1*$^{-/-}$ mice compared to *Spg11*$^{+/+}$ and *Spg11*$^{-/-}$ mice are determined by one-way ANOVA and Tukey's post hoc test (*p < 0.05, **p < 0.01, ***p < 0.001). Corresponding data from *Spg11*$^{+/+}$ and *Spg11*$^{-/-}$ mice, as shown in figure 7, are presented here again.

Surprisingly, even though *Rag1*-deficiency restored the densities of RBPMS$^+$ RGCs, retinal thinning, typically detected in *Spg11*$^{-/-}$ mice, was not ameliorated (Figure 19a, b). Of note, visual acuity remained unaffected by *Rag1*-deficiency (data not shown).
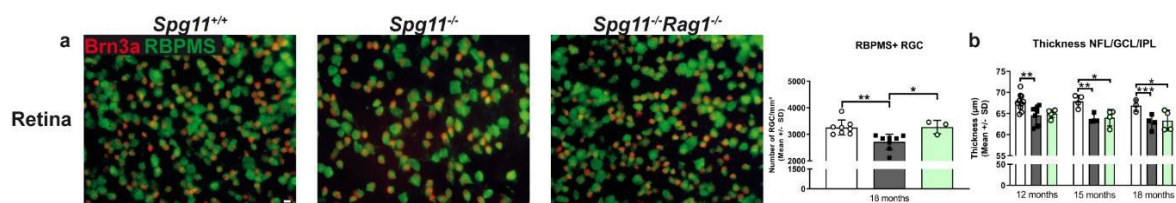
Figure 19: *Rag1*-deficiency restores the densities of RBPMS⁺ RGCs while retinal thinning remains unaffected.
(**a**) Representative images of Brn3a/RBPMS⁺ RGCs in whole-mount retinae of 18-month-old *Spg11⁺/⁺*, *Spg11⁻/⁻* and *Spg11⁻/⁻Rag1⁻/⁻* mice (left) and corresponding quantification (right). Scale bar: 50 µm. *Rag1*-deficiency restores the densities of RBPMS⁺ RGC. Most RBPMS⁺ cells are Brn3a⁺. (**b**) Longitudinal analysis of the thickness of the innermost retinal composite layer (NFL/GCL/IPL) of *Spg11⁺/⁺, Spg11⁻/⁻* and *Spg11⁻/⁻Rag1⁻/⁻* mice by OCT. *Rag1*-deficiency does not reduce retinal thinning of *Spg11⁻/⁻* mice. Error bars represent standard deviations (circles, squares = mean value of one mouse). Significance of *Spg11⁻/⁻Rag1⁻/⁻* mice compared to *Spg11⁺/⁺* and *Spg11⁻/⁻* mice is determined by one-way ANOVA and Tukey's post hoc test (*$p < 0.05$, **$p < 0.01$, ***$p < 0.001$). Corresponding data from *Spg11⁺/⁺* and *Spg11⁻/⁻* mice, as shown in figure 8, are presented here again.

Regarding the innate immune system, even though *Rag1*-deficiency did not reduce the overall number of microglia, we could see a clear reduction of microglial activation in the ON, CC and CB of 18-month-old *Spg11⁻/⁻Rag1⁻/⁻* mice compared to *Spg11⁻/⁻* mice (Figure 20a – h). Of note, the number of Sn⁺ microglia was generally low in CO compared to the other investigated compartments (Figure 20f).
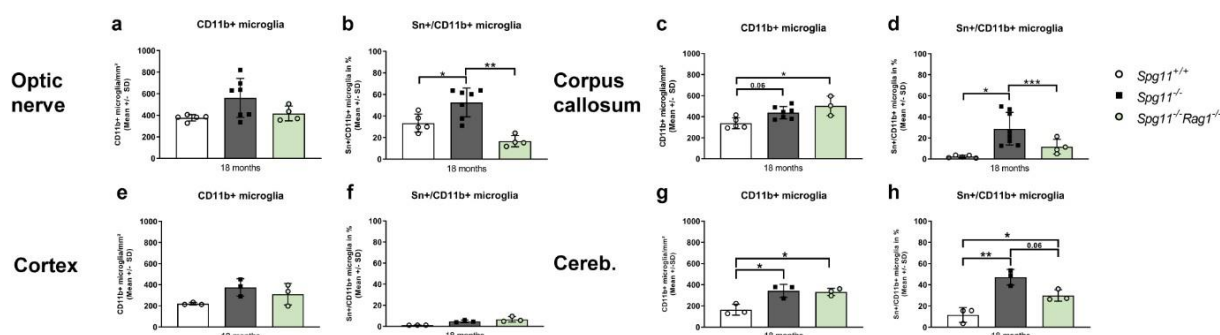
Figure 20: *Rag1*-deficiency leads to reduced expression of the microglial activation marker Sn in the CNS of *Spg11⁻/⁻* mice.
(**a, c, e, g**) Quantification of CD11b⁺ cells in distinct CNS compartments of 18-month-old *Spg11⁺/⁺*, *Spg11⁻/⁻* and *Spg11⁻/⁻Rag1⁻/⁻* mice. *Rag1*-deficiency does not reduce the number of CD11b⁺ cells in (**a**) longitudinal ON sections, or coronal sections of (**c**) CC, (**e**) CO, or (**g**) CB. (**b, d, f, h**) *Rag1*-deficiency reduces the percentage of CD11b⁺ cells showing the microglial activation marker Sn in (**b**) ON, (**d**) CC and (**h**) CB, but not in (**f**) CO where Sn⁺ microglial cells are generally rare. Error bars represent the standard deviations (circles, squares = mean value of one mouse). Significance of *Spg11⁻/⁻Rag1⁻/⁻* mice compared to *Spg11⁺/⁺* and *Spg11⁻/⁻* mice is determined by one-way ANOVA and Tukey's post hoc test (*$p < 0.05$, **$p < 0.01$, ***$p < 0.001$). Corresponding data from *Spg11⁺/⁺* and *Spg11⁻/⁻* mice, as shown in figure 6, are presented here again.

While lymphocytes were absent in *Spg11⁺/⁺Rag1⁻/⁻* mice (data not shown), *Rag1*-deficiency did not alter the number of SMI32⁺ axonal spheroids or the number or activation status of microglial

cells in the ON (Figure 21a – c). The number of RBPMS$^+$ RGCs in the retina of 18-month-old
Spg11$^{+/+}$ mice remained unchanged by *Rag1*-deficiency (Figure 21d).
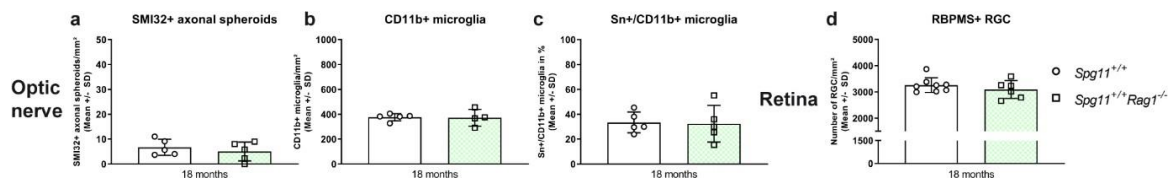
Figure 21: *Rag1*-deficiency does not affect histopathology of *Spg11$^{+/+}$* mice.
(a – c) Quantification of SMI32$^+$ axonal spheroids, CD11b$^+$ microglia, and microglial activation status in longitudinal ON sections of 18-month-old *Spg11$^{+/+}$* and *Spg11$^{+/+}$Rag1$^{-/-}$* mice. **(a)** *Rag1*-deficiency does not alter the number of SMI32$^+$ axonal spheroids, **(b)** CD11b$^+$ microglia or **(c)** microglial activation status. **(d)** Quantification of RBPMS$^+$ RGCs in whole-mount retinae of 18-month-old *Spg11$^{+/+}$* and *Spg11$^{+/+}$Rag1$^{-/-}$* mice. *Rag1*-deficiency does not alter the number RBPMS$^+$ RGCs. Most RBPMS$^+$ RGCs are Brn3a$^+$. Error bars represent the standard deviations (circles, squares = mean value of one mouse). Significance of *Spg11$^{+/+}$Rag1$^{-/-}$* mice compared to *Spg11$^{+/+}$* is determined by Two-tailed Student's t-test. Corresponding data from *Spg11$^{+/+}$* mice, as shown in figure 6, 7 and 8, are presented here again.

The previously presented data strengthened our hypothesis that secondary inflammation does play a role in the development of axonopathic features and neuronal loss in our mouse model for SPG11 and led us to the question whether lack of lymphocytes could also lead to an improved functional phenotype, typically disturbed in *Spg11$^{-/-}$* mice.

5.6 Genetic inactivation of the adaptive immune system ameliorates gait coordination of *Spg11$^{-/-}$* mice

As an important clinical read-out, we wanted to investigate whether the amelioration of the histopathological abnormalities in the CNS of *Spg11$^{-/-}$* mice by *Rag1*-deficiency led to functional improvement. Therefore, we investigated the walking pattern of *Spg11$^{-/-}$Rag1$^{-/-}$* mice at 6 and 18 months of age (Figure 22).

Indeed, *Rag1*-deficiency led to a substantial improvement of the altered walking pattern, typically detected in *Spg11$^{-/-}$* mice and rescued the abnormalities in gait coordination (Figure 22a – g). While the paw angle movement vector variation and the regularity index of *Spg11$^{-/-}$* mice was restored to wt levels at 18 months (Figure 22c, g), the paw angle body axis variation, the step cycle variation and the print position was corrected at 6 and 18 months (Figure 22d – f). However, parameters reflecting strength remained unaffected by *Rag1*-deficiency (Figure 22h – j).
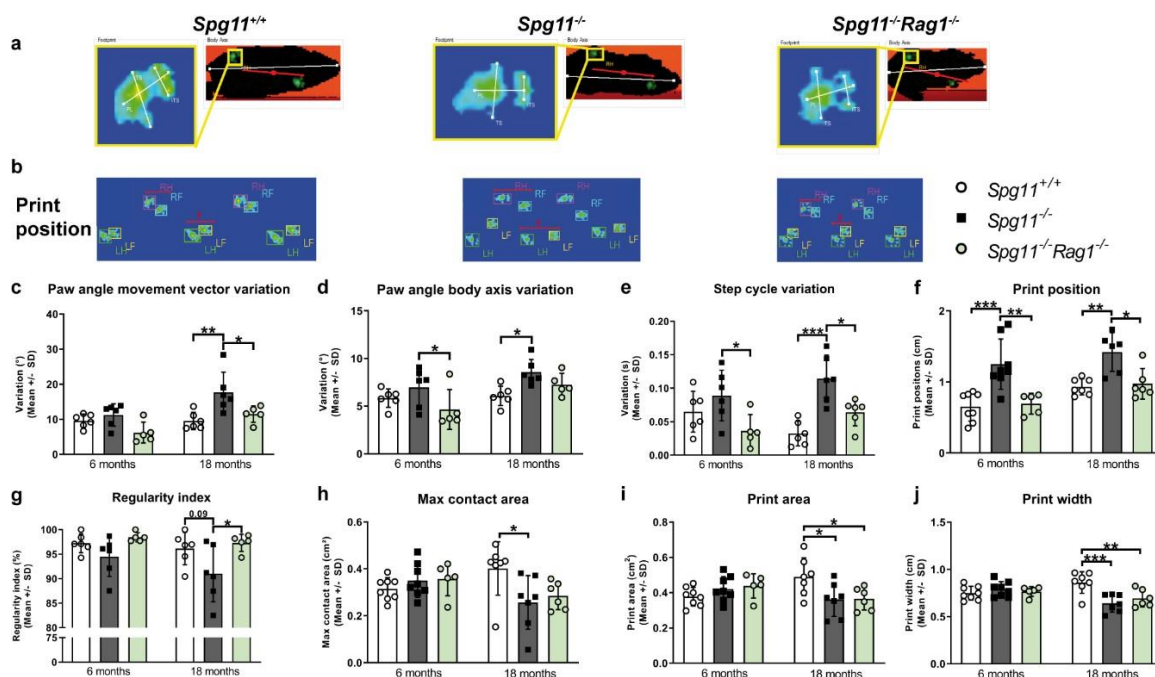
Figure 22: *Rag1*-deficiency improves gait coordination of *Spg11⁻ᐟ⁻* mice.

(a) Representative images of body contour, footprints and (b) print positions of 18-month-old *Spg11⁺ᐟ⁺*, *Spg11⁻ᐟ⁻* and *Spg11⁻ᐟ⁻Rag1⁻ᐟ⁻* mice while crossing the CatWalk device (ITS: intermediate toe spread; TS: toe spread; PL: print length; RF: right front paw; LF: left front paw; RH: right hind paw; LH: left hind paw). Red line (top) indicates the body axis, red line segment (bottom) indicates print position. (c) In *Spg11⁻ᐟ⁻* mice, *Rag1*-deficiency ameliorates the paw angle movement vector variation at 18 months, (d) the paw angle body axis variation at 6 months and (e) the step cycle variation at 6 and 18 months. (f) In *Spg11⁻ᐟ⁻* mice, *Rag1*-deficiency corrects the print position at 6 and 18 months, while (g) the regularity index, is corrected at 18 months. (h) In *Spg11⁻ᐟ⁻* mice, *Rag1*-deficiency does not affect the maximal contact area, (i) the print area, or (j) the print width of the hind paws. Error bars represent the standard deviations (circles, squares = mean value of three consecutive runs of one mouse). Significance of *Spg11⁻ᐟ⁻Rag1⁻ᐟ⁻* mice compared to *Spg11⁺ᐟ⁺* and *Spg11⁻ᐟ⁻* mice is determined by one-way ANOVA and Tukey's post hoc test (*$p < 0.05$, **$p < 0.01$, ***$p < 0.001$). Corresponding data from *Spg11⁺ᐟ⁺* and *Spg11⁻ᐟ⁻* mice, as shown in figure 9, are presented here again.

Even though *Rag1*-deficiency corrected the stride length and number of steps of *Spg11⁻ᐟ⁻* mice at 6 months, there was no rescuing effect at 18 months (Figure 23a, b). The number of steps needed to cross the walkway was unexpectantly increased in 18-month-old *Spg11⁻ᐟ⁻Rag1⁻ᐟ⁻* mice compared to both, wt and *Spg11⁻ᐟ⁻* mice (Figure 23b).
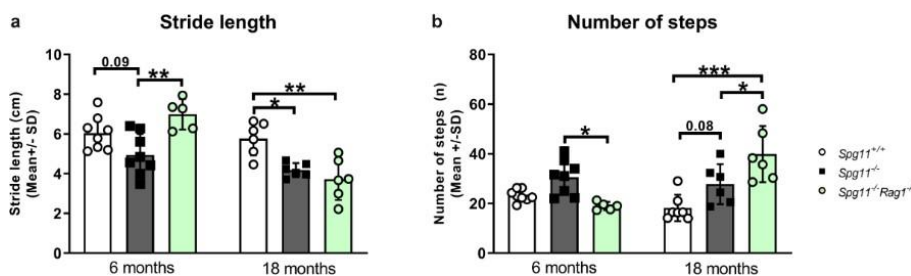
Figure 23: *Rag1*-deficiency fails to improve selected gait abnormalities of 18-month-old *Spg11⁻ᐟ⁻* mice.

(a) *Rag1*-deficiency restores the stride length of *Spg11⁻ᐟ⁻* mice to wt levels at 6 but not 18 months.
(b) *Rag1*-deficiency restores the number of steps needed to cross the walkway of *Spg11⁻ᐟ⁻* mice to wt

levels at 6 months, while this parameter is unexpectedly increased at 18 months. Error bars represent the standard deviations (circles, squares = mean value of three consecutive runs of one mouse). Significance of *Spg11⁻/⁻Rag1⁻/⁻* mice compared to *Spg11⁺/⁺* and *Spg11⁻/⁻* mice is determined by one-way ANOVA and Tukey's post hoc test (*$p < 0.05$, **$p < 0.01$, ***$p < 0.001$). Corresponding data from *Spg11⁺/⁺* and *Spg11⁻/⁻* mice, as shown in figure 10, are presented here again.

Of note, while *Rag1*-deficiency did not change most gait parameters of 18-month-old *Spg11⁺/⁺* mice (Figure 24a – h), it led to a small but significant increase in the number of steps needed to cross the walkway, which was accompanied by a tendency towards a lower stride length (Figure 24i, j), resembling the unexpected finding in *Spg11⁻/⁻Rag1⁻/⁻* mice.
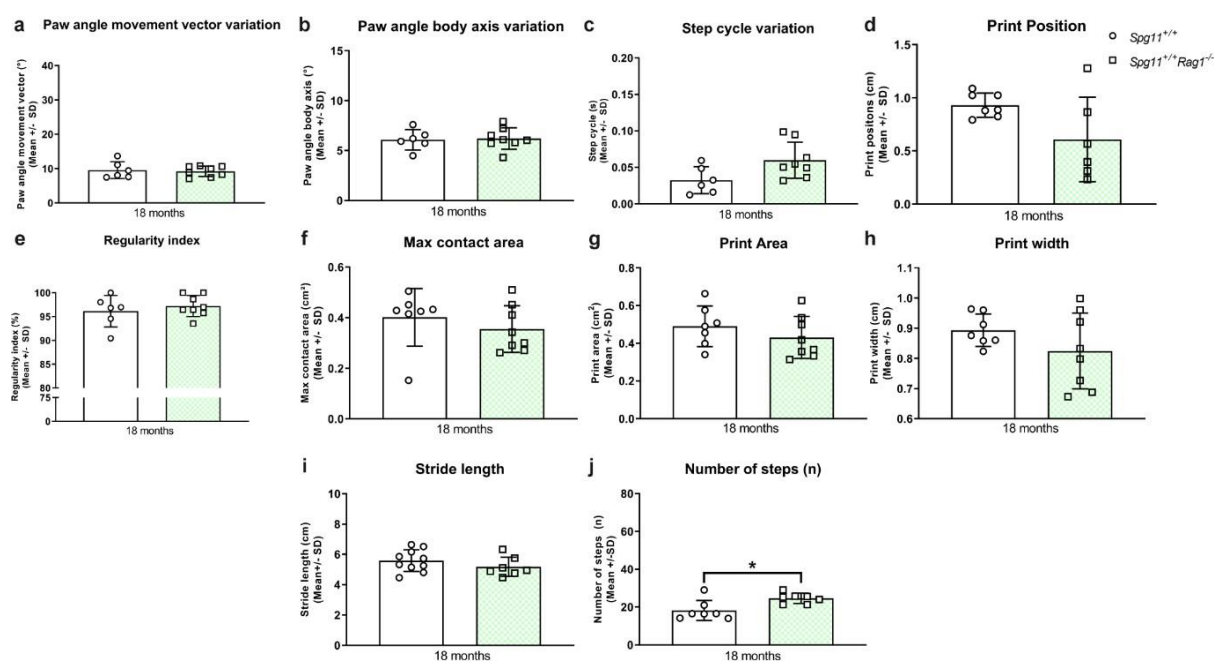
Figure 24: *Rag1*-deficiency increases the number of steps needed to cross the walkway of *Spg11⁺/⁺* mice.
(a) *Rag1*-deficiency does not alter the paw angle movement vector variation, **(b)** the paw angle body axis variation, **(c)** the step cycle variation, **(d)** the print position, **(e)** the regularity index, or **(f)** the maximal contact area, **(g)** the print area, and **(h)** the print width of the hind paws of *Spg11⁺/⁺* mice. **(i)** *Rag1*-deficiency leads to a tendency towards a lower stride length of *Spg11⁺/⁺* mice, **(j)** which in turn leads to a significant increase in the number of steps needed to cross the walkway. Error bars represent the standard deviations (circles, squares = mean value of three consecutive runs of one mouse). Significance of *Spg11⁺/⁺Rag⁻/⁻* mice compared to *Spg11⁺/⁺* mice is determined by Two-tailed Student's t-test. Corresponding data from *Spg11⁺/⁺* mice, as shown in figure 9 and 10, are presented here again.

Interestingly, while *Rag1*-deficiency dampened body weight loss of male *Spg11⁻/⁻* mice from 12 months onwards, leading to a significantly increased body weight at 18 months, it did not affect the body weight of female *Spg11⁻/⁻* mice (Figure 25a, b).
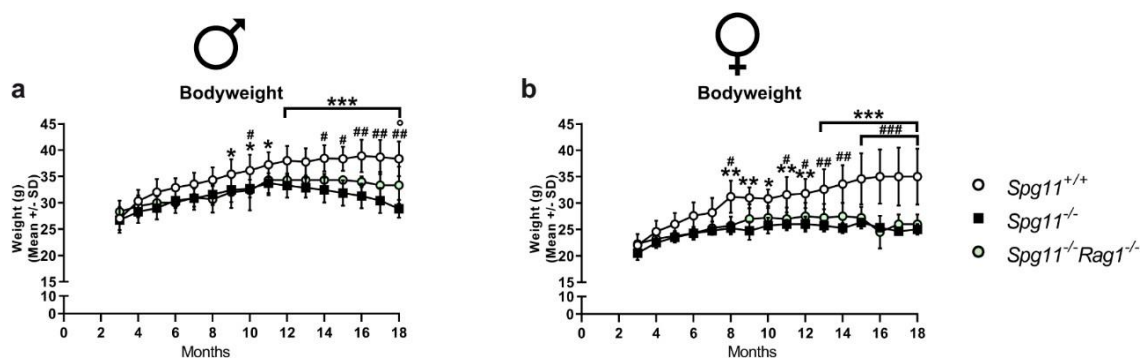
Figure 25: *Rag1*-deficiency dampens body weight loss of male but not female *Spg11*^{-/-} mice.
(a) Body weight of male *Spg11*^{+/+}, *Spg11*^{-/-} and *Spg11*^{-/-}*Rag1*^{-/-} mice starting from 3 months. *Rag1*-deficiency dampens body weight loss of male *Spg11*^{-/-} mice from 12 months onwards. **(b)** Body weight of female *Spg11*^{+/+}, *Spg11*^{-/-} and *Spg11*^{-/-}*Rag1*^{-/-} mice starting from 3 months. *Rag1*-deficiency does influence body weight of female *Spg11*^{-/-} mice. Error bars represent standard deviations (circles, squares = mean value of one age point). Significance of *Spg11*^{-/-}*Rag1*^{-/-} compared to *Spg11*^{+/+} and *Spg11*^{-/-} mice is determined by two-way ANOVA with multiple comparisons. Stars (*) indicate the significance of *Spg11*^{-/-} mice compared to *Spg11*^{+/+} mice (*$p < 0.05$, **$p < 0.01$, ***$p < 0.001$). Hashtags (#) indicate the significance of *Spg11*^{-/-}*Rag1*^{-/-} mice compared to *Spg11*^{+/+} mice (#$p < 0.05$, ##$p < 0.01$, ###$p < 0.001$). Circles (°) indicate the significance of *Spg11*^{-/-}*Rag1*^{-/-} mice compared to *Spg11*^{-/-} mice (°$p < 0.05$). Corresponding data from *Spg11*^{+/+} and *Spg11*^{-/-} mice, as shown in figure 11, are presented here again.

Of note, *Rag1*-deficiency did not alter the body weight of male or female *Spg11*^{+/+} mice (data not shown).

In summary, *Rag1*-deficiency ameliorated gait coordination of *Spg11*^{-/-} mice and dampened the body weight loss of male mutant mice, while features related to strength and stride length or body weight of female mice were not improved.

5.7 Genetic inactivation of the adaptive immune system ameliorates social behavior of *Spg11*^{-/-} mice

We next investigated whether *Rag1*-deficiency could ameliorate the behavioral abnormalities of *Spg11*^{-/-} mice, by using the previously described behavioral test battery (Figure 1).

As we have detected substantial abnormalities in social behavior of *Spg11*^{-/-} mice, we investigated the influence of *Rag1*-deficiency on these alterations. We found that *Rag1*-deficiency restored the social interest and novelty preference of male *Spg11*^{-/-} mice to wt levels at 18 months (Figure 26a – c). Interestingly, even though the social novelty preference was restored, the time spent with unfamiliar animals during the social novelty trial (trial 2) remained reduced (Figure 26d). To exclude the possibility that *Rag1*-deficiency alone changed behavioral aspects, *Spg11*^{+/+}*Rag1*^{-/-} mice were investigated. *Rag1*-deficiency did not affect the social interest or novelty behavior of male *Spg11*^{+/+} mice (Figure 26a – d).

Figure 26: *Rag1*-deficiency ameliorates social behavior of male *Spg11*^{-/-} mice.

(a) Representative images of social interest (trial 1, left) and novelty (trial 2, right) analysis of 18-month-old male *Spg11*^{+/+}(top row), *Spg11*^{+/+}*Rag1*^{-/-}(2nd row), *Spg11*^{-/-}(3rd row), and *Spg11*^{-/-}*Rag1*^{-/-} mice (bottom row). Light square indicates the center zone of the arena, green area indicates the border zone. Red line represents the walking track. Mouse 1 indicates in which cage the first unfamiliar mouse is placed, mouse 2 in which second unfamiliar mouse is placed. (b) Social interest and novelty preference in 6-, 12- and 18-month-old and (c) 18-month-old (enlarged) male mice. *Rag1*-deficiency restores social interest and novelty preference of 18-month-old male *Spg11*^{-/-} mice. Chance indicates equal time spent with the empty cage/animals (50%). (d) *Rag1*-deficiency does not alter the time spent with animal of male *Spg11*^{-/-} mice. *Rag1*-deficiency does not alter the social behavior of male *Spg11*^{+/+}mice. Error bars represent standard deviations (circles, squares = value of one mouse). Significance of *Spg11*^{+/+}*Rag1*^{-/-} compared to *Spg11*^{+/+}and *Spg11*^{-/-} mice, and significance of *Spg11*^{-/-}*Rag1*^{-/-} compared to *Spg11*^{+/+}and *Spg11*^{-/-} mice is determined by one-way ANOVA and Tukey's post hoc test (*$p < 0.05$, **$p < 0.01$, ***$p < 0.001$). Corresponding data from *Spg11*^{+/+}and *Spg11*^{-/-}mice, as shown in figure 12, are presented here again.

Rag1-deficiency did not only restore the social interest and novelty preference of female *Spg11*^{-/-} mice to wt levels (Figure 27a – c), but it also increased the time 18-month-old female mutant mice spent with the unfamiliar animals in the social interest (trial 1) and novelty trial (trial 2) (Figure 27d), hence, restoring the social behavior of female *Spg11*^{-/-} mice to wt levels. Of note, *Rag1*-deficiency did not alter the social interest or novelty behavior of female *Spg11*^{+/+} mice (Figure 27a – d).
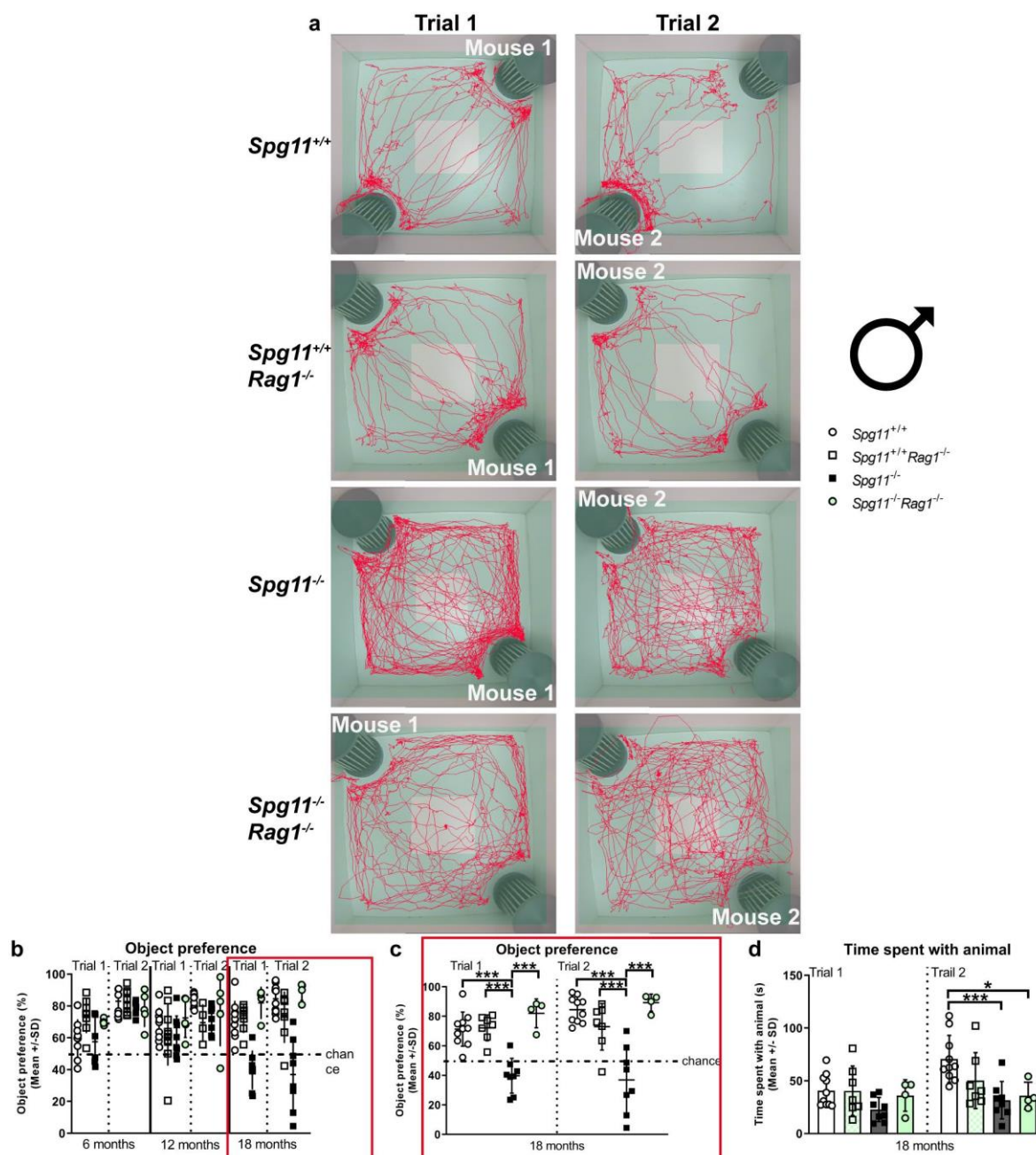

Figure 27: *Rag1*-deficiency ameliorates social behavior of female *Spg11*^{-/-} mice.
(**a**) Representative images of social interest (trial 1, left) and novelty (trial 2, right) analysis of 18-month-old female *Spg11*^{+/+} (top row), *Spg11*^{+/+}*Rag1*^{-/-} (2nd row), *Spg11*[-/-](3rd row), and *Spg11*^{-/-}*Rag1*^{-/-} mice (bottom row). Light square indicates the center zone of the arena, green area indicates the border zone. Red line represents the walking track. Mouse 1 indicates in which cage the first unfamiliar mouse is placed, mouse 2 in which the second unfamiliar mouse is placed. (**b**) Social interest and novelty

preference in 6-, 12- and 18-month-old and **(c)** 18-month-old (enlarged) female mice. *Rag1*-deficiency restores social interest and novelty preference in 18-month-old female *Spg11⁻/⁻* mice. Chance indicates equal time spent with the empty cage/animals (50%). **(d)** *Rag1*-deficiency increases the time female *Spg11⁻/⁻* mice spend with the unfamiliar animals in the social interest (trial 1) and novelty trial (trial 2). Of note, *Rag1*-deficiency does not alter the social behavior of female *Spg11⁺/⁺* mice. Error bars represent standard deviations (circles, squares = value of one mouse). Significance of *Spg11⁺/⁺Rag1⁻/⁻* compared to *Spg11⁺/⁺* and *Spg11⁻/⁻* mice, and significance of *Spg11⁻/⁻Rag1⁻/⁻* compared to *Spg11⁺/⁺* and *Spg11⁻/⁻* mice is determined by one-way ANOVA and Tukey's post hoc test ($*p < 0.05$, $**p < 0.01$, $***p < 0.001$). Corresponding data from *Spg11⁺/⁺* and *Spg11⁻/⁻* mice, as shown in figure 13, are presented here again.

Next, we investigated if *Rag1*-deficiency had an impact on non-spatial, short-term memory formation and recognition using the NOR analysis (Figure 28). *Rag1*-deficiency did not alter memory formation and recognition in male or female *Spg11⁻/⁻* or *Spg11⁺/⁺* mice, as they showed the expected object preferences in the training (trial 1) and test trial (trial 2) (Figure 28a, b).
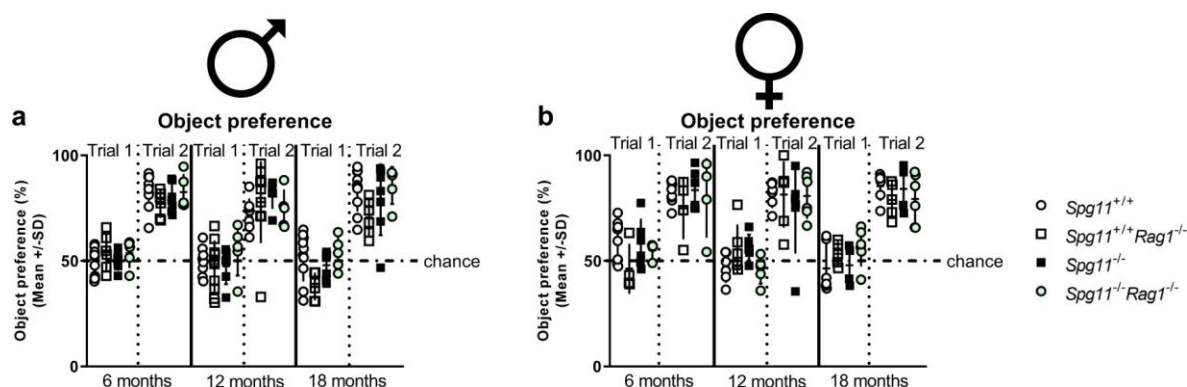
Figure 28: *Rag1*-deficiency does not alter object preference of *Spg11⁻/⁻* mice in NOR.
(a) *Rag1*-deficiency does not alter the object preference in NOR of male or **(b)** female *Spg11⁻/⁻* or *Spg11⁺/⁺* mice. Chance indicates equal time spent with both objects (50%). Error bars represent standard deviations (circles, squares = value of one mouse). Significance of *Spg11⁺/⁺Rag1⁻/⁻* compared to *Spg11⁺/⁺* and *Spg11⁻/⁻* mice, and significance of *Spg11⁻/⁻Rag1⁻/⁻* compared to *Spg11⁺/⁺* and *Spg11⁻/⁻* mice is determined by one-way ANOVA and Tukey's post hoc test. Corresponding data from *Spg11⁺/⁺* and *Spg11⁻/⁻* mice, as shown in figure 14, are presented here again.

The OF analysis revealed that *Rag1*-deficiency did not reduce hyperactivity-like behavior of male or female *Spg11⁻/⁻* mice (Figure 29). Surprisingly, male, and female *Spg11⁻/⁻Rag1⁻/⁻* mice walked a greater distance and showed a higher movement duration than *Spg11⁻/⁻* mice at 6 months (Figure 29a – c, f – h). While the walking distance and movement duration increased in *Spg11⁻/⁻* mice between 6 and 18 months, it remained unchanged in *Rag1*-deficient *Spg11⁻/⁻* mice, leading to similar values at 18 months (Figure 29a – c, f – h). *Rag1*-deficiency did not affect the time spent in the center zone (Figure 29d), or the time spent rearing of male *Spg11⁻/⁻* mice (Figure 29e). Female *Spg11⁻/⁻Rag1⁻/⁻* mice spent more time in the center zone compared to their wt littermates (Figure 29i), while the time spent rearing remained unaffected (Figure 29j). Of

note, *Rag1*-deficiency did not alter the behavior of male or female *Spg11*^{+/+} mice (Figure 29a – j).
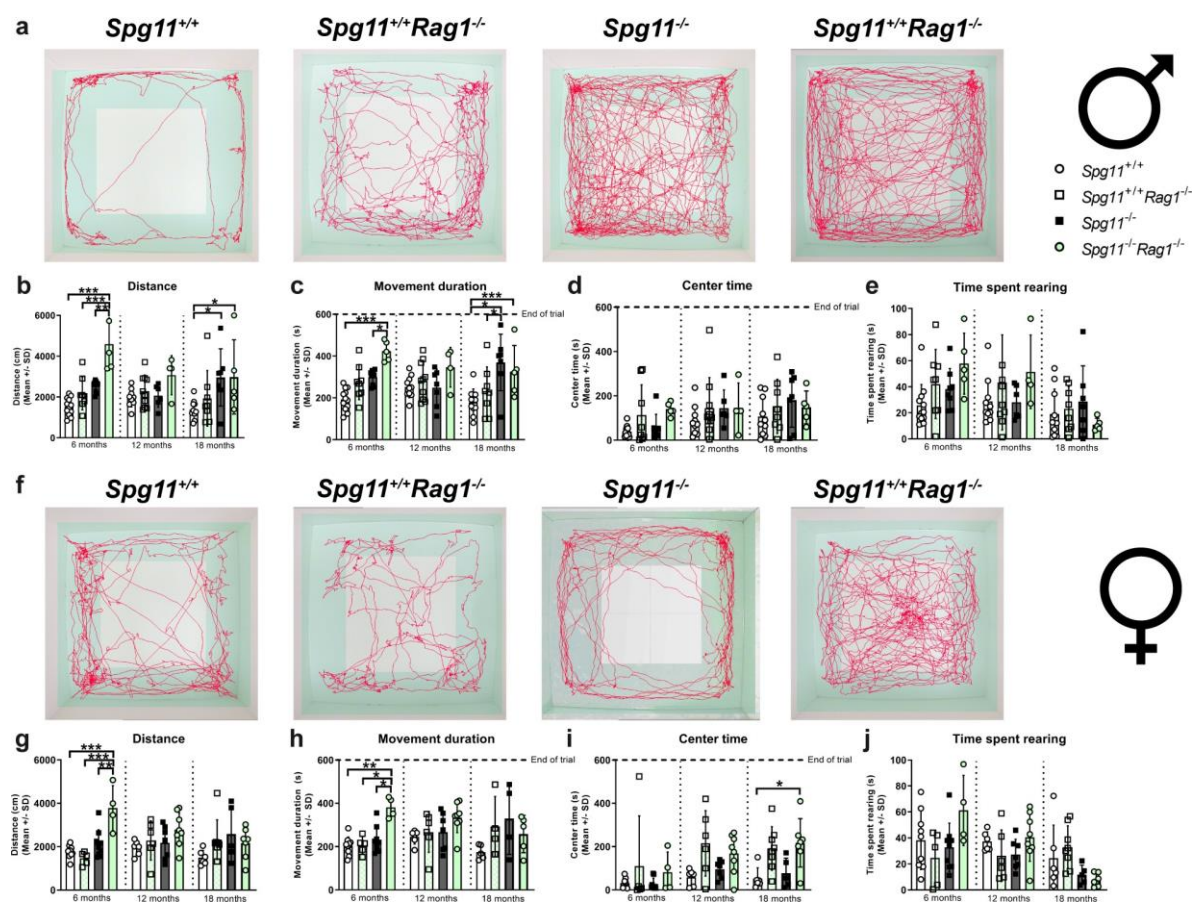
Figure 29: *Rag1*-deficiency does not ameliorate hyperactivity-like behavior of *Spg11*^{-/-} mice.

(**a**) Representative images of OF analysis of 18-month-old male *Spg11*^{+/+}, *Spg11*^{+/+}*Rag1*^{-/-}, *Spg11*^{-/-}, and *Spg11*^{-/-}*Rag1*^{-/-} mice. Light square indicates the center zone of the arena, green area indicates the border zone. Red line represents the walking track. (**b**) Male *Spg11*^{-/-}*Rag1*^{-/-} mice walk a greater distance than all other investigated groups at 6 months. *Rag1*-deficiency does not reduce the walking distance, typically increase in male *Spg11*^{-/-} mice, at 18 months. (**c**) Accordingly, male *Spg11*^{-/-}*Rag1*^{-/-} mice have a higher movement duration than all other investigated groups at 6 months. *Rag1*-deficiency does not reduce the movement duration, typically increased in male *Spg11*^{-/-} mice, at 18 months. (**d**) *Rag1*-deficiency does not alter the center time or (**e**) time spent rearing of male *Spg11*^{-/-} mice. Of note, *Rag1*-deficiency does not alter the behavior of male *Spg11*^{+/+} mice. (**f**) Representative images of OF analysis of 18-month-old female *Spg11*^{+/+}, *Spg11*^{+/+}*Rag1*^{-/-}, *Spg11*^{-/-}, and *Spg11*^{-/-}*Rag1*^{-/-} mice. Light square indicates the center zone of the arena, green area indicates the border zone. Red line represents the walking track. (**g**) Female *Spg11*^{-/-}*Rag1*^{-/-} mice walk a greater distance than all other investigated groups at 6 months, while there is no significant difference at the other investigated ages. (**h**) Accordingly, female *Spg11*^{-/-}*Rag1*^{-/-} mice have a higher movement duration than all other investigated groups at 6 months. (**i**) Female *Spg11*^{-/-}*Rag1*^{-/-} spend more time in the center zone of the arena compared to wt littermates at 18 months. (**j**) *Rag1*-deficiency does not alter the time spent rearing of female *Spg11*^{-/-} mice. Of note, *Rag1*-deficiency does not alter the behavior of female *Spg11*^{+/+} mice. Error bars represent standard deviations (circles, squares = value of one mouse). Significance of *Spg11*^{+/+}*Rag1*^{-/-} compared to *Spg11*^{+/+} and *Spg11*^{-/-} mice, and significance of *Spg11*^{-/-}*Rag1*^{-/-} compared to *Spg11*^{+/+} and *Spg11*^{-/-} mice is determined by one-way ANOVA and Tukey's post hoc test (*$p < 0.05$, **$p < 0.01$, ***$p < 0.001$). Corresponding data from *Spg11*^{+/+} and *Spg11*^{-/-} mice, as shown in figure 15, are presented here again.

Regarding the anxiety-related parameters, *Rag1*-deficiency did not lead to behavioral changes of male *Spg11*$^{-/-}$ mice (Figure 30a – e). While *Rag1*-deficiency did not alter the latency to enter the light compartment of female *Spg11*$^{-/-}$ mice (Figure 30g), it restored the walking distance, and time spent in the light compartment, typically increased in 18-month-old female *Spg11*$^{-/-}$ mice, to wt levels (Figure 30f, h, i). The time spent in the center zone remained unaffected by *Rag1*-deficiency (Figure 30j). Interestingly, *Rag1*-deficiency had distinct effects on male and female *Spg11*$^{+/+}$ mice. In male *Spg11*$^{+/+}$ mice, *Rag1*-deficiency led to a tendency towards an increased latency to enter the light compartment at 18 months, with multiple mice not entering the arena (Figure 30a, b). Consequently, they showed a tendency towards less walking distance and less time spent in the light compartment than their wt littermates, while the center time remained unaffected (Figure 30c – e). Female *Rag1*-deficient *Spg11*$^{+/+}$ mice walked less distance, and showed a tendency towards less time spent in the light compartment compared to their wt littermates at 6 months of age (Figure 30h, i), while the latency to enter and the center time remained unaffected (Figure 30 g, j).
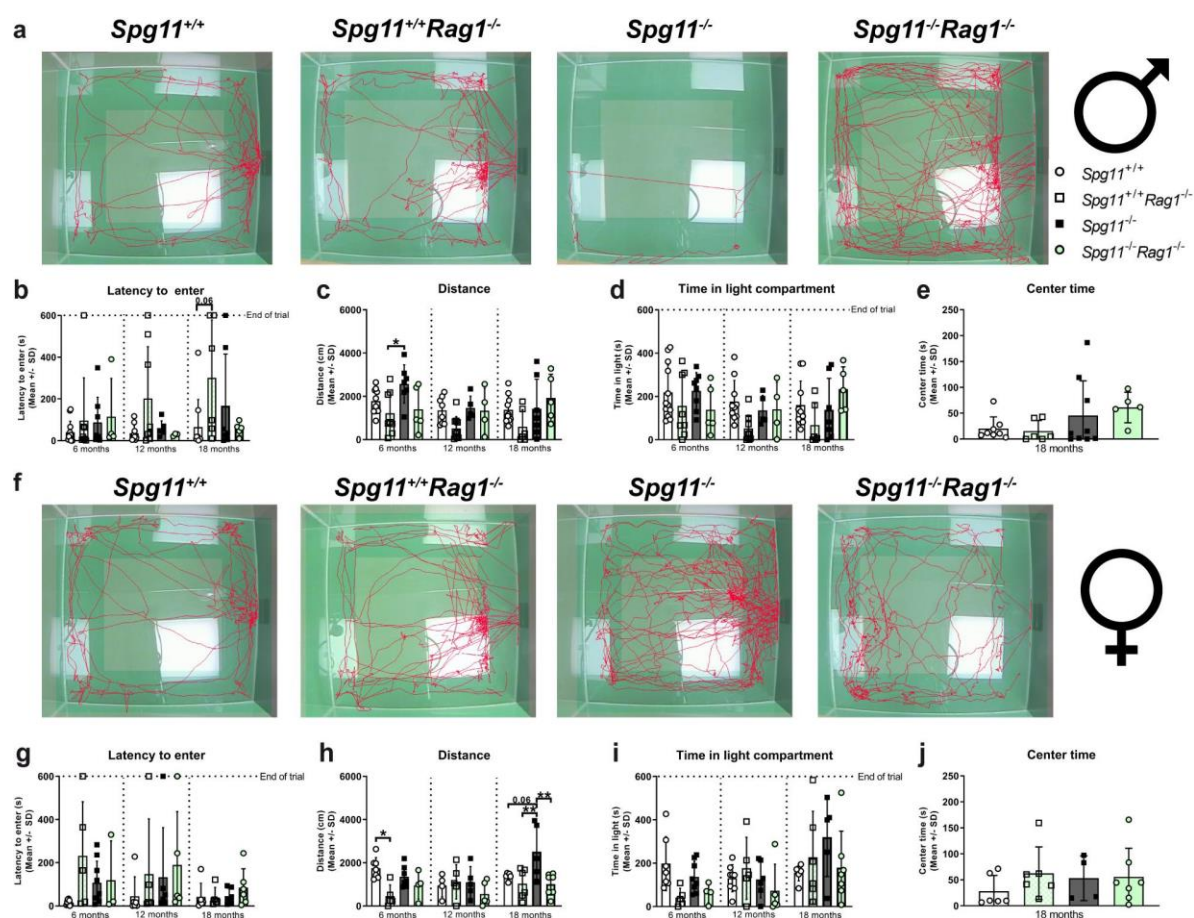
Figure 30: *Rag1*-deficiency restores anxiety-like behavior of female *Spg11*$^{-/-}$ mice.
(a) Representative images of DLB analysis of 18-month-old male *Spg11*$^{+/+}$, *Spg11*$^{+/+}$*Rag1*$^{-/-}$, *Spg11*$^{-/-}$, and *Spg11*$^{-/-}$*Rag1*$^{-/-}$ mice. Light square indicates the center zone of the arena. Red line represents the walking track. **(b – e)** *Rag1*-deficiency does not affect anxiety-like behavior of male *Spg11*$^{-/-}$ mice. **(b)** *Rag1*-deficiency increases the latency to enter and shows a tendency towards reduced **(c)** walking

distance and **(d)** time in light compartment of 18-month-old $Spg11^{+/+}$ mice. **(e)** $Rag1$-deficiency does not alter the center time of male mice. **(f)** Representative images of DLB analysis of 18-month-old female $Spg11^{+/+}$, $Spg11^{+/+}Rag1^{-/-}$, $Spg11^{-/-}$, and $Spg11^{-/-}Rag1^{-/-}$ mice. Light square indicates the center zone of the arena. Red line represents the walking track. **(g)** $Rag1$-deficiency does not change the latency to enter of female $Spg11^{-/-}$ mice. **(h)** $Rag1$-deficiency restores the walking distance and **(i)** time spent in light compartment, typically increased in 18-month-old female $Spg11^{-/-}$ mice. $Rag1$-deficiency decreases these parameters in 6-month-old female $Spg11^{+/+}$ mice. **(j)** $Rag1$-deficiency does not alter the center time of female mice. Error bars represent standard deviations (circles, squares = value of one mouse). Significance of $Spg11^{+/+}Rag1^{-/-}$ compared to $Spg11^{+/+}$ and $Spg11^{-/-}$ mice, and significance of $Spg11^{-/-}Rag1^{-/-}$ compared to $Spg11^{+/+}$ and $Spg11^{-/-}$ mice is determined by one-way ANOVA and Tukey's post hoc test (*$p < 0.05$, **$p < 0.01$). Corresponding data from $Spg11^{+/+}$ and $Spg11^{-/-}$ mice, as shown in figure 16, are presented here again.

$Rag1$-deficiency did not influence the walking distance of male or female $Spg11^{-/-}$ mice in the CAR analysis, resembling the findings of the OF analysis (Figure 31a, b, f, g). Interestingly, $Rag1$-deficiency reduced the time spent leaning over the edge of the platform, typically increased in 18-month-old male $Spg11^{-/-}$ mice (Figure 31c), showing the same tendency in female $Spg11^{-/-}Rag1^{-/-}$ mice (Figure 31h). However, it did not ameliorate the reduced latency to jump off the platform or the abnormal CAR of male or female $Spg11^{-/-}$ mice, at the same age (Figure 31d, e, i, j). Interestingly, male, and female $Rag1$-deficienct $Spg11^{-/-}$ mice showed an abnormal CAR already at 12 months of age, which was not present in $Spg11^{-/-}$ mice at this timepoint (Figure 31e, j). Surprisingly, $Rag1$-deficient male $Spg11^{+/+}$ mice also showed an abnormal CAR from 12 months of age onwards (Figure 31e). In contrast, $Rag1$-deficiency did not alter the impulsivity-like behavior of female $Spg11^{+/+}$ mice (Figure 31f – i).
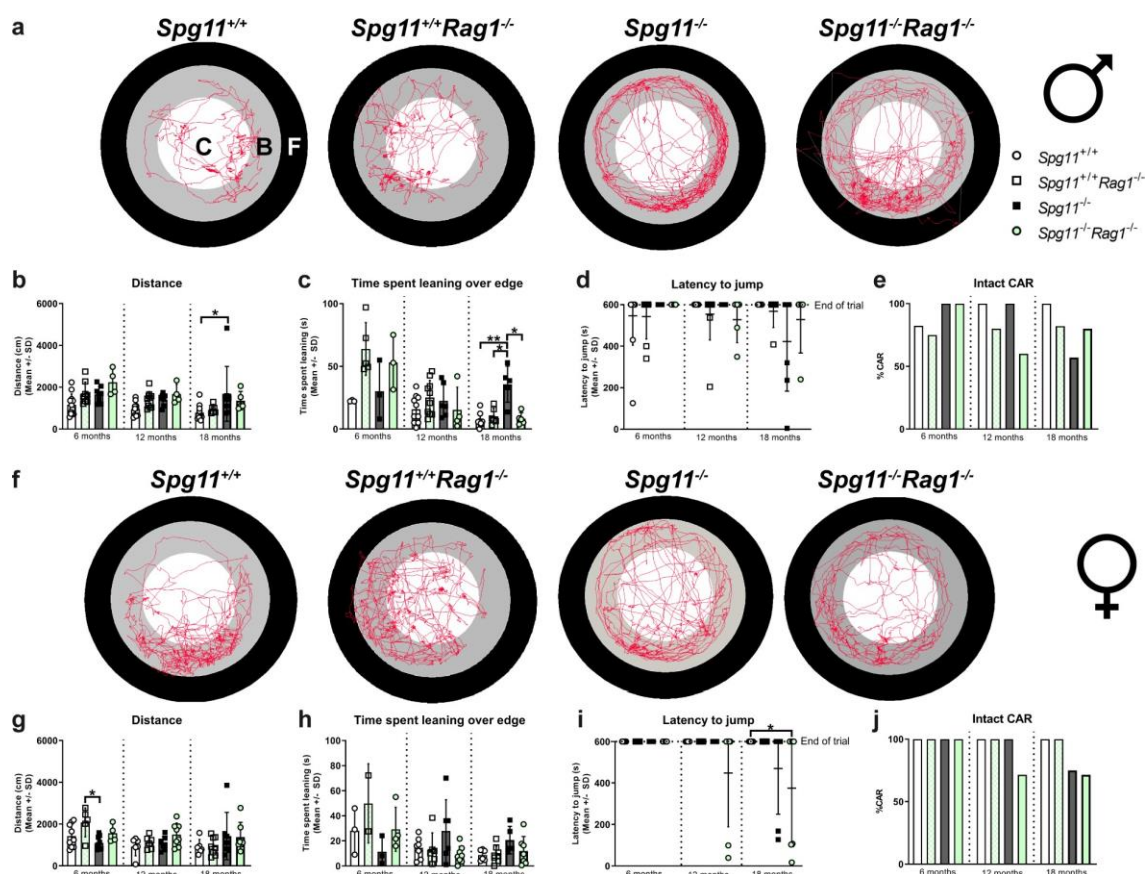
Figure 31: *Rag1*-deficiency reduces the time spent leaning over the edge of the platform of *Spg11^{-/-}* mice.
(a) Representative images of CAR analysis of 18-month-old male *Spg11^{+/+}*, *Spg11^{+/+}Rag1^{-/-}*, *Spg11^{-/-}*, and *Spg11^{-/-}Rag1^{-/-}* mice. Red line represents the walking track (C= center zone, white; B= border zone, grey; F = floor zone, black). (b) *Rag1*-deficiency does not affect the walking distance of male *Spg11^{-/-}* mice. (c) *Rag1*-deficiency reduces the time spent leaning over the edge of the platform of 18-month-old male *Spg11^{-/-}* mice. Of note, *Rag1*-deficiency does not alter these parameters in male *Spg11^{+/+}* mice. (d) *Rag1*-deficiency does not alter the latency to jump of male *Spg11^{-/-}* mice, while it is reduced in *Spg11^{+/+}Rag1^{-/-}* mice compared to wt mice at 12 and 18 months. (e) *Rag1*-deficient *Spg11^{-/-}* mice display an abnormal CAR compared to mutant mice at 12 months, while there is no difference at 18 months. *Spg11^{+/+}Rag1^{-/-}* mice display an abnormal CAR compared to wt mice at 12 and 18 months. (f) Representative images of CAR analysis of 18-month-old female *Spg11^{+/+}*, *Spg11^{+/+}Rag1^{-/-}*, *Spg11^{-/-}*, and *Spg11^{-/-} Rag1^{-/-}* mice. Red line represents the walking track. (g) *Rag1*-deficiency does not alter the walking distance of female *Spg11^{-/-}* mice. (h) *Rag1*-deficiency leads to a tendency towards reduced time spent leaning over edge of the platform of female *Spg11^{-/-}* mice. (i) *Rag1*-deficiency does not alter the latency to jump of female *Spg11^{-/-}* mice. (j) *Rag1*-deficiency leads to an abnormal CAR in 12-month-old *Spg11^{-/-}* mice, while there is no difference at 18 months. *Rag1*-deficiency does not affect female *Spg11^{+/+}* mice. Error bars represent standard deviations (circles, squares = value of one mouse). Significance of *Spg11^{+/+}Rag1^{-/-}* compared to *Spg11^{+/+}* and *Spg11^{-/-}* mice, and significance of *Spg11^{-/-}Rag1^{-/-}* compared to *Spg11^{+/+}* and *Spg11^{-/-}* mice is determined by one-way ANOVA and Tukey's post hoc test (*$p < 0.05$, **$p < 0.01$, ***$p < 0.001$). Corresponding data from *Spg11^{+/+}* and *Spg11^{-/-}* mice, as shown in figure 17, are presented here again.

The previously presented data indicate that *Rag1*-deficiency ameliorated the social behavior of male and female *Spg11^{-/-}* mice, showing even more pronounced effects for the latter group. Furthermore, *Rag1*-deficiency corrected the abnormal anxiety-like behavior, typically present in female *Spg11^{-/-}* mice. *Rag1*-deficiency did not reduce hyperactivity-like behavior of male or

female $Spg11^{-/-}$ mice. Interestingly, while $Rag1$-deficiency could ameliorate some aspects of impulsivity-like behavior others remained unaffected. Of note, while $Spg11^{+/+}$ mice remained mostly unaffected by $Rag1$-deficiency, $Spg11^{+/+}Rag1^{-/-}$ showed increase anxiety-like behavior. Taken together, these findings indicate that secondary inflammation does not only contribute to neuropathological and gait alterations but also, in part, to behavioral abnormalities.

5.8 Early treatment with clinically approved immunomodulators reduces neuroinflammation in white and grey matter compartments of the CNS, ameliorates neural damage and reduces walking pattern abnormalities of $Spg11^{-/-}$ mice

As shown above, the absence of an adaptive immune response led to a substantial amelioration of histopathological and clinical features, typically present in $Spg11^{-/-}$ mice. Therefore, we investigated whether we could ex ploit this finding to develop a possible treatment approach, by pharmacologically targeting lymphocytes as a likely clinically relevant translation of the genetic inactivation. We made use of already available and FDA-approved immunomodulators fingolimod (FTY720) and teriflunomide, both in use for treatment of MS (Bar-Or *et al.*, 2014; Melzer & Meuth, 2014). As a pharmacological proof-of-principle, we used an early treatment approach starting at 3 months of age (Figure 32).
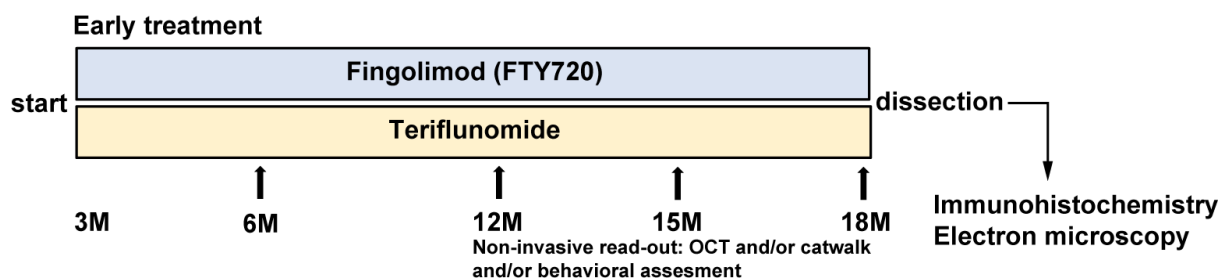
Figure 32: Treatment regime for early treatment of $Spg11^{-/-}$ mice with fingolimod or teriflunomide.
Schematic representation of the treatment regimens comprising early and late treatment using fingolimod (FTY720) or teriflunomide as medications in the drinking water. "Early treatment" starts at 3 months of age and lasted for 450 days. Non-invasive read-outs during the treatment are indicated by arrows, allowing longitudinal studies.

We first investigated whether treatment with the aforementioned immunomodulators led to a reduction in the number of T-lymphocytes (Figure 33). Indeed, treatment of $Spg11^{-/-}$ mice with either immunomodulator led to a significant reduction in the number of CD8$^+$ T-lymphocytes in the ON (Figure 33a), CC (Figure 33c), CO (Figure 33e), and CB (Figure 33g) at 18 months. The anyhow low number of CD4$^+$ T-lymphocytes showed only a non-significant, mild trend towards reduction by either treatment approach (Figure 33b, d, f, h).

Figure 33: Early treatment with fingolimod or teriflunomide reduces the number of CD8$^+$ T-lymphocytes in white and grey matter compartments of *Spg11$^{-/-}$* mice.

(a, c, e, g) Representative images of CD8$^+$ T-lymphocytes (arrows) in distinct CNS compartments of 18-month-old *Spg11$^{+/+}$*, *Spg11$^{-/-}$*, and *Spg11$^{-/-}$* mice after treatment with fingolimod (FTY720) or teriflunomide (left) and corresponding quantification (right). Nuclei are labeled with DAPI (blue). Scale bar: 10 µm. (a) CD8$^+$ T-lymphocytes in longitudinal sections of ON, and in coronal sections of (c) CC, (e) CO and (g) CB. Note that in all compartments treatment with either immunomodulator reduces the increased number of CD8$^+$ T-lymphocytes, typically present in *Spg11$^{-/-}$* mice. (b, d, f, h) Quantification of CD4$^+$ T-lymphocytes in distinct CNS compartments of 18-month-old *Spg11$^{+/+}$*, *Spg11$^{-/-}$*, and treated *Spg11$^{-/-}$* mice. (b) Note that treatment with either immunomodulator fails to significantly reduce the number of CD4$^+$ T-lymphocytes in ON, (d) CC, (f) CO, or (h) CB. Error bars represent the standard deviations (circles, squares, triangles = mean value of one mouse). Significance of treated *Spg11$^{-/-}$* mice compared to *Spg11$^{+/+}$* and *Spg11$^{-/-}$* mice is determined by one-way ANOVA and Tukey's post hoc test (*p < 0.05, **p < 0.01). Corresponding data from *Spg11$^{+/+}$* and *Spg11$^{-/-}$* mice, as shown in figure 3, are presented here again.

In the SC of *Spg11$^{-/-}$* mice, neither the relatively small number of CD8$^+$ nor CD4$^+$ T-lymphocytes responded to the early treatment approach (Figure 34a, b).
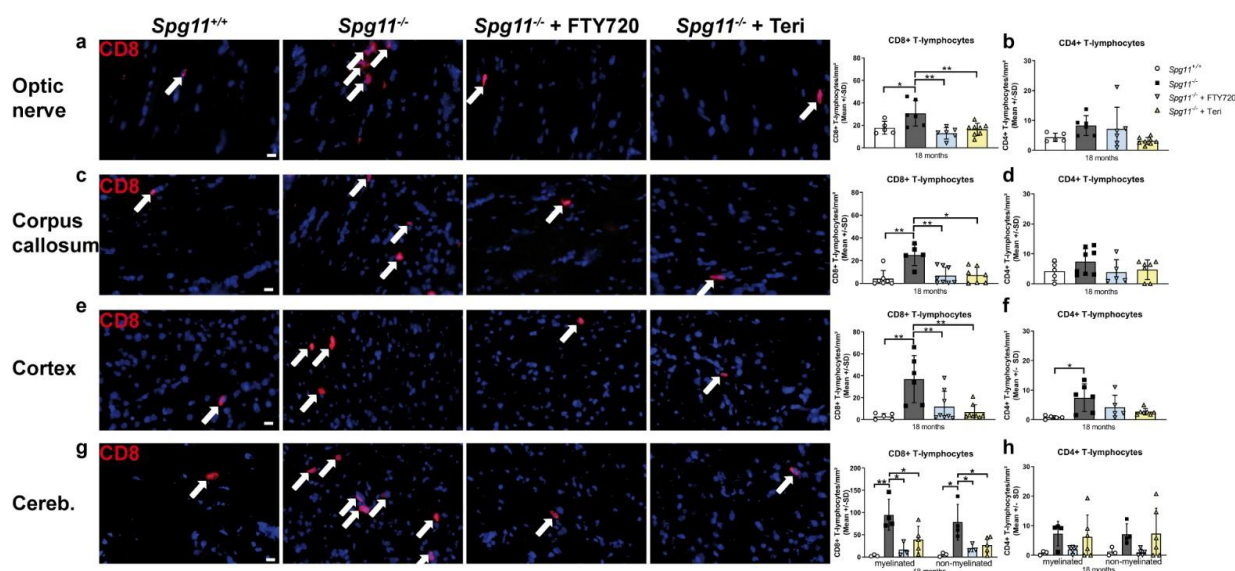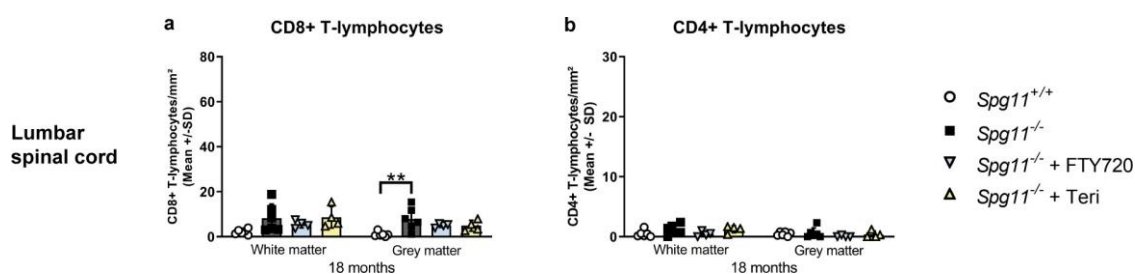

Figure 34: Early treatment with fingolimod or teriflunomide does not reduce the number of CD8$^+$ T-lymphocytes in SC of *Spg11$^{-/-}$* mice.

(a) Quantification of CD8$^+$ T-lymphocytes in coronal sections of SC of 18-month-old *Spg11$^{+/+}$*, *Spg11$^{-/-}$* and *Spg11$^{-/-}$* mice after treatment with fingolimod (FTY720) or teriflunomide. In SC of *Spg11$^{-/-}$* mice, treatment does not reduce the only mildly increased number of CD8$^+$ T-lymphocytes, typically present in *Spg11$^{-/-}$* mice. (b) Quantification of CD4$^+$ T-lymphocytes in SC of 18-month-old *Spg11$^{+/+}$*, *Spg11$^{-/-}$* and treated *Spg11$^{-/-}$* mice. In SC of *Spg11$^{-/-}$* mice, treatment does not affect the number of CD4$^+$ T-lymphocytes. Error bars represent the standard deviations (circles, squares, triangles = mean value of one mouse). Significance of treated *Spg11$^{-/-}$* mice compared to *Spg11$^{+/+}$* and *Spg11$^{-/-}$* mice is determined by one-way ANOVA and Tukey's post hoc test (**p < 0.01). Corresponding data from *Spg11$^{+/+}$* and *Spg11$^{-/-}$* mice, as shown in figure 4, are presented here again.

Of note, the impact of early treatment with fingolimod or teriflunomide on microglia was generally low (Figure 35a – j). The early treatment failed to reduce the mildly upregulated number of CD11b$^+$ microglia in ON, CC, CO, CB and white and grey matter of SC of 18-month-old *Spg11*$^{-/-}$ mice (Figure 35a, c, e, g, i). As opposed to *Rag1*-deficiency, early treatment did not lead to a reduction of microglial activation in these compartments at 18 months (Figure 35b, d, h, j). Of note, in CO, activated microglial cells were always rare (Figure 35f).
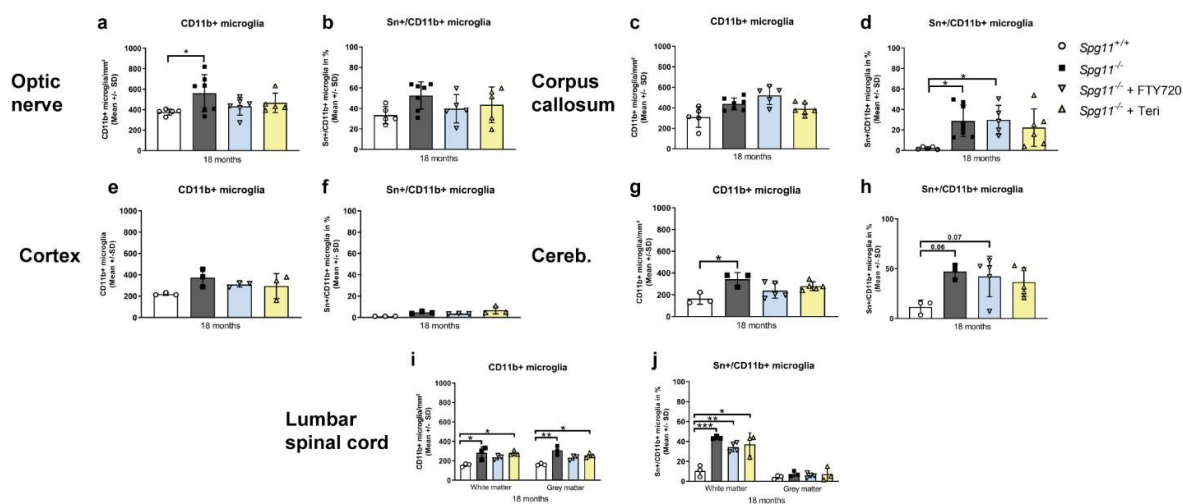
Figure 35: Early treatment with fingolimod or teriflunomide does not reduce microgliosis in the CNS of *Spg11*$^{-/-}$ mice.
(a, c, e, g, i) Quantification of the number of CD11b$^+$ cells, in longitudinal sections of **(a)** ON and in coronal sections of **(c)** CC, **(e)** CO, **(g)** CB and **(i)** SC of 18-month-old *Spg11*$^{+/+}$, *Spg11*$^{-/-}$ and *Spg11*$^{-/-}$ mice treated with fingolimod (FTY720) or teriflunomide. Treatment fails to reduce the increase in the number of CD11b$^+$ cells, typically occurring in *Spg11*$^{-/-}$ mice. **(b, d, f, h, j)** Percentage of CD11b$^+$ cells showing the microglial activation marker Sn in **(b)** ON, **(d)** CC, **(f)** CO, **(h)** CB and **(j)** SC of 18-month-old *Spg11*$^{+/+}$, *Spg11*$^{-/-}$ and treated *Spg11*$^{-/-}$ mice. In ON, CC, CB, and SC, treatment fails to reduce the increase of Sn$^+$ cells, typically occurring in *Spg11*$^{-/-}$ mice. In CO of *Spg11*$^{+/+}$, *Spg11*$^{-/-}$ and treated *Spg11*$^{-/-}$ mice, Sn$^+$ cells are rare. Error bars represent the standard deviations (circles, squares, triangles = mean value of one mouse). Significance of treated *Spg11*$^{-/-}$ mice compared to *Spg11*$^{+/+}$ and *Spg11*$^{-/-}$ mice is determined by one-way ANOVA and Tukey's post hoc test (*$p < 0.05$). Corresponding data from *Spg11*$^{+/+}$ and *Spg11*$^{-/-}$ mice, as shown in figure 6, are presented here again.

As we have seen that treatment with fingolimod or teriflunomide led to a substantial reduction in the number of CD8$^+$ T-lymphocytes, we wanted to investigate whether it could also ameliorate neural and axonal perturbation. Therefore, we investigated the different CNS compartments for histopathological alterations. Early treatment of *Spg11*$^{-/-}$ mice resulted in a reduction of axonopathic features in ON, as investigated by ultrastructural EM analysis (Figure 36a, b). Correspondingly, we detected a substantial reduction of axonal loss and ON atrophy, while redundant myelin was increased at 18 months of age (Figure 36c – e). The number of SMI32$^+$ axonal spheroids in ON, CC, CO, and CB was significantly reduced, corroborating the beneficial effect of the early treatment seen by EM (Figure 36f – i). Conversely, treatment with

fingolimod or teriflunomide did not dampen the brain weight decline of $Spg11^{-/-}$ mice, reminiscent of the finding in $Rag1$-deficient $Spg11^{-/-}$ mice (Figure 36j).
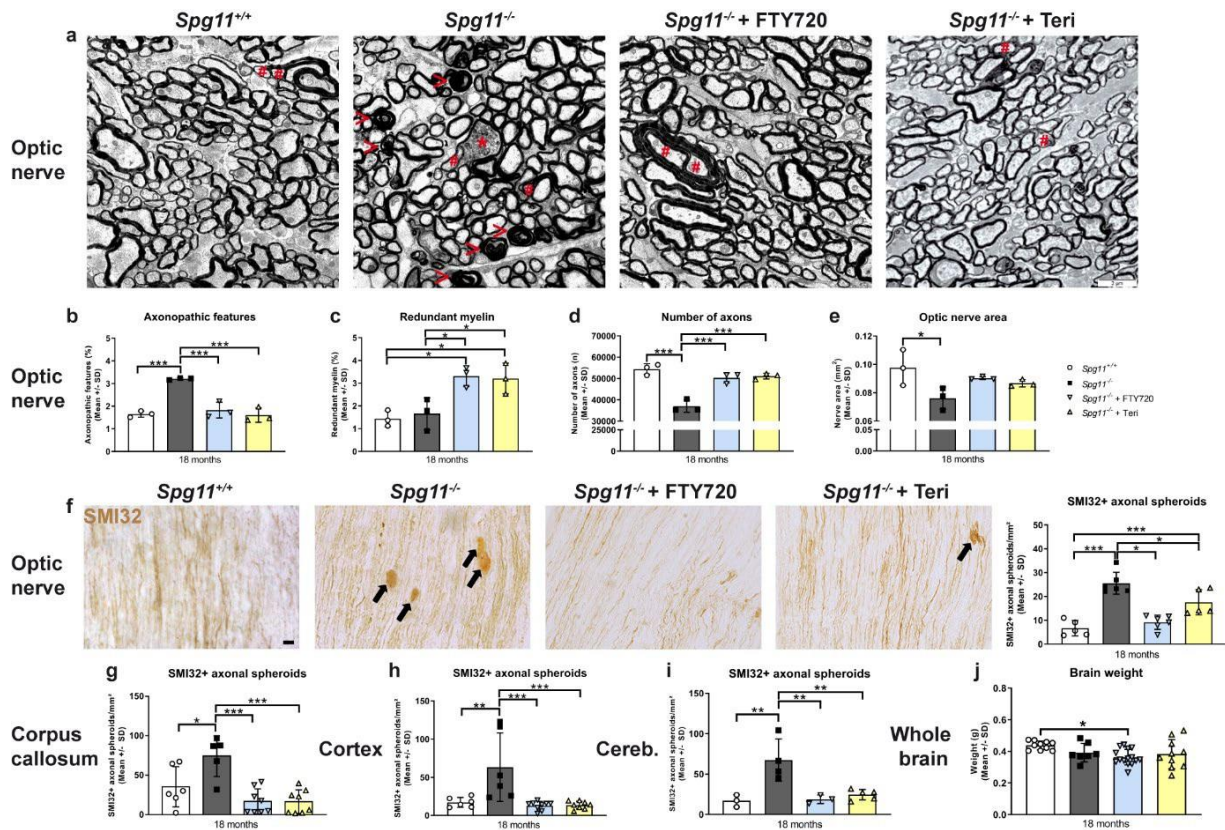
Figure 36: Early treatment with fingolimod or teriflunomide reduces neural damage in the CNS of $Spg11^{-/-}$ mice.

(a) Representative electron micrographs of ON cross sections of 18-month-old $Spg11^{+/+}$, $Spg11^{-/-}$, and $Spg11^{-/-}$ mice after treatment with fingolimod (FTY720) or teriflunomide and (b – e) EM-based quantification of pathological alterations. Asterisks indicate axonopathic features, hashtags axons with redundant myelin, open arrowheads myelin fragments. Scale bar: 2 µm. (b) Treatment reduces axonopathic features, typically occurring in $Spg11^{-/-}$ mice. (c) Redundant myelin becomes more frequent in $Spg11^{-/-}$ mice after treatment. (d) The number of axons and (e) ON area, typically reduced in $Spg11^{-/-}$ mice, are preserved after treatment. (f) Representative images of SMI32$^+$ axonal spheroids (arrows) in longitudinal ON sections of 18-month-old $Spg11^{+/+}$, $Spg11^{-/-}$, and treated $Spg11^{-/-}$ mice (left) and corresponding quantification (right). Scale bar: 10 µm. Treatment reduces the increase in the number of SMI32$^+$ axonal spheroids, typically occurring in $Spg11^{-/-}$ mice. (g) Quantification of SMI32$^+$ axonal spheroids in coronal sections of CC, (h) CO and (i) CB of $Spg11^{+/+}$, $Spg11^{-/-}$, and treated $Spg11^{-/-}$ mice. In all compartments, treatment reduces the increase in the number of SMI32$^+$ axonal spheroids, typically occurring in $Spg11^{-/-}$ mice. (j) Treatment does not dampen brain weight decline, typically occurring in $Spg11^{-/-}$ mice. Error bars represent the standard deviations (circles, squares, triangles = mean value of one mouse). Significance of treated mutant mice compared to $Spg11^{+/+}$ and $Spg11^{-/-}$ mice is determined by one-way ANOVA and Tukey's post hoc test (*$p < 0.05$, **$p < 0.01$, ***$p < 0.001$). Corresponding data from $Spg11^{+/+}$ and $Spg11^{-/-}$ mice, as shown in figure 7, are presented here again.

The mild loss of RGCs, typically occurring in $Spg11^{-/-}$ mice, was prevented by the early treatment with fingolimod or teriflunomide (Figure 37a). Interestingly, thinning of the inner retinal layers, as investigated by OCT, was not ameliorated in $Spg11^{-/-}$ mice, another parallel finding to the $Rag1$-deficient $Spg11^{-/-}$ mice (Figure 37b).
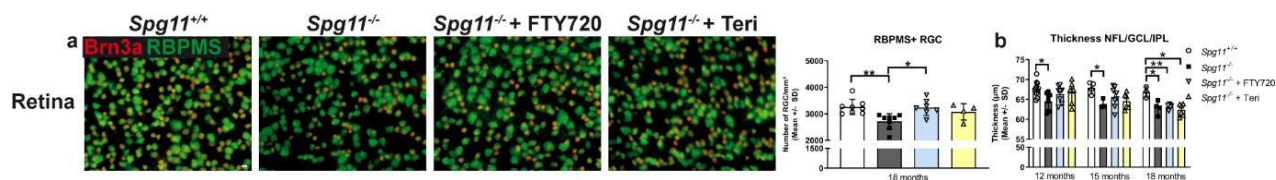
Figure 37: Early treatment with fingolimod or teriflunomide restores the densities of RBPMS$^+$ RGCs of *Spg11$^{-/-}$* mice, while retinal thinning remains unaffected.
(**a**) Representative images of Brn3a/RBPMS$^+$ RGCs in whole-mount retinae of 18-month-old *Spg11$^{+/+}$*, *Spg11$^{-/-}$*, and *Spg11$^{-/-}$* mice treated with fingolimod (FTY720) or teriflunomide (left) and corresponding quantification (right). Scale bar: 50 µm. Treatment restores densities of RBPMS$^+$ RGC. Most RBPMS$^+$ cells are Brn3a$^+$. (**b**) Longitudinal analysis of the thickness of the innermost retinal composite layer (NFL/GCL/IPL) of *Spg11$^{+/+}$*, *Spg11$^{-/-}$*, and treated *Spg11$^{-/-}$* mice by OCT. Treatment does not reduce retinal thinning, typically occurring in *Spg11$^{-/-}$* mice. Error bars represent the standard deviations (circles, squares, triangles = mean value of one mouse). Significance of treated mutant mice compared to *Spg11$^{+/+}$* and *Spg11$^{-/-}$* mice is determined by one-way ANOVA and Tukey's post hoc test (*$p < 0.05$, **$p < 0.01$, ***$p < 0.001$). Corresponding data from *Spg11$^{+/+}$* and *Spg11$^{-/-}$* mice, as shown in figure 8, are presented here again.

Of note, early treatment of *C57BL6/J* (*B6J*) mice with fingolimod or teriflunomide reduced the number of CD8$^+$ and CD4$^+$ T-lymphocytes in ON at 18 months (Figure 38a, b). The number and activation status of microglia remained unaffected by the treatment (Figure 38c, d). Interestingly, the number of SMI32$^+$ axonal spheroids in ON of 18-month-old *B6J* mice treated with either immunomodulator was also reduced (Figure 38e). Early treatment of *B6J* mice had no effect on the number of RBPMS$^+$ RGCs (Figure 38f) or on the brain weight (Figure 38g).
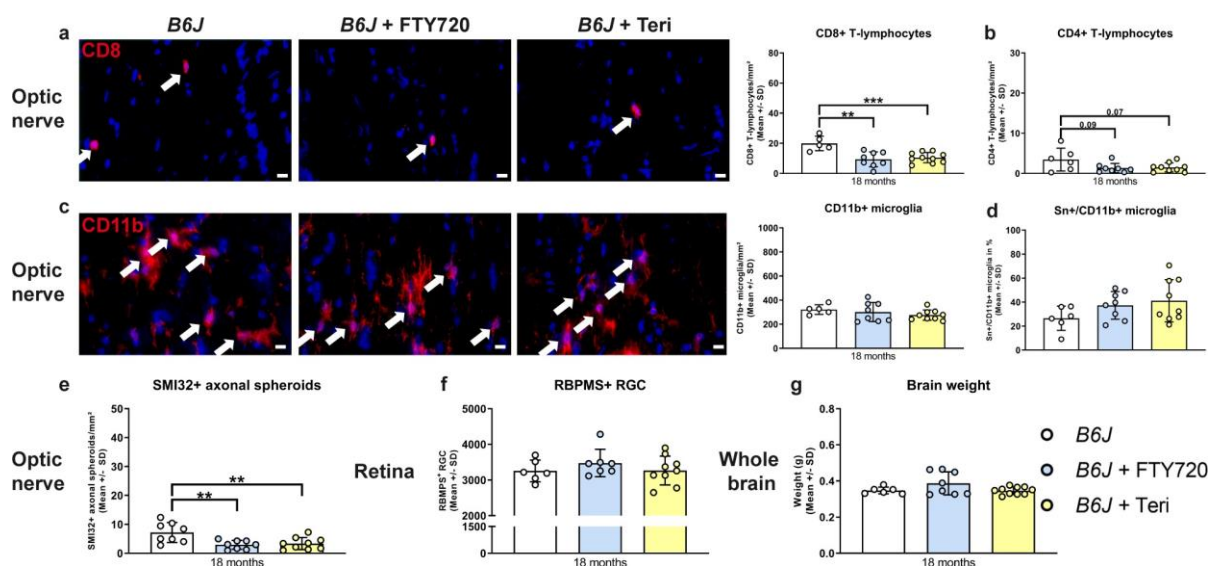
Figure 38: **Early treatment with fingolimod or teriflunomide reduces the number of T-lymphocytes and SMI32$^+$ axonal spheroids in ON of *B6J* mice.**
(**a**) Representative images of CD8$^+$ T-lymphocytes (red, arrows) in longitudinal ON sections of 18-month-old *B6J* mice and *B6J* mice treated with fingolimod (FTY720) or teriflunomide (left) and corresponding quantification (right). Nuclei are labeled with DAPI (blue). Scale bar: 10 µm. Treatment reduces the number of CD8$^+$ T-lymphocytes in ON of *B6J* mice. (**b**) Quantification of CD4$^+$ T-lymphocytes in ON of 18-month-old *B6J* and treated *B6J* mice. Treatment reduces the number of CD4$^+$ T-lymphocytes. (**c**) Representative images of CD11b$^+$ microglia (red, arrows) in ON of 18-month-old

B6J and treated *B6J* mice (left) and corresponding quantification (right). Nuclei are labeled with DAPI (blue). Scale bar: 10 µm. Treatment does not affect the number of CD11b^{+} microglia in *B6J* mice. **(d)** Percentage of CD11b^{+} cells showing the microglial activation marker Sn in ON of 18-month-old *B6J* and treated *B6J* mice. In ON of *B6J* mice, treatment does not alter the amount of Sn^{+} cells. **(e)** Quantification of SMI32^{+} axonal spheroids in ON of 18-month-old *B6J* and treated *B6J* mice. Treatment reduces the number of SMI32^{+} axonal spheroids. **(f)** Quantification of RBPMS[+] RGCs in whole-mount retinae of 18-month-old *B6J* and treated *B6J* mice. Treatment does not alter the number of RBPMS[+] RGCs. **(g)** Brain weight of 18-month-old *B6J* and treated *B6J* mice. Treatment does not alter the brain weight. Error bars represent the standard deviations (circles = mean value of one mouse). Significance of treated *B6J* mice compared to *B6J* mice is determined by one-way ANOVA and Tukey's post hoc test (**$p < 0.01$, ***$p < 0.001$).

We also investigated the effect of early treatment with immunomodulators on the walking pattern of 6- and 18-month-old *Spg11*^{-/-} mice (Figure 39a – j). Similar to our genetic approach, we detected partial amelioration of gait coordination, but not strength, in 18-month-old treated *Spg11*^{-/-} mice (Figure 39a – j). The paw angle movement vector variation showed a trend towards amelioration after treatment with either immunomodulator while the step cycle variation was significantly improved by the treatment with fingolimod (Figure 39c, e). Treatment with both drugs led to a trend towards a reduced print position at 6 and 18 months, while the regularity index was significantly improved at 18 months (Figure 39f, g). As mentioned above, and reminiscent of our findings in *Rag1*-deficient *Spg11*^{-/-} mice, features representing strength remained unaffected by the treatment with either immunomodulator (Figure 39h – j).
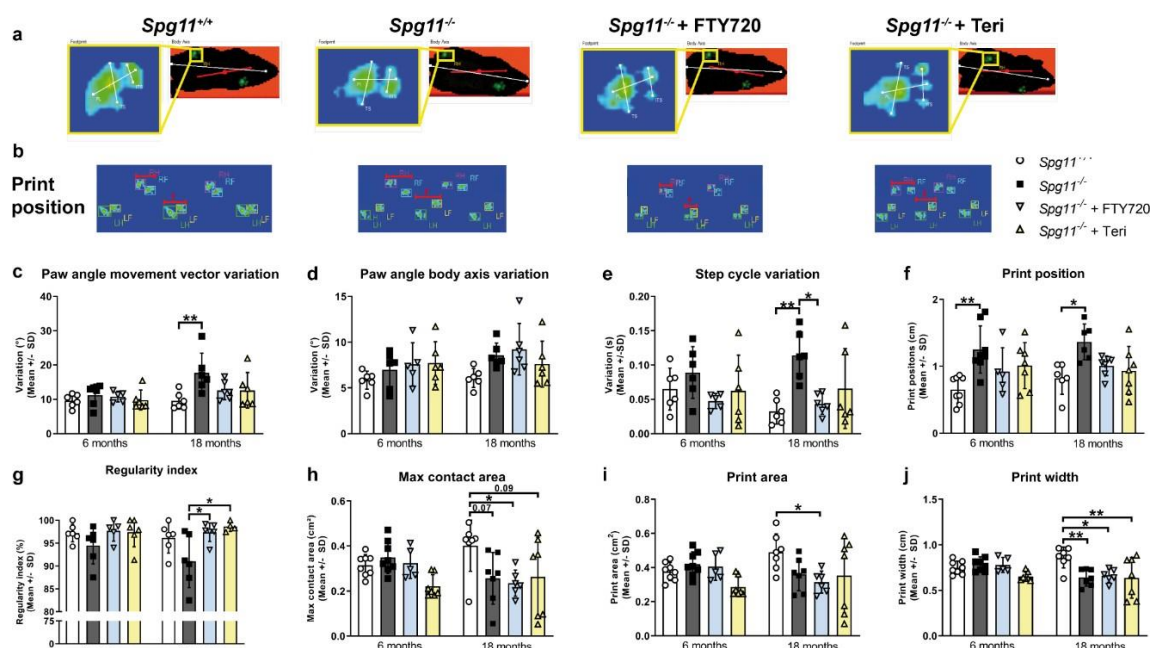
Figure 39: Early treatment with fingolimod or teriflunomide improves gait coordination of *Spg11*^{-/-} mice.
(a) Representative images of a body contour, footprints and **(b)** print positions of 18-month-old *Spg11*^{+/+}, *Spg11*^{-/-}, and *Spg11*^{-/-} mice after treatment with fingolimod (FTY720) or teriflunomide while crossing the CatWalk device (ITS: intermediate toe spread; TS: toe spread; PL: print length; RF: right

front paw; LF: left front paw; RH: right hind paw; LH: left hind paw). Red line (top) indicates the body axis, red line segment (bottom) indicates print position. (**c**) Treated $Spg11^{-/-}$ mice show a tendency towards a reduced paw angle movement vector variation at 18 months while (**d**) the paw angle body axis variation is not affected. (**e**) In $Spg11^{-/-}$ mice, treatment ameliorates the step cycle variation at 18 months. (**f**) In $Spg11^{-/-}$ mice, treatment shows a tendency towards an ameliorated print position at 6 and 18 months, while (**g**) the regularity index is ameliorated at 18 months. (**h**) In $Spg11^{-/-}$ mice, treatment does not affect the maximal contact area, (**i**) the print area, or (**j**) the print width of the hind paws. Error bars represent the standard deviations (circles, squares, triangles = mean value of three consecutive runs of one mouse). Significance of treated mutant mice compared to $Spg11^{+/+}$ and $Spg11^{-/-}$ mice is determined by one-way ANOVA and Tukey's post hoc test (*$p < 0.05$, **$p < 0.01$, ***$p < 0.001$). Corresponding data from $Spg11^{+/+}$ and $Spg11^{-/-}$ mice, as shown in figure 9, are presented here again.

Neither treatment with fingolimod nor treatment with teriflunomide had effects on the stride length and number of steps $Spg11^{-/-}$ mice needed to cross the walkway (Figure 40a, b).
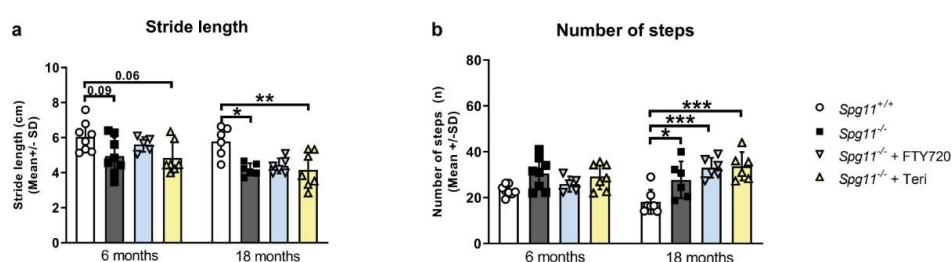
Figure 40: Early treatment with fingolimod or teriflunomide fails to improve selected gait abnormalities of $Spg11^{-/-}$ mice.
(**a**) In $Spg11^{-/-}$ mice, early treatment does not affect the stride length or (**b**) number of steps. Error bars represent the standard deviations (circles, squares, triangles = mean value of three consecutive runs of one mouse). Significance of treated mutant mice compared to $Spg11^{+/+}$ and $Spg11^{-/-}$ mice is determined by one-way ANOVA and Tukey's post hoc test (*p < 0.05, **p < 0.01, ***p < 0.001). Corresponding data from $Spg11^{+/+}$ and $Spg11^{-/-}$ mice, as shown in figure 10, are presented here again.

Of note, we could not detect any effect of treatment with fingolimod or teriflunomide on the walking pattern of *B6J* mice (Figure 41a – l).
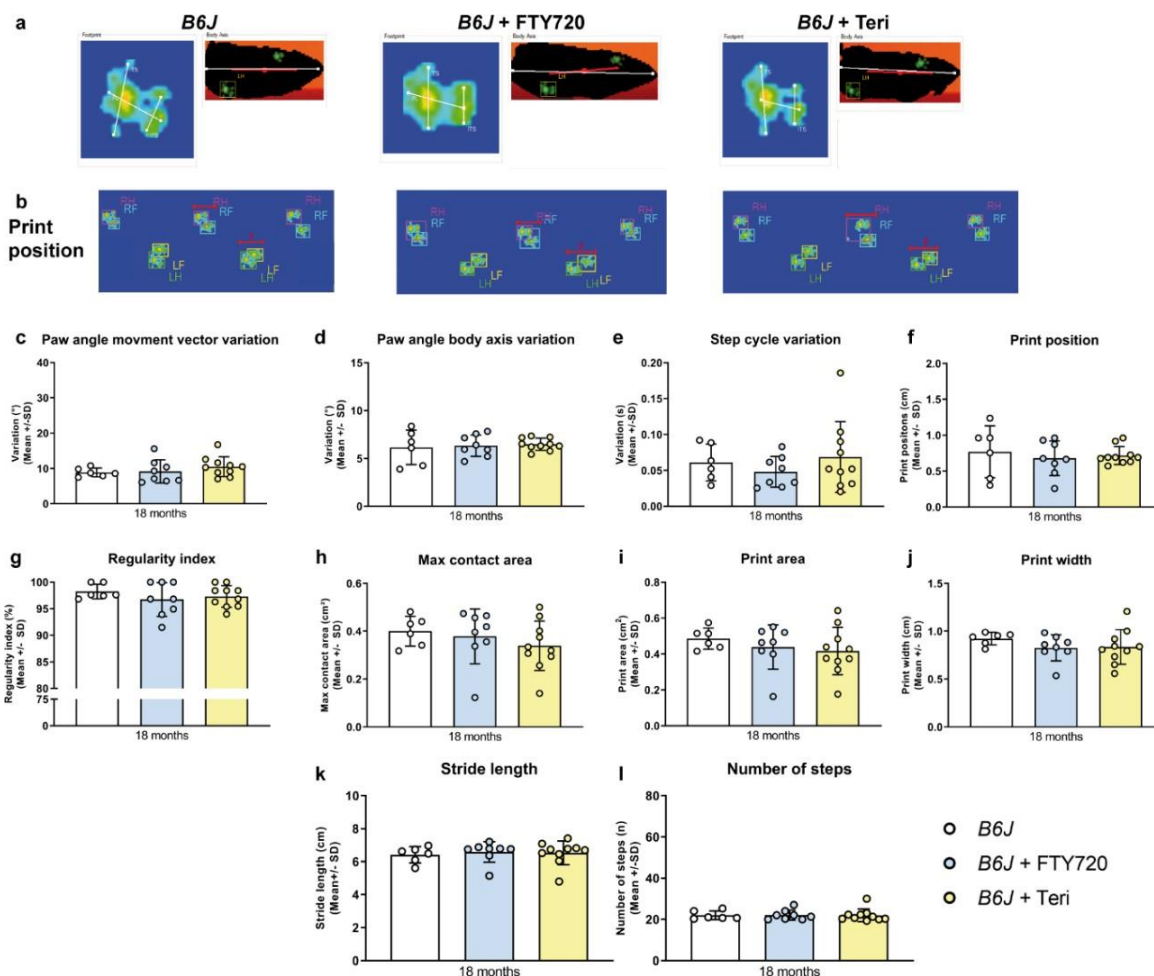
Figure 41: Early treatment with fingolimod or teriflunomide does not affect walking pattern of *B6J* mice.
(**a**) Representative images of a body contour, footprints and (**b**) print positions of 18-month-old *B6J* and *B6J* mice after treatment with fingolimod (FTY720) or teriflunomide while crossing the CatWalk device (ITS: intermediate toe spread; TS: toe spread; PL: print length; RF: right front paw; LF: left front paw; RH: right hind paw; LH: left hind paw). Red line (top) indicates the body axis, red line segment (bottom) indicates print position. (**c**) Treatment of *B6J* mice does not affect the paw angle movement vector, (**d**) the paw angle body axis, or (**e**) the step cycle variation. (**f**) Treatment of *B6J* mice does not affect the print position, (**g**) the regularity index, or the (**h**) the maximal contact, (**i**) the print area, or (**j**) the print width of the hind paws. (**k**) Treatment of *B6J* mice does not affect the stride length, or (**l**) number of steps. Error bars represent the standard deviations (circles = mean value of three consecutive runs of one mouse). Significance of treated *B6J* mice compared to *B6J* mice is determined by one-way ANOVA and Tukey's post hoc test.

As opposed to *Rag1*-deficiency, treatment could not dampen the body weight loss of male or female *Spg11⁻/⁻* mice (Figure 42a, b). Of note, in male *Spg11⁻/⁻* mice treatment with teriflunomide led to body weight loss compared to wt mice from 6 months onwards, while treatment with fingolimod led to body weight loss from 9 months onwards (Figure 42a).
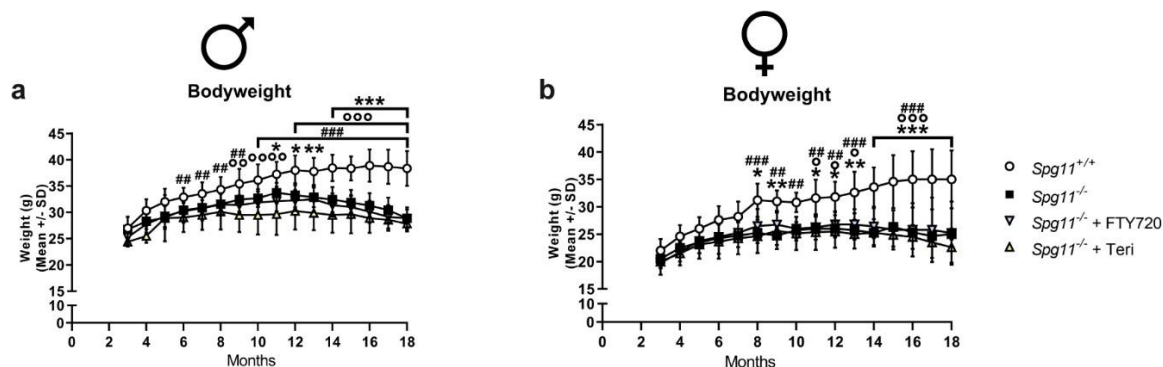
Figure 42: Early treatment with fingolimod or teriflunomide does not ameliorate body weight loss of *Spg11^-/-* mice.

(a) Body weight of male *Spg11^+/+*, *Spg11^-/-* and *Spg11^-/-* mice treated with fingolimod (FTY720) or teriflunomide mice starting at 3 months. Early treatment with fingolimod or teriflunomide does not dampen body weight loss of male *Spg11^-/-* mice. Treatment of male *Spg11^-/-* mice with teriflunomide leads to body weight loss compared to wt mice starting at 6 months, while treatment with fingolimod leads to body weight loss starting at 9 months. **(b)** Weight of female *Spg11^+/+*, *Spg11^-/-* and treated *Spg11^-/-* mice starting at 3 months. Treatment does not reduce weight loss of female *Spg11^-/-* mice. Error bars represent standard deviations (circles, squares, triangles = mean value at one age point). Significance of treated *Spg11^-/-* mice compared to *Spg11^+/+* and *Spg11^-/-* mice is determined by one-way ANOVA and Tukey's post hoc test. Stars (*) indicate the significance of *Spg11^-/-* mice compared to *Spg11^+/+* mice ($*p < 0.05$, $*p < 0.01$, $***p < 0.001$). Circles (°) indicate the significance of *Spg11^-/-* mice treated with fingolimod compared to *Spg11^+/+* mice ($°p < 0.05$, $°p < 0.01$, $°p < 0.001$). Hashtags (#) indicate the significance of *Spg11^-/-* mice treated with teriflunomide compared to *Spg11^+/+* mice ($\#p < 0.05$, $\#\#p < 0.01$, $\#\#\#p < 0.001$). Corresponding data from *Spg11^+/+* and *Spg11^-/-* mice, as shown in figure 11, are presented here again.

Of note, treatment with teriflunomide led to loss of body weight of male and female *B6J* mice, while fingolimod showed the same tendency only in females (Figure 43a, b).
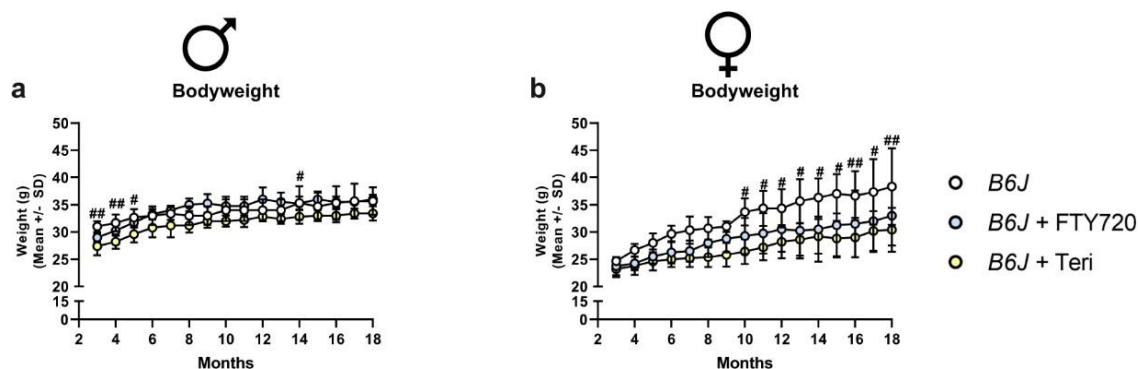
Figure 43: Early treatment with fingolimod or teriflunomide reduces the body weight of *B6J* mice.

(a) Body weight of male *B6J* mice and *B6J* mice treated with fingolimod (FTY720) or teriflunomide starting at 3 months. Male *B6J* mice treated with teriflunomide show reduced body weight compared to untreated *B6J* mice from 3 – 5 months and at 14 months of age. Early treatment with fingolimod does not influence the body weight of male *B6J* mice. **(b)** Body weight of female *B6J* mice and treated *B6J* mice starting at 3 months. Treatment with teriflunomide reduces the body weight of female *B6J* mice from 10 months onwards, while treatment with fingolimod shows the same tendency. Error bars represent standard deviations (circles = mean value at one age point). Significance of treated *B6J* mice compared to *B6J* mice is determined by two-way ANOVA and multiple comparisons. Hashtags (#) indicate the significance of *B6J* mice treated with teriflunomide compared to *B6J* mice ($\#p < 0.05$, $\#\#p < 0.005$).

In summary, pharmacological targeting of lymphocytes with fingolimod or teriflunomide improved histopathological alteration and distinct walking pattern abnormalities, without reaching the effectivity of genetic depletion of the adaptive immune system. Of note, treatment of *B6J* mice reduced the number of T-lymphocytes and axonal spheroids in the ON and did not alter the walking pattern, while it did reduced the body weight of mice.

5.9 Early treatment with clinically approved immunomodulators ameliorates social behavior of *Spg11*$^{-/-}$ mice

Since we could show that behavioral abnormalities of *Spg11*$^{-/-}$ mice are partially driven by the adaptive immune system, we investigated whether immunomodulatory treatment, as a more clinically relevant approach, could lead to similar beneficial effects.

Indeed, we could see striking benefits of the early treatment with either immunomodulator on the social behavior of *Spg11*$^{-/-}$ mice (Figure 44; Figure 45). Treatment restored social interest (trial 1) and novelty (trial 2) preference of male *Spg11*$^{-/-}$ mice to wt levels (Figure 44a – c). Interestingly, and resembling the findings in *Rag1*-deficient *Spg11*$^{-/-}$ mice, even though the social interest and novelty preference was restored, treatment did not increase the time male *Spg11*$^{-/-}$ mice spent with the unfamiliar animals in the social novelty trial (trial 2) (Figure 44d).

Figure 44: Early treatment with fingolimod or teriflunomide ameliorates social behavior of male *Spg11$^{-/-}$* mice.

(a) Representative images of social interest (trial 1, left) and novelty (trial 2, right) analysis of 18-month-old male *Spg11$^{+/+}$* (top row), *Spg11$^{-/-}$*(2nd row), and *Spg11$^{-/-}$* mice treated with fingolimod (FTY720) (3rd row) or teriflunomide (bottom row). Light square indicates the center zone of the arena, green area indicates the border zone. Red line represents the walking track. Mouse 1 indicates in which cage the first unfamiliar mouse was placed, mouse 2 in which the second unfamiliar mouse was placed. **(b)** Social preference of male *Spg11$^{+/+}$*, *Spg11$^{-/-}$* or treated *Spg11$^{-/-}$* mice at 6-, 12-, and 18- months and **(c)** at 18 months (enlarged). Early treatment with either immunomodulator restores social interest and novelty preference of 18-month-old male *Spg11$^{-/-}$* mice. Chance indicates equal time spent with the empty cage/animals (50%). **(d)** Early treatment with fingolimod or teriflunomide does not increase the time male *Spg11$^{-/-}$* mice spent with the unfamiliar animals in the social novelty trial (trial 2). Error bars represent standard deviations (circles, squares, triangles = value of one mouse). Significance of treated *Spg11$^{-/-}$* mice compared to *Spg11$^{+/+}$* and *Spg11$^{-/-}$* mice, is determined by one-way ANOVA and Tukey's post hoc test (**$p < 0.01$, ***$p < 0.001$). Corresponding data from *Spg11$^{+/+}$* and *Spg11$^{-/-}$* mice, as shown in figure 12, are presented here again.

Remarkably, the early treatment with teriflunomide had even more pronounced effects on female $Spg11^{-/-}$ mice, resembling our previous findings in $Spg11^{-/-}Rag11^{-/-}$ mice (Figure 45). Treatment with teriflunomide did not only restore the social interest (trial 1) and novelty preference (trial 2) of female $Spg11^{-/-}$ mice to wt levels, but treated mice also spent significantly more time with the unfamiliar animal in the social interest trial (trial 1) and there was the same tendency in the social novelty trial (trial 2) (Figure 45a – d). Treatment with fingolimod also increased the social interest and novelty preference of 18-month-old female $Spg11^{-/-}$ mice, albeit not to the same degree as treatment with teriflunomide (Figure 45a – c). Interestingly treatment with fingolimod did not increase the time female $Spg11^{-/-}$ mice spent with the unfamiliar mice (Figure 45d).

Figure 45: Early treatment with fingolimod or teriflunomide ameliorates social behavior of female *Spg11⁻ᐟ⁻* mice.

(a) Representative images of social interest (trial 1, left) and novelty (trial 2, right) analysis of 18-month-old female *Spg11⁺ᐟ⁺* (top row), *Spg11⁻ᐟ⁻*(2nd row), and *Spg11⁻ᐟ⁻* mice treated with fingolimod (FTY720) (3rd row) or teriflunomide (bottom row). Light square indicates the center zone of the arena, green area indicates the border zone. Red line represents the walking track. Mouse 1 indicates in which cage the first unfamiliar mouse was place, mouse 2 in which the second unfamiliar mouse was placed. (b) Social preference of female *Spg11⁺ᐟ⁺*, *Spg11⁻ᐟ⁻* or treated *Spg11⁻ᐟ⁻* mice at 6-, 12-, and 18- months and (c) at 18 months (enlarged). Treatment with either immunomodulator increases the social interest and novelty preference of 18-month-old female *Spg11⁻ᐟ⁻* mice, while the effect of teriflunomide treatment is more pronounced. Chance indicates equal time spent with the empty cage/animals (50%). (d) Treatment with teriflunomide, but not fingolimod, increases the time female *Spg11⁻ᐟ⁻* mice spent with the unfamiliar animal in the social interest trial (trial 1) and shows the same tendency in the social novelty trial (trial 2) at 18 months. Error bars represent standard deviations (circles, squares, triangles = value of one mouse). Significance of treated *Spg11⁻ᐟ⁻* mice compared to *Spg11⁺ᐟ⁺* and *Spg11⁻ᐟ⁻* mice, is determined by one-way ANOVA and Tukey's post hoc test (*$p < 0.05$, *$p < 0.01$, ***$p < 0.001$). Corresponding data from *Spg11⁺ᐟ⁺* and *Spg11⁻ᐟ⁻* mice, as shown in Figure 13, are presented here again.

To ensure that early treatment did not change behavior of wt mice, *B6J* mice were treated with fingolimod or teriflunomide using the same treatment approach as previously described (Figure 32). Early treatment did not alter social interest (trial 1) or novelty preference (trial 2) of male *B6J* mice compared to untreated littermates (Figure 46a – c). The time treated mice spent with the unfamiliar animals also remained unaffected by either treatment (Figure 46d).
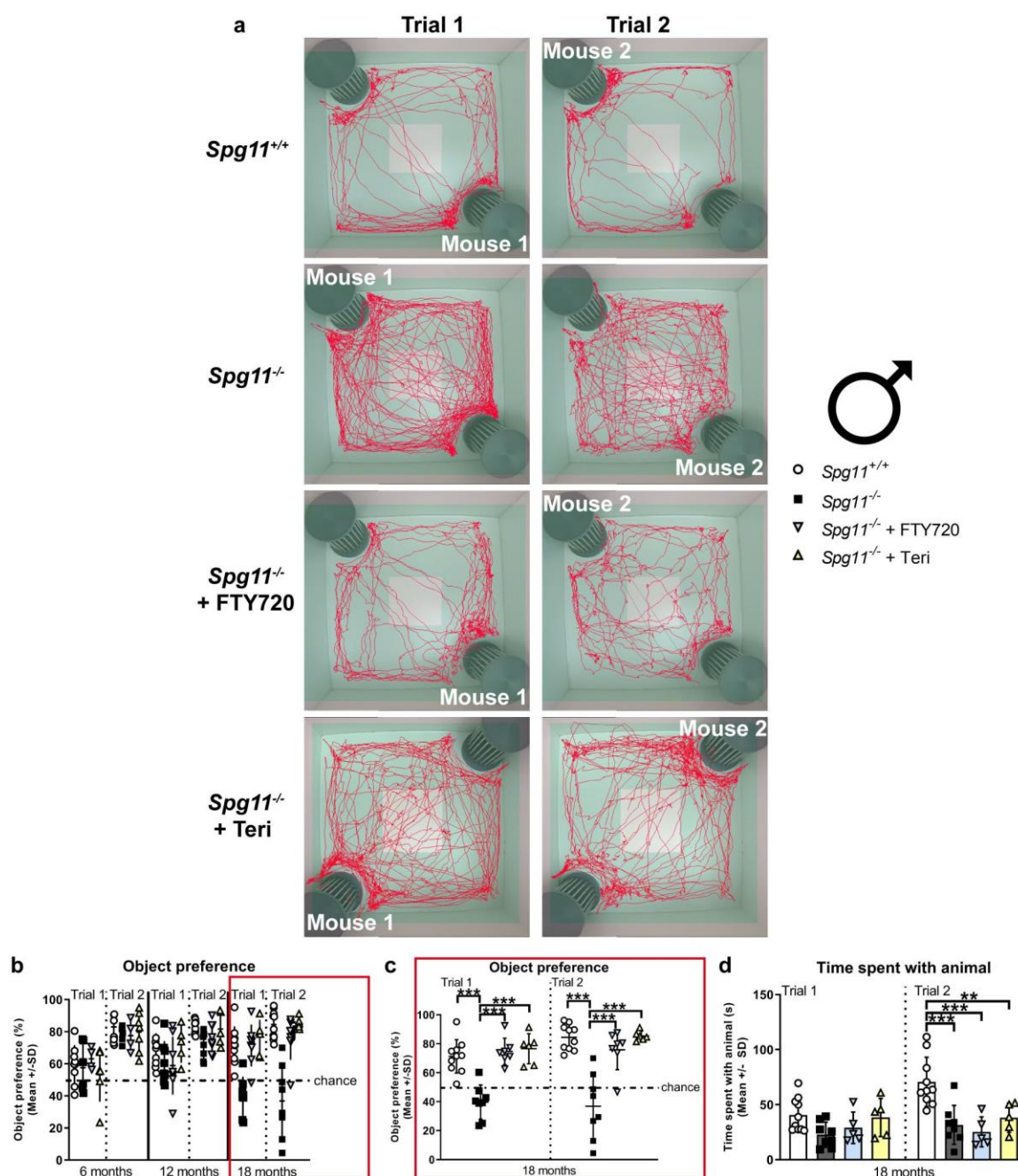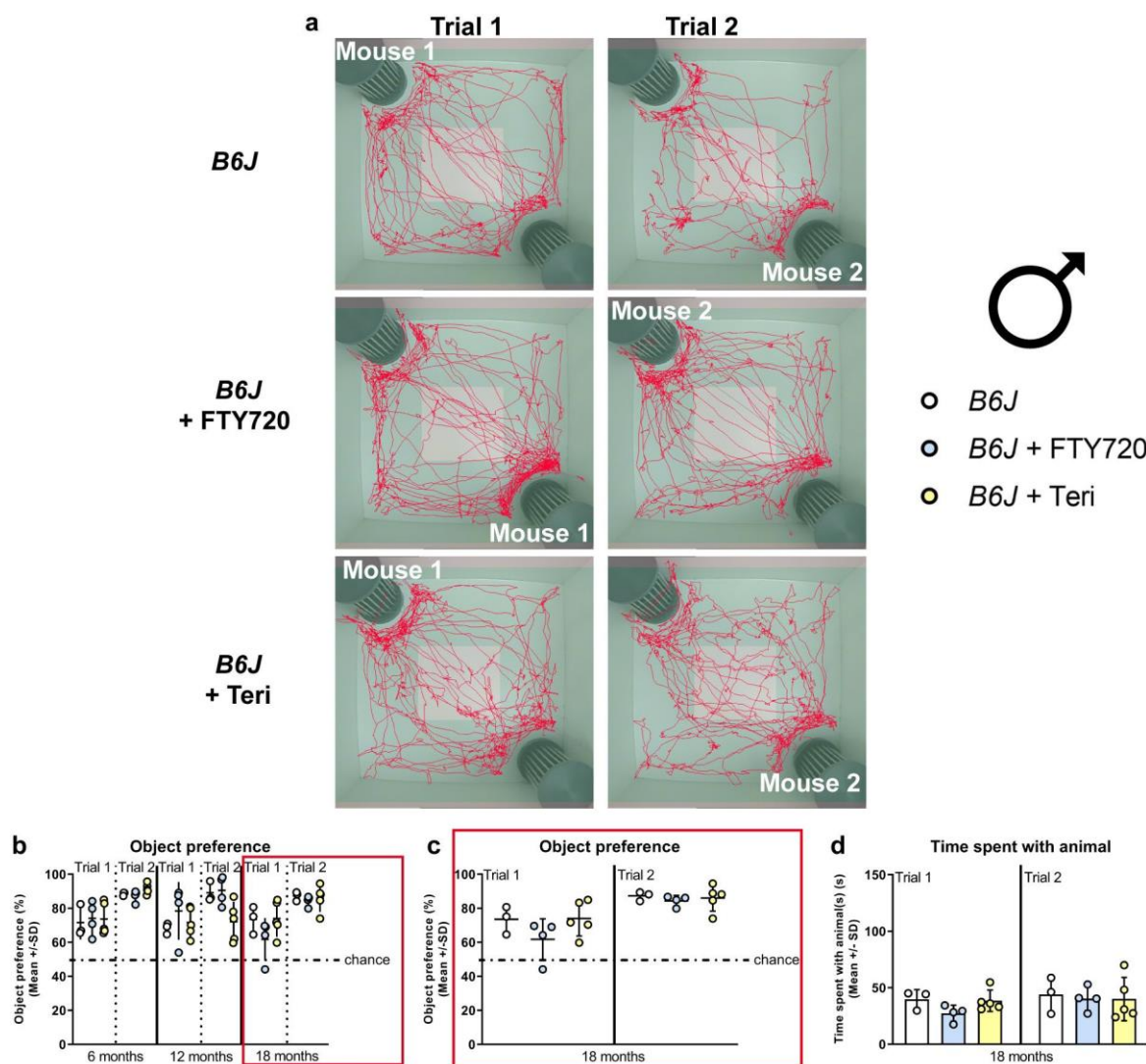

Figure 46: Early treatment with fingolimod or teriflunomide does not alter social behavior of male *B6J* mice.
(a) Representative images of social interest (trial 1, left) and novelty (trial 2, right) analysis of 18-month-old male *B6J* (top row) and *B6J* mice treated with fingolimod (FTY720) (2nd row) or teriflunomide (bottom row). Light square indicates the center zone of the arena, green area indicates the border zone. Red line represents the walking track. Mouse 1 indicates in which cage the first unfamiliar mouse was placed, mouse 2 in which the second unfamiliar mouse was placed. **(b)** Social preference of *B6J* or treated *B6J* mice at 6-, 12-, and 18- months and **(c)** at 18 months (enlarged). Treatment does not alter social interest and novelty preference of male *B6J* mice. Chance indicates equal time spent with the empty cage/animals (50%). **(d)** Treatment does not alter the time male *B6J* mice spent with the unfamiliar animals in the social interest (trial 1) or novelty trial (trial 2) at 18 months. Error bars represent standard deviations (circles = value of one mouse). Significance of treated *B6J* mice compared to *B6J* mice is determined by one-way ANOVA and Tukey's post hoc test.

Similarly, treatment of female *B6J* mice with either immunomodulator did not alter social interest (trial 1) or novelty preference (trial 2) (Figure 47a – c). The time treated mice spent with the unfamiliar animals during both trials remained unaffected (Figure 47a – d).
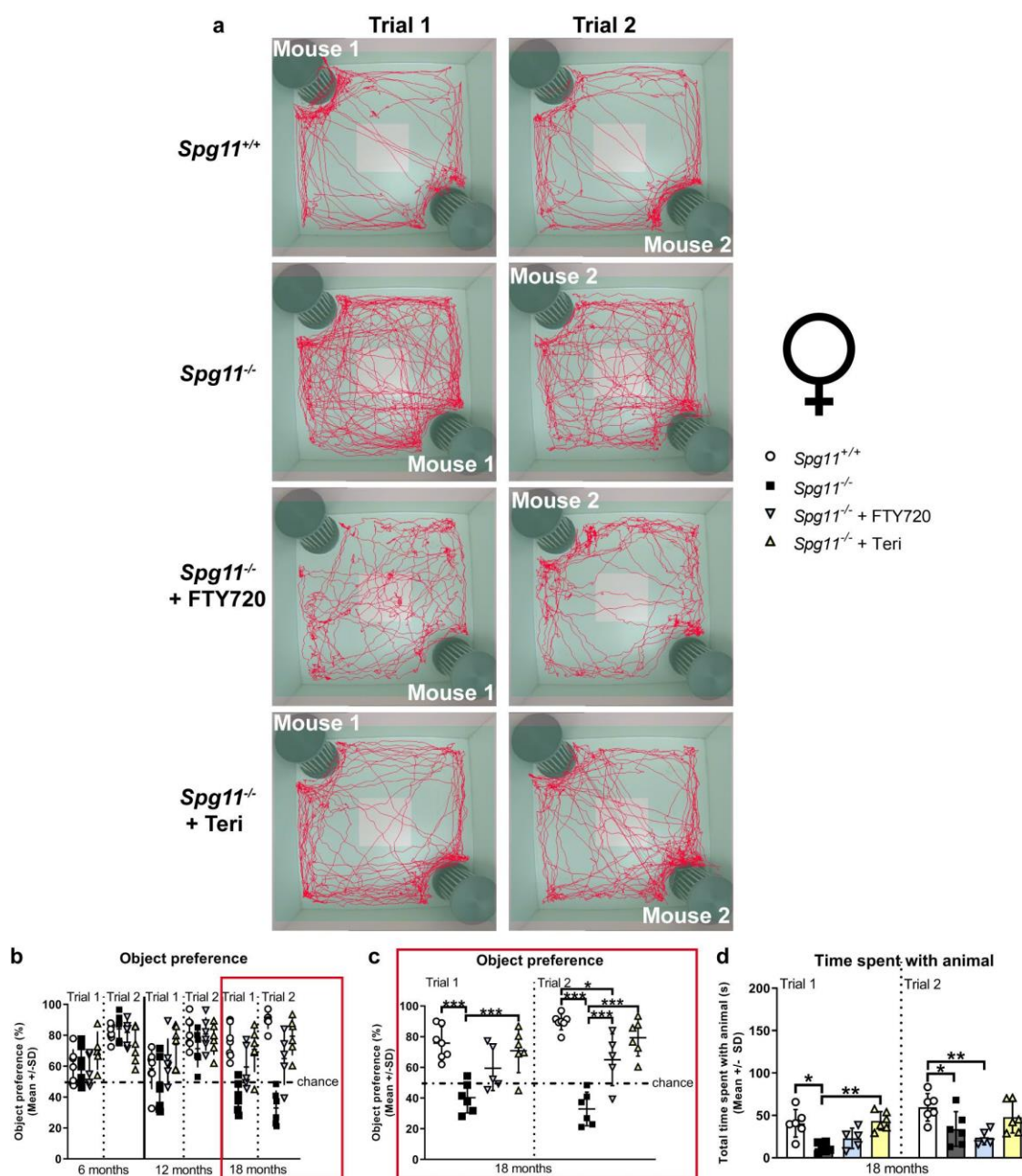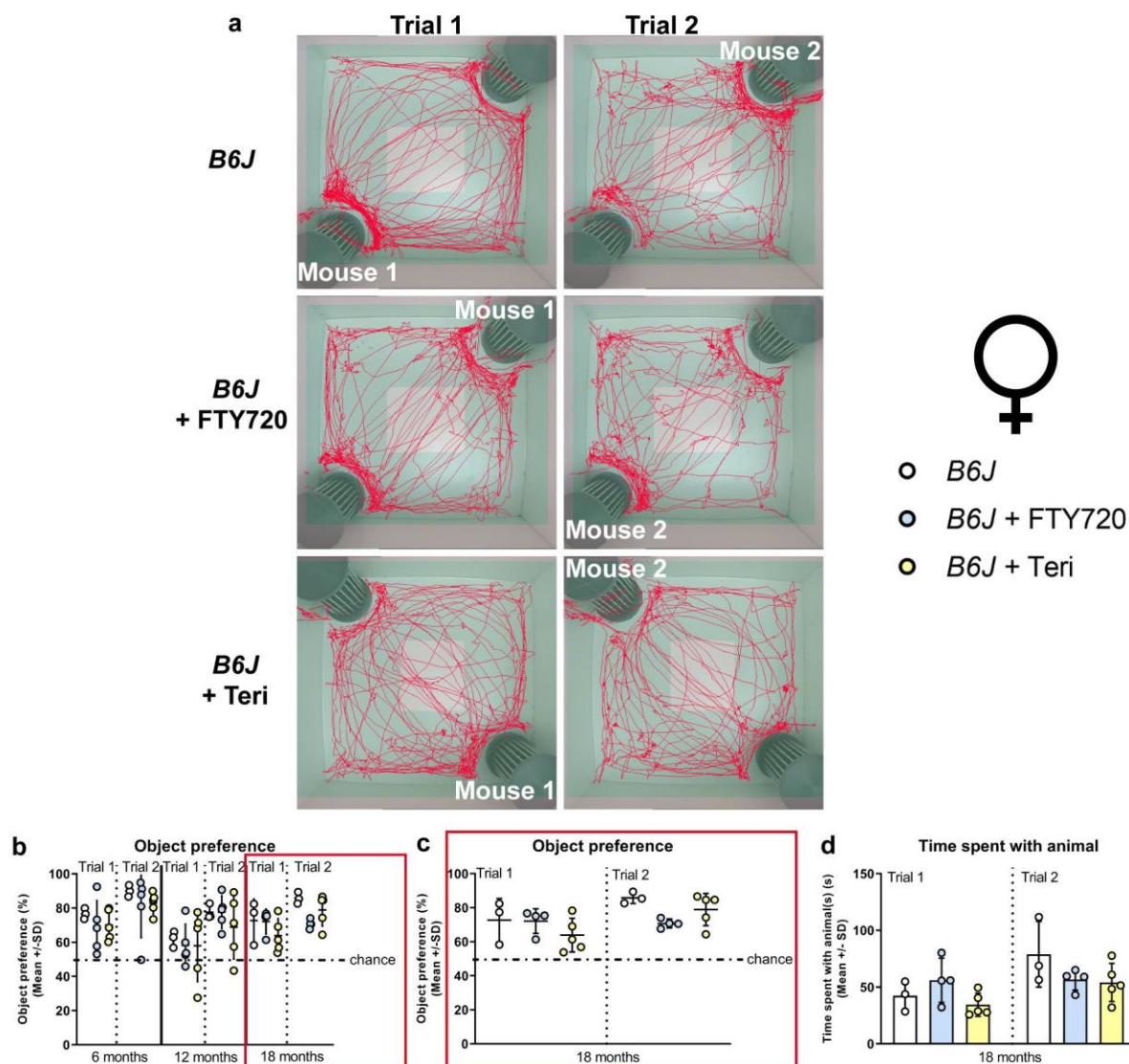

Figure 47: Early treatment with fingolimod or teriflunomide does not alter social behavior of female *B6J* mice.
(a) Representative images of social interest (trial 1, left) and novelty (trial 2, right) analysis of 18-month-old female *B6J* (top row) and *B6J* mice treated with fingolimod (FTY720) (2nd row) or teriflunomide (bottom row). Light square indicates the center zone of the arena, green area indicates the border zone. Red line represents the walking track. Mouse 1 indicates in which cage the first unfamiliar mouse was placed, mouse 2 in which the second unfamiliar mouse was placed. **(b)** Social preference of *B6J* or treated *B6J* mice at 6-, 12-, and 18- months and **(c)** at 18 months (enlarged). Treatment does not alter social interest and novelty preference of female *B6J* mice. Chance indicates equal time spent with the empty cage/animals (50%). **(d)** Treatment does not alter the time female *B6J* mice spent with the unfamiliar animals in the social interest (trial 1) or novelty trial (trial 2) at 18 months. Error bars represent standard deviations (circles = value of one mouse). Significance of treated *B6J* mice compared to untreated *B6J* mice is determined by one-way ANOVA and Tukey's post hoc test.

We saw no change in non-spatial, short-term memory formation and recognition after early treatment of male or female $Spg11^{-/-}$ mice with fingolimod or teriflunomide (Figure 48a, b).
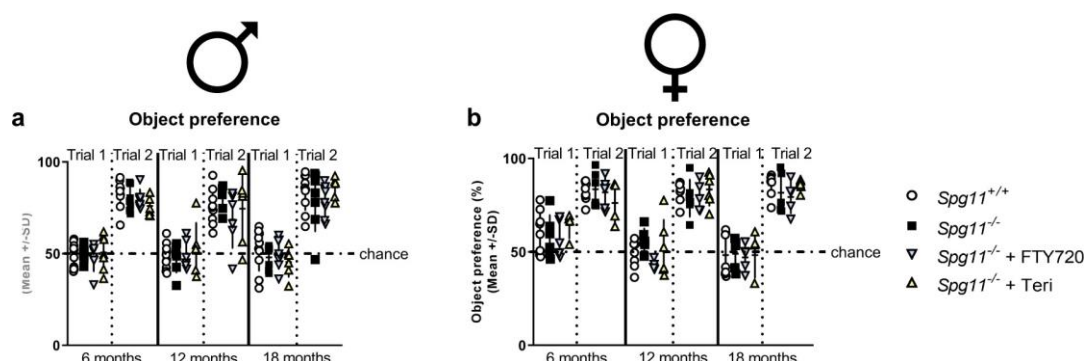
Figure 48: Early treatment with fingolimod or teriflunomide does not alter object preference in NOR of $Spg11^{-/-}$ mice.
(a) Treatment with neither fingolimod (FTY720) nor teriflunomide impacts the object preference in NOR of male or **(b)** female $Spg11^{-/-}$ mice. Chance indicates equal time spent with both objects (50%). Error bars represent standard deviations (circles, squares, triangles = value of one mouse). Significance of treated Spg11-/- mice compared to $Spg11^{+/+}$ and $Spg11^{-/-}$ mice, is determined by one-way ANOVA and Tukey's post hoc test. Corresponding data from $Spg11^{+/+}$ and $Spg11^{-/-}$ mice, as shown in Figure 14, are presented here again.

Accordingly, early treatment of male or female *B6J* mice with fingolimod or teriflunomide did not alter the non-spatial, short-term memory formation and recognition (Figure 49a, b).
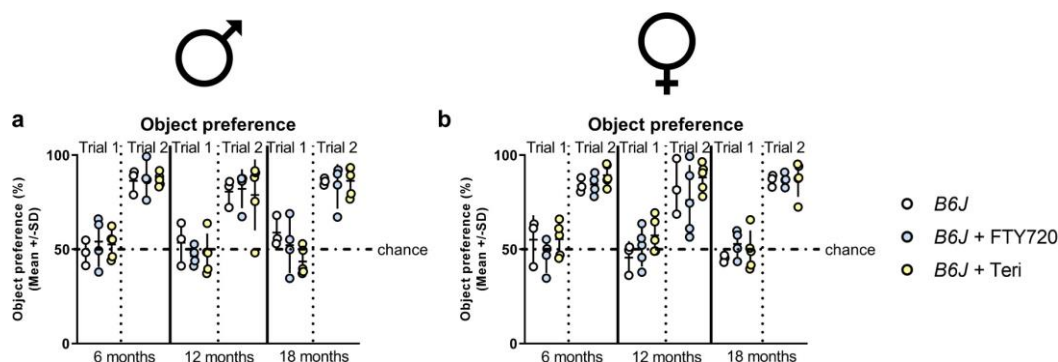
Figure 49: Early treatment with fingolimod or teriflunomide does not alter object preference in NOR of *B6J* mice.
(a) Early treatment with neither fingolimod (FTY720) nor teriflunomide impacts the object preference in NOR of male **(b)** or female *B6J* mice. Chance indicates equal time spent with both objects (50%). Error bars represent standard deviations (circles = value of one mouse). Significance of treated *B6J* mice compared to untreated *B6J* mice is determined by one-way ANOVA and Tukey's post hoc test.

Using the OF analysis, we found that treatment with fingolimod, but not teriflunomide, reduced the walking distance and movement duration, typically increased in male $Spg11^{-/-}$ mice, at 6 months (Figure 50a – c). No effect of treatment with either immunomodulator on these parameters was detectable at a later age (Figure 50a – c). Early treatment did not change the time spent in the center zone or time spent rearing of male $Spg11^{-/-}$ mice (Figure 50d, e). Early

treatment of female *Spg11⁻/⁻* mice with fingolimod, but not teriflunomide, led to a trend towards a reduced walking distance and movement duration at 18 months (Figure 50f – h), while the center time and time spent rearing remained unaffected after either treatment (Figure 50i, j).
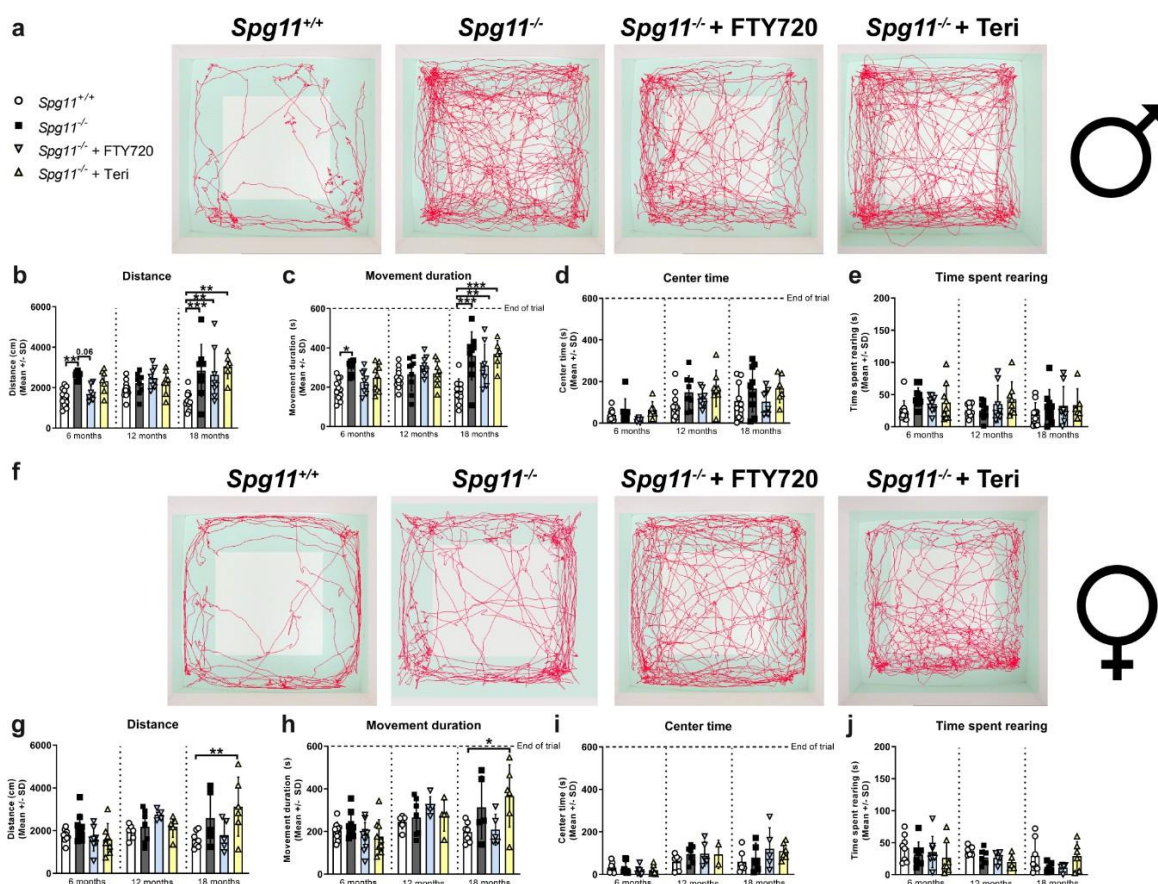
Figure 50: Early treatment with fingolimod, but not teriflunomide, reduces hyperactivity-like behavior of *Spg11⁻/⁻* mice.
(a) Representative images of OF analysis of 18-month-old male *Spg11⁺/⁺*, *Spg11⁻/⁻* and *Spg11⁻/⁻* mice treated with fingolimod (FTY720) or teriflunomide. Light square indicates the center zone of the arena, green area indicates the border zone. Red line represents the walking track. (b) Treatment with fingolimod, but not teriflunomide, reduces the walking distance (c) and movement duration of 6-month-old male *Spg11⁻/⁻* mice, while neither treatment affects these parameters at 12 or 18 months. (d) Treatment does not alter the center time or (e) time spent rearing of male *Spg11⁻/⁻* mice. (f) Representative images of OF analysis of 18-month-old female *Spg11⁺/⁺*, *Spg11⁻/⁻* and treated *Spg11⁻/⁻* mice. Light square indicates the center zone of the arena, green area indicates the border zone. Red line represents the walking track. (g) Treatment with fingolimod, but not teriflunomide, leads to a trend towards a reduced walking distance and (h) movement duration of 18-month-old female *Spg11⁻/⁻* mice. (i) Treatment of female *Spg11⁻/⁻* mice does not alter the center time or (j) the time spent rearing. Error bars represent standard deviations (circles, squares, triangles = value of one mouse). Significance of treated *Spg11⁻/⁻* mice compared to *Spg11⁺/⁺* and *Spg11⁻/⁻* mice, is determined by one-way ANOVA and Tukey's post hoc test (*p<0.05, **$p < 0.01$, ***$p < 0.001$). Corresponding data from *Spg11⁺/⁺* and *Spg11⁻/⁻* mice, as shown in Figure 15, are presented here again.

Interestingly, early treatment of male *B6J* mice with fingolimod or teriflunomide led to a tendency towards increased walking distance and movement duration at 6 and 18 months compared to untreated mice, suggesting hyperactivity-like behavior (Figure 51a – c). Treatment

with teriflunomide increased the time 6- and 12-month-old male *B6J* mice spent in the center zone of the arena compared to untreated mice (Figure 51d), while treatment with fingolimod led to the same tendency but only at 12 months (Figure 51d). Male *B6J* mice treated with either immunomodulator spent more time rearing than untreated mice from 12 months onwards (Figure 51e). In female *B6J* mice treatment with fingolimod, but not teriflunomide, led to an increased walking distance and showed a tendency towards an increased movement duration compared to untreated mice at 18 months, suggesting hyperactivity-like behavior (Figure 51f – h). The center time and the time treated female *B6J* mice spent rearing remained unchanged (Figure 51i, j).

Figure 51: Early treatment with fingolimod or teriflunomide increases some aspects of hyperactivity-like behavior of *B6J* mice.
(**a**) Representative images of OF analysis of 18-month-old male *B6J* and *B6J* mice treated with fingolimod (FTY720) or teriflunomide. Light square indicates the center zone of the arena, green area indicates the border zone. Red line represents the walking track. (**b**) Treatment with either immunomodulator leads to a tendency towards an increased walking distance and (**c**) movement duration in 18-month-old male *B6J* mice. (**d**) Treatment with teriflunomide increases the center time of male *B6J* mice at 6 and 12 months, while fingolimod shows the same tendency at 12 months. (**e**) Treatment with teriflunomide increases the time spent rearing of 6- and 12-month-old male *B6J* mice, and treatment with fingolimod leads to the same tendency. (**f**) Representative images of OF analysis of 18-month-old female *B6J* and treated *B6J* mice. Light square indicates the center zone of the arena, green area indicates the border zone. Red line represents the walking track. (**g**) Treatment with fingolimod, but not teriflunomide, increases the walking distance and (**h**) movement duration in 18-

month-old female *B6J* mice. **(i)** Treatment of female *B6J* mice does not alter the center time or **(j)** the time spent rearing. Error bars represent standard deviations (circles = value of one mouse). Significance of treated *B6J* mice compared to *B6J* mice is determined by one-way ANOVA and Tukey's post hoc test (*$p < 0.05$).

Regarding the anxiety-like behavior, early treatment with neither fingolimod nor teriflunomide changed the behavior of male *Spg11$^{-/-}$* mice (Figure 52a – e). In female mutant mice, which typically show a reduced anxiety-like behavior under non-treatment conditions, treatment with fingolimod led to an increased time to enter the light compartment (Figure 52f, g). Of note, treatment of mutant mice with fingolimod increased the latency to enter also compared to wt mice (Figure 52g). Accordingly, the walking distance, and the time spent in the light compartment, or the center zone were reduced at the same age (Figure 52h – j). Treatment with teriflunomide showed the same tendencies, albeit not to the same degree as fingolimod (Figure 52h, i), while the center time remained unchanged by the treatment (Figure 52j).
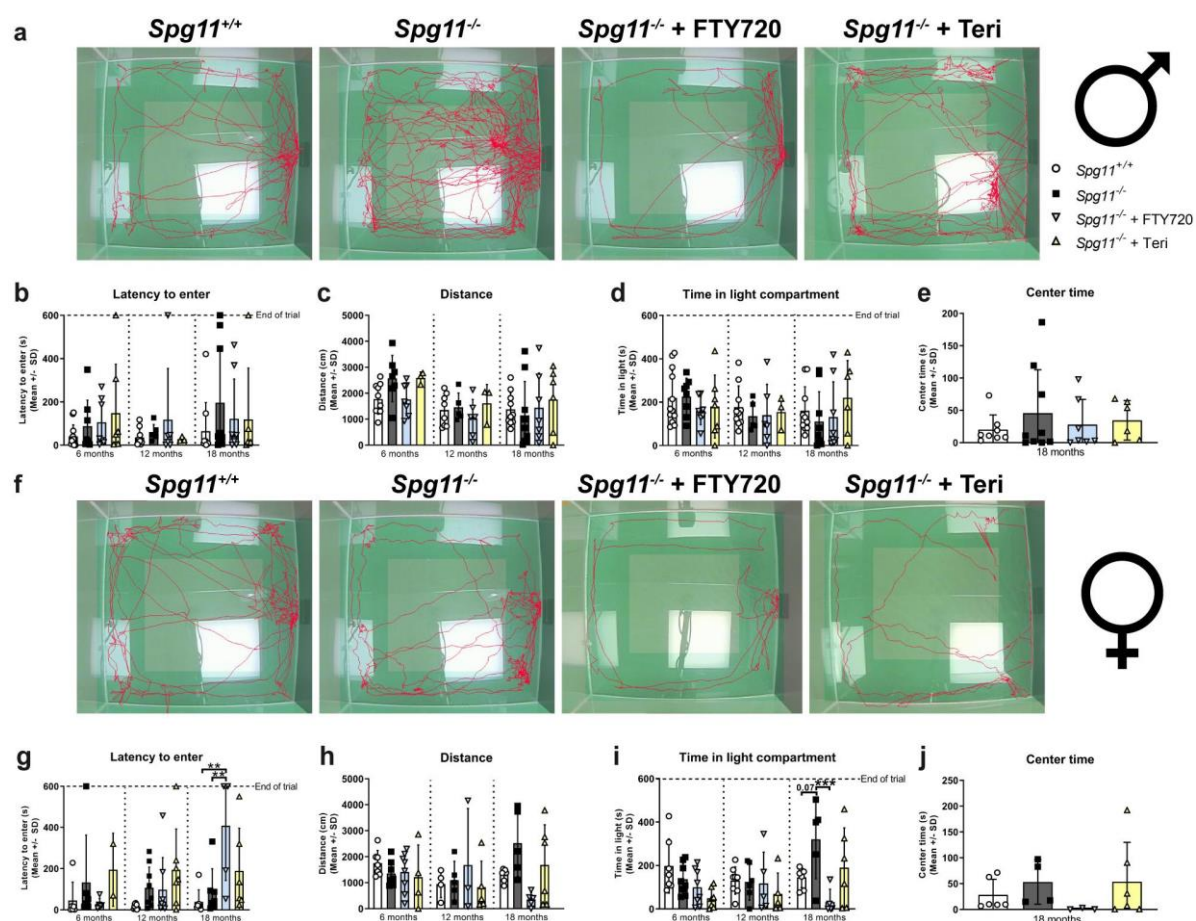
Figure 52: Early treatment with fingolimod or teriflunomide restores anxiety-like behavior of female *Spg11$^{-/-}$* mice.
(a) Representative images of DLB analysis of 18-month-old male *Spg11$^{+/+}$*, *Spg11$^{-/-}$* and *Spg11$^{-/-}$* mice treated with fingolimod (FTY720) or teriflunomide. Light square indicates the center zone of the arena. Red line represents the walking track. **(b)** Treatment does not alter latency to enter, **(c)** walking distance, **(d)** time in light compartment, or **(e)** center time of male *Spg11$^{-/-}$* mice. **(f)** Representative images of

77

DLB analysis of 18-month-old female $Spg11^{+/+}$ and treated $Spg11^{-/-}$ mice. Light square indicates the center zone of the arena. Red line represents the walking track. **(g)** Treatment with fingolimod, but not teriflunomide, increases the latency to enter of female $Spg11^{-/-}$ mice compared to wt and mutant mice. **(h)** Treatment with fingolimod reduces the walking distance and **(i)** time in the light compartment of 18-month-old female $Spg11^{-/-}$ mice, while teriflunomide shows the same tendency. **(j)** Treatment with fingolimod, but not teriflunomide, leads to a tendency towards a reduced time 18-month-old female $Spg11^{-/-}$ mice spend in the center zone. Error bars represent standard deviations (circles, squares, triangles = value of one mouse). Significance of treated $Spg11^{-/-}$ mice compared to $Spg11^{+/+}$ and $Spg11^{-/-}$ mice, is determined by one-way ANOVA and Tukey's post hoc test (**$p < 0.01$, ***$p < 0.001$). Corresponding data from $Spg11^{+/+}$ and $Spg11^{-/-}$ mice, as shown in figure 16, are presented here again.

Early treatment of male or female *B6J* mice with fingolimod or teriflunomide did not alter the latency to enter, walking distance, time in light compartment or center time in the DLB analysis (Figure 53a – j).

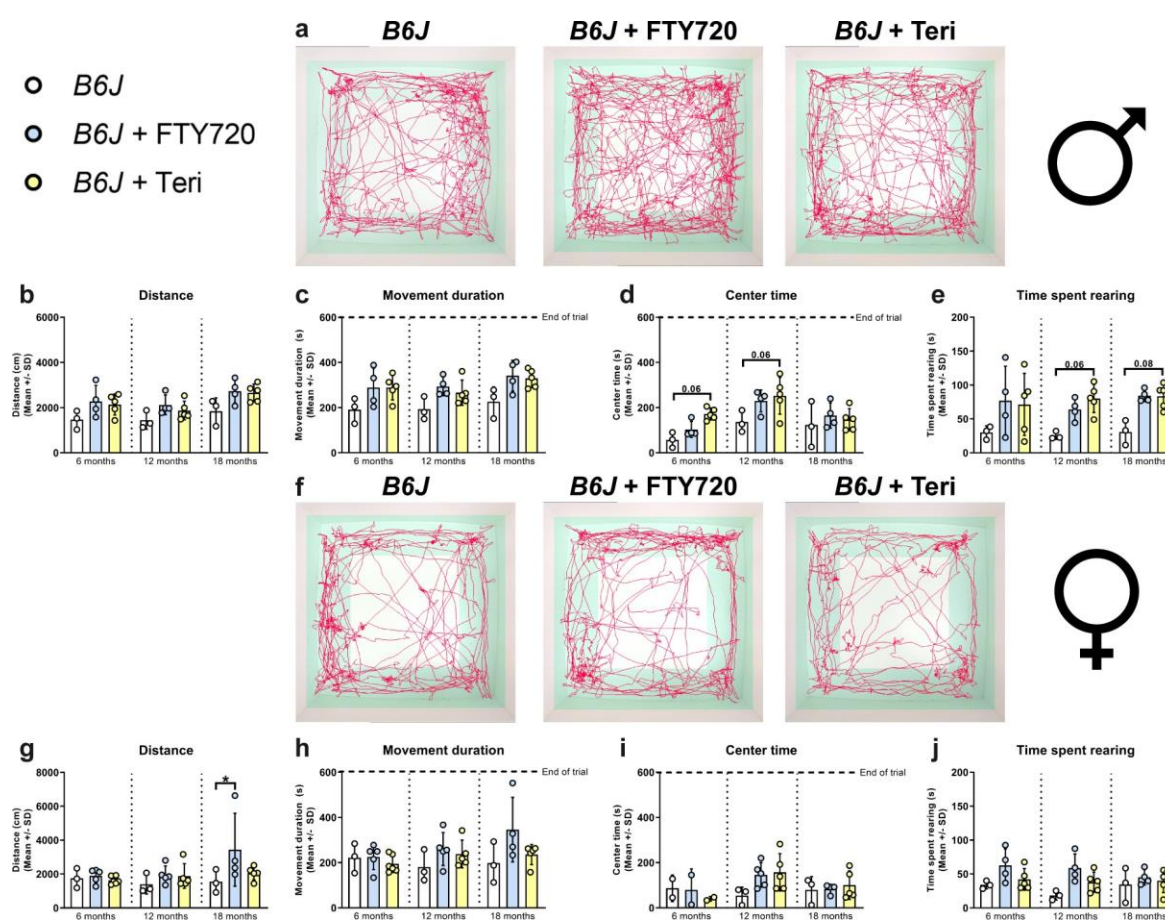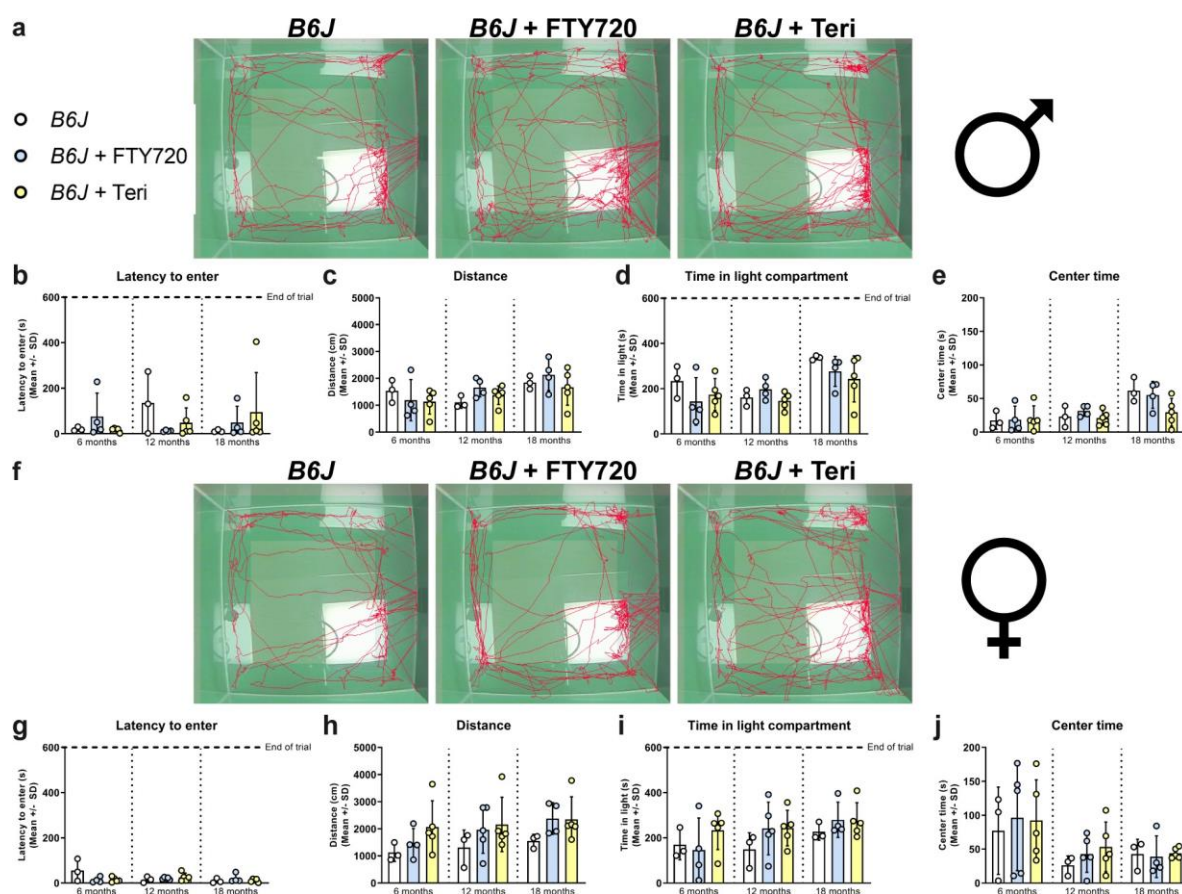**Figure 53: Early treatment with fingolimod or teriflunomide does not alter anxiety-like behavior of *B6J* mice.**
(a) Representative images of DLB analysis of 18-month-old male *B6J* and *B6J* mice treated with fingolimod (FTY720) or teriflunomide. Light square indicates the center zone of the arena. Red line represents the walking track. **(b)** Treatment does not alter latency to enter, **(c)** walking distance, **(d)** time in light compartment, or **(e)** center time of male *B6J* mice. **(f)** Representative images of DLB analysis of 18-month-old female *B6J* and treated *B6J* mice. Light square indicates the center zone of the arena. Red line represents the walking track. **(g)** Treatment does not alter the latency to enter, **(h)** walking distance, **(i)** time in light compartment, or **(j)** center time of female *B6J* mice. Error bars represent standard deviations (circles = value of one mouse). Significance of treated *B6J* mice compared to untreated *B6J* mice is determined by one-way ANOVA and Tukey's post hoc test.

Similar to what we have seen in *Rag1*-deficient mice, treatment with fingolimod or teriflunomide did not reduce the walking distance of male *Spg11⁻ᐟ⁻* mice in the CAR analysis (Figure 54a, b) and even though treatment with either immunomodulators could reduce the time male mutant mice spent leaning over the edge of the platform, the latency to jump and abnormal CAR was not ameliorated (Figure 54c – e). In female *Spg11⁻ᐟ⁻* mice, treatment with fingolimod, but not teriflunomide, led a tendency towards a reduced time spent leaning over the edge of the platform, while the other parameters remained unaffected by both treatments (Figure 54f – j).
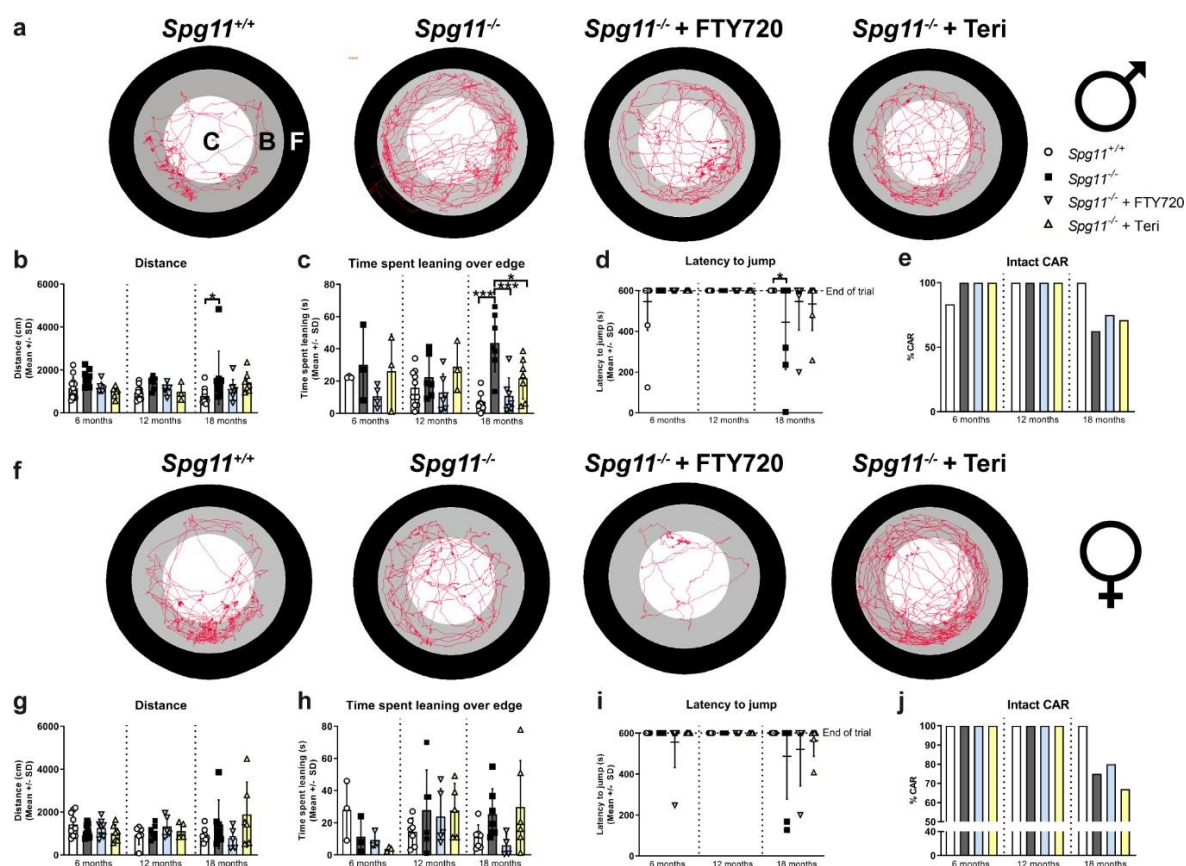
Figure 54: Early treatment with fingolimod or teriflunomide reduces time spent leaning over the edge of the platform of *Spg11⁻ᐟ⁻* mice.
(**a**) Representative images of CAR analysis of 18-month-old male *Spg11⁺ᐟ⁺*, *Spg11⁻ᐟ⁻* and *Spg11⁻ᐟ⁻* mice treated with fingolimod (FTY720) or teriflunomide. Red line represents the walking track (C= center zone, white; B= border zone, grey; F = floor zone, black). (**b**) Treatment does not reduce the walking distance of male *Spg11⁻ᐟ⁻* mice at 18 months. (**c**) Treatment reduces the time spent leaning over the edge of the platform of 18-month-old male *Spg11⁻ᐟ⁻* mice. (**d**) Treatment does not ameliorate the latency to jump or (**e**) CAR of male 18-month-old male *Spg11⁻ᐟ⁻* mice. (**f**) Representative images of CAR analysis of 18-month-old female *Spg11⁺ᐟ⁺*, *Spg11⁻ᐟ⁻* and treated *Spg11⁻ᐟ⁻* mice. Red line represents the walking track. (**g**) Treatment does not alter the walking distance of female *Spg11⁻ᐟ⁻* mice. (**h**) Treatment of female *Spg11⁻ᐟ⁻* mice with fingolimod, but not teriflunomide, shows a tendency towards a reduced time spent leaning over the edge of the platform at 18 months (**i**) Treatment does not ameliorate the latency to jump or (**j**) CAR of 18-month-old female *Spg11⁻ᐟ⁻* mice. Error bars represent standard deviations (circles, squares, triangles = value of one mouse). Significance of treated mutant mice compared to *Spg11⁺ᐟ⁺* and *Spg11⁻ᐟ⁻* mice is determined by one-way ANOVA and Tukey's post hoc test (*$p < 0.05$, ***$p < 0.001$). Corresponding data from *Spg11⁺ᐟ⁺* and *Spg11⁻ᐟ⁻* mice, as shown in Figure 17, are presented here again.

Treatment of male *B6J* mice with either fingolimod or teriflunomide increased the walking distance at 6, 12 and 18 months, resembling the findings in the OF analysis (Figure 55a, b). Furthermore, treatment with fingolimod increased the time spent leaning over the edge of the platform of 18-month-old male *B6J* mice (Figure 55c). Surprisingly, we detected a reduced latency to jump off the platform and an abnormal CAR in untreated male *B6J* mice, which was not altered by treatment with either immunomodulator (Figure 55d, e). In female *B6J* mice treatment with fingolimod did not lead to behavioral changes in the CAR analysis (Figure 55f – j). Treatment with teriflunomide led to a reduced latency to jump off the platform and an abnormal CAR when compared to untreated mice at 12 months, while the other parameters remained unaffected (Figure 55f – j).
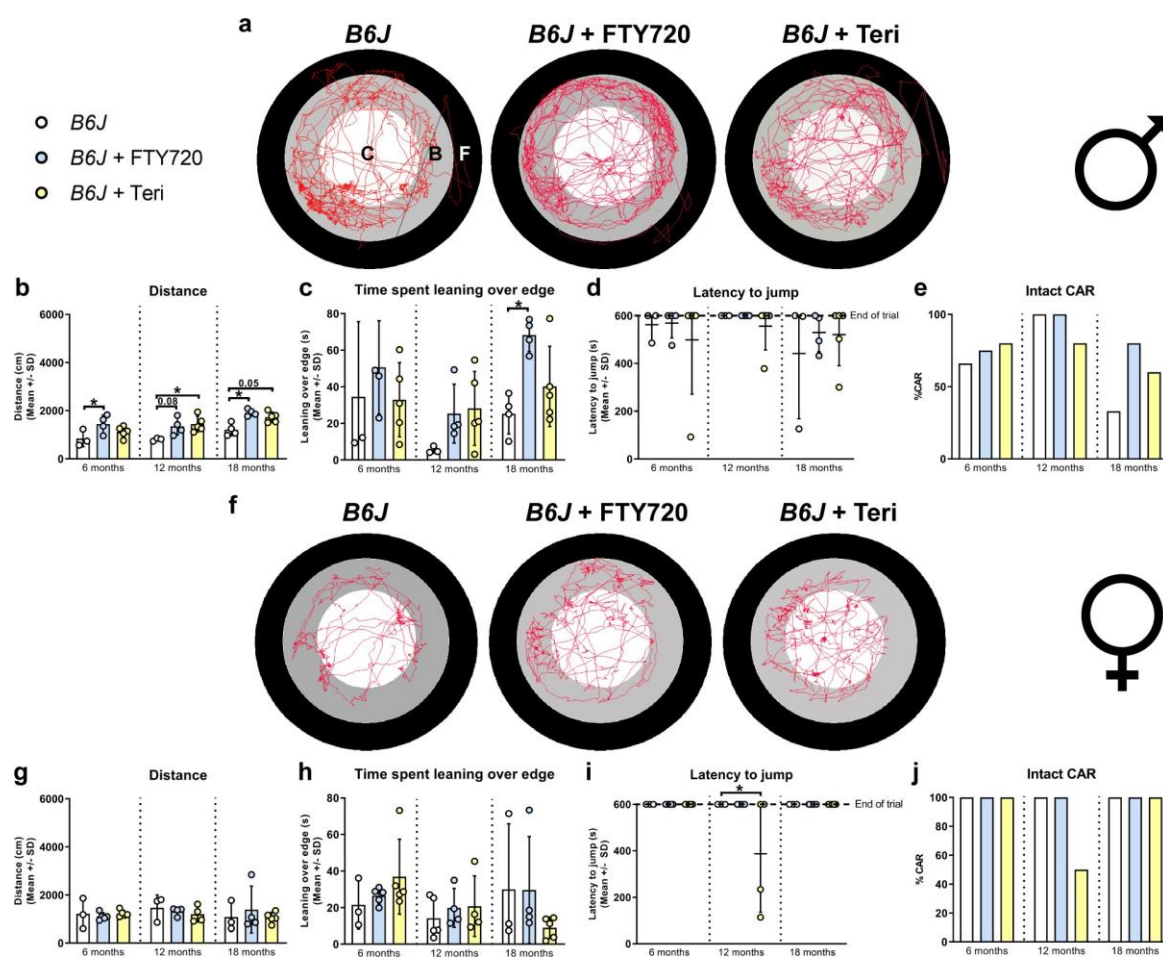
Figure 55: Early treatment with fingolimod or teriflunomide increases aspects of impulsivity-like behavior of *B6J* mice.
(a) Representative images of CAR analysis of 18-month-old male *B6J* and *B6J* mice treated with fingolimod (FTY720) or teriflunomide. Red line represents the walking track (C= center zone, white; B= border zone, grey; F = floor zone, black). (b) Treatment with either immunomodulators increases the walking distance of male *B6J* mice compared to untreated mice at all investigated ages. (c) Treatment with fingolimod increases the time spent leaning over edge in male 18-month-old *B6J* mice compared to untreated mice. (d) Untreated male *B6J* mice show jumping behavior and (e) abnormal CAR. Treatment does not alter these parameters. (f) Representative images of CAR analysis of 18-month-old female *B6J* and treated *B6J* mice. Red line represents the walking track. (g) Treatment does not alter the

walking distance or **(h)** time spent leaning over edge of female *B6J* mice. **(i)** Treatment with teriflunomide, but not fingolimod, reduces the latency to jump of 12-, but not 6- or 18-month-old female *B6J* mice compared to untreated mice. **(j)** Female *B6J* mice treated with teriflunomide, but not fingolimod, display an abnormal CAR at 12 months compared to untreated mice. Error bars represent standard deviations (circles = value of one mouse). Significance of treated *B6J* mice compared to untreated *B6J* mice is determined by one-way ANOVA and Tukey's post hoc test (*$p < 0.05$).

In summary, we here show that pharmacological immunomodulation could substantially improve the abnormal social behavior of *Spg11$^{-/-}$* mice, as well as anxiety-like behavior and some aspects of impulsivity- behavior. Resembling our findings in *Rag1*-deficient *Spg11$^{-/-}$* mice, treatment did not affect hyperactivity-like behavior. Interestingly, and somewhat surprisingly, treatment of *B6J* mice with fingolimod or teriflunomide led to increased hyperactivity-like behavior.

5.10 Late treatment with clinically approved immunomodulators ameliorates pathological alterations and improves gait coordination of *Spg11$^{-/-}$* mice

After having shown that early treatment of mutant mice starting at 3 months of age led to a substantial alleviation of distinct disease features and improved clinical alterations, typically present in *Spg11$^{-/-}$* mice, we started the treatment at 15 months of age, when the disease had already developed (Figure 56). This is a more clinically relevant therapeutic setup, as patients usually seek medical help when symptoms have already occurred, and the disease has progressed.
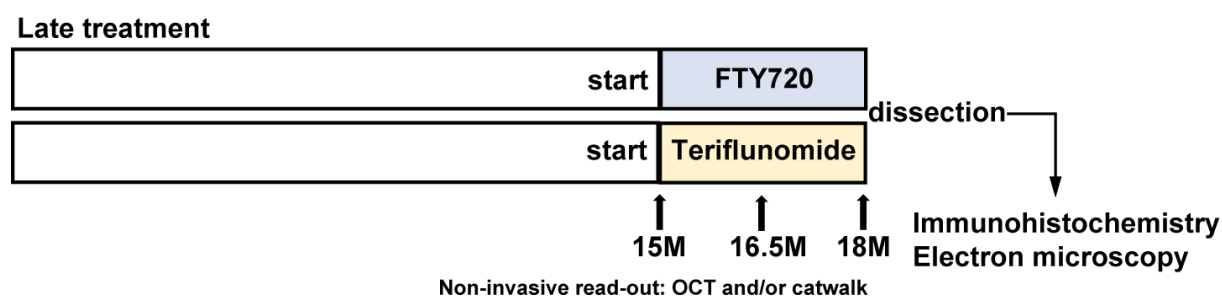
Figure 56: Treatment regime for late treatment of *Spg11$^{-/-}$* mice with fingolimod or teriflunomide.
Schematic representation of the late treatment using fingolimod (FTY720) or teriflunomide as medications in the drinking water. "Late treatment" starts when histopathological and clinical features are present, at 15 months of age, and lasted for 90 days. Non-invasive read-outs during the treatment are indicated by arrows, allowing longitudinal studies.

Following the late treatment of mutant mice, we did not detect a reduction of CD8$^+$ or CD4$^+$ T-lymphocytes in ON (Figure 57a, b). However, and unlike the effect we saw in ON, late treatment of *Spg11$^{-/-}$* mice caused a substantial decline in the number of CD8$^+$, but also in the number of the less frequent CD4$^+$ T-lymphocytes in the CC, CO and CB (Figure 57c– h).
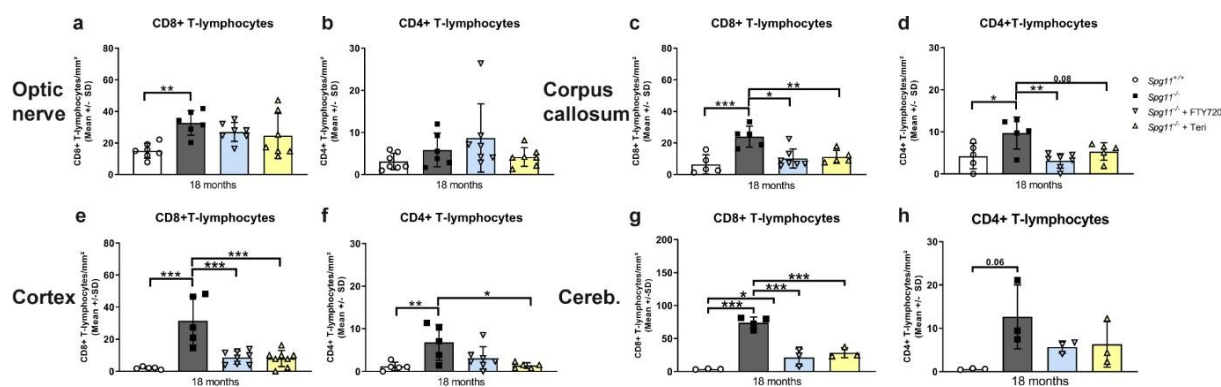
Figure 57: **Late treatment with fingolimod or teriflunomide reduces inflammation by CD8⁺ and CD4⁺ T-lymphocytes in white and grey matter compartments of *Spg11⁻ᐟ⁻* mice.** **(a, c, e, g)** Quantification of CD8⁺ T-lymphocytes in distinct CNS compartments of *Spg11⁺ᐟ⁺*, *Spg11⁻ᐟ⁻*, and *Spg11⁻ᐟ⁻* mice after treatment with fingolimod or teriflunomide at distinct ages. **(a)** CD8⁺ T-lymphocytes in longitudinal ON sections, and coronal sections of **(c)** CC, **(e)** CO and **(g)** CB. Note that in all compartments, except ON, treatment with either of the immunomodulator attenuates the number of CD8⁺ T-lymphocytes, typically increased in *Spg11⁻ᐟ⁻* mice. **(b, d, f, h)** Quantification of CD4⁺ T-lymphocytes in distinct CNS compartments of 18-month-old *Spg11⁺ᐟ⁺*, *Spg11⁻ᐟ⁻*, and treated *Spg11⁻ᐟ⁻* mice. **(b)** Treatment does not reduce the generally low number of CD4⁺ T-lymphocytes in ON, but they are reduced in **(d)** CC, **(f)** CO and **(h)** CB. Error bars represent the standard deviations (circles, squares, triangles = mean value of one mouse). Significance of treated mutant mice compared to *Spg11⁺ᐟ⁺* and *Spg11⁻ᐟ⁻* mice is determined by one-way ANOVA and Tukey's post hoc test (*$p < 0.05$, **$p < 0.01$, *** $p < 0.001$).

Ultrastructural investigation of ON by EM revealed that axonopathic features showed only a mild trend towards reduction (Figure 58a, b). Interestingly, late treatment with fingolimod, but not teriflunomide, caused a trend towards an increase of axons with redundant myelin (Figure 58c), possibly reminiscent of the unexpected findings upon early treatment with both drugs (compare with Figure 36c). Late treatment with fingolimod or teriflunomide did not significantly change axon loss of *Spg11⁻ᐟ⁻* mice (Figure 58d). Accordingly, there was no effect on the area of the ON after late treatment (Figure 58e). Using IC, we saw that only treatment with teriflunomide, but not fingolimod significantly reduced the number of SMI32⁺ axonal spheroids in ON (Figure 58f), while late treatment with both drugs substantially reduced the number of spheroids in CC, CO and CB (Figure 58g – i), a finding that is in accordance with the effect of the late treatment on inflammation in these compartments. Reminiscent of *Rag1*-deficient and early treated *Spg11⁻ᐟ⁻* mice, late treatment with either fingolimod or teriflunomide did not dampen brain weight decline of 18-month-old *Spg11⁻ᐟ⁻* mice (Figure 58j).

Figure 58: Late treatment with fingolimod or teriflunomide reduces neural damage in the CNS of *Spg11*^{-/-} mice.

(**a**) Representative electron micrographs of ON cross sections of 18-month-old *Spg11*^{+/+}, *Spg11*^{-/-}, and *Spg11*^{-/-} mice treated with fingolimod or teriflunomide and (**b – e**) EM-based quantification of pathological alterations. Asterisks indicate axonopathic features, hashtags axons with redundant myelin, open arrowheads myelin fragments. Scale bar: 2 µm. (**b**) Treatment with teriflunomide, but not fingolimod, shows a trend towards reduction of axonopathic features, typically occurring in *Spg11*^{-/-} mice. (**c**) Redundant myelin becomes more frequent after treatment with fingolimod. (**d**) Late treatment with neither fingolimod nor teriflunomide preserves the number of axons or (**e**) ON area of *Spg11*^{-/-} mice. (**f**) Representative images of SMI32⁺ axonal spheroids (arrows) in longitudinal ON sections of 18-month-old *Spg11*^{+/+}, *Spg11*^{-/-}, and treated *Spg11*^{-/-} mice (left) and corresponding quantification (right). Scale bar: 10 µm. Late treatment with teriflunomide, but not fingolimod, reduces the increase in the number of SMI32⁺ spheroids, typically occurring in *Spg11*^{-/-} mice. (**g**) Late treatment with either immunomodulator reduces the formation of SMI32⁺ axonal spheroids, typically occurring in *Spg11*^{-/-} mice, in coronal sections of CC, (**h**) CO, and (**i**) CB. (**j**) Late treatment does not increase dampen brain decline, typically occurring in *Spg11*^{-/-} mice. Error bars represent the standard deviations (circles, squares, triangles = mean value of one mouse). Significance compared to *Spg11*^{+/+} and *Spg11*^{-/-} mice is determined by one-way ANOVA and Tukey's post hoc test (*$p < 0.05$, **$p < 0.01$, ***$p < 0.001$).

Similar to *Rag1*-deficient *Spg11*^{-/-} mice and the early treatment approach, there was no effect on retinal thickness by the late treatment approach, as revealed by OCT analysis (Figure 59a).
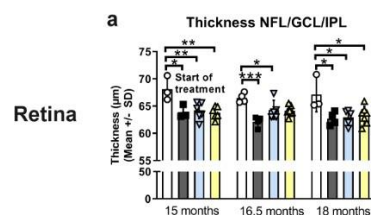
Figure 59: Late treatment with fingolimod or teriflunomide does not restore retinal thickness of *Spg11^{-/-}* mice.

(a) Longitudinal analysis of the thickness of the innermost retinal composite layer (NFL/GCL/IPL) of *Spg11^{+/+}, Spg11^{-/-},* and *Spg11^{-/-}* mice treated with fingolimod (FTY720) or teriflunomide, by OCT. Treatment does not reduce retinal thinning of *Spg11^{-/-}* mice. Error bars represent the standard deviations (circles, squares, triangles = mean value of one mouse). Significance of treated *Spg11^{-/-}* mice compared to *Spg11^{+/+}* and *Spg11^{-/-}* mice is determined by one-way ANOVA and Tukey's post hoc test (*$p < 0.05$, **$p < 0.01$, ***$p < 0.001$).

Regarding the clinical readout of this study, late treatment with fingolimod or teriflunomide resulted in significantly improved gait characteristics (Figure 60a – l). Treatment with teriflunomide significantly improved the paw angle body axis variation of *Spg11^{-/-}* mice at 18 months (Figure 60c), while treatment with either drug substantially reduced the step cycle variation and restored the regularity index at the same age (Figure 60e, g). All these parameters share the common feature that, in the absence of treatment, they still progress between the ages of 15 and 18 months. The other parameters, including strength parameters, stride length and number of steps do not progress anymore between these timepoints and late treatment with fingolimod or teriflunomide did not affect them (Figure 60a, c, f, h – l).
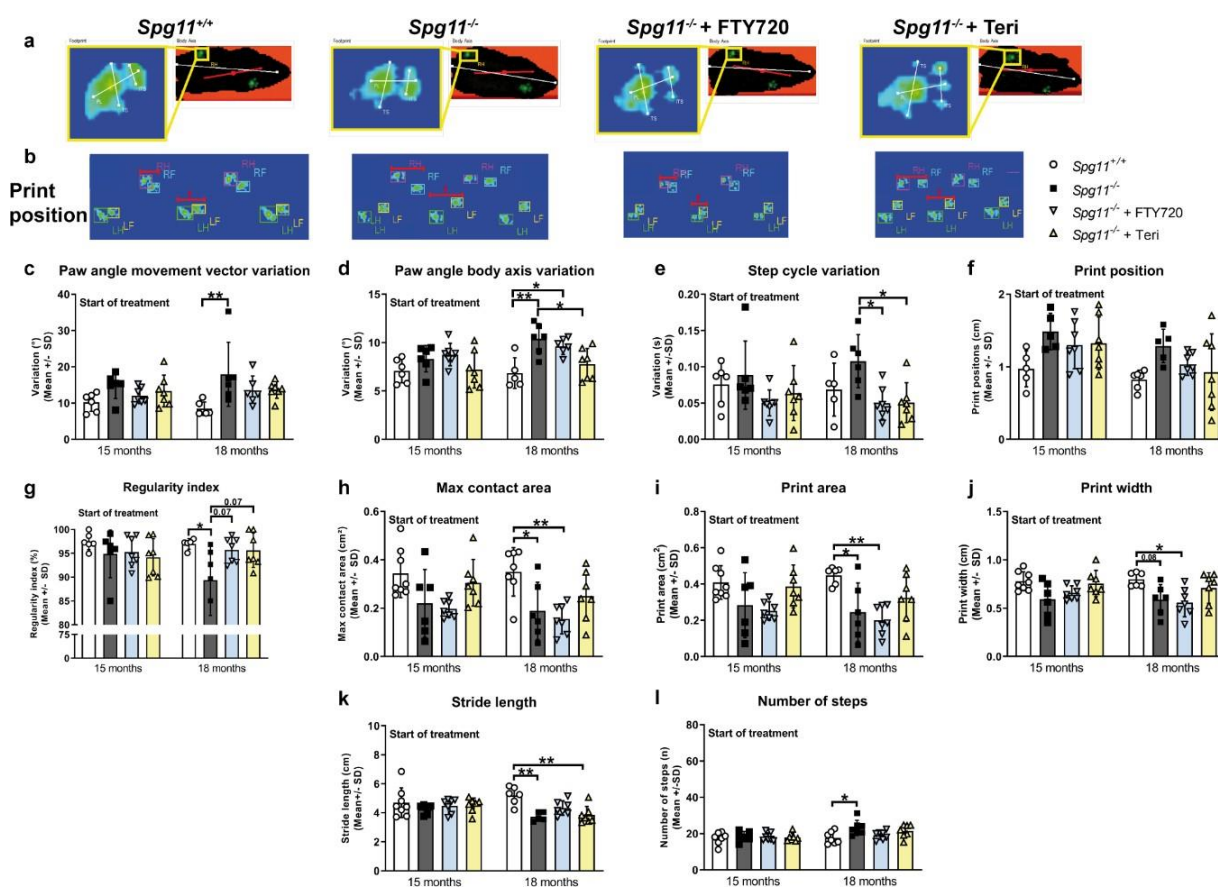
Figure 60: Late treatment with fingolimod or teriflunomide improves abnormalities related to gait coordination of *Spg11⁻/⁻* mice.

(a) Representative images of body contours, footprints and (b) print positions of 18-month-old *Spg11⁺/⁺*, *Spg11⁻/⁻*, and *Spg11⁻/⁻* mice after treatment with fingolimod (FTY720) or teriflunomide, while crossing the CatWalk device (ITS: intermediate toe spread; TS: toe spread; PL: print length; RF: right front paw; LF: left front paw; RH: right hind paw; LH: left hind paw). Red line (top) indicates the body axis, red line segment (bottom) indicates print position. (c) In *Spg11⁻/⁻* mice, treatment does not ameliorate paw angle movement vector variation and (d) only treatment with teriflunomide reduces the paw angle body axis variation at 18 months. (e) In *Spg11⁻/⁻* mice, treatment with fingolimod and teriflunomide ameliorates the step cycle variation at 18 months. (f) In *Spg11⁻/⁻* mice, treatment does not ameliorate the print position. (g) In *Spg11⁻/⁻* mice, treatment with either immunomodulator ameliorates the regularity index at 18 months. (h) In *Spg11⁻/⁻* mice, treatment does not ameliorate the maximal contact area, (i) the print area, or (j) the print width of the hind paws. (k) In *Spg11⁻/⁻* mice, treatment does not alter stride length or (l) number of steps. Error bars represent the standard deviations (circles, squares, triangles = mean value of three consecutive runs of one mouse). Significance of *Spg11⁻/⁻* mice compared to *Spg11⁺/⁺* mice and treated *Spg11⁻/⁻* mice compared to *Spg11⁺/⁺* and *Spg11⁻/⁻* mice is determined by one-way ANOVA and Tukey's post hoc test ($*p < 0.05$, $**p < 0.01$, $***p < 0.001$).

In summary, most histopathological alterations and some parameters of gait coordination responded to the treatment, even when started relatively late in the disease progression, provided these parameters still progressed between the ages of 15 and 18 months.

Due to limited amounts of experimental animals, we had to omit the impact of late pharmacological treatment on behavioral tests. This must presently remain a topic for future experiments.

6 Discussion

Previously conducted studies in models of SPG11 focused on neuropathological and clinical alterations (Varga *et al.*, 2015; Branchu *et al.*, 2017). In this study, we demonstrate a robust impact of CNS inflammation on disease progression in a mouse model of SPG11. We could demonstrate that this model for a hereditary neurodegenerative disease shows distinct gait characteristics and behavioral abnormalities, recapitulating features also present in patients. The role of inflammation as a disease amplifier was not only refined to the histopathological findings but extended to the gait and behavioral abnormalities, a finding that could be of great importance to other genetically-mediated diseases.

6.1 CD8^{+} T-lymphocytes are likely candidates to amplify disease progression in *Spg11^{-/-}* mice

While we observed an increase in number and activation of microglia in this SPG11 mouse model, we here focused on the impact of T-lymphocytes as – from a translational point of view – targetable pathogenic immune cells in other neuroinflammatory diseases like MS (Melzer & Meuth, 2014; Klotz *et al.*, 2019). We found that CD4^{+} and CD8^{+} T-lymphocytes showed a robustly increased number in all investigated CNS compartments. CD8^{+} T-lymphocytes did not only outnumber CD4^{+} T-lymphocytes in the parenchyma of all investigated CNS compartments, but the occurrence and accumulation in *Spg11^{-/-}* mice also correlated with the development of axonopathic and clinical alterations. This suggests that CD8^{+} T-lymphocytes are likely the main pathogenic player among the adaptive immune cells in *Spg11^{-/-}* mice. We found that CD8^{+} T-lymphocytes were often closely associated with perturbed axons, suggesting a direct and detrimental impact. Supporting the implication of CD8^{+} T-lymphocytes, *Rag1*-deficiency led not only to a preservation of axons but also to a robust amelioration of the disease outcome in *Spg11^{-/-}* mice. Remarkably, in other models of genetically mediated CNS disorders or during normal aging our group could prove that CD8^{+} T-lymphocytes are indeed the major pathogenic player using bone-marrow transplant experiments (Ip *et al.*, 2006; Kroner *et al.*, 2010; Ip *et al.*, 2012; Groh *et al.*, 2013; Groh *et al.*, 2016a; Groh *et al.*, 2021b). While reconstitution of *Rag1*-deficient mutant or aged *Rag1*-deficient mice with *Cd4^{-/-}* bone marrow did not retain diminished axonal degeneration, mice reconstituted with *Cd8^{-/-}* bone marrow not only showed reduced axonal degeneration but also significant clinical improvements, like an increased NFL/GCL/IPL thickness, as measured by OCT, and a better rotarod performance (Ip *et al.*, 2006; Kroner *et al.*, 2010; Ip *et al.*, 2012; Groh *et al.*, 2013; Groh *et al.*, 2016a; Groh *et al.*, 2021b). These findings further underline the pathogenic impact of CD8^{+} T-lymphocytes not

only on a histopathological but also on a clinical level. Strikingly, this could be seen among different hereditary CNS diseases, e.g., PMS, SPG2, and NCL as well as normal aging (Ip *et al.*, 2006; Kroner *et al.*, 2010; Ip *et al.*, 2012; Groh *et al.*, 2013; Groh *et al.*, 2016a; Groh *et al.*, 2017; Groh *et al.*, 2021b). Moreover, we saw a disproportional increase of $CD8^+CXCR6^+CXCR4^-CD103^+$ T-lymphocytes, a subpopulation of $CD8^+$ T-lymphocytes, in the brains of *Spg11$^{-/-}$* mice by flow cytometry. These markers for activation and cytotoxicity have been previously identified in disturbed white matter of normal aging mice (Groh *et al.*, 2021b) and have also been found to be expressed by $CD8^+$ T-lymphocytes in active white matter lesions of MS patients (Machado-Santos *et al.*, 2018; Lassmann, 2019; Fransen *et al.*, 2020).

These previously described observations reveal striking commonalities of $CD8^+$ T-lymphocytes in lysosomal storage diseases, myelin-related CNS disorders, primary neuroinflammatory diseases and normal aging and strongly suggest that $CD8^+$ T-lymphocytes amplify disease progression in the present model of SPG11.

6.2 Damage of myelinated axons is amplified by neuroinflammation in *Spg11$^{-/-}$* mice

Spatacsin, the culprit gene leading to SPG11, has initially been reported to be expressed by neurons (Murmu *et al.*, 2011; Perez-Branguli *et al.*, 2014; Pozner *et al.*, 2020). Its absence leads to cytoskeletal abnormalities and axonopathic changes in human-derived neurons *in vitro* (Perez-Branguli *et al.*, 2014). Therefore, it is possible that such perturbed neurons may foster neuroinflammation in the living organism which can lead to or amplify neuronal damage. However, recent large-scale brain mapping projects revealed that oligodendrocytes show an additional robust expression of *Spg11* (Sjostedt *et al.*, 2020). Hence, the absence of spatacsin in these cells could also lead to pathogenic neuroinflammation, likely directed against the oligodendrocytes. In oligodendroglial (*Plp1*) mutant mice (Ip *et al.*, 2006; Kroner *et al.*, 2010; Groh *et al.*, 2016a) axonal spheroids and perturbed myelinated axons are similarly associated with $CD8^+$ T-lymphocytes, and the axonal damage is strongly dependent on these immune cells. This implicates that oligodendrocytic mutations alone are sufficient to induce perturbation in myelinated axons via glia-directed neuroinflammation, likely pointing towards altered axon-glia interactions. We propose that impaired axon-glia interaction also accounts for redundant myelin being prone to degenerate, as it leads to a dysregulation of myelin-axon signaling and aberrant myelin synthesis, further underscoring its implication in axonal perturbation. This in turn could lead to an immune response targeted against the myelin sheath, as seen in neuroinflammatory diseases, like MS (Hohlfeld & Wekerle, 2001). The fact that *Spg11$^{-/-}$* mice treated with fingolimod or teriflunomide show a preservation of axon numbers, even though

they still display a high percentage of redundant myelin, further strengthens this hypothesis. Interestingly, recent studies in experimental autoimmune encephalomyelitis (EAE) revealed that experimentally induced demyelination can rescue initially myelinated axons from inflammatory attack, reflecting that perturbed myelin can indeed be a risk factor for axonal degeneration under neuroinflammatory conditions (Schäffner *et al.*, 2021). Importantly, recent studies have shown that while CD8^{+} T-lymphocytes accumulate in distinct diseases and during normal aging of the CNS, there are multiple subsets within the CD8^{+} T-lymphocyte pool, which display some differences in gene expression and heterogeneity, are functionally distinct and can have different roles *in vivo* (Dressman & Elyaman, 2022; Groh *et al.*, unpublished data). These observations demonstrate an overarching, detrimental role of CD8^{+} T-lymphocytes in not only SPG11, but also various other disease conditions as exemplified above. Furthermore, it may also impressively reflect their common neural target structure in the form of vulnerable, myelinated axons.

By using bone marrow transplant approaches it was shown that Granzyme B (GzmB) is mechanistically involved in T-lymphocyte driven axonal degeneration in *Plp1* overexpressing mice (Ip *et al.*, 2012; Kroner *et al.*, 2010) and during normal aging (Groh *et al.*, 2021b). GzmB is a cytotoxic serine protease that is enriched in CD8^{+} T-lymphocytes carrying markers for chronic activation and cytotoxicty (Groh *et al.*, 2021b). Upon antigen recognition, GzmB, together with perforin becomes concentrated and eventually released from cytotoxic granules by CD8^{+} T-lymphocytes (Chowdhury & Lieberman, 2008; Dressman & Elyaman, 2022). This in turn activates distinct pathways of cell damage in target cells and induces demyelination (Shi *et al.*, 2005; Chowdhury & Lieberman, 2008; Dressman & Elyaman, 2022). Perforin has a critical role in trafficking granzymes, as it can either lead to release of granzymes from endosomes or can form pores in plasma membranes that enables granzyme to enter the cytosol of target cells (Keefe *et al.*, 2005; Cullen & Martin, 2008). This mechanism is a likely driver of CD8^{+} T-lymphocyte mediated cytotoxicity (Chowdhury & Lieberman, 2008), and could therefore also be involved in axonal degeneration in this mouse model for SPG11.

6.3   Damage of cell bodies is amplified by neuroinflammation in *Spg11*^{-/-} mice

Spg11^{-/-} mice show loss of RGCs, as seen in retinal flat mount preparations using RGC-specific antibodies, most likely due to damage of myelinated axons. Programmed axonal degeneration, also known als Wallerian degeneration (WD), has been shown to occure not only following injury but also in chronic CNS inflammatory disorders such as MS or during EAE (Dziedzic *et al.*, 2010; Singh *et al.*, 2017). Sterile alpha and TIR motif-containing 1 (*SARM1)* has been

identified as a key mediator of Wallerian degeneration (WD), acting downstream of neuroinflammation (Ko *et al.*, 2020). Interestingly, deletion of *Sarm1* rescues Wallerian-like axonopathy in a nicotinamide mononucleotide adenylyltransferase 2 (*Nmnat2*)-deficient mouse model (Gilley *et al.*, 2017), and *Sarm1* knockout protects against axonal degeneration during EAE (Viar *et al.*, 2020). Of note, *SARM1* variants were found to be enriched in HSP patients (Gilley *et al.*, 2021), making it plausible that it might be involved in axonal degeneration in this mouse model. Activation of *SARM1* promotes axon death through NAD^+ cleavage, followed by decreased ATP levels leading to a bioenergetic crisis of the axon, axonal degeneration, and a subsequent loss of the cell body (Gerdts *et al.*, 2015; Essuman *et al.*, 2017). Therefore, our findings may not only implicate myelinated axons as vulnerable target structures but consequently also their cell bodies, i.e., RGCs. Of note, $Spg11^{-/-}$ mice also show loss of Purkinje cells (PCs), that are not only implicated in impaired gait coordination but also disturbed social behavior (Van Overwalle *et al.*, 2020; Cutando *et al.*, 2022), which is discussed in more detail in a later section. An unexpected observation was that neither *Rag1*-deficiency nor treatment with fingolimod or teriflunomide could rescue the concomitant retinal thinning as identified by OCT in $Spg11^{-/-}$ mice. We hypothesize that a persistent reduction of dendritic areas in the inner plexiform layer (IPL) contributes to retinal thinning in the $Spg11^{-/-}$ mutants, rather than loss of RGCs alone, as the latter is prevented by targeting lymphocytes. Reduced dendritic areas in IPL, in addition to loss of RGCs, have been observed in mice carrying mutant human *PLP1* genes (Groh *et al.*, 2018) and in aging mice (Groh *et al.*, 2021b), but, in contrast to the present model, could be dampened by targeting the adaptive immune system. As *Rag1*-deficiency did not delay retinal thinning, we propose that this is not directly connected to the adaptive immune response, at least in this mouse model for SPG11. We would, thus, like to hypothesize that activated microglia cells - not targeted in the present study - substantially contribute to the reduction of the dendritic areas in the IPL of $Spg11^{-/-}$ mice. Indeed, activated microglial cells were found in distinct retinal layers under different disease conditions (Langmann, 2007; Rojas *et al.*, 2014), including AD (Salobrar-Garcia *et al.*, 2020) and MS (Choi *et al.*, 2021). Moreover, targeting microglial cells led to reduced retinal thinning in mice after experimental retinal vein occlusion (Jovanovic *et al.*, 2020) and in mice expressing a functional null mutation of the human *PLP1* gene (Groh *et al.*, 2019). Interestingly, microglial cells also express spatacsin (Hauser *et al.*, 2020; Sjostedt *et al.*, 2020) and could therefore be affected by spatacsin deficiency, making the pathogenic mechanism even more complex. We identified microglia cells as being activated in distinct CNS compartments of $Spg11^{-/-}$ mice, even though we do not know whether they are indeed activated by such cell autonomous mechanisms. Microglial cells

play an important role in many other CNS disorders (Keren-Shaul *et al.*, 2017; Deczkowska *et al.*, 2018a; Deczkowska *et al.*, 2018b) and can initiate an increased recruitment of pathogenic CD8^{+} T-lymphocytes (Mohebiany *et al.*, 2020). Using sialoadhesin (Sn) as a microglial activation marker, we could show that *Rag1*-deficiency reduced the activation of microglia in CNS compartments. This argues against the possibility that spatacsin deficiency causes microglial activation solely by a cell-autonomous mechanism. Previous work showed that loss of brain weight was ameliorated after depletion of microglia in CLN1 mice (Berve *et al.*, 2020). We detected brain weight decline in *Spg11*^{-/-} mice. However, neither *Rag1*-deficiency nor pharmacological treatment could dampen the loss of brain weight of *Spg11*^{-/-} mice. This is surprising, as axonal perturbation in the brain is considerably reduced by all approaches and previous studies have shown that treatment with immunomodulators could significantly dampen brain weight decline in mouse models for CLN1 and CLN3 (Groh *et al.*, 2017; 2021a). This might possibly point towards involvement of microglia. It would be interesting to target microglial cells by either a genetic approach, e.g., CX3CR1 or Sn knockout mice, or by a pharmacological approach, e.g., treatment with the CSF1R-inhibitor PLX5622, to determine the influence of microglia on disease progression. Of note, more cells including circulating leukocytes express spatacsin (Hauser *et al.*, 2020; Sjostedt *et al.*, 2020), adding to the complexity of the disease's pathomechanism. To decipher which cell type(s) induce neuroinflammation in *Spg11*^{-/-} mice, studies in cell-specific knockout models are needed.

6.4 Immune modulation improves histopathological alterations and walking pattern abnormalities of *Spg11*^{-/-} mice

One of the most important points of this study concerns the potential translational impact. Up to this day treatment options for HSP diseases are confined to mostly spasmolytic drugs, botulinum toxin and physiotherapy (Boutry *et al.*, 2019a; Gumeni *et al.*, 2021). In this study, we open the possibility to target a more causal, disease-amplifying mechanism. Genetic inactivation of the adaptive immune system by crossbreeding *Spg11*^{-/-} mice with *Rag1*-deficient mice, used as a proof-of-concept, led to axon preservation in multiple compartments of the CNS, and robustly improved the clinical outcome. Using the clinically established immunomodulators fingolimod and teriflunomide (Brinkmann *et al.*, 2010; Chun & Brinkmann, 2011; Melzer & Meuth, 2014) in a subsequent translational approach, we dampened adaptive immune reactions. In an early treatment approach, starting at three months of age, we could show that treatment with either immunomodulator recapitulated the findings of the proof-of-principle experiments, preserving the axonal integrity. The impact of the

treatment on clinical features is of relevance with regard of the possible translational benefits. We divided our clinical investigations into two different subsets: the gait analysis and the behavioral analysis.

Regarding the gait analysis, we included two important features: gait coordination and strength. Both are well depicted by the CatWalk analysis used in our study. We detected increased variability of interlimb coordination and stepping pattern as well as reduced rhythmicity of gait in *Spg11*$^{-/-}$ mice, a finding that was similarly detected in a mouse model of cerebellar ataxia (Lang *et al.*, 2020). Therefore, we propose that the altered gait coordination of *Spg11*$^{-/-}$ mice reflects atactic features. Not only genetic depletion of lymphocytes by *Rag1*-deficiency but importantly also treatment with the immunomodulators fingolimod or teriflunomide robustly ameliorated these atactic gait features. This was accompanied by histopathological improvements of possibly relevant compartments, like CB, CO and CC, that all showed robust neuroinflammation in *Spg11*$^{-/-}$ mice. Of particular relevance might be disturbed cerebellar components, like axons of PCs, as they are the histopathological base of cerebellar ataxia in different mouse models (Grusser-Cornehls & Baurle, 2001; Manto, 2009) and patients (Koeppen, 2018). Our observation that neuroinflammation by CD8$^+$ T-lymphocytes was most prominent in CB and that targeting these cells robustly improved axonal structures and ataxia corroborate the implication of cerebellar components. The *robotic* mouse mutant suffers from a mutation in the PC-specific transcription factor *Af4*, which leads to progressive adult-onset PC loss (Isaacs *et al.*, 2003; Oliver *et al.*, 2007). Interestingly, the occurrence of ataxic-like gate characteristics, like variation of direction of movement, appear when axonal "torpedoes" form in the CB (Isaacs *et al.*, 2003; Oliver *et al.*, 2007), identical to what we call spheroids. Previous studies in this SPG11 mouse model could indeed show an age-dependent loss of PCs of *Spg11*$^{-/-}$ mice (Branchu *et al.*, 2017). These observations support our hypothesis, that mitigating inflammation-related axonal perturbation by either a genetic approach or immunomodulation improves atactic features.

The other investigated parameter using the CatWalk analysis was strength, depicted as a reduction of maximal contact area, print width and print area of the hind paws. It has been shown that sciatic nerve injury in mice or muscle injury in rats can lead to a reduced print area and print width (Bozkurt *et al.*, 2008) and that this could be due to muscular atrophy and loss of strength (Hoke & Brushart, 2010; Gronholdt-Klein *et al.*, 2019). Interestingly, even if the sciatic index, an index for functional recovery of the sciatic nerve, normalized after injury, mice still showed a smaller print area than pre-injury (Bozkurt *et al.*, 2008), possibly due to the slow regeneration of muscular atrophy. Therefore, it is plausible to assume that a reduction of these

print parameters does indeed implicate strength loss in this SPG11 mouse model. Interestingly, we did not see an effect of genetic or pharmacological targeting of lymphocytes on the gait parameters reflecting strength. Previous studies could show a loss of large motor neurons in the spinal cord (SC) of *Spg11*^{-/-} mice (Branchu *et al.*, 2017). However, T-lymphocytes were rare in the SC of *Spg11*^{-/-} mice which could point towards predominantly non-immune-related neural damage in this compartment. Based on studies conducted in humans, peripheral nerves are likely affected in this mouse model, possibly contributing to reduced strength (Klebe *et al.*, 2015; Montecchiani *et al.*, 2016; Boutry *et al.*, 2019a). Interestingly, while we did not investigate pathological features in peripheral nerves of *Spg11*^{-/-} mice, inflammation by T-lymphocytes was rarely detected (data not shown). Previous studies in a model for the most frequently inherited neuropathy, Charcot-Marie-Tooth (CMT) 1A disease, showed that T-lymphocytes were mildly upregulated in peripheral nerves (Kobsar *et al.*, 2005) and the disease progression was not ameliorated by *Rag1*-deficiency (Kohl *et al.*, 2010). Instead, targeting of endoneurial macrophages could substantially alleviate the neuropathic symptoms in this mouse model underscoring the role of macrophage-mediated inflammation (Klein *et al.*, 2022). However, in other CMT subtypes low grade secondary inflammation by T-lymphocytes is responsible for deterioration of pathological features (Schmid *et al.*, 2000; Maurer *et al.*, 2001; Kobsar *et al.*, 2003), underlining the complexity of peripheral nerve pathology. All together, we here show that particularly those gait parameters reflecting cerebellar ataxia, a feature typical for complicated HSP forms like SPG11, are improved by pharmacological immunomodulation, while parameters reflecting strength are not affected by the treatment. Presently, there are no standardized, reliable measures available to characterize parameters reflecting spasticity in mice (Wieters *et al.*, 2021). Therefore, we were not able to analyze this in our SPG11 mouse model, even though spasticity is another important feature of HSPs. Of note, in a similar SPG11 model, Varga *et al.* used the "foot-base-angle" to investigate a combined spastic and ataxic gait (Varga *et al.*, 2015). It would be interesting to investigate this further regarding its dependency on inflammation. Importantly, to fully understand the gait-related improvement by immunomodulation and its translational impact, there is need to "harmonize" gait parameters seen in patients with potentially related features in *Spg11*^{-/-} mice and other HSP-related models.

Previous studies in another SPG11 mouse models could demonstrate that mice showed reduced body weight from 12 months onwards (Varga *et al.*, 2015), a similar finding to what we saw in male *Spg11*^{-/-} mice. However, female *Spg11*^{-/-} mice showed body weight loss at already at 8 months. We do not know if the aforementioned study used both male and female mice, or only

male mice, which could explain the observed differences. Interestingly, *Rag1*-deficiency dampened body weight loss of male *Spg11⁻ᐟ⁻* mice, while it did not in female mutant mice, and treatment with fingolimod or teriflunomide failed to dampen body weight loss of males or females. Surprisingly, treatment with teriflunomide led to a body weight reduction in both male and female *B6J* mice compared to untreated mice, while treatment with fingolimod showed the same tendency, indicating that treatment with immunomodulators alone is sufficient to induce body weight loss. One explanation for this might be the hyperactivity-like behavior of mice. While neither *Rag1*-deficiency nor treatment with immunomodulators could reduce this behavior in *Spg11⁻ᐟ⁻* mice, treatment increased it in *B6J* mice.

6.5 Immune modulation improves social abnormalities of *Spg11⁻ᐟ⁻* mice

Another research area we focused on is the historically more neglected and only insufficiently researched behavioral involvement. In humans, neuropsychological abnormalities are a comorbidity in many CNS diseases like AD, PD, MS, multiple system atrophy and HSPs (Becker *et al.*, 1988; St Clair *et al.*, 1988; Brassington & Marsh, 1998; Osmolak *et al.*, 2012; Barcelos *et al.*, 2018; Faber *et al.*, 2018a). However, the underlying reasons remain mainly elusive, and translation from mouse to men is difficult. Previous work could show that secondary inflammation due to white matter abnormalities leads to depression- and catatonia-like behavior in mice, symptoms implicated in schizophrenia, bipolar disorder and major depressive disorder in humans (Hagemeyer *et al.*, 2012; Janova *et al.*, 2018). Here, we established a behavioral test battery that revealed abnormalities in social behavior, exploratory behavior, anxiety-like behavior, and impulsivity-like behavior in *Spg11⁻ᐟ⁻* mice. Substantial social abnormalities were detected in both, male and female *Spg11⁻ᐟ⁻* mice. An ongoing study by Klebe *et al.* (unpublished data; University hospital Essen; University hospital Wuerzburg) provides evidence that this recapitulates the behavioral changes typical for patients. Of note, social abnormalities of *Spg11⁻ᐟ⁻* mice were not due to disturbed memory formation or recognition, as they did not show cognitive abnormalities in the NOR analysis. While it is known that cognitive dysfunction is a prominent feature in HSPs (Faber *et al.*, 2016), new data suggests that even though SPG11 patients show major deficits in memory functions, recognition is stable on a low level (Klebe *et al.*, unpublished data), possibly explaining the intact object recognition in this SPG11 model. *Spg11⁻ᐟ⁻* mice showed signs of hyperactivity-like behavior and previous studies could provide evidence that SPG11 patients show signs of attention deficit/hyperactivity syndrome (ADHD) (Wijemanne *et al.* 2015). Interestingly, we found some sex-specific differences between male and female mice regarding the anxiety- and impulsivity-

like behavior. While female *Spg11^-/-* mice showed reduced anxiety-like behavior compared to male mutant mice, male *Spg11^-/-* mice showed increased impulsivity-like behavior. In contrast, female patients are more prone to depression and anxiety (Klebe *et al.*, unpublished data), which is not reflected by this SPG11 mouse model. However, male patients show pronounced impulsivity behavior and disinhibition (Klebe *et al.*, unpublished data). Therefore, our SPG11 mouse model reflects most aspects of neuropsychological abnormalities seen in patients. Of note, social, anxiety-like, and impulsivity-like behavior was affected in an age-dependent manner after 12 months which correlates with the progressive accumulation of CD8$^+$ T-lymphocytes in the CNS of *Spg11^-/-* mice, possibly pointing towards an immune-mediated development.

Indeed, *Rag1*-deficiency and treatment with either immunomodulator robustly restored the social behavior of male and female *Spg11^-/-* mice. Interestingly, a study by McGowan *et al.* indicated that *Rag1*-deficient mice showed impaired social recognition memory (McGowan *et al.*, 2011). In contrast to our study, these experiments focused largely on social memory using retention intervals after presentation of a social stimulus (McGowan *et al.*, 2011). Importantly, social behavior of *Rag1*-deficient mice was comparable to those of wt mice after a retention phase of 30 minutes (McGowan *et al.*, 2011), indicating that *Rag1*-deficiency does not generally alter social behavior. Of note, especially treatment with fingolimod has been shown to be beneficial in other diseases regarding social abnormalities, e.g., it attenuated social deficits in a rat model of autism (Wu *et al.*, 2017) and in a mouse model of EAE (de Bruin *et al.*, 2016; Wu *et al.*, 2017; Shi *et al.*, 2018). Recently, it has been shown that cerebellar dopamine D2 receptors (D2R), that are preferentially expressed on PCs and regulate synaptic efficacy onto them, are implicated in social behavior of male mice during adulthood (Cutando *et al.*, 2022). Altered levels of D2R in PCs did not only alter sociability, but also preference for social novelty without affecting motor functions (Cutando *et al.*, 2022). While the study by Cutando *et al.* showed that D2R activation leads to abnormal social behavior, other studies linked altered structures and loss of PCs, leading to decreased excitability, to disturbed social behavior (Tsai *et al.*, 2012; Reith *et al.*, 2013; Sudarov, 2013). Furthermore, it was shown that humans with autism spectrum disorder (ASD), characterized by atypical social interaction, show loss of PCs (Bauman & Kemper, 2005; Amaral *et al.*, 2008), further strengthening the implication of PCs in social behavior. The here presented mouse model shows a progressive loss of PCs (Branchu *et al.*, 2017), and an unproportionally high increase of inflammation in the CB. Genetic or pharmacological intervention robustly reduced inflammation and axonal damage, suggesting that disturbed social behavior could be due to an immune-mediated perturbation or loss of PCs,

possibly implicating altered D2R levels. Our findings support the notion that cerebellar dysfunction plays a prominent role in SPG11, not only in the development of gait abnormalities but also in the development of abnormal social behavior. It further strengthens the hypothesis that inflammation by CD8^{+} T-lymphocytes has an overarching role in the disease progression, possibly also implicating their relevance for other diseases presenting with disturbed social behavior. Of note, genetic and pharmacological intervention showed stronger effects on the social behavior of female compared to male mice. This might be due to the fact, that female mice are intrinsically more social than male mice (An *et al.*, 2011).

Memory formation and recognition remained unaffected in this mouse model, yet, previous studies reported different findings regarding memory deficits of *Rag1*-deficient mice in NOR in young (Smith *et al.*, 2014) vs adult (Faraco *et al.*, 2018) mice. While Smith *et al.* found impaired cognitive function in young *Rag1*-deficient mice, Faraco *et al.* did not see this effect in adult mice. A more recent investigation (Groh *et al.*, 2021b) and the here presented data support the latter study, suggesting that ablation of T-lymphocytes alone does not interfere with cognitive function.

Abnormalities that occurred early in *Spg11*^{-/-} mice, i.e., hyperactivity-like behavior, could not be ameliorated by either the genetic or pharmacological targeting of lymphocytes. The early development of these symptoms could point towards an inflammation-independent mechanism. Locomotor activity is in part regulated by the activity of mesolimbic dopaminergic neurons that originate in the ventral tegmental area and project to the ventral striatum (Koob & Swerdlow, 1988; Szczypka *et al.*, 2001). Interestingly, previous studies could provide evidence that SPG11 patients show signs of ADHD (Wijemanne *et al.* 2015), which is linked to mutations in the dopamine receptor (DR) and/or dopamine transporter (DAT) (Cook *et al.*, 1995; Kuntsi & Stevenson, 2000; Sagvolden *et al.*, 2005). Accordingly, DAT knockout and knockdown mice, hyperdopaminergic mouse models for ADHD and mania-relevant behaviors, show increased hyperactivity- and impulsivity-like behavior (Ralph *et al.*, 2001; Rossi & Yin, 2015; Kwiatkowski *et al.*, 2019). A clinical study indeed reported reduced DAT density as a common finding in SPG11 patients (Faber *et al.*, 2018b), indicating that altered dopamine levels may also play a role in hyperactivity-like behavior of this SPG11 mouse model. Interestingly, dopamine itself has emerged as a major regulator of inflammation (Pacheco *et al.*, 2014; Vidal & Pacheco, 2020), as it can activate and lead to migration of CD8^{+} T-lymphocytes (Levite *et al.*, 2001; Watanabe *et al.*, 2006). Of note, some SPG11 patients show indications of a disrupted presynaptic dopaminergic system (Faber *et al.*, 2018b) and there have been reports of

parkinsonism in SPG11 patients, partly with positive response to levodopa treatment (Anheim *et al.*, 2009; Paisan-Ruiz *et al.*, 2010; Guidubaldi *et al.*, 2011; Vanderver *et al.*, 2012; Wijemanne *et al.*, 2015).

Regarding anxiety-related parameters, genetic and pharmacological treatment approaches counteracted the reduced anxiety-like behavior of female *Spg11⁻/⁻* mice. Some studies indicated that *Rag1*-deficiency leads to increased anxiety- and depression-like behavior in mice (Rattazzi *et al.*, 2013; Smith *et al.*, 2014), and indeed *Rag1*-deficiency increased anxiety-like behavior of wt mice in our study. Surprisingly, treatment with fingolimod increased anxiety-like behavior of female *Spg11⁻/⁻* mice compared to wt mice, as opposed to restoring it to wt levels. Therefore, it is possible that the effect of *Rag1*-deficiency and pharmacological treatment is mainly due to an increase of anxiety-like behavior as opposed to a correction of the behavioral phenotype. Of note, the increased anxiety-like behavior was not due to decreased exploratory behavior. Conversely, previous studies indicated that treatment with fingolimod reduced anxiety-like behavior in a mouse model of EAE (Bonfiglio *et al.*, 2017) while other studies provided evidence that treatment with fingolimod did not affect anxiety-like behavior in a mouse model for chronic unpredictable stress or in a rat model of genetic epilepsy (di Nuzzo *et al.*, 2015; Leo *et al.*, 2017). We did not find an effect of treatment with immunomodulators on anxiety-like behavior of *B6J* mice. Previous studies suggested that the absence of CD4⁺, rather than CD8⁺, T-lymphocytes is responsible for impaired emotional behavior (Rattazzi *et al.*, 2013). As treatment of wt mice showed little effect on the generally low number of CD4⁺ T-lymphocytes, this could explain the unchanged anxiety-related parameters. Of note, other studies provided evidence of a mechanistic link between anxiety-like behavior and microglial activation, especially in the amygdala and the hippocampus (Sawada *et al.*, 2014; Stein *et al.*, 2017; Wang *et al.*, 2018). However, we did not analyze microglia in these compartments. It should be subject of future experiments to determine the connection of *Rag1*-deficiency/pharmacological treatment, microglial activation, and anxiety-like behavior.

Regarding impulsivity-like behavior, *Rag1*-deficiency or pharmacological treatment could reduce the time *Spg11⁻/⁻* mice spent leaning over the edge of the platform, but not their jumping behavior. It is therefore possible, that jumping behavior and leaning behavior in mice are not dependent on each other and, while jumping behavior might be linked to hyperactivity-like behavior, leaning behavior is influenced by secondary inflammation. Indeed, it has been shown that inflammatory markers are elevated in humans and mice that display traits linked to impulsivity and aggression (Beurel & Jope, 2014; Logsdon *et al.*, 2016; Kim *et al.*, 2020). In a

rat model of TBI reduction of neuroinflammation led to a significant reduction of impulsivity-like behavior in the elevated platform maze test (Logsdon *et al.*, 2016). Of note, it has been demonstrated that Olig2 conditional knockout mice, resulting in impaired oligodendroglial maturation, show increased impulsivity-like behavior (Chen *et al.*, 2015), linking impulsivity-like behavior to defects in oligodendrocytes. As spatacsin is robustly expressed in oligodendrocytes, the increase in impulsivity-like behavior could also be due to a direct perturbation of oligodendrocytes.

This is, to our knowledge, the first study also examining the effects of long-term treatment with immunomodulators on behavioral properties of wt mice. Interestingly, while most parameters remained unaffected by the treatment, treated wt mice showed increased hyperactivity-like behavior, a finding that should also be investigated in humans receiving long-term treatment.

Taken together, our results indicate, that secondary neuroinflammation plays a role in the development of abnormal social behavior, strongly implicating cerebellar dysfunction and involvement of PCs. Furthermore, neuroinflammation influences the development of anxiety-like behavior, and some aspects of impulsivity-like behavior. These findings further demonstrate the overarching and detrimental role of CD8$^+$ T-lymphocytes, implicating the efficacy of treatment in this mouse model for SPG11 and pointing into the direction for a translational treatment approach in humans.

6.6 Late treatment with immunomodulators can still improve histopathological and clinical outcome in *Spg11$^{-/-}$* mice

Another aim of this study was to determine the efficacy of relatively late pharmacological immunomodulation, i.e., starting treatment at a timepoint where neurodegeneration is ongoing and histopathological and clinical symptoms are already prominent, as it has also been done in other genetically-mediated CNS disorders (Groh *et al.*, 2021a). This is a scenario of high clinical relevance, as patients are usually diagnosed with the disease after symptoms have already emerged. Indeed, we provide evidence that late treatment with immunomodulators leads to histopathological benefits. Additionally, progression of ataxia could still be halted even in the late treatment approach, given the respective parameters worsened within the therapeutic time window in untreated *Spg11$^{-/-}$* mice. Interestingly, in the late treatment approach the progression of the ataxia-related parameter "paw angle variation related to body axis" was only halted by treatment with teriflunomide. It is possible that this relates to the different mechanisms of actions of fingolimod and teriflunomide. While fingolimod impairs the

emigration of lymphocytes from the lymph nodes (Brinkmann *et al.*, 2010; Chun & Brinkmann, 2011; Melzer & Meuth, 2014), teriflunomide is a cytostatic that constantly blocks proliferation and effector mechanisms of distinct, activated subtypes, particularly of $CD8^+$ T-lymphocytes (Bar-Or *et al.*, 2014; Melzer & Meuth, 2014; Tilly *et al.*, 2021). Therefore, it is possible that fingolimod is less effective when T-lymphocytes become tissue resident within the brain, while it is plausible to assume that teriflunomide might be the more effective drug in later treatment conditions in SPG11. Due to limited numbers of experimental animals available we were not able to perform the behavioral analysis after late treatment. As the findings after late treatment partially recapitulate the findings of the early treatment, regarding histopathological alterations and gait coordination, we hypothesize that it may have similar effects on the behavioral outcome. However, this hypothesis must presently remain a topic for future experiments.

6.7 Fingolimod and teriflunomide: adverse and direct effects

Even though fingolimod and teriflunomide have been shown to be well-tolerated, safe and beneficial in diseases involving T-lymphocytes as a major player, clinical monitoring of adverse side effects is necessary during treatment. The most common serious adverse effects after treatment with fingolimod include dose-dependent cardiovascular events, such as bradycardia, macular edema, laboratory abnormalities in the liver, and abnormalities in blood enzyme levels (Kappos *et al.*, 2010; Willis & Cohen, 2013; Gold *et al.*, 2014; Gajofatto *et al.*, 2015; Khatri, 2016). Of note, most effects were mild to moderate in severity even after long-term treatment (Ziemssen *et al.*, 2022). Importantly, treatment with fingolimod leads to lymphopenia, which in turn results in an increased risk of infections and opportunistic infections (Cohen & Chun, 2011). Furthermore, prolonged lymphopenia is associated with increased cancer incidence (Menetrier-Caux *et al.*, 2019). However, due to the efficacy of fingolimod treatment regarding relapses, disability progression, lesion activity and brain volume loss in MS, its oral route administration, as well as the safety, and tolerability profile, it is, up to this day, an attractive treatment option for RRMS. The most common adverse events during treatment with teriflunomide include diarrhea, nausea, high blood pressure, hair thinning or decreased hair density, and elevated alanine aminotransferase levels (Fragoso & Brooks, 2015). Importantly and in contrast to fingolimod, which impairs the emigration of lymphocytes from the lymph nodes (Brinkmann *et al.*, 2010; Chun & Brinkmann, 2011; Melzer & Meuth, 2014), teriflunomide blocks the proliferation and effector mechanisms of distinct, activated T-lymphocyte subtypes (Bar-Or *et al.*, 2014; Melzer & Meuth, 2014; Tilly *et al.*, 2021), while having only a small effect on the peripheral count of lymphocytes and neutrophils (Fragoso &

Brooks, 2015). Remarkably, only mild infections and no opportunistic infections were observed, even in a long-term follow-up study after 8.5 years (Confavreux *et al.*, 2012), making it an attractive agent for treatment of RRMS.

One must also keep in mind, that pleiotropic, immune-unrelated functions have been postulated for both drugs that might be directly neuroprotective, e.g., fingolimod leading to increased neurite growth, enhanced synaptic plasticity in the hippocampus or increased levels of brain-derived neurotrophic factor (BDNF) and teriflunomide directly affecting microglia and astrocytes *in vitro* (Deogracias *et al.*, 2012; Bar-Or *et al.*, 2014; Miguez *et al.*, 2015; Edling *et al.*, 2017; Segura-Ulate *et al.*, 2017; Schira *et al.*, 2019). Concerning this study, both drugs had remarkable and similar effects on the outcome of histopathological and behavioral changes, even though they differ considerably regarding their immunomodulatory mechanism. Of note, we did not detect adverse effects after treatment with either immunomodulator. Previous studies showed that treatment with fingolimod or teriflunomide failed to further improve the pathology in *Rag1*-deficient CLN1 mice (Groh *et al.*, 2021a), suggesting that the effects were primarily immune-related. We didn't see beneficial effects of treatment with either immunomodulator compared to *Rag1*-deficiency, instead *Rag1*-deficiency was more effective regarding most parameters, possibly pointing towards a primarily immune-mediated mechanism in SPG11. More studies would be needed to ensure that the here shown effects are due to the immunomodulatory functions of the drugs alone, rather than additional direct neuroprotective effects, e.g., treating *Rag1*-deficient mice with fingolimod or teriflunomide. However, due to limited amounts of experimental animals, we had to omit the impact of pharmacological treatment in *Rag1*-deficient mice.

6.8   Proposed mechanism and conclusion

We propose the following mechanism for the role of inflammation in SPG11, as exemplified in the retinotectal system and the folium of the cerebellum (Figure 61): Based on our observations, *Spg11*$^{-/-}$ mice display substantial neuroinflammation, possibly targeted against myelinated axons, resulting in axonal perturbation and loss of cell bodies, like RGCs and PCs. Loss of PCs in the CB most likely leads to abnormal gait coordination as well as social abnormalities (Figure 61). *Rag1*-deficiency, resulting in a model without mature T- and B-lymphocytes and therefore devoid of an adaptive immune response, reduces microglial activation, axonal perturbation, and neuronal loss (Figure 61). Additionally, gait coordination and social abnormalities are improved, likely due to a restored number of PCs in the CB (Figure 61). As a clinically relevant translation of the genetic inactivation of the adaptive immune system we investigated the

pharmacological inhibition of lymphocytes with the immunomodulators fingolimod or teriflunomide, which are in wide use for the treatment of MS. While treatment with either immunomodulator does not influence microglial numbers or activation, it leads to a substantial reduction of inflammation by cytotoxic CD8$^+$ T-lymphocytes and ameliorates the histopathological and clinical disease outcome in an early and, more importantly, late treatment approach (Figure 61). Therefore, we here identify neuroinflammation as a targetable and disease-amplifying mechanism in a model of SPG11.
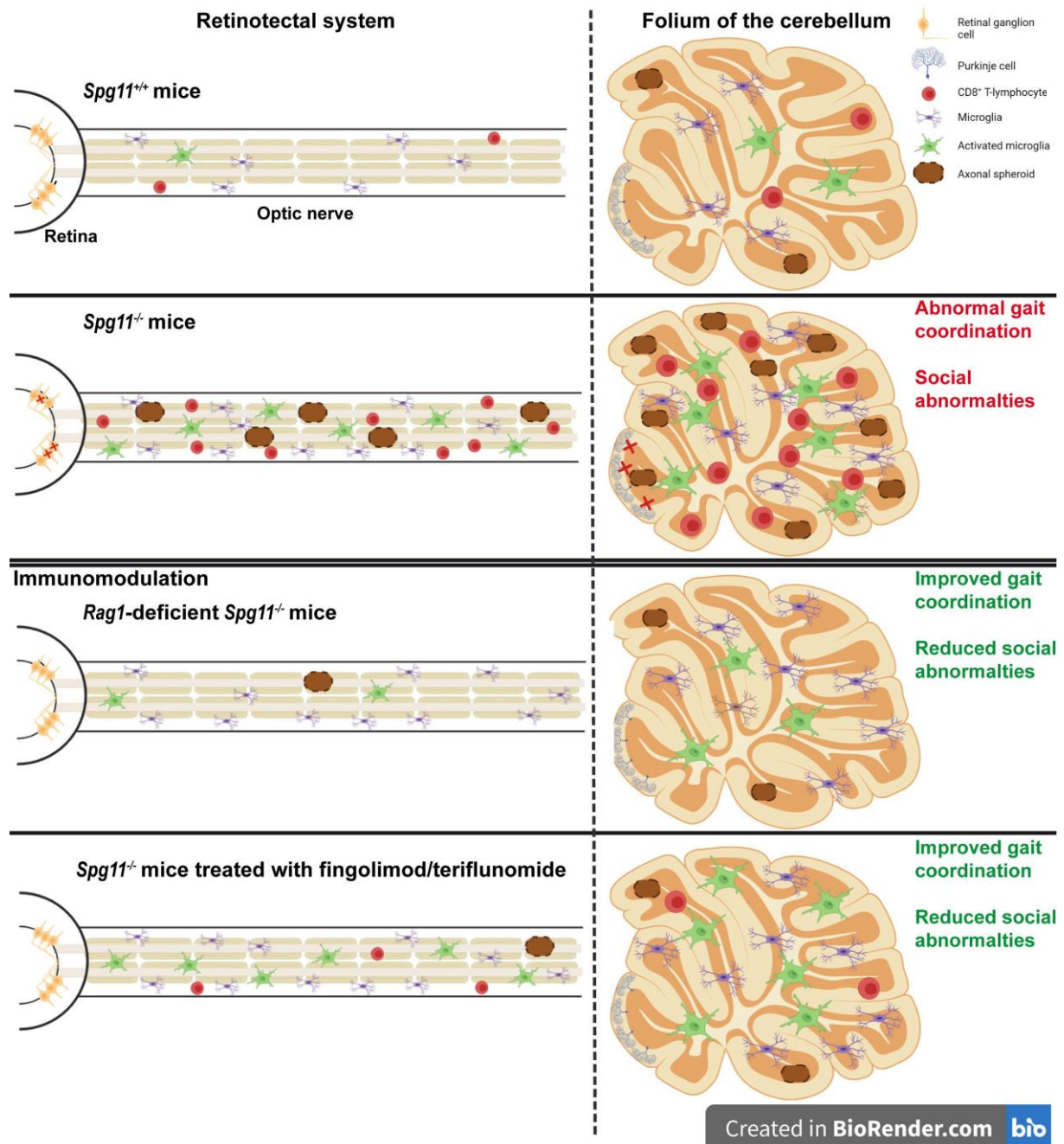

Figure 61: Secondary inflammation acts as a disease amplifier in SPG11.
Mechanistic involvement of inflammation in SPG11, as exemplified in the retinotectal system (left) and folium of the cerebellum (right). $Spg11^{-/-}$ mice (2nd row) show a substantial increase in axonal perturbation (seen as SMI32$^+$ axonal spheroids; brown) and neuronal loss (seen as loss of RGCs (yellow,

left) or PCs (blue, right)) compared to $Spg11^{+/+}$ mice (1st row). This is accompanied by an increase of cytotoxic $CD8^+$ T-lymphocytes (red), microglial numbers (purple) and microglial activation (green). The degeneration of PCs in the cerebellum likely contribute to gait alterations and social abnormalities, typically present in $Spg11^{-/-}$ mice. $Rag1$-deficiency (3rd row), resulting in a model devoid of an adaptive immune response, reduces microglial activation and substantially ameliorates axonal perturbation and neuron loss, likely contributing to improved gait coordination, and social abnormalities. The translational approach using fingolimod (FTY720) or teriflunomide in an early and more clinically relevant, late treatment approach also leads to substantial reduction of inflammation by $CD8^+$ T-lymphocytes and a consequent amelioration of histopathological and clinical disease progression. Of note, treatment does not reduce microglial activation. This indicates that secondary inflammation is causally involved in the disease progression of SPG11. Scheme by Hörner et $al.$, unpublished (generated with BioRender).

To make our approach eventually translatable, providing evidence of neuroinflammation in the CNS of SPG11 patients is necessary. While our group was able to demonstrate an elevated number of $CD8^+$ T-lymphocytes in brains of CLN2 and CLN3 patients (Groh et $al.$, 2017) and normal white matter of older humans (Groh et $al.$, 2021b), corresponding tissue samples of SPG11 patients were, to the best of our knowledge, not available. However, cytokine signatures and immune cell activation in blood and the cerebrospinal fluid are becoming more interesting for monitoring CNS-associated immune processes also in other, more frequent neurodegenerative diseases (Schroder et $al.$, 2018; Oh et $al.$, 2021). Therefore, identifying such biomarkers of neuroinflammation in SPG11 might provide a direct rationale and important readout for repurposing clinically established disease-modifying treatments. Our study may then give hope that immunomodulation could become a potent option to make the presently poorly treatable disease more bearable for patients and their relatives.

7 References

Amaral, D.G., Schumann, C.M. & Nordahl, C.W. (2008) Neuroanatomy of autism. *Trends Neurosci*, **31**, 137-145.

An, X.L., Zou, J.X., Wu, R.Y., Yang, Y., Tai, F.D., Zeng, S.Y., Jia, R., Zhang, X., Liu, E.Q. & Broders, H. (2011) Strain and sex differences in anxiety-like and social behaviors in C57BL/6J and BALB/cJ mice. *Exp Anim*, **60**, 111-123.

Anheim, M., Lagier-Tourenne, C., Stevanin, G., Fleury, M., Durr, A., Namer, I.J., Denora, P., Brice, A., Mandel, J.L., Koenig, M. & Tranchant, C. (2009) SPG11 spastic paraplegia. A new cause of juvenile parkinsonism. *J Neurol*, **256**, 104-108.

Bar-Or, A., Pachner, A., Menguy-Vacheron, F., Kaplan, J. & Wiendl, H. (2014) Teriflunomide and its mechanism of action in multiple sclerosis. *Drugs*, **74**, 659-674.

Barcelos, L.B., Saad, F., Giacominelli, C., Saba, R.A., de Carvalho Aguiar, P.M., Silva, S.M.A., Borges, V., Bertolucci, P.H.F. & Ferraz, H.B. (2018) Neuropsychological and clinical heterogeneity of cognitive impairment in patients with multiple system atrophy. *Clin Neurol Neurosurg*, **164**, 121-126.

Bauman, M.L. & Kemper, T.L. (2005) Neuroanatomic observations of the brain in autism: a review and future directions. *Int J Dev Neurosci*, **23**, 183-187.

Becker, J.T., Huff, F.J., Nebes, R.D., Holland, A. & Boller, F. (1988) Neuropsychological function in Alzheimer's disease. Pattern of impairment and rates of progression. *Arch Neurol*, **45**, 263-268.

Bennett, M.L., Bennett, F.C., Liddelow, S.A., Ajami, B., Zamanian, J.L., Fernhoff, N.B., Mulinyawe, S.B., Bohlen, C.J., Adil, A., Tucker, A., Weissman, I.L., Chang, E.F., Li, G., Grant, G.A., Hayden Gephart, M.G. & Barres, B.A. (2016) New tools for studying microglia in the mouse and human CNS. *Proc Natl Acad Sci U S A*, **113**, E1738-1746.

Berve, K., West, B.L., Martini, R. & Groh, J. (2020) Sex- and region-biased depletion of microglia/macrophages attenuates CLN1 disease in mice. *J Neuroinflammation*, **17**, 323.

Beurel, E. & Jope, R.S. (2014) Inflammation and lithium: clues to mechanisms contributing to suicide-linked traits. *Transl Psychiatry*, **4**, e488.

Blackstone, C. (2012) Cellular pathways of hereditary spastic paraplegia. *Annu Rev Neurosci*, **35**, 25-47.

Blackstone, C. (2018) Hereditary spastic paraplegia. *Handb Clin Neurol*, **148**, 633-652.

Blackstone, C., O'Kane, C.J. & Reid, E. (2011) Hereditary spastic paraplegias: membrane traffic and the motor pathway. *Nat Rev Neurosci*, **12**, 31-42.

Bogie, J.F., Boelen, E., Louagie, E., Delputte, P., Elewaut, D., van Horssen, J., Hendriks, J.J. & Hellings, N. (2018) CD169 is a marker for highly pathogenic phagocytes in multiple sclerosis. *Mult Scler*, **24**, 290-300.

Bonfiglio, T., Olivero, G., Merega, E., Di Prisco, S., Padolecchia, C., Grilli, M., Milanese, M., Di Cesare Mannelli, L., Ghelardini, C., Bonanno, G., Marchi, M. & Pittaluga, A. (2017) Prophylactic versus Therapeutic Fingolimod: Restoration of Presynaptic Defects in Mice Suffering from Experimental Autoimmune Encephalomyelitis. *PLoS One*, **12**, e0170825.

Boutry, M., Morais, S. & Stevanin, G. (2019a) Update on the Genetics of Spastic Paraplegias. *Curr Neurol Neurosci Rep*, **19**, 18.

Boutry, M., Pierga, A., Matusiak, R., Branchu, J., Houllegatte, M., Ibrahim, Y., Balse, E., El Hachimi, K.H., Brice, A., Stevanin, G. & Darios, F. (2019b) Loss of spatacsin impairs cholesterol trafficking and calcium homeostasis. *Commun Biol*, **2**, 380.

Bozkurt, A., Deumens, R., Scheffel, J., O'Dey, D.M., Weis, J., Joosten, E.A., Fuhrmann, T., Brook, G.A. & Pallua, N. (2008) CatWalk gait analysis in assessment of functional recovery after sciatic nerve injury. *J Neurosci Methods*, **173**, 91-98.

Branchu, J., Boutry, M., Sourd, L., Depp, M., Leone, C., Corriger, A., Vallucci, M., Esteves, T., Matusiak, R., Dumont, M., Muriel, M.P., Santorelli, F.M., Brice, A., El Hachimi, K.H., Stevanin, G. & Darios, F. (2017) Loss of spatacsin function alters lysosomal lipid clearance leading to upper and lower motor neuron degeneration. *Neurobiology of disease*, **102**, 21-37.

Brassington, J.C. & Marsh, N.V. (1998) Neuropsychological aspects of multiple sclerosis. *Neuropsychol Rev*, **8**, 43-77.

Brinkmann, V., Billich, A., Baumruker, T., Heining, P., Schmouder, R., Francis, G., Aradhye, S. & Burtin, P. (2010) Fingolimod (FTY720): discovery and development of an oral drug to treat multiple sclerosis. *Nat Rev Drug Discov*, **9**, 883-897.

Brown, W.S., Jeeves, M.A., Dietrich, R. & Burnison, D.S. (1999) Bilateral field advantage and evoked potential interhemispheric transmission in commissurotomy and callosal agenesis. *Neuropsychologia*, **37**, 1165-1180.

Chang, J., Lee, S. & Blackstone, C. (2014) Spastic paraplegia proteins spastizin and spatacsin mediate autophagic lysosome reformation. *J Clin Invest*, **124**, 5249-5262.

Chen, X., Zhang, W., Li, T., Guo, Y., Tian, Y., Wang, F., Liu, S., Shen, H.Y., Feng, Y. & Xiao, L. (2015) Impairment of Oligodendroglia Maturation Leads to Aberrantly Increased Cortical Glutamate and Anxiety-Like Behaviors in Juvenile Mice. *Front Cell Neurosci*, **9**, 467.

Choi, S., Guo, L. & Cordeiro, M.F. (2021) Retinal and Brain Microglia in Multiple Sclerosis and Neurodegeneration. *Cells*, **10**.

Chowdhury, D. & Lieberman, J. (2008) Death by a thousand cuts: granzyme pathways of programmed cell death. *Annu Rev Immunol*, **26**, 389-420.

Chun, J. & Brinkmann, V. (2011) A mechanistically novel, first oral therapy for multiple sclerosis: the development of fingolimod (FTY720, Gilenya). *Discov Med*, **12**, 213-228.

Cohen, J.A. & Chun, J. (2011) Mechanisms of fingolimod's efficacy and adverse effects in multiple sclerosis. *Ann Neurol*, **69**, 759-777.

Confavreux, C., Li, D.K., Freedman, M.S., Truffinet, P., Benzerdjeb, H., Wang, D., Bar-Or, A., Traboulsee, A.L., Reiman, L.E., O'Connor, P.W. & Group, T.M.S.T. (2012) Long-term follow-up of a phase 2 study of oral teriflunomide in relapsing multiple sclerosis: safety and efficacy results up to 8.5 years. *Mult Scler*, **18**, 1278-1289.

Cook, E.H., Jr., Stein, M.A., Krasowski, M.D., Cox, N.J., Olkon, D.M., Kieffer, J.E. & Leventhal, B.L. (1995) Association of attention-deficit disorder and the dopamine transporter gene. *Am J Hum Genet*, **56**, 993-998.

Cullen, S.P. & Martin, S.J. (2008) Mechanisms of granule-dependent killing. *Cell Death Differ*, **15**, 251-262.

Cutando, L., Puighermanal, E., Castell, L., Tarot, P., Belle, M., Bertaso, F., Arango-Lievano, M., Ango, F., Rubinstein, M., Quintana, A., Chedotal, A., Mameli, M. & Valjent, E. (2022) Cerebellar dopamine D2 receptors regulate social behaviors. *Nat Neurosci*, **25**, 900–911

Daoud, H., Zhou, S., Noreau, A., Sabbagh, M., Belzil, V., Dionne-Laporte, A., Tranchant, C., Dion, P. & Rouleau, G.A. (2012) Exome sequencing reveals SPG11 mutations causing juvenile ALS. *Neurobiol Aging*, **33**, 839 e835-839.

de Bruin, N.M., Schmitz, K., Schiffmann, S., Tafferner, N., Schmidt, M., Jordan, H., Haussler, A., Tegeder, I., Geisslinger, G. & Parnham, M.J. (2016) Multiple rodent models and behavioral measures reveal unexpected responses to FTY720 and DMF in experimental autoimmune encephalomyelitis. *Behav Brain Res*, **300**, 160-174.

De Leon Reyes, N.S., Bragg-Gonzalo, L. & Nieto, M. (2020) Development and plasticity of the corpus callosum. *Development*, **147**.

Deczkowska, A., Amit, I. & Schwartz, M. (2018a) Microglial immune checkpoint mechanisms. *Nature neuroscience*, **21**, 779-786.

Deczkowska, A., Keren-Shaul, H., Weiner, A., Colonna, M., Schwartz, M. & Amit, I. (2018b) Disease-Associated Microglia: A Universal Immune Sensor of Neurodegeneration. *Cell*, **173**, 1073-1081.

Denora, P.S., Smets, K., Zolfanelli, F., Ceuterick-de Groote, C., Casali, C., Deconinck, T., Sieben, A., Gonzales, M., Zuchner, S., Darios, F., Peeters, D., Brice, A., Malandrini, A., De Jonghe, P., Santorelli, F.M., Stevanin, G., Martin, J.J. & El Hachimi, K.H. (2016) Motor neuron degeneration in spastic paraplegia 11 mimics amyotrophic lateral sclerosis lesions. *Brain*, **139**, 1723-1734.

Deogracias, R., Yazdani, M., Dekkers, M.P., Guy, J., Ionescu, M.C., Vogt, K.E. & Barde, Y.A. (2012) Fingolimod, a sphingosine-1 phosphate receptor modulator, increases BDNF levels and improves symptoms of a mouse model of Rett syndrome. *Proc Natl Acad Sci U S A*, **109**, 14230-14235.

Depienne, C., Stevanin, G., Brice, A. & Durr, A. (2007) Hereditary spastic paraplegias: an update. *Curr Opin Neurol*, **20**, 674-680.

di Nuzzo, L., Orlando, R., Tognoli, C., Di Pietro, P., Bertini, G., Miele, J., Bucci, D., Motolese, M., Scaccianoce, S., Caruso, A., Mauro, G., De Lucia, C., Battaglia, G., Bruno, V., Fabene, P.F. & Nicoletti, F. (2015) Antidepressant activity of fingolimod in mice. *Pharmacol Res Perspect*, **3**, e00135.

Dressman, D. & Elyaman, W. (2022) T Cells: A Growing Universe of Roles in Neurodegenerative Diseases. *Neuroscientist*, **28**, 335-348.

Dziedzic, T., Metz, I., Dallenga, T., Konig, F.B., Muller, S., Stadelmann, C. & Bruck, W. (2010) Wallerian degeneration: a major component of early axonal pathology in multiple sclerosis. *Brain Pathol*, **20**, 976-985.

Edling, A., Woodworth, L., Rajiv, A., Mahan, A., Garron, T., Nellwyn, H. & Siders, B. (2017) Teriflunomide Impacts Primary Microglia and Astrocyte Functions In Vitro (P2.348). *Neurology* **88** P2.348.

Essuman, K., Summers, D.W., Sasaki, Y., Mao, X., DiAntonio, A. & Milbrandt, J. (2017) The SARM1 Toll/Interleukin-1 Receptor Domain Possesses Intrinsic NAD(+) Cleavage Activity that Promotes Pathological Axonal Degeneration. *Neuron*, **93**, 1334-1343 e1335.

Faber, I., Branco, L.M.T. & Franca Junior, M.C. (2016) Cognitive dysfunction in hereditary spastic paraplegias and other motor neuron disorders. *Dement Neuropsychol*, **10**, 276-279.

Faber, I., Martinez, A.R.M., de Rezende, T.J.R., Martins, C.R., Jr., Martins, M.P., Lourenco, C.M., Marques, W., Jr., Montecchiani, C., Orlacchio, A., Pedroso, J.L., Barsottini, O.G.P., Lopes-Cendes, I. & Franca, M.C., Jr. (2018a) SPG11 mutations cause widespread white matter and basal ganglia abnormalities, but restricted cortical damage. *Neuroimage Clin*, **19**, 848-857.

Faber, I., Martinez, A.R.M., Martins, C.R., Jr., Maia, M.L., Souza, J.P., Lourenco, C.M., Marques, W., Jr., Montecchiani, C., Orlacchio, A., Pedroso, J.L., Barsottini, O.G.P., Ramos, C.D., Lopes-Cendes, I., Friedman, J.H., Amorim, B.J. & Franca, M.C., Jr. (2018b) SPG11-related parkinsonism: Clinical profile, molecular imaging and l-dopa response. *Mov Disord*, **33**, 1650-1656.

Faraco, G., Brea, D., Garcia-Bonilla, L., Wang, G., Racchumi, G., Chang, H., Buendia, I., Santisteban, M.M., Segarra, S.G., Koizumi, K., Sugiyama, Y., Murphy, M., Voss, H., Anrather, J. & Iadecola, C. (2018) Dietary salt promotes neurovascular and cognitive dysfunction through a gut-initiated TH17 response. *Nat Neurosci*, **21**, 240-249.

Faul, F., Erdfelder, E., Lang, A.G. & Buchner, A. (2007) G*Power 3: A flexible statistical power analysis program for the social, behavioral, and biomedical sciences. *Behav Res Methods*, **39**, 175-191.

Finsterer, J., Loscher, W., Quasthoff, S., Wanschitz, J., Auer-Grumbach, M. & Stevanin, G. (2012) Hereditary spastic paraplegias with autosomal dominant, recessive, X-linked, or maternal trait of inheritance. *J Neurol Sci*, **318**, 1-18.

Fragoso, Y.D. & Brooks, J.B. (2015) Leflunomide and teriflunomide: altering the metabolism of pyrimidines for the treatment of autoimmune diseases. *Expert Rev Clin Pharmacol*, **8**, 315-320.

Fransen, N.L., Hsiao, C.C., van der Poel, M., Engelenburg, H.J., Verdaasdonk, K., Vincenten, M.C.J., Remmerswaal, E.B.M., Kuhlmann, T., Mason, M.R.J., Hamann, J., Smolders, J. & Huitinga, I. (2020) Tissue-resident memory T cells invade the brain parenchyma in multiple sclerosis white matter lesions. *Brain*, **143**, 1714-1730.

Gajofatto, A., Turatti, M., Monaco, S. & Benedetti, M.D. (2015) Clinical efficacy, safety, and tolerability of fingolimod for the treatment of relapsing-remitting multiple sclerosis. *Drug Healthc Patient Saf*, **7**, 157-167.

Galli, E., Hartmann, F.J., Schreiner, B., Ingelfinger, F., Arvaniti, E., Diebold, M., Mrdjen, D., van der Meer, F., Krieg, C., Nimer, F.A., Sanderson, N., Stadelmann, C., Khademi, M., Piehl, F., Claassen, M., Derfuss, T., Olsson, T. & Becher, B. (2019) GM-CSF and CXCR4 define a T helper cell signature in multiple sclerosis. *Nat Med*, **25**, 1290-1300.

Geevasinga, N., Menon, P., Sue, C.M., Kumar, K.R., Ng, K., Yiannikas, C., Kiernan, M.C. & Vucic, S. (2015) Cortical excitability changes distinguish the motor neuron disease phenotypes from hereditary spastic paraplegia. *Eur J Neurol*, **22**, 826-831.

Gerdts, J., Brace, E.J., Sasaki, Y., DiAntonio, A. & Milbrandt, J. (2015) SARM1 activation triggers axon degeneration locally via NAD(+) destruction. *Science*, **348**, 453-457.

Gilley, J., Jackson, O., Pipis, M., Estiar, M.A., Al-Chalabi, A., Danzi, M.C., van Eijk, K.R., Goutman, S.A., Harms, M.B., Houlden, H., Iacoangeli, A., Kaye, J., Lima, L., Queen Square, G., Ravits, J., Rouleau, G.A., Schule, R., Xu, J., Zuchner, S., Cooper-Knock, J., Gan-Or, Z., Reilly, M.M. & Coleman, M.P. (2021) Enrichment of SARM1 alleles encoding variants with constitutively hyperactive NADase in patients with ALS and other motor nerve disorders. *Elife*, **10**.

Gilley, J., Ribchester, R.R. & Coleman, M.P. (2017) Sarm1 Deletion, but Not Wld(S), Confers Lifelong Rescue in a Mouse Model of Severe Axonopathy. *Cell Rep*, **21**, 10-16.

Gold, R., Comi, G., Palace, J., Siever, A., Gottschalk, R., Bijarnia, M., von Rosenstiel, P., Tomic, D., Kappos, L. & Investigators, F.S. (2014) Assessment of cardiac safety during fingolimod treatment initiation in a real-world relapsing multiple sclerosis population: a phase 3b, open-label study. *J Neurol*, **261**, 267-276.

Gorman, M.P., Golomb, M.R., Walsh, L.E., Hobson, G.M., Garbern, J.Y., Kinkel, R.P., Darras, B.T., Urion, D.K. & Eksioglu, Y.Z. (2007) Steroid-responsive neurologic relapses in a child with a proteolipid protein-1 mutation. *Neurology*, **68**, 1305-1307.

Groh, J., Berve, K. & Martini, R. (2017) Fingolimod and Teriflunomide Attenuate Neurodegeneration in Mouse Models of Neuronal Ceroid Lipofuscinosis. *Mol Ther*, **25**, 1889-1899.

Groh, J., Berve, K. & Martini, R. (2021a) Immune modulation attenuates infantile neuronal ceroid lipofuscinosis in mice before and after disease onset. *Brain Commun*, **3**, fcab047.

Groh, J., Friedman, H.C., Orel, N., Ip, C.W., Fischer, S., Spahn, I., Schaffner, E., Horner, M., Stadler, D., Buttmann, M., Varallyay, C., Solymosi, L., Sendtner, M., Peterson, A.C. & Martini, R. (2016a) Pathogenic inflammation in the CNS of mice carrying human PLP1 mutations. *Hum Mol Genet*, **25**, 4686-4702.

Groh, J., Horner, M. & Martini, R. (2018) Teriflunomide attenuates neuroinflammation-related neural damage in mice carrying human PLP1 mutations. *J Neuroinflammation*, **15**, 194.

Groh, J., Klein, D., Berve, K., West, B.L. & Martini, R. (2019) Targeting microglia attenuates neuroinflammation-related neural damage in mice carrying human PLP1 mutations. *Glia*, **67**, 277-290.

Groh, J., Knöpper, K., Arampatzi, P., Yuan, X., Lößlein, L., Saliba, A.-E., Kastenmüller, W. & Martini, R. (2021b) Accumulation of cytotoxic T cells in the aged CNS leads to axon degeneration and contributes to cognitive and motor decline. *Nature Aging*, **1**, 357–367.

Groh, J., Kuhl, T.G., Ip, C.W., Nelvagal, H.R., Sri, S., Duckett, S., Mirza, M., Langmann, T., Cooper, J.D. & Martini, R. (2013) Immune cells perturb axons and impair neuronal survival in a mouse model of infantile neuronal ceroid lipofuscinosis. *Brain : a journal of neurology*, **136**, 1083-1101.

Groh, J. & Martini, R. (2017) Neuroinflammation as modifier of genetically caused neurological disorders of the central nervous system: Understanding pathogenesis and chances for treatment. *Glia*, **65**, 1407-1422.

Groh, J., Ribechini, E., Stadler, D., Schilling, T., Lutz, M.B. & Martini, R. (2016b) Sialoadhesin promotes neuroinflammation-related disease progression in two mouse models of CLN disease. *Glia*, **64**, 792-809.

Groh, J., Stadler, D., Buttmann, M. & Martini, R. (2014) Non-invasive assessment of retinal alterations in mouse models of infantile and juvenile neuronal ceroid lipofuscinosis by spectral domain optical coherence tomography. *Acta Neuropathol Commun*, **2**, 54.

Gronholdt-Klein, M., Altun, M., Becklen, M., Dickman Kahm, E., Fahlstrom, A., Rullman, E. & Ulfhake, B. (2019) Muscle atrophy and regeneration associated with behavioural loss and recovery of function after sciatic nerve crush. *Acta Physiol (Oxf)*, **227**, e13335.

Grusser-Cornehls, U. & Baurle, J. (2001) Mutant mice as a model for cerebellar ataxia. *Prog Neurobiol*, **63**, 489-540.

Guidubaldi, A., Piano, C., Santorelli, F.M., Silvestri, G., Petracca, M., Tessa, A. & Bentivoglio, A.R. (2011) Novel mutations in SPG11 cause hereditary spastic paraplegia associated with early-onset levodopa-responsive Parkinsonism. *Mov Disord*, **26**, 553-556.

Gumeni, S., Vantaggiato, C., Montopoli, M. & Orso, G. (2021) Hereditary Spastic Paraplegia and Future Therapeutic Directions: Beneficial Effects of Small Compounds Acting on Cellular Stress. *Front Neurosci*, **15**, 660714.

Hagemeyer, N., Goebbels, S., Papiol, S., Kastner, A., Hofer, S., Begemann, M., Gerwig, U.C., Boretius, S., Wieser, G.L., Ronnenberg, A., Gurvich, A., Heckers, S.H., Frahm, J., Nave, K.A. & Ehrenreich, H. (2012) A myelin gene causative of a catatonia-depression syndrome upon aging. *EMBO Mol Med*, **4**, 528-539.

Hanein, S., Martin, E., Boukhris, A., Byrne, P., Goizet, C., Hamri, A., Benomar, A., Lossos, A., Denora, P., Fernandez, J., Elleuch, N., Forlani, S., Durr, A., Feki, I., Hutchinson, M., Santorelli, F.M., Mhiri, C., Brice, A. & Stevanin, G. (2008) Identification of the SPG15 gene, encoding spastizin, as a frequent cause of complicated autosomal-recessive spastic paraplegia, including Kjellin syndrome. *Am J Hum Genet*, **82**, 992-1002.

Harding, A.E. (1983) Classification of the hereditary ataxias and paraplegias. *Lancet*, **1**, 1151-1155.

Hauser, S., Schuster, S., Heuten, E., Hoflinger, P., Admard, J., Schelling, Y., Velic, A., Macek, B., Ossowski, S. & Schols, L. (2020) Comparative Transcriptional Profiling of Motor Neuron Disorder-Associated Genes in Various Human Cell Culture Models. *Front Cell Dev Biol*, **8**, 544043.

Hirst, J., Barlow, L.D., Francisco, G.C., Sahlender, D.A., Seaman, M.N., Dacks, J.B. & Robinson, M.S. (2011) The fifth adaptor protein complex. *PLoS Biol*, **9**, e1001170.

Hirst, J., Borner, G.H., Edgar, J., Hein, M.Y., Mann, M., Buchholz, F., Antrobus, R. & Robinson, M.S. (2013) Interaction between AP-5 and the hereditary spastic paraplegia proteins SPG11 and SPG15. *Mol Biol Cell*, **24**, 2558-2569.

Hohlfeld, R. & Wekerle, H. (2001) Immunological update on multiple sclerosis. *Curr Opin Neurol*, **14**, 299-304.

Hoke, A. & Brushart, T. (2010) Introduction to special issue: Challenges and opportunities for regeneration in the peripheral nervous system. *Exp Neurol*, **223**, 1-4.

Hooten, K.G., Beers, D.R., Zhao, W. & Appel, S.H. (2015) Protective and Toxic Neuroinflammation in Amyotrophic Lateral Sclerosis. *Neurotherapeutics*, **12**, 364-375.

Hörner, M., Groh, J., Klein, D., Ilg, W., Schols, L., Dos Santos, S., Bergmann, A., Klebe, S., Cauhape, M., Branchu, J., El Hachimi, K.H., Stevanin, G., Darios, F. & Martini, R. (2022) CNS-associated T-lymphocytes in a mouse model of Hereditary Spastic Paraplegia type 11 (SPG11) are therapeutic targets for established immunomodulators. *Exp Neurol*, **355**, 114119.

Ip, C.W., Isaias, I.U., Kusche-Tekin, B.B., Klein, D., Groh, J., O'Leary, A., Knorr, S., Higuchi, T., Koprich, J.B., Brotchie, J.M., Toyka, K.V., Reif, A. & Volkmann, J. (2016) Tor1a+/- mice develop dystonia-like movements via a striatal dopaminergic dysregulation triggered by peripheral nerve injury. *Acta Neuropathol Commun*, **4**, 108.

Ip, C.W., Kroner, A., Bendszus, M., Leder, C., Kobsar, I., Fischer, S., Wiendl, H., Nave, K.A. & Martini, R. (2006) Immune cells contribute to myelin degeneration and axonopathic changes in mice overexpressing proteolipid protein in oligodendrocytes. *J Neurosci*, **26**, 8206-8216.

Ip, C.W., Kroner, A., Crocker, P.R., Nave, K.A. & Martini, R. (2007) Sialoadhesin deficiency ameliorates myelin degeneration and axonopathic changes in the CNS of PLP overexpressing mice. *Neurobiol Dis*, **25**, 105-111.

Ip, C.W., Kroner, A., Groh, J., Huber, M., Klein, D., Spahn, I., Diem, R., Williams, S.K., Nave, K.A., Edgar, J.M. & Martini, R. (2012) Neuroinflammation by cytotoxic T-lymphocytes impairs retrograde axonal transport in an oligodendrocyte mutant mouse. *PLoS One*, **7**, e42554.

Isaacs, A.M., Oliver, P.L., Jones, E.L., Jeans, A., Potter, A., Hovik, B.H., Nolan, P.M., Vizor, L., Glenister, P., Simon, A.K., Gray, I.C., Spurr, N.K., Brown, S.D., Hunter, A.J. & Davies, K.E. (2003) A mutation in Af4 is predicted to cause cerebellar ataxia and cataracts in the robotic mouse. *J Neurosci*, **23**, 1631-1637.

Janova, H., Arinrad, S., Balmuth, E., Mitjans, M., Hertel, J., Habes, M., Bittner, R.A., Pan, H., Goebbels, S., Begemann, M., Gerwig, U.C., Langner, S., Werner, H.B., Kittel-Schneider, S., Homuth, G., Davatzikos, C., Volzke, H., West, B.L., Reif, A., Grabe, H.J., Boretius, S., Ehrenreich, H. & Nave, K.A. (2018) Microglia ablation alleviates myelin-associated catatonic signs in mice. *J Clin Invest*, **128**, 734-745.

Jovanovic, J., Liu, X., Kokona, D., Zinkernagel, M.S. & Ebneter, A. (2020) Inhibition of inflammatory cells delays retinal degeneration in experimental retinal vein occlusion in mice. *Glia*, **68**, 574-588.

Kandel, E.R., Schwartz, J.H. & Jessell, T.M. (2000) *Principles of neural science*. McGrawHill, New York.

Kappos, L., Radue, E.W., O'Connor, P., Polman, C., Hohlfeld, R., Calabresi, P., Selmaj, K., Agoropoulou, C., Leyk, M., Zhang-Auberson, L., Burtin, P. & Group, F.S. (2010) A placebo-controlled trial of oral fingolimod in relapsing multiple sclerosis. *N Engl J Med*, **362**, 387-401.

Keefe, D., Shi, L., Feske, S., Massol, R., Navarro, F., Kirchhausen, T. & Lieberman, J. (2005) Perforin triggers a plasma membrane-repair response that facilitates CTL induction of apoptosis. *Immunity*, **23**, 249-262.

Keren-Shaul, H., Spinrad, A., Weiner, A., Matcovitch-Natan, O., Dvir-Szternfeld, R., Ulland, T.K., David, E., Baruch, K., Lara-Astaiso, D., Toth, B., Itzkovitz, S., Colonna, M., Schwartz, M. & Amit, I. (2017) A Unique Microglia Type Associated with Restricting Development of Alzheimer's Disease. *Cell*, **169**, 1276-1290 e1217.

Khatri, B.O. (2016) Fingolimod in the treatment of relapsing-remitting multiple sclerosis: long-term experience and an update on the clinical evidence. *Ther Adv Neurol Disord*, **9**, 130-147.

Khundadze, M., Kollmann, K., Koch, N., Biskup, C., Nietzsche, S., Zimmer, G., Hennings, J.C., Huebner, A.K., Symmank, J., Jahic, A., Ilina, E.I., Karle, K., Schols, L., Kessels, M., Braulke, T., Qualmann, B., Kurth, I., Beetz, C. & Hubner, C.A. (2013) A hereditary spastic paraplegia mouse model supports a role of ZFYVE26/SPASTIZIN for the endolysosomal system. *PLoS Genet*, **9**, e1003988.

Kim, J.S., Kang, E.S., Bahk, Y.C., Jang, S., Hong, K.S. & Baek, J.H. (2020) Exploratory Analysis of Behavioral Impulsivity, Pro-inflammatory Cytokines, and Resting-State Frontal EEG Activity Associated With Non-suicidal Self-Injury in Patients With Mood Disorder. *Front Psychiatry*, **11**, 124.

Klebe, S., Stevanin, G. & Depienne, C. (2015) Clinical and genetic heterogeneity in hereditary spastic paraplegias: from SPG1 to SPG72 and still counting. *Rev Neurol (Paris)*, **171**, 505-530.

Klein, D., Groh, J., Yuan, X., Berve, K., Stassart, R., Fledrich, R. & Martini, R. (2022) Early targeting of endoneurial macrophages alleviates the neuropathy and affects abnormal Schwann cell differentiation in a mouse model of Charcot-Marie-Tooth 1A. *Glia*, **70**, 1100-1116.

Klotz, L., Eschborn, M., Lindner, M., Liebmann, M., Herold, M., Janoschka, C., Torres Garrido, B., Schulte-Mecklenbeck, A., Gross, C.C., Breuer, J., Hundehege, P., Posevitz, V., Pignolet, B., Nebel, G., Glander, S., Freise, N., Austermann, J., Wirth, T., Campbell, G.R., Schneider-Hohendorf, T., Eveslage, M., Brassat, D., Schwab, N., Loser, K., Roth, J., Busch, K.B., Stoll, M., Mahad, D.J., Meuth, S.G., Turner, T., Bar-Or, A. & Wiendl, H. (2019) Teriflunomide treatment for multiple sclerosis modulates T cell mitochondrial respiration with affinity-dependent effects. *Sci Transl Med*, **11**, eaao5563.

Ko, K.W., Milbrandt, J. & DiAntonio, A. (2020) SARM1 acts downstream of neuroinflammatory and necroptotic signaling to induce axon degeneration. *J Cell Biol*, **219**, e201912047.

Kobsar, I., Berghoff, M., Samsam, M., Wessig, C., Maurer, M., Toyka, K.V. & Martini, R. (2003) Preserved myelin integrity and reduced axonopathy in connexin32-deficient mice lacking the recombination activating gene-1. *Brain*, **126**, 804-813.

Kobsar, I., Hasenpusch-Theil, K., Wessig, C., Muller, H.W. & Martini, R. (2005) Evidence for macrophage-mediated myelin disruption in an animal model for Charcot-Marie-Tooth neuropathy type 1A. *J Neurosci Res*, **81**, 857-864.

Kobsar, I., Maurer, M., Ott, T. & Martini, R. (2002) Macrophage-related demyelination in peripheral nerves of mice deficient in the gap junction protein connexin 32. *Neurosci Lett*, **320**, 17-20.

Koeppen, A.H. (2018) The neuropathology of the adult cerebellum. *Handb Clin Neurol*, **154**, 129-149.

Kohl, B., Groh, J., Wessig, C., Wiendl, H., Kroner, A. & Martini, R. (2010) Lack of evidence for a pathogenic role of T-lymphocytes in an animal model for Charcot-Marie-Tooth disease 1A. *Neurobiol Dis*, **38**, 78-84.

Koob, G.F. & Swerdlow, N.R. (1988) The functional output of the mesolimbic dopamine system. *Ann N Y Acad Sci*, **537**, 216-227.

Kroner, A., Ip, C.W., Thalhammer, J., Nave, K.A. & Martini, R. (2010) Ectopic T-cell specificity and absence of perforin and granzyme B alleviate neural damage in oligodendrocyte mutant mice. *Am J Pathol*, **176**, 549-555.

Kroner, A., Schwab, N., Ip, C.W., Ortler, S., Gobel, K., Nave, K.A., Maurer, M., Martini, R. & Wiendl, H. (2009) Accelerated course of experimental autoimmune encephalomyelitis in PD-1-deficient central nervous system myelin mutants. *Am J Pathol*, **174**, 2290-2299.

Kuntsi, J. & Stevenson, J. (2000) Hyperactivity in children: a focus on genetic research and psychological theories. *Clin Child Fam Psychol Rev*, **3**, 1-23.

Kwiatkowski, M.A., Hellemann, G., Sugar, C.A., Cope, Z.A., Minassian, A., Perry, W., Geyer, M.A. & Young, J.W. (2019) Dopamine transporter knockdown mice in the behavioral pattern monitor: A robust, reproducible model for mania-relevant behaviors. *Pharmacol Biochem Behav*, **178**, 42-50.

Lang, J., Haas, E., Hubener-Schmid, J., Anderson, C.J., Pulst, S.M., Giese, M.A. & Ilg, W. (2020) Detecting and Quantifying Ataxia-Related Motor Impairments in Rodents Using Markerless Motion Tracking With Deep Neural Networks. *Annu Int Conf IEEE Eng Med Biol Soc*, **2020**, 3642-3648.

Langmann, T. (2007) Microglia activation in retinal degeneration. *J Leukoc Biol*, **81**, 1345-1351.

Lassmann, H. (2019) The changing concepts in the neuropathology of acquired demyelinating central nervous system disorders. *Curr Opin Neurol*, **32**, 313-319.

Leo, A., Citraro, R., Amodio, N., De Sarro, C., Gallo Cantafio, M.E., Constanti, A., De Sarro, G. & Russo, E. (2017) Fingolimod Exerts only Temporary Antiepileptogenic Effects but Longer-Lasting Positive Effects on Behavior in the WAG/Rij Rat Absence Epilepsy Model. *Neurotherapeutics*, **14**, 1134-1147.

Levite, M., Chowers, Y., Ganor, Y., Besser, M., Hershkovits, R. & Cahalon, L. (2001) Dopamine interacts directly with its D3 and D2 receptors on normal human T cells, and activates beta1 integrin function. *Eur J Immunol*, **31**, 3504-3512.

Lin, J.Z., Zheng, H.H., Ma, Q.L., Wang, C., Fan, L.P., Wu, H.M., Wang, D.N., Zhang, J.X. & Zhan, Y.H. (2020) Cortical Damage Associated With Cognitive and Motor Impairment in Hereditary Spastic Paraplegia: Evidence of a Novel SPAST Mutation. *Front Neurol*, **11**, 399.

Logsdon, A.F., Lucke-Wold, B.P., Nguyen, L., Matsumoto, R.R., Turner, R.C., Rosen, C.L. & Huber, J.D. (2016) Salubrinal reduces oxidative stress, neuroinflammation and impulsive-like behavior in a rodent model of traumatic brain injury. *Brain Res*, **1643**, 140-151.

Machado-Santos, J., Saji, E., Troscher, A.R., Paunovic, M., Liblau, R., Gabriely, G., Bien, C.G., Bauer, J. & Lassmann, H. (2018) The compartmentalized inflammatory response in the multiple sclerosis brain is composed of tissue-resident CD8+ T lymphocytes and B cells. *Brain*, **141**, 2066-2082.

Manto, M. (2009) Mechanisms of human cerebellar dysmetria: experimental evidence and current conceptual bases. *J Neuroeng Rehabil*, **6**, 10.

Marteyn, A. & Baron-Van Evercooren, A. (2016) Is involvement of inflammation underestimated in Pelizaeus-Merzbacher disease? *J Neurosci Res*, **94**, 1572-1578.

Maurer, M., Schmid, C.D., Bootz, F., Zielasek, J., Toyka, K.V., Oehen, S. & Martini, R. (2001) Bone marrow transfer from wild-type mice reverts the beneficial effect of genetically mediated immune deficiency in myelin mutants. *Mol Cell Neurosci*, **17**, 1094-1101.

McGowan, P.O., Hope, T.A., Meck, W.H., Kelsoe, G. & Williams, C.L. (2011) Impaired social recognition memory in recombination activating gene 1-deficient mice. *Brain Res*, **1383**, 187-195.

Melzer, N. & Meuth, S.G. (2014) Disease-modifying therapy in multiple sclerosis and chronic inflammatory demyelinating polyradiculoneuropathy: common and divergent current and future strategies. *Clin Exp Immunol*, **175**, 359-372.

Menetrier-Caux, C., Ray-Coquard, I., Blay, J.Y. & Caux, C. (2019) Lymphopenia in Cancer Patients and its Effects on Response to Immunotherapy: an opportunity for combination with Cytokines? *J Immunother Cancer*, **7**, 85.

Merrill, J.E., Hanak, S., Pu, S.F., Liang, J., Dang, C., Iglesias-Bregna, D., Harvey, B., Zhu, B. & McMonagle-Strucko, K. (2009) Teriflunomide reduces behavioral, electrophysiological, and histopathological deficits in the Dark Agouti rat model of experimental autoimmune encephalomyelitis. *Journal of neurology*, **256**, 89-103.

Metzler, B., Gfeller, P., Wieczorek, G., Li, J., Nuesslein-Hildesheim, B., Katopodis, A., Mueller, M. & Brinkmann, V. (2008) Modulation of T cell homeostasis and alloreactivity under continuous FTY720 exposure. *International immunology*, **20**, 633-644.

Miguez, A., Garcia-Diaz Barriga, G., Brito, V., Straccia, M., Giralt, A., Gines, S., Canals, J.M. & Alberch, J. (2015) Fingolimod (FTY720) enhances hippocampal synaptic plasticity and memory in Huntington's disease by preventing p75NTR up-regulation and astrocyte-mediated inflammation. *Hum Mol Genet*, **24**, 4958-4970.

Mohebiany, A.N., Ramphal, N.S., Karram, K., Di Liberto, G., Novkovic, T., Klein, M., Marini, F., Kreutzfeldt, M., Hartner, F., Lacher, S.M., Bopp, T., Mittmann, T., Merkler, D. & Waisman, A. (2020) Microglial A20 Protects the Brain from CD8 T-Cell-Mediated Immunopathology. *Cell Rep*, **30**, 1585-1597 e1586.

Mombaerts, P., Iacomini, J., Johnson, R.S., Herrup, K., Tonegawa, S. & Papaioannou, V.E. (1992) RAG-1-deficient mice have no mature B and T lymphocytes. *Cell*, **68**, 869-877.

Montecchiani, C., Pedace, L., Lo Giudice, T., Casella, A., Mearini, M., Gaudiello, F., Pedroso, J.L., Terracciano, C., Caltagirone, C., Massa, R., St George-Hyslop, P.H., Barsottini, O.G., Kawarai, T. & Orlacchio, A. (2016) ALS5/SPG11/KIAA1840 mutations cause autosomal recessive axonal Charcot-Marie-Tooth disease. *Brain*, **139**, 73-85.

Murmu, R.P., Martin, E., Rastetter, A., Esteves, T., Muriel, M.P., El Hachimi, K.H., Denora, P.S., Dauphin, A., Fernandez, J.C., Duyckaerts, C., Brice, A., Darios, F. & Stevanin, G. (2011) Cellular distribution and subcellular localization of spatacsin and spastizin, two proteins involved in hereditary spastic paraplegia. *Mol Cell Neurosci*, **47**, 191-202.

Nair, A.B. & Jacob, S. (2016) A simple practice guide for dose conversion between animals and human. *J Basic Clin Pharm*, **7**, 27-31.

Oh, H., Leventhal, O., Channappa, D., Henderson, V.W., Wyss-Coray, T., Lehallier, B. & Gate, D. (2021) Methods to investigate intrathecal adaptive immunity in neurodegeneration. *Mol Neurodegener*, **16**, 3.

Oliver, P.L., Keays, D.A. & Davies, K.E. (2007) Behavioural characterisation of the robotic mouse mutant. *Behav Brain Res*, **181**, 239-247.

Orlacchio, A., Babalini, C., Borreca, A., Patrono, C., Massa, R., Basaran, S., Munhoz, R.P., Rogaeva, E.A., St George-Hyslop, P.H., Bernardi, G. & Kawarai, T. (2010) SPATACSIN mutations cause autosomal recessive juvenile amyotrophic lateral sclerosis. *Brain*, **133**, 591-598.

Osmolak, A.M., Wallenberg, R.B. & Caplan, J.P. (2012) Hereditary spastic paraplegia and psychosis: connected by the corpus callosum? *Psychosomatics*, **53**, 81-84.

Pacheco, R., Contreras, F. & Zouali, M. (2014) The dopaminergic system in autoimmune diseases. *Front Immunol*, **5**, 117.

Paisan-Ruiz, C., Guevara, R., Federoff, M., Hanagasi, H., Sina, F., Elahi, E., Schneider, S.A., Schwingenschuh, P., Bajaj, N., Emre, M., Singleton, A.B., Hardy, J., Bhatia, K.P., Brandner, S., Lees, A.J. & Houlden, H. (2010) Early-onset L-dopa-responsive parkinsonism with pyramidal signs due to ATP13A2, PLA2G6, FBXO7 and spatacsin mutations. *Mov Disord*, **25**, 1791-1800.

Parodi, L., Fenu, S., Stevanin, G. & Durr, A. (2017) Hereditary spastic paraplegia: More than an upper motor neuron disease. *Rev Neurol (Paris)*, **173**, 352-360.

Paul, L.K., Van Lancker-Sidtis, D., Schieffer, B., Dietrich, R. & Brown, W.S. (2003) Communicative deficits in agenesis of the corpus callosum: nonliteral language and affective prosody. *Brain Lang*, **85**, 313-324.

Pelosi, L., Lanzillo, B., Perretti, A., Santoro, L., Blumhardt, L. & Caruso, G. (1991) Motor and somatosensory evoked potentials in hereditary spastic paraplegia. *J Neurol Neurosurg Psychiatry*, **54**, 1099-1102.

Perez-Branguli, F., Mishra, H.K., Prots, I., Havlicek, S., Kohl, Z., Saul, D., Rummel, C., Dorca-Arevalo, J., Regensburger, M., Graef, D., Sock, E., Blasi, J., Groemer, T.W., Schlotzer-Schrehardt, U., Winkler, J. & Winner, B. (2014) Dysfunction of spatacsin leads to axonal pathology in SPG11-linked hereditary spastic paraplegia. *Hum Mol Genet*, **23**, 4859-4874.

Pirau, L. & Lui, F. (2021) Frontal Lobe Syndrome. *StatPearls*, Treasure Island (FL).

Pozner, T., Regensburger, M., Engelhorn, T., Winkler, J. & Winner, B. (2020) Janus-faced spatacsin (SPG11): involvement in neurodevelopment and multisystem neurodegeneration. *Brain*, **143**, 2369-2379.

Prinz, M., Erny, D. & Hagemeyer, N. (2017) Ontogeny and homeostasis of CNS myeloid cells. *Nat Immunol*, **18**, 385-392.

Puech, B., Lacour, A., Stevanin, G., Sautiere, B.G., Devos, D., Depienne, C., Denis, E., Mundwiller, E., Ferriby, D., Vermersch, P. & Defoort-Dhellemmes, S. (2011) Kjellin syndrome: long-term neuro-ophthalmologic follow-up and novel mutations in the SPG11 gene. *Ophthalmology*, **118**, 564-573.

Ralph, R.J., Paulus, M.P., Fumagalli, F., Caron, M.G. & Geyer, M.A. (2001) Prepulse inhibition deficits and perseverative motor patterns in dopamine transporter knock-out mice: differential effects of D1 and D2 receptor antagonists. *J Neurosci*, **21**, 305-313.

Rattazzi, L., Piras, G., Ono, M., Deacon, R., Pariante, C.M. & D'Acquisto, F. (2013) CD4(+) but not CD8(+) T cells revert the impaired emotional behavior of immunocompromised RAG-1-deficient mice. *Transl Psychiatry*, **3**, e280.

Reith, R.M., McKenna, J., Wu, H., Hashmi, S.S., Cho, S.H., Dash, P.K. & Gambello, M.J. (2013) Loss of Tsc2 in Purkinje cells is associated with autistic-like behavior in a mouse model of tuberous sclerosis complex. *Neurobiol Dis*, **51**, 93-103.

Renvoise, B., Chang, J., Singh, R., Yonekawa, S., FitzGibbon, E.J., Mankodi, A., Vanderver, A., Schindler, A., Toro, C., Gahl, W.A., Mahuran, D.J., Blackstone, C. & Pierson, T.M. (2014) Lysosomal abnormalities in hereditary spastic paraplegia types SPG15 and SPG11. *Ann Clin Transl Neurol*, **1**, 379-389.

Rojas, B., Gallego, B.I., Ramirez, A.I., Salazar, J.J., de Hoz, R., Valiente-Soriano, F.J., Aviles-Trigueros, M., Villegas-Perez, M.P., Vidal-Sanz, M., Trivino, A. & Ramirez, J.M. (2014) Microglia in mouse retina contralateral to experimental glaucoma exhibit multiple signs of activation in all retinal layers. *J Neuroinflammation*, **11**, 133.

Rossi, M.A. & Yin, H.H. (2015) Elevated dopamine alters consummatory pattern generation and increases behavioral variability during learning. *Front Integr Neurosci*, **9**, 37.

Rubegni, A., Battisti, C., Tessa, A., Cerase, A., Doccini, S., Malandrini, A., Santorelli, F.M. & Federico, A. (2017) SPG2 mimicking multiple sclerosis in a family identified using next generation sequencing. *J Neurol Sci*, **375**, 198-202.

Sagvolden, T., Russell, V.A., Aase, H., Johansen, E.B. & Farshbaf, M. (2005) Rodent models of attention-deficit/hyperactivity disorder. *Biol Psychiatry*, **57**, 1239-1247.

Salinas, S., Proukakis, C., Crosby, A. & Warner, T.T. (2008) Hereditary spastic paraplegia: clinical features and pathogenetic mechanisms. *Lancet Neurol*, **7**, 1127-1138.

Salobrar-Garcia, E., Mendez-Hernandez, C., Hoz, R., Ramirez, A.I., Lopez-Cuenca, I., Fernandez-Albarral, J.A., Rojas, P., Wang, S., Garcia-Feijoo, J., Gil, P., Salazar, J.J. & Ramirez, J.M. (2020) Ocular Vascular Changes in Mild Alzheimer's Disease Patients: Foveal Avascular Zone, Choroidal Thickness, and ONH Hemoglobin Analysis. *J Pers Med*, **10**, 231.

Sawada, A., Niiyama, Y., Ataka, K., Nagaishi, K., Yamakage, M. & Fujimiya, M. (2014) Suppression of bone marrow-derived microglia in the amygdala improves anxiety-like behavior induced by chronic partial sciatic nerve ligation in mice. *Pain*, **155**, 1762-1772.

Schäffner, E., Edgar, J., Lehning, M., Strauß, J., Bosch-Queralt, M., Wieghofer, P., Berghoff, S., Krueger, M., Morawski, M., Reinert, T., Möbius, W., Barrantes-Freer, A., Prinz, M., Reich, D., Flügel, A., Stadelmann, C., Fledrich, R., Stassart, R. & Nave, K. (2021) Myelin insulation as a risk factor for axonal degeneration in autoimmune demyelinating disease, bioRxiv, 13 Nov 2021.

Schira, J., Heinen, A., Poschmann, G., Ziegler, B., Hartung, H.P., Stuhler, K. & Kury, P. (2019) Secretome analysis of nerve repair mediating Schwann cells reveals Smad-dependent trophism. *FASEB J*, **33**, 4703-4715.

Schmid, C.D., Stienekemeier, M., Oehen, S., Bootz, F., Zielasek, J., Gold, R., Toyka, K.V., Schachner, M. & Martini, R. (2000) Immune deficiency in mouse models for inherited peripheral neuropathies leads to improved myelin maintenance. *J Neurosci*, **20**, 729-735.

Schroder, J.B., Pawlowski, M., Meyer Zu Horste, G., Gross, C.C., Wiendl, H., Meuth, S.G., Ruck, T. & Warnecke, T. (2018) Immune Cell Activation in the Cerebrospinal Fluid of Patients With Parkinson's Disease. *Front Neurol*, **9**, 1081.

Seehafer, S.S. & Pearce, D.A. (2006) You say lipofuscin, we say ceroid: defining autofluorescent storage material. *Neurobiol Aging*, **27**, 576-588.

Segura-Ulate, I., Yang, B., Vargas-Medrano, J. & Perez, R.G. (2017) FTY720 (Fingolimod) reverses alpha-synuclein-induced downregulation of brain-derived neurotrophic factor mRNA in OLN-93 oligodendroglial cells. *Neuropharmacology*, **117**, 149-157.

Shi, D., Tian, T., Yao, S., Cao, K., Zhu, X., Zhang, M., Wen, S., Li, L., Shi, M. & Zhou, H. (2018) FTY720 attenuates behavioral deficits in a murine model of systemic lupus erythematosus. *Brain Behav Immun*, **70**, 293-304.

Shi, L., Keefe, D., Durand, E., Feng, H., Zhang, D. & Lieberman, J. (2005) Granzyme B binds to target cells mostly by charge and must be added at the same time as perforin to trigger apoptosis. *J Immunol*, **174**, 5456-5461.

Singh, S., Dallenga, T., Winkler, A., Roemer, S., Maruschak, B., Siebert, H., Bruck, W. & Stadelmann, C. (2017) Relationship of acute axonal damage, Wallerian degeneration, and clinical disability in multiple sclerosis. *J Neuroinflammation*, **14**, 57.

Sjostedt, E., Zhong, W., Fagerberg, L., Karlsson, M., Mitsios, N., Adori, C., Oksvold, P., Edfors, F., Limiszewska, A., Hikmet, F., Huang, J., Du, Y., Lin, L., Dong, Z., Yang, L., Liu, X., Jiang, H., Xu, X., Wang, J., Yang, H., Bolund, L., Mardinoglu, A., Zhang, C., von Feilitzen, K., Lindskog, C., Ponten, F., Luo, Y., Hokfelt, T., Uhlen, M. & Mulder, J. (2020) An atlas of the protein-coding genes in the human, pig, and mouse brain. *Science*, **367**.

Slabicki, M., Theis, M., Krastev, D.B., Samsonov, S., Mundwiller, E., Junqueira, M., Paszkowski-Rogacz, M., Teyra, J., Heninger, A.K., Poser, I., Prieur, F., Truchetto, J., Confavreux, C., Marelli, C., Durr, A., Camdessanche, J.P., Brice, A., Shevchenko, A., Pisabarro, M.T., Stevanin, G. & Buchholz, F. (2010) A genome-scale DNA repair RNAi screen identifies SPG48 as a novel gene associated with hereditary spastic paraplegia. *PLoS Biol*, **8**, e1000408.

Smith, C.J., Emge, J.R., Berzins, K., Lung, L., Khamishon, R., Shah, P., Rodrigues, D.M., Sousa, A.J., Reardon, C., Sherman, P.M., Barrett, K.E. & Gareau, M.G. (2014) Probiotics normalize the gut-brain-microbiota axis in immunodeficient mice. *Am J Physiol Gastrointest Liver Physiol*, **307**, G793-802.

Soderblom, C. & Blackstone, C. (2006) Traffic accidents: molecular genetic insights into the pathogenesis of the hereditary spastic paraplegias. *Pharmacol Ther*, **109**, 42-56.

St Clair, D., Blackburn, I., Blackwood, D. & Tyrer, G. (1988) Measuring the course of Alzheimer's disease. A longitudinal study of neuropsychological function and changes in P3 event-related potential. *Br J Psychiatry*, **152**, 48-54.

Stein, D.J., Vasconcelos, M.F., Albrechet-Souza, L., Cereser, K.M.M. & de Almeida, R.M.M. (2017) Microglial Over-Activation by Social Defeat Stress Contributes to Anxiety- and Depressive-Like Behaviors. *Front Behav Neurosci*, **11**, 207.

Stevanin, G., Azzedine, H., Denora, P., Boukhris, A., Tazir, M., Lossos, A., Rosa, A.L., Lerer, I., Hamri, A., Alegria, P., Loureiro, J., Tada, M., Hannequin, D., Anheim, M., Goizet, C., Gonzalez-Martinez, V., Le Ber, I., Forlani, S., Iwabuchi, K., Meiner, V., Uyanik, G., Erichsen, A.K., Feki, I., Pasquier, F., Belarbi, S., Cruz, V.T., Depienne, C., Truchetto, J., Garrigues, G., Tallaksen, C., Tranchant, C., Nishizawa, M., Vale, J., Coutinho, P., Santorelli, F.M., Mhiri, C., Brice, A., Durr, A. & SPATAX consortium (2008a) Mutations in SPG11 are frequent in autosomal recessive spastic paraplegia with thin corpus callosum, cognitive decline and lower motor neuron degeneration. *Brain*, **131**, 772-784.

Stevanin, G., Ruberg, M. & Brice, A. (2008b) Recent advances in the genetics of spastic paraplegias. *Curr Neurol Neurosci Rep*, **8**, 198-210.

Stevanin, G., Santorelli, F.M., Azzedine, H., Coutinho, P., Chomilier, J., Denora, P.S., Martin, E., Ouvrard-Hernandez, A.M., Tessa, A., Bouslam, N., Lossos, A., Charles, P., Loureiro, J.L., Elleuch, N., Confavreux, C., Cruz, V.T., Ruberg, M., Leguern, E., Grid, D., Tazir, M., Fontaine, B., Filla, A., Bertini, E., Durr, A. & Brice, A. (2007) Mutations in SPG11, encoding spatacsin, are a major cause of spastic paraplegia with thin corpus callosum. *Nat Genet*, **39**, 366-372.

Sudarov, A. (2013) Defining the role of cerebellar Purkinje cells in autism spectrum disorders. *Cerebellum*, **12**, 950-955.

Szczypka, M.S., Kwok, K., Brot, M.D., Marck, B.T., Matsumoto, A.M., Donahue, B.A. & Palmiter, R.D. (2001) Dopamine production in the caudate putamen restores feeding in dopamine-deficient mice. *Neuron*, **30**, 819-828.

Tesson, C., Koht, J. & Stevanin, G. (2015) Delving into the complexity of hereditary spastic paraplegias: how unexpected phenotypes and inheritance modes are revolutionizing their nosology. *Hum Genet*, **134**, 511-538.

Tilly, G., Cadoux, M., Garcia, A., Morille, J., Wiertlewski, S., Pecqueur, C., Brouard, S., Laplaud, D. & Degauque, N. (2021) Teriflunomide Treatment of Multiple Sclerosis Selectively Modulates CD8 Memory T Cells. *Front Immunol*, **12**, 730342.

Timmerman, V., Clowes, V.E. & Reid, E. (2013) Overlapping molecular pathological themes link Charcot-Marie-Tooth neuropathies and hereditary spastic paraplegias. *Exp Neurol*, **246**, 14-25.

Toupenet Marchesi, L., Leblanc, M. & Stevanin, G. (2021) Current Knowledge of Endolysosomal and Autophagy Defects in Hereditary Spastic Paraplegia. *Cells*, **10**, 1678.

Tsai, P.T., Hull, C., Chu, Y., Greene-Colozzi, E., Sadowski, A.R., Leech, J.M., Steinberg, J., Crawley, J.N., Regehr, W.G. & Sahin, M. (2012) Autistic-like behaviour and cerebellar dysfunction in Purkinje cell Tsc1 mutant mice. *Nature*, **488**, 647-651.

Ueda, M. & Kusunoki, S. (2011) [Autoimmune neuropathies: diagnosis, treatment, and recent topics]. *Brain Nerve*, **63**, 549-555.

Urban, S.L., Jensen, I.J., Shan, Q., Pewe, L.L., Xue, H.H., Badovinac, V.P. & Harty, J.T. (2020) Peripherally induced brain tissue-resident memory CD8(+) T cells mediate protection against CNS infection. *Nat Immunol*, **21**, 938-949.

Van Overwalle, F., Manto, M., Cattaneo, Z., Clausi, S., Ferrari, C., Gabrieli, J.D.E., Guell, X., Heleven, E., Lupo, M., Ma, Q., Michelutti, M., Olivito, G., Pu, M., Rice, L.C., Schmahmann, J.D., Siciliano, L., Sokolov, A.A., Stoodley, C.J., van Dun, K., Vandervert, L. & Leggio, M. (2020) Consensus Paper: Cerebellum and Social Cognition. *Cerebellum*, **19**, 833-868.

Vanderver, A., Tonduti, D., Auerbach, S., Schmidt, J.L., Parikh, S., Gowans, G.C., Jackson, K.E., Brock, P.L., Patterson, M., Nehrebecky, M., Godfrey, R., Zein, W.M., Gahl, W. & Toro, C. (2012) Neurotransmitter abnormalities and response to supplementation in SPG11. *Mol Genet Metab*, **107**, 229-233.

Varga, R.E., Khundadze, M., Damme, M., Nietzsche, S., Hoffmann, B., Stauber, T., Koch, N., Hennings, J.C., Franzka, P., Huebner, A.K., Kessels, M.M., Biskup, C., Jentsch, T.J., Qualmann, B., Braulke, T., Kurth, I., Beetz, C. & Hubner, C.A. (2015) In Vivo Evidence for Lysosome Depletion and Impaired Autophagic Clearance in Hereditary Spastic Paraplegia Type SPG11. *PLoS Genet*, **11**, e1005454.

Vavla, M., Paparella, G., Papayannis, A., Pascuzzo, R., Girardi, G., Pellegrini, F., Capello, G., Prosdocimo, G. & Martinuzzi, A. (2019) Optical Coherence Tomography in a Cohort of Genetically Defined Hereditary Spastic Paraplegia: A Brief Research Report. *Front Neurol*, **10**, 1193.

Viar, K., Njoku, D., Secor McVoy, J. & Oh, U. (2020) Sarm1 knockout protects against early but not late axonal degeneration in experimental allergic encephalomyelitis. *PLoS One*, **15**, e0235110.

Vidal, P.M. & Pacheco, R. (2020) Targeting the Dopaminergic System in Autoimmunity. *J Neuroimmune Pharmacol*, **15**, 57-73.

Wang, Y.L., Han, Q.Q., Gong, W.Q., Pan, D.H., Wang, L.Z., Hu, W., Yang, M., Li, B., Yu, J. & Liu, Q. (2018) Microglial activation mediates chronic mild stress-induced depressive- and anxiety-like behavior in adult rats. *J Neuroinflammation*, **15**, 21.

Warshawsky, I., Rudick, R.A., Staugaitis, S.M. & Natowicz, M.R. (2005) Primary progressive multiple sclerosis as a phenotype of a PLP1 gene mutation. *Ann Neurol*, **58**, 470-473.

Watanabe, Y., Nakayama, T., Nagakubo, D., Hieshima, K., Jin, Z., Katou, F., Hashimoto, K. & Yoshie, O. (2006) Dopamine selectively induces migration and homing of naive CD8+ T cells via dopamine receptor D3. *J Immunol*, **176**, 848-856.

Wieters, F., Weiss Lucas, C., Gruhn, M., Buschges, A., Fink, G.R. & Aswendt, M. (2021) Introduction to spasticity and related mouse models. *Exp Neurol*, **335**, 113491.

Wijemanne, S., Shulman, J.M., Jimenez-Shahed, J., Curry, D. & Jankovic, J. (2015) SPG11 Mutations Associated With a Complex Phenotype Resembling Dopa-Responsive Dystonia. *Mov Disord Clin Pract*, **2**, 149-154.

Willis, M.A. & Cohen, J.A. (2013) Fingolimod therapy for multiple sclerosis. *Semin Neurol*, **33**, 37-44.

Wolf-Schnurrbusch, U.E., Ceklic, L., Brinkmann, C.K., Iliev, M.E., Frey, M., Rothenbuehler, S.P., Enzmann, V. & Wolf, S. (2009) Macular thickness measurements in healthy eyes using six different optical coherence tomography instruments. *Invest Ophthalmol Vis Sci*, **50**, 3432-3437.

Wu, H., Wang, X., Gao, J., Liang, S., Hao, Y., Sun, C., Xia, W., Cao, Y. & Wu, L. (2017) Fingolimod (FTY720) attenuates social deficits, learning and memory impairments, neuronal loss and neuroinflammation in the rat model of autism. *Life Sci*, **173**, 43-54.

Zagha, E., Casale, A.E., Sachdev, R.N., McGinley, M.J. & McCormick, D.A. (2013) Motor cortex feedback influences sensory processing by modulating network state. *Neuron*, **79**, 567-578.

Ziemssen, T., Lang, M., Schmidt, S., Albrecht, H., Klotz, L., Haas, J., Lassek, C., Lang, S., Winkelmann, V.E., Ettle, B., Schulze-Topphoff, U. & Pangaea study group (2022) Long-term real-world effectiveness and safety of fingolimod over 5 years in Germany. *J Neurol*, **269**, 3276-3285.

8 Appendix

8.1 Technical equipment

BioPhotometer 6131		Eppendorf (Hamburg, Germany)
Biosphere Filter Tips		Sarstedt (Nuernbrecht, Germany)
Catwalk XT 10.6		Noldus (Weimar, Germany)
Centrifuges		
	Biofuge 15R	Heraeus (Hanau, Germany)
	Biofuge Pico	Heraeus (Hanau, Germany)
	Centrifuge 5424	Eppendorf (Hamburg, Germany)
Cryostat CM 3050S		Leica (Wetzlar, Germany)
FACSLyric		BD Biosciences (San Jose, USA)
Freezer		Liebherr (Biberach, Germany)
Dry block thermostat TBD-120		Hartenstein (Wuerzburg, Germany)
Dry block thermostat TBD-100		Hartenstein (Wuerzburg, Germany)
Gel chambers		
	Horizontal Mini Gel System	Peqlab (Erlangen, Germany)
	Mini-PROTEAN3® cell	Bio-Rad (Munich, Germany)
	Mini-Trans-Blot® cell	Bio-Rad (Munich, Germany)
Gel imager		Intas (Goettingen, Germany)
Hamilton syringes		Hamilton (Höchst, Germany)
Heating plate		Medax (Neumuenster, Germany)
Homogenizer MICCRA D-8		ART (Muehlheim, Germany)
MicroAmp® Fast 96-well reaction plate		Applied Biosystems (Darmstadt, Germany)
Microscopes		
	ApoTome 2	Zeiss (Oberkochen, Germany)
	Axiophot 2	Zeiss (Oberkochen, Germany)
	CM10	Philips (Hamburg, Germany)
	LEO 906 E	Zeiss (Oberkochen, Germany)
Object slides superfrost		Langenbrinck (Teningen, Germany)
Olympus Veleta camera system		Olympus (Hamburg, Germany)
Optical adhesive covers		Applied Biosystems (Darmstadt, Germany)
Optodrum		Striatech (Tübingen, Germany)
Spectralis® OCT		Heidelberg Engineering (Heidelberg, Germany)
PapPen		SCI (Munich, Germany)
PCR tubes		Hartenstein (Wuerzburg, Germany)
Perfusion pump Reglo		Ismatec (Glattbrugg, Switzerland)
ProScan Slow Scan CCD camera		Pro Scan (Lagerlechfeld, Germany)

Pipettes

	Abimed (Berlin, Germany)
	Eppendorf (Hamburg, Germany)
	Gilson (Bad Camberg, Germany
Power supply	Bio-RAD (Munich, Germany)

Thermocycler

	Step One Plus Real Time PCR System	Applied Biosystems (Darmstadt, Germany
	Mastercycler gradient	Eppendorf (Hamburg, Germany)
	Primus96 advanced	Peqlab (Erlangen, Germany)
Ultracut		Leica (Wetzlar, Germany)

8.2   Software

Adobe Photoshop CS6	Adobe (San Jose, USA)
Catwalk XT 10.6	Noldus (Weimar, Germany)
CellQuest Pro	BD Biosciences (San Jose, USA)
EthoVision XT 11	Noldus (Weimar, Germany)
EthoVision XT 15	Noldus (Weimar, Germany)
Flowjo version 10	BD Biosciences (San Jose, USA)
FluoView	Olympus (Hamburg, Germany)
GraphPad Prism 7	GraphPad Software (San Diego, USA)
ImageJ	NIH (Bethesda, USA)
iTEM	Olympus (Hamburg, Germany)
Microsoft Office 2016	Microsoft (Redmond, USA)
Optodrum	Striatech (Tübingen, Germany)
Research Heyex	Heidelberg Engineering (Heidelberg, Germany)
ZEN 3.0	Zeiss (Oberkochen, Germany)

8.3   Reagents

Acetone	Invitrogen (Karlsruhe, Germany)
Accutase	Merck Millipore (Massachusetts, USA)
Agarose	Carl Roth (Karlsruhe, Germany)
AmpliTaq DNA Polymerase	Polymerase Applied Biosystems (Darmstadt, Germany)
Aqua-Poly/Mount®	Polysciences (Eppelheim, Germany)
Avidin-Biotin blocking kit	Vector Laboratories (Burlingame, USA)
Boric acid	Merck (Darmstadt, Germany)
Bovine serum albumin 96%	Sigma-Aldrich (Munich, Germany)
Bromphenol blue	Sigma-Aldrich (Munich, Germany)

Cacodylic acid	Serva (Heidelberg, Germany)
Chloroform	Sigma-Aldrich (Munich, Germany)
DAPI	Sigma-Aldrich (Munich, Germany)
Diethyl pyrocarbonate (DEPC)	Sigma-Aldrich (Munich, Germany)
1, 4-Dithiothreitol (DTT)	Sigma-Aldrich (Munich, Germany)
Ethylenediaminetetraacetic acid (EDTA)	Merck (Darmstadt, Germany)
Ethanol	Sigma-Aldrich (Munich, Germany)
Gel Star DNA-Dye	Lonza (Basel, Switzerland)
Glycine	Sigma-Aldrich (Munich, Germany)
Glycerol	Merck (Darmstadt, Germany)
Glycogen	Roche (Mannheim, Germany)
HD Green DNA-Dye	Intas (Göttingen, Germany)
Heparin	Ratiopharm (Ulm, Germany)
HEPES	Carl Roth (Karlsruhe, Germany)
IGEPAL CA-630	Sigma-Aldrich (Munich, Germany)
Ketavet	Pfizer (Berlin, Germany)
Methanol	Sigma-Aldrich (Munich, Germany)
2-Methylbutane	Carl Roth (Karlsruhe, Germany)
Orange DNA Loading Dye (6X)	Thermo Fisher Scientific (Darmstadt, Germany)
O'RangeRuler™ 100+500 bp DNA Ladder	Thermo Fisher Scientific (Darmstadt, Germany)
Page Ruler Plus prestained protein ladde	Thermo Fisher Scientific (Darmstadt, Germany)
40 % Percoll	GE Healthcare (Munich, Germany)
Polyacrylamid	Carl Roth (Karlsruhe, Germany)
Primers	Sigma-Aldrich (Munich, Germany)
Potassium chloride	Merck (Darmstadt, Germany)
Potassium di-hydrogen phosphate	Merck (Darmstadt, Germany)
Protease inhibitor cocktail set	Calbiochem (Darmstadt, Germany)
Sodium chloride solution	Merck (Darmstadt, Germany)
Sodium dodecyl sulfate (SDS)	Carl Roth (Karlsruhe, Germany)
Sucrose	Carl Roth (Karlsruhe, Germany)
Tetramethylethylenediamine (TEMED)	Sigma-Aldrich (Munich, Germany)
Tissue-Tek® O.C.T.™ Compound	Sakura (Alphen aan den Rijn, Netherlands)
Tris(hydroxymethyl)aminomethane (Tris)	Merck (Darmstadt, Germany)
Tris-HCl	Merck (Darmstadt, Germany)
TritonX-100	Carl Roth (Karlsruhe, Germany)
Tween-20	Carl Roth (Karlsruhe, Germany)
Tween-80	Carl Roth (Karlsruhe, Germany)
Vitro-Clud®	Langebrinck (Teningen, Germany)
Xylavet	CP-Pharma (Burgdorf, Germany)

8.4   Buffer and solutions

Anaesthetics	1.2% Ketaminhydrochloride
	0.08% Xylazinhydrochloride
	0.9% NaCl
Cacodylate buffer	0.1 M cacodylic acid
	Dissolved in distilled water
	pH 7.4
Cresyl vioelt solution	0.1% cresyl violet
	1% acetic acid
DABCO	25% PBS
	75% Glycerol
	25 mg/ml 1,4-diazabicyclo[2.2.2]octane
Erythrocyte lysis buffer	0.15 M NH4Cl
	1 mM KHCO3
	0.1 mM Na2EDTA
	pH 7.4
	sterile filtration
FACS buffer	1% BSA
	0.1% NaAzide
	in PBS
	sterile filtration
10% FCS in PBS	10% FCS
	in PBS
Gel running buffer (10x)	0.25M Tris
	1.92M Glycin
	1% SDS
	Store at 4°C
Haematoxylin	50 mg/ml KAl(SO4)2
	1 mg/ml Haematoxylin
	0.2 mg/ml NaIO3
	2% acetic acid

Methylene blue	1% Methylene blue
	1% Azure II
	40% Saccharose
	pH9.2
PBS (1x)	137 mM NaCl
	2.7 mM KCl
	1.5 mM KH2PO4
	8.1 mM Na2HPO4
	pH 7.4
Ponceau S	1% Trichloroacetic acid
	0.1% Ponceau S
	Store protected from light
Spurr's medium	10 g Vinyl/ERL
	6 g DER 736
	26 g NSA
	0.4 g DMAE

8.5 Primers

SPG11

SPG11 FW	5′-GCCAAGGTATGCACCAGACGGGG-3′
SPG11 Rev	5′-TCCTGCCCTTCACCACGTCAGG-3′

RAG1

RAG-1F1	5'-GAGGTTCCGCTACGACTCTG-3'
RAG-1F2	5'-CCGGACAAGTTTTTCAT-CGT-3'
RAG-1R	5'-TGGATGTGGAATTGTTGCGAG-3'

8.6   Antibodies

Primary antibodies

Antibodies	Company	Host	Dilution	Fixation	Additives
Brn3a	Santa Cruz	Goat	1/100	2% PFA	2% Triton
CD4	Serotec	Rat	1/1000	Acetone	None
CD8	Serotec	Rat	1/500	Acetone	None
CD11b	Serotec	Rat	1/100	4% PFA	0.3% Triton
CD169(Sn)	Serotec	Rat	1/300	Acetone	None
RBPMS	Merck	Guinea pig	1/300	2% PFA	2% Triton
SMI32	Covance	Mouse	1/1000	4%PFA	None
TMEM119	Abcam	Rabbit	1/500	2% PFA	2% Triton-X

Secondary antibodies

Reactivity	Company	Host	Dilution	Conjugation
Rat IgG	Dianova	Goat	1/300	Cy3
Mouse IgG	Dianova	Donkey	1/300	Cy3
Rabbit IgG	Dianova	Goat	1/300	Cy3
Goat IgG	Dianova	Donkey	1/300	Cy3
Rat IgG	Dianova	Goat	1/300	Cy2
Mouse IgG	Dianova	Goat	1/300	Cy2
Guinea pig IgG	Dianova	Donkey	1/500	AF488
Rat IgG	Vector	Rabbit	1/100	Biotin
Mouse IgG	Vector	Goat	1/100	Biotin

FACS antibodies

Antibody	Company	Host	Dilution
CD8a PerCP/Cyanine5.5	BioLegend	Rat	1/100
CD16/32	BD Biosciences	Rat	1/200
CD45 APC	BioLegend	Rat	1/100
CD103 BV605	BioLegend	Armenian hamster	1/100
CXCR4 PE	BioLegend	Rat	1/100
CXCR6 PE/Cyanine7	BioLegend	Rat	1/100
Ly-6A/E FITC	BioLegend	Rat	1/100

9 Abbreviations

AF	Alexafluor
ALS	Amyotrophic lateral sclerosis
AP-5	Adaptor protein complex 5
ASD	Autism spectrum disorder
BDNF	Brain-derived neurotrophic factor
Brn3a	Brain-specific homeobox(POU domain protein 3A)
BSA	Bovine serum albumin
°C	Degree Celsius
CAR	Cliff-avoidance-reaction
CB	Cerebellum
CC	Corpus callosum
CD	Cluster of differentiation
CIDP	Chronic inflammatory demyelinating polyneuropathy
CLN1	Neuronal ceroid lipofuscinosis type 1
CLN3	Neuronal ceroid lipofuscinosis type 3
cm	Centimeter
CMT	Charcot-Marie-Tooth disease
CMAP	Compound muscle action potential
CNS	Central nervous system
CO_2	Carbon dioxide
CO	Cortex
Cy	Cyanine
d	Degree
DA	Dopamine
DABCO	1,4-Diazabicyclo[2.2.2]octane
DAPI	4',6-Diamidino-2-phenylindole
DAT	Dopamine transporter
DR	Dopamine receptor
DRD2	Dopamine receptor 2
DLB	Dark-light-box
DNA	Deoxyribonucleic acid
DMSO	Dimethyl sulfoxide
DOHDH	Dihydroorotate dehydrogenase
EAE	Experimental autoimmune encephalomyelitis
EP1	Prostaglandin E receptor 1
FACS	Fluorescence activated cell sorting
FTY720	Fingolimod
g	Gravitational acceleration
GA	Glutaraldehyde
GBS	Guillain-Barré-syndrome
GFAP	Glial fibrillary acidic protein
GFP	Green fluorescent protein
GzmB	Granzyme B
HSP	Hereditary spastic paraplegia
Iba1	Ionized calcium-binding adapter molecule 1

IC	Immunocytochemistry
IgG	Immunoglobulin G
IgM	Immunoglobulin M
i.v.	Intravenously
LAMP1	Lysosomal-associated membrane protein 1
LMN	Lower motor neuron
Lx	Lux
min	Minutes
MS	Multiple sclerosis
NCL	Neuronal ceroid lipofuscinosis
NMNAT	Nicotinamide mononucleotide adenylyltransferease
NOR	Novel object recognition
OCT	Optic coherence tomography
OF	Open field
ON	Optic nerve
PBS	Phosphate buffered saline
PC	Purkinje cell
PCR	Polymerase chain reaction
PFA	Paraformaldehyde
PD-1	Programmed cell death 1
PLP	Proteolipid protein
PNS	Peripheral nervous system
PMS	Progressive multiple sclerosis
Rag1	Recombination activating gene 1
RBPMS	RNA Binding Protein, MRNA Processing Factor
RGC	Retinal ganglion cell
RNA	Ribonucleic acid
RNFL	Retinal nerve fiber layer
s	Seconds
S1P	Sphingosine-1-phosphate
SARM1	Sterile alpha and TIR motif containing 1
SC	Spinal cord
SD-OCT	Spectral domain OCT
SI	Social interaction and novelty
Sn	Sialoadhesin
SPG2	Hereditary spastic paraplegia type 2
SPG11	Hereditary spastic paraplegia type 11
SPG15	Hereditary spastic paraplegia type 15
SPG48	Hereditary spastic paraplegia type 48
TCC	Thin corpus callosum
TCR	T-cell receptor
Teri	Teriflunomide
TMEM	Transmembrane protein family members
TNFα	Tumor necrosis factor-alpha
UPN	Upper motor neuron
V	Five
WD	Wallerian degeneration

Wt   Wild-type

10 Curriculum vitae

11 Publications

11.1 Original articles in peer-reviewed international journals

Hörner, M., Groh, J., Klein, D., Ilg, W., Schöls, L., Dos Santos, S., Bergmann, A., Klebe, S., Cauhape, M., Branchu, J., El Hachimi, K., Stevanin, G., Darios, F., & Martini, R. (2022) CNS-associated T-lymphocytes in a mouse model of Hereditary Spastic Paraplegia type 11 (SPG11) are therapeutic targets for established immunomodulators**. Experiment. Neurol. **355**, 114119, doi: 10.1016/j.expneurol.2022.114119

Publications previous/unrelated to PhD project

Groh, J., **Hörner, M**. & Martini, R. (2018) Teriflunomide attenuates neuroinflammation-related neural damage in mice carrying human PLP1 mutations. *J Neuroinflammation* **15**, 194, doi:10.1186/s12974-018-1228-z

Groh, J., Friedman H.C., Orel N., Ip C.W., Fischer S., Spahn I., Schäffner E., **Hörner M.**, Stadler, D., Buttmann, M., Varallyay, C., Solymosi, L., Sendtner, M., Peterson, A.C., Martini, R. (2016) Pathogenic inflammation in the CNS of mice carrying human PLP1 mutations. *Hum Mol Genet* **25**, 4686-4702, doi:10.1093/hmg/ddw296

11.2 Oral presentations

Hörner M., *et al.* (2018), SPG11 and SPG15 advisory meeting, Cambridge; Role of inflammation in spastic paraplegia type 11

Hörner M., *et al.* (2019), TreatHSP/Tom-Wahlig-Symposium, Weimar; Physical exercise as a possible therapy for hereditary spastic paraplegia type 2

Hörner M., *et al.* (2019), Autumn school, Translational Neuroscience, Wuerzburg; Evidence for a pathogenic role of neuroinflammation in hereditary spastic paraplegia type 11

Hörner M., *et al.* (2020), TreatHSP/Tom-Wahlig-Symposium, online; Neuropsychological aspects in SPG-11

Hörner M., *et al.* (2021), TreatHSP/Tom-Wahlig-Symposium, Essen; Neuroinflammation in a mouse model of Hereditary Spastic Paraplegia type 11 (SPG11) as target for established immunomodulators

Hörner M., *et al.* (2021), Autumn school, Translational Neuroscience, Wuerzburg; Speed talk; Neuroinflammation in a mouse model of Hereditary Spastic Paraplegia type 11 (SPG11) as target for established immunomodulators

11.3 Poster presentations

Hörner M., *et al.* (2018), IZKF retreat 2018, Kloster Banz; Evidence for a pathogenic role of neuroinflammation in hereditary spastic paraplegia type 11, Poster price

Hörner M., *et al.* (2018), From rare to care, Tutzing; Evidence for a pathogenic role of neuroinflammation in hereditary spastic paraplegia type 11

Hörner M., *et al.* (2019), Current topics in myelin research, Kassel; Evidence for a role of neuroinflammation in hereditary spastic paraplegia type 11

Hörner M., *et al.* (2019), Eureka! Graduate School of Life Sciences Symposium, Wuerzburg; Evidence for a pathogenic role of neuroinflammation in hereditary spastic paraplegia type 11

12 Danksagung